Design, Synthesis and Application of Fluorogenic Probes for Selective Detection of Ionic Analytes in Physiological Condition

A Dissertation Submitted for Partial Fulfillment for the Degree of

Doctor of Philosophy

by

Chirantan Kar

(Roll No. 09612230)

Thesis Supervisor

Prof. Gopal Das

Department of Chemistry

Indian Institute of Technology Guwahati

June – 2014

In dedication to my Parents for

making me who I am and my wife for

supporting me all the way

INDIAN INSTITUTE OF TECHNOLOGY GUWAHATI

Department of Chemistry

STATEMENT

I do hereby declare that the matter embodied in this thesis is the result of investigations carried out by me in the Department of Chemistry, Indian Institute of Technology Guwahati, India, under the guidance of Dr. Gopal Das, Professor (Department of Chemistry), Indian Institute of Technology Guwahati, India.

In keeping with the general practice of reporting scientific observations, due acknowledgements have been made wherever this work is based on the findings of other investigators.

June, 2014 (**Chirantan Kar**)

IIT Guwahati

INDIAN INSTITUTE OF TECHNOLOGY GUWAHATI

Department of Chemistry

CERTIFICATE

This is to certify that Chirantan Kar has been working under my supervision since January, 2010 as a regular registered Ph. D. student. His thesis entitled **"Design, synthesis and application of fluorogenic probes for selective detection of ionic analytes in physiological condition"** is an authentic record of the results obtained from the research work carried out under my supervision in the Department of Chemistry, Indian Institute of Technology Guwahati, Assam, India. I am forwarding his thesis to submit for the award of degree of Doctor of Philosophy, from this institute. I certify that he has fulfilled all the requirements according to the rules of this institute regarding the investigations embodied in his thesis and this work has not been submitted elsewhere for a degree.

Dr. Gopal Das
(Thesis Supervisor)
Professor
Department of Chemistry
IIT Guwahati
Assam - 781 039, India

Acknowledgement

At the very onset, I would like to express my deepest gratitude to my father Chitta Ranjan Kar and mother Lekha Kar, two people with irrational and unbreakable belief on me. Their unconditional love and support made me reach this stage of my life. I am highly indebted to my PhD supervisor, Dr. Gopal Das for his guidance, constant supervision and encouragement for keeping me involved. He allowed me to see things from different point of view I could never understand, his invaluable insight and experience helped me to explore the domain of my work assembled in this thesis. His continuous support and inspiration always motivated me in hard times.

Besides my supervisor, I would also like to extend my heartiest thanks to the doctoral committee members, Dr. Sandeep Paul, Dr. Debasis Manna, Dr. Biplab Mondal, for their periodic evaluation of my work and valuable suggestion. I shall always be obliged to Dr. Aiyagari Ramesh for his admirable support throughout my research work. I also wish to thank staff members of chemistry department especially Nilyotpal da and Aniruddha da, they were always there when I needed. I would also thank Dr. BLD for the help he has rendered through these years; I truly believe that he is the man behind the substantial output of our analytical instruments. My sincere thanks to the staffs of Central Instruments facility, for their help and in hand guidance to several analytical instruments, required during my research work.

Alongside I have always felt lucky that I got wonderful seniors like Avijit da, Bimlesh da, bedo da, Sandeep da, amazing buddy like Jiban and extraordinary juniors like Md Najbul, Romen, Abhijit, Barun, Soham, Nilotpal. My days in these few years never started without having the morning tea with you people, you are real friends and fellow warrior. Keep up the fight. I am always a phone call away. I shall always be obliged to Arghya da- mentor and friend who taught me the basics of lab techniques, without your support I would have given this up a long time ago.

I also owe my obligations to my other seniors, batch mate and juniors of PhD fraternity of chemistry department for their help and support.

In context to the thesis work, I had the opportunity to mingle with the seniors and friends of the Center for Biotechnology, IIT Guwahati. I owe my gratitude to Manab da, Sudip, Tyagu (Thiyagarajan), Sandipan for their unconditional support and all the help they extended from time to time whenever required.

I take this opportunity to thank my friend Debu, Saumik, Amrik, Avra da, Guddu, Sourit, Chaki, Papu, Bappa, Piku, Sumit, Rajasree and Payel for being a source of encouragement and love throughout this time. I would also like to thank all M. Sc and B. Tech batches here in IIT Guwahati, and hostel mates, Debraj, Ravindra Patil, Mandar, Rajeev, Sayantan, Prasanta, Ashim, Deb da, Tuhin, Indranil, Kaushik, Hridesh I came across in these years. Also big thanks to Srimanta and Saroj for supporting me in countless occasions. I would also like to thank Chandani and Moumita (IIT Kharagpur) for their assistance and well-wishing.

Hearty thanks to Monorima, for dealing with my stubbornness, to bear with me for so long throughout this phase even in frustrating times, and for dealing with all my absence from many family occasions with a smile. All this is meaningless without you. I would also like to offer my thanks to two of my little brothers Sankha and Saheb and my sister Sneha for their untiring smile and love for me throughout my life, my relationship with them goes beyond the common gene we share.

No words would suffice to express my feelings for my teachers to whom I owe debt for their kindness and benevolence; Pinaki sir, Basudeb sir, Anirban sir, Pradipta sir, Sandip da, Sanju da, Amit da, Khokon da and many others from my school, college and university who gave me the direction and insightful informations to march forward in this field.

Finally, I would like to thank the Microsoft Corporation for presenting the MS word, from grammar checks to synonyms, from equations to symbols, without this software, the thesis would have taken another five years.

Still many names are missing whose contribution and help is worth mentioning.

Chirantan

SYNOPSIS

The contents of this thesis entitled **"Design, synthesis and application of fluorogenic probes for selective detection of ionic analytes in physiological condition"** have been divided into six chapters based on the results of experimental work performed during the research period.

Chapter 1: Introduction

This chapter provides a brief introduction on 'Design and application of sensor molecule' for ionic species. Cationic and anionic charged species are omnipresent and their importance in chemical, biological, medical, environmental, and industrial processes cannot be underestimated. Over the past several decades, a large number of acyclic and macrocyclic compounds have been synthesized for colorimetric detection of ionic species and recently designing of fluorescence responsive sensors for anions and cations is an emerging field of study. Our focus is to develop sensor molecules for optical as well as fluorescence detection of ionic analytes.

The design, synthesis and application of fluorescent and/or colorimetric molecular probes that selectively and specifically respond to the presence of a specific analyte (metal ions or anions) in a more or less complex matrix is a strong research area involving organic, inorganic, analytical and physical chemistry, all of them converging into the multidisciplinary field of supramolecular chemistry. According to this premise, it is possible to say that in the last decades, the chemistry of sensor materials has entered a phase of creation going further than pure research in chemistry.

In 1994 Czarnik gave the definition of a fluorescent chemosensor as an abiotic molecular device formed by three well defined components: a binding site, a fluorophore and a mechanism for communication between both. At that point, the classical design of fluorescence chemosensors or probes was born. Later the fluorophore-spacer-receptor model grows up with the strong contribution of De Silva and co-workers. In this way, a chemosensor device is conceived to avoid classical expensive and laborious analytical methodologies and to allow in situ and real time detections and quantification of analytes at the lowest cost possible. In a world of fast and unpredictable changes it is extremely necessary to develop new chemosensors; applications cover from process control, environmental monitoring, food control and food analysis, medical diagnosis and

treatment, and many other disciplines need more sophisticated and specific sensing systems for their development, including chemistry, biology, medicine, military security, new materials, nano-devices and environmental science. The list of attractive analytes to be detected is extensive, however, among all possible analytes, metal ions and anions occupy a central task in all aspects of human life and development.

According to the recent literature molecular probes with optical responses at longer wavelength region of the spectra are particularly gaining special interest. Radiation with longer wavelength can penetrate much deeper into the sample, since there is no or limited absorption and scattering. Additionally, there is no interference of autofluorescence generated from the chromophores and macromolecules present in the analytic samples. Thus, the work in this thesis focuses on the design and continuous modification of the fluorogenic ligands for obtaining the spectral response at a longer wavelength region of the spectra.

Chapter 2: Experimental methods and characterization

In this chapter, a detailed report of the various reagents used in the detail synthesis of the receptors, their synthetic procedures, crystallization details, binding study and specifications of analytical instruments employed in the characterization of synthesized compounds and their various complexes.

Chapter 3: A quinoline based fluorophoric probe for sensing of Fe^{3+} ions by switch ON green fluorescence and application of the metal-ligand complex as a selective sensor for F^- ions.

This chapter describes a newly synthesized quinoline functionalized fluorophoric Schiff base **L_1** and it's colorimetric and fluorescence responses toward various metal ions in mixed aqueous media. The ligand exhibited high selectivity towards Fe^{3+} in presence of large excess of other competing ions with certain observable optical and fluorescence changes. These spectral changes are significant enough in the visible region of the spectrum and thus enable naked eye detection. The efficiency of **L_1** in detecting Fe^{3+} ions was also checked in presence of relevant complex biomacromolecules viz. met-hemoglobin, fetal bovine serum and human serum albumin. **L_1** was also found to be enough sensitive for visual detection of Fe^{3+} ions in native iron pools of banana pith. Studies revealed that **L_1-Fe** complex formation is fully reversible in presence of fluoride anion with very high selectivity. Further, fluorescence microscopic studies demonstrated that compound **L_1** could also be used as an imaging probe for detection of uptake of these

ions in model human cells. This selective sensing behaviour of $\mathbf{L_1}$ towards Fe^{3+} was explained via CHEF process where theoretical calculations also supported the premise.

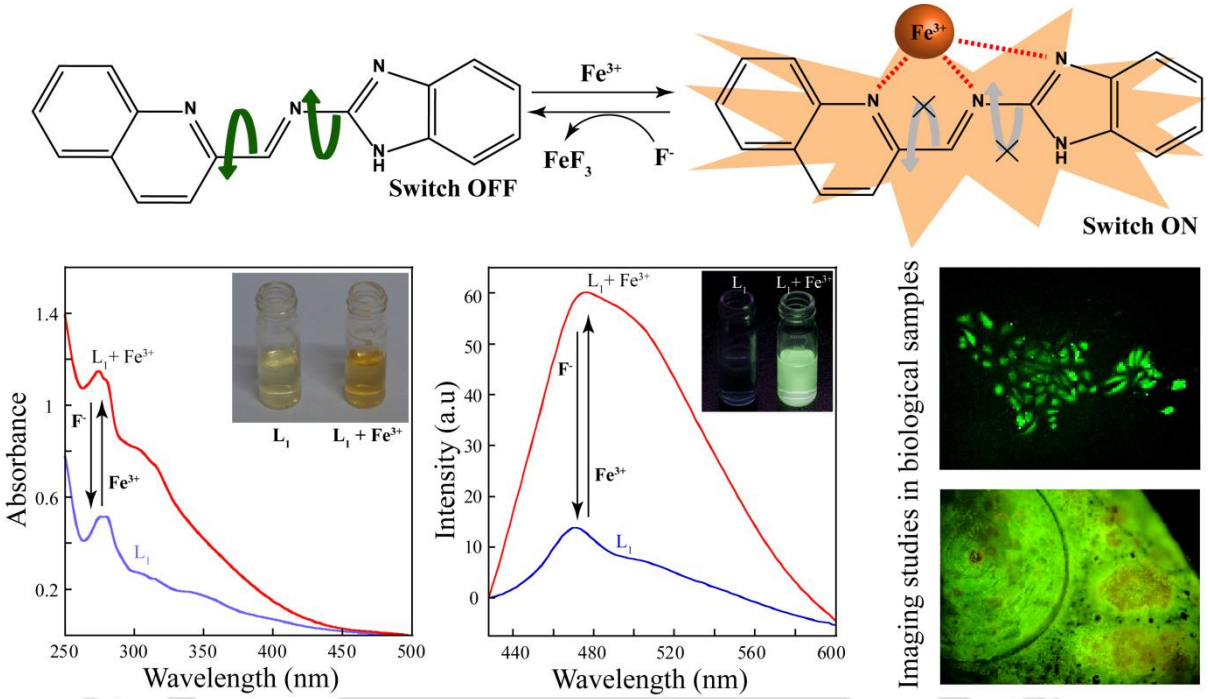

Scheme 1. A comprehensive representation of the research work included in this chapter

Chapter 4: A CHEF based ratiometric sensor for selective detection of Cu^{2+} ions by switch ON Yellow fluorescence.

This chapter describes a newly synthesized 1-amino-2-naphthol functionalized fluorophoric ligand $\mathbf{L_2}$, which specifically binds Cu^{2+} in presence of large excess of other competing ions with observable changes in their electronic and fluorescence spectral behavior. These spectral changes are significant enough in visible region of the spectrum and thus enable naked eye detection. As $\mathbf{L_2}$ displays Cu^{2+} ions dependent spectral changes at two different wavelengths of the emission spectra so it can be used as a ratiometric sensor for the analyte with minimal interference of environmental conditions and background disturbances. The coordination of Cu^{2+} with $\mathbf{L_2}$ force the molecule to attain a planar geometry with an increased opportunity of charge transfer throughout the π-system, leading to a highly conjugated geometry with sufficient enhancement of the fluorescence intensity, from which fluorogenic and ratiometric detection of Cu^{2+} ions are possible. Further, fluorescence microscopic studies confirmed that the reagent $\mathbf{L_2}$ could also be used as an imaging probe for detection and uptake of Cu^{2+} ions in HeLa cells.

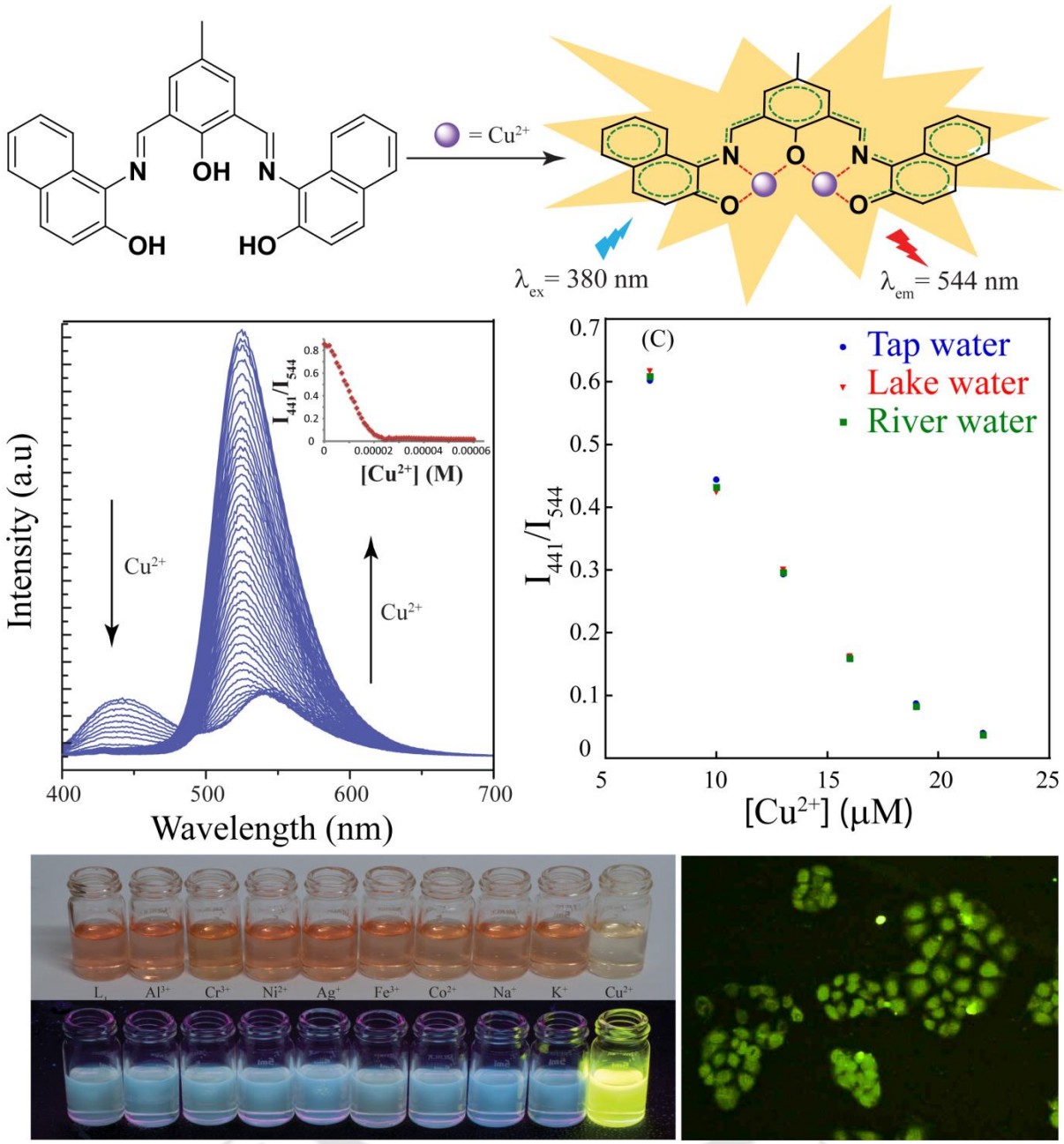

Scheme 2. A comprehensive representation of the research work included in this chapter

Chapter 5: A single Probe to sense Al^{3+} Colorimetrically and Cd^{2+} by Turn-ON orange Fluorescence

This chapter describes a pyridine-2-carbohydrazide functionalized conjugated fluorophoric Schiff base ligand **L_3** specifically sense Al^{3+} and Cd^{2+} ions through significant changes in their absorption and emission spectral behavior, respectively, in physiological condition. The spectral changes are in the visible region of the spectrum and thus facilitate naked eye detection. Apart from the visible changes, an in-field device application was demonstrated by sensing these ions in paper strips coated with **L_3**. The

crystal structure of the **L_3-Cd** complex provided a mechanistic insight of the metal coordination attribute of **L_3**. Interestingly, fluorescence microscopic studies demonstrated that the ligand **L_3** could also be used as an effective probe in imaging experiments for detection of intracellular Cd^{2+} ions in HeLa cells.

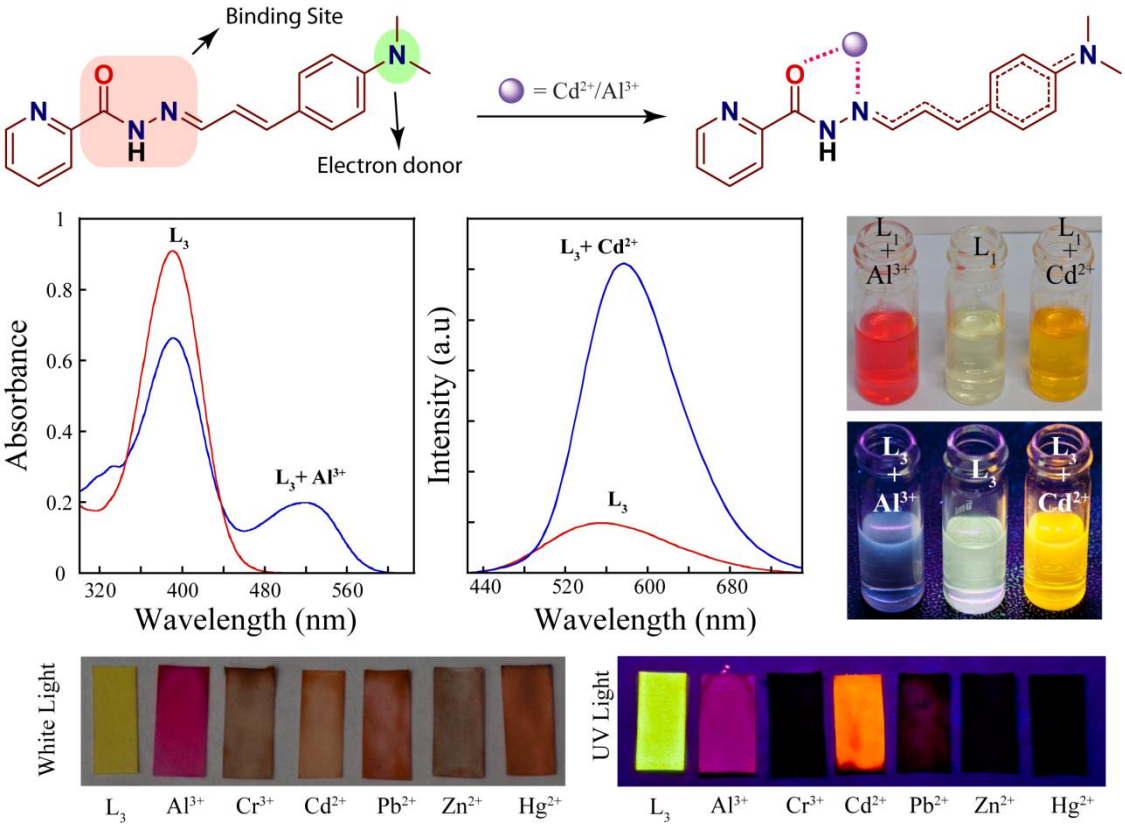

Scheme 3. A comprehensive representation of the research work included in this chapter

Chapter 6: A rhodamine based fluorophoric probe for sensing of Cu^{2+} ions by switch ON red fluorescence and application of the metal-ligand complex as a selective sensor for S^{2-} ions.

This chapter describes a newly synthesized indole functionalized rhodamine derivative **L_4**, which specifically bind to Cu^{2+} in presence of large excess of other competing ions with visually observable changes in their electronic and fluorescence spectral behavior. These spectral changes are significant enough in the NIR and visible region of the spectrum and thus enable naked eye detection. The receptor, **L_4** could be employed as a resonance energy transfer (RET) based sensor for detection of Cu^{2+} based on the process involving the donor indole and the acceptor Cu^{2+} bound xanthene fragment. Studies reveal that **L_4-Cu** complex is selectively and fully reversible in presence of sulfide anions. Further,

fluorescence microscopic studies confirmed that the reagent **L_4** could also be used as an imaging probe for detection of uptake of these ions in HeLa cells.

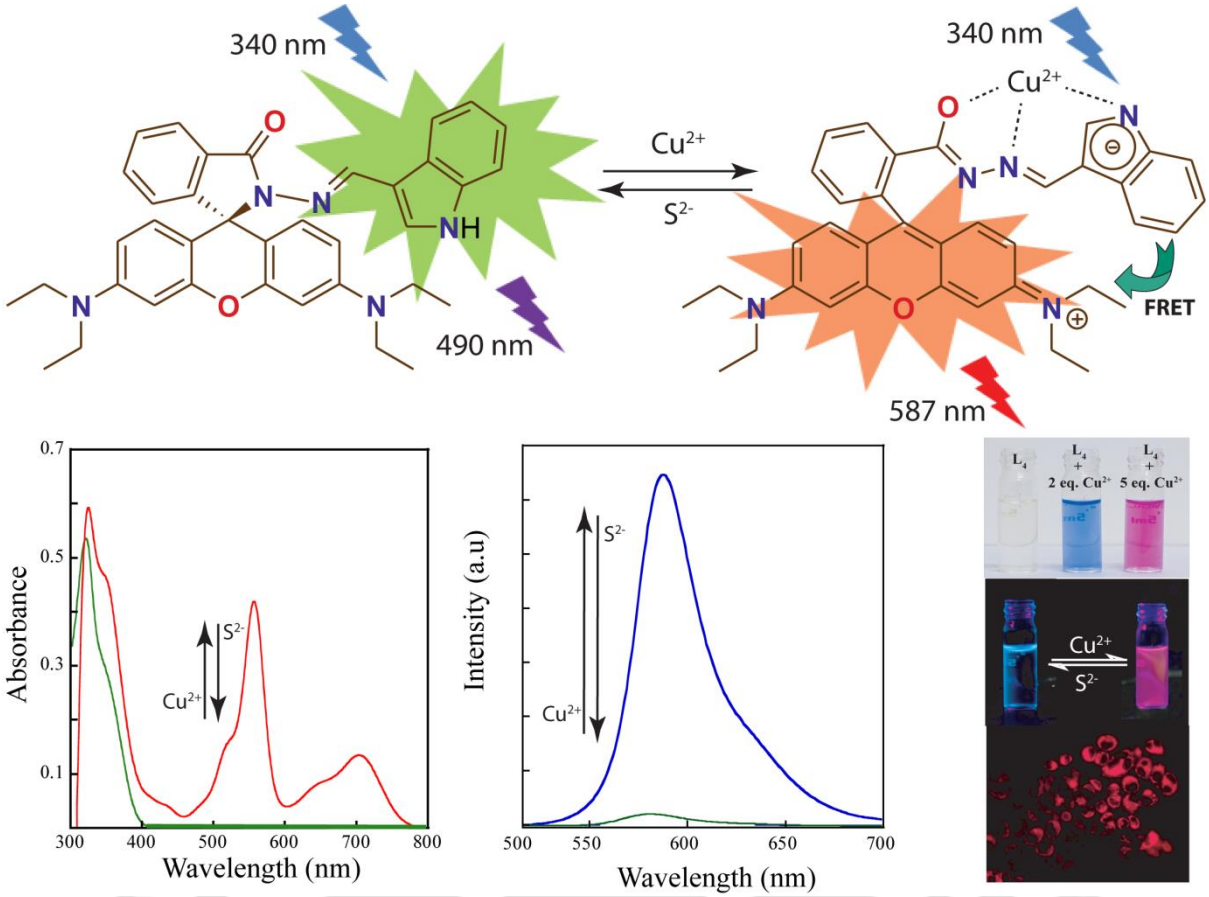

Scheme 4. A comprehensive representation of the research work included in this chapter

Conclusion and future perspective

To conclude, this thesis provides some significant results in the domain of 'supramolecular chemistry of cation and anion sensing' where the cation and anion binding capability of some newly synthesized fluorogenic receptors were explored in solution state and solid state as well. In general the present findings provide deep insight into the design and application of fluorogenic receptor for selective sensing of ionic guests in environmental as well as biological samples. Each fluorogenic receptor molecule has shown an interesting property in presence of a specific ionic guest.

The receptor **L_1** has been shown to selectively detect Fe^{3+} ion *via* formation of chelation induced fluorescence emission mechanism and subsequently formed **L_1-Fe** complex undergoes dissociation selectively in presence of F^- ions. Thus **L_1** can be used for selective detection of Fe^{3+} and F^- in aqueous medium as well as biological milieu by switch ON/OFF green fluorescence. Whereas, receptor **L_2** with Cu^{2+} induced planar geometry

shows a switch ON response at the yellow region of the emission spectra. In case of **L_3** we have introduced an electron donor site and a binding site separated by a conjugated system, the binding of metal ions to **L_3** increase the possibility of charge transfer through the system and the fluorescence response is obtained at further longer region of the spectra. To further shift the optical as well as fluorescence response to far more longer region in chapter 6 we have chosen a well-known fluorophoric moiety, Rhodamine B and further modified it by introducing an indole moiety. The rhodamine based fluorophoric probe **L_4** has been shown to efficiently sense Cu^{2+} ions in the NIR region of the optical spectra and also exhibit switch ON red fluorescence. The **L_4-Cu** complex undergoes dissociation selectively in presence of S^{2-} ions with complete regeneration of the spectral properties. Overall, these results give a clear idea about some of the important factors for designing chemosensors, such as the type of donor-atoms, size and flexibility that determines the selectivity, efficiency and the wavelength region of the spectral response.

Fluorescence and colorimetric chemo-sensorial chemistry has grown considerably since the pioneering work of Sousa with the naphthalene compounds. After the Nobel Prize in supramolecular chemistry in 1987 to Charles J. Pedersen, Jean-Marie Lehn and Donald J. Cram, the design and application of fluorescent molecular devices increased exponentially. The possibility of a precise molecular recognition between a chemosensor and their guests has many applications in analytical chemistry, supramolecular science, biochemistry, physical chemistry, medicinal chemistry, toxicology, forensic sciences and applicable disciplines even to the modern nanosciences. However, for these applications to reach their prospective basic work is in tuning the receptor molecule in such a way that it is easily soluble in aqueous media and the spectral response is vivid and at longer end of the spectra. Although the results included in this thesis are extremely useful from a fundamental viewpoint, there is other challenging aspects in supramolecular chemistry that need to be developed, basically from an applicative approach. Research in these areas with a focus on technological and biomedical applications, based upon the remarkable cation, anion and neutral molecular sensing appear to be forthcoming.

Contents

Chapter 1

Introduction:

Chemistry of Fluorogenic Sensing

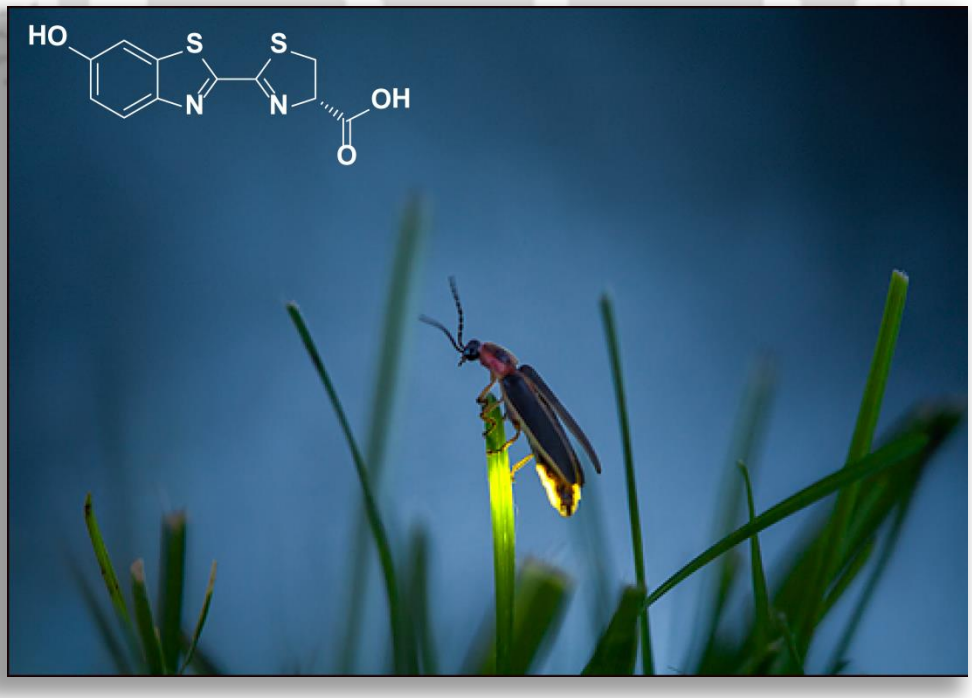

Chapter 1

1.1. Fluorogenic sensors: An Introduction

In the middle of the 19th century G. Stokes reported that the fluorescence emission spectrum appears at a longer wavelength than the excitation spectra,[1.1] which is known as ‘‘Stokes shift’’ and this physical observation initiated the conceptual basis for the fluorimetric analysis. The first publication that reports the uses of luminescence as an analytical tool was by Harvey in 1923. Harvey reported the minimum of concentration required of the molecule luciferin,[1.1] a light-emitting biological dye found in some organisms capable of bioluminescence, to detect visible light.[1.2] Later, Sousa and Larson discussed the use of some functionalized naphthalene crown-ether ligands to describe the concept of a fluorescence chemosensor, [1.2] for alkaline metal ion detection.[1.3] The design, synthesis and application of fluorescent and/or colorimetric receptor molecules that display selective response in presence of a specific analyte (metal ions or anions) in a more or less complex matrix is a vast and strong research area involving organic, inorganic, analytical and physical chemistry, all of them converging into the multidisciplinary field of supramolecular chemistry. According to this premise, we can say that in the last decades, the chemistry of sensor materials has entered a phase of creation going further than pure research in chemistry.

According to Czarnik a fluorescent chemosensor is an abiotic molecular device formed by three well defined constituents: a binding site, a fluorophore and a mechanism for communication between both.[1.4] At that point, the classical design of fluorescence chemosensors or probes was born. This model of fluorophore-spacer-receptor further grows up with the contribution of De Silva and co-workers.[1.5] In this manner, a chemosensor device is considered to avoid classical costly and difficult analytical methodologies and to allow in situ and real time detections and quantification of analytes at the lowest cost possible. In this unpredictably fast changing world it is extremely necessary to develop new chemosensors; applications cover from process control, food control, food analysis and environmental monitoring, medical diagnosis and treatment, and many other disciplines need more sophisticated and specific sensing systems for their

development, including chemistry, biology, medicine, military security, new materials, nano-devices and environmental science.[1.6–1.11] The list of attractive analytes to be sensed is wide-ranging, however, among all possible analytes, metal ions and anions occupy a central place in all vital physiological process of human life and development.

Recently chemists have adopted a practical approach for the design of new and well-organized chemical sensors which takes accurate advantage of the principles of supramolecular chemistry.[1.12,1.13] The ‘‘bottom-up’’ approach starts the design of a more efficient device usually referred as molecular probes or chemosensors, which are much more efficient device from the molecular level than classical macroscopic devices and chemical sensors.[1.14,1.15] A step forward involves the integration of chemosensors into a really macroscopic sensory device without any loss of important properties such as sensitivity and selectivity. In this way new application strategies based on sol–gel materials, polymers, glass and gold surfaces, micelle aggregates, silica nanoparticles, quantum dots or magnetic nanoparticles have been developed for new chemosensing materials.[1.16–1.18] Many factors make fluorescence one of the most effective mechanisms to report chemical recognition events, but the most significant one is due to the analytical implications, that fluorescence spectroscopy does not need any reference and it consume no analytes. All these aims can be easily modified by changing three basic constituents the receptor unit, the signalling unit and the spacer units.

ICT (internal charge transfer), PET (photoinduced electron transfer), EET (electronic energy transfer) and monomer-excimer formation (MEF) are the most extensively studied processes which are used for sensing purposes.[1.19] Numerous works have been published recently concerning fluorescence or colorimetric sensors for metal cations and anions where the above mentioned photo-physical mechanisms are very well discussed.[1.19–1.27] Alternatively, colorimetric molecular devices have attracted much scientific attention due to the so called ‘‘naked-eye’’ detection, which reduces the use of expensive and complicated equipment to metal-ion measurements. A close examination reveals that the analyte detection by the probes is usually attained through one of the following reaction mechanisms: (1) protonation-deprotonation; (2) complexation (including direct complexation and competitive displacement complexation); (3) cleavage and formation of covalent bonds; and (4) redox reaction. The work involved in this thesis mainly discusses design and application of sensor molecule which shows selective response through

Complexation mechanism (including direct complexation and competitive displacement complexation).

1.2. Complexation- based chromogenic and fluorogenic probes

Designing a complexation-based chromogenic and fluorogenic probes involves two different stratagies: one is direct complexation, and the other is competitive displacement complexation. In the strategy of direct complexation, the receptor unit and the signaling unit are covalently linked, and the resulting probes can directly complex with analyte via the following ways: coordination, electrostatic interaction, or hydrogen bonding. This strategy is a major one in the development of complexation based chromogenic and fluorogenic probes, and the probes based on such a mechanism usually have the advantage of rapid spectroscopic response and good reversibility, which are significant for monitoring the dynamic change in the analyte concentration.

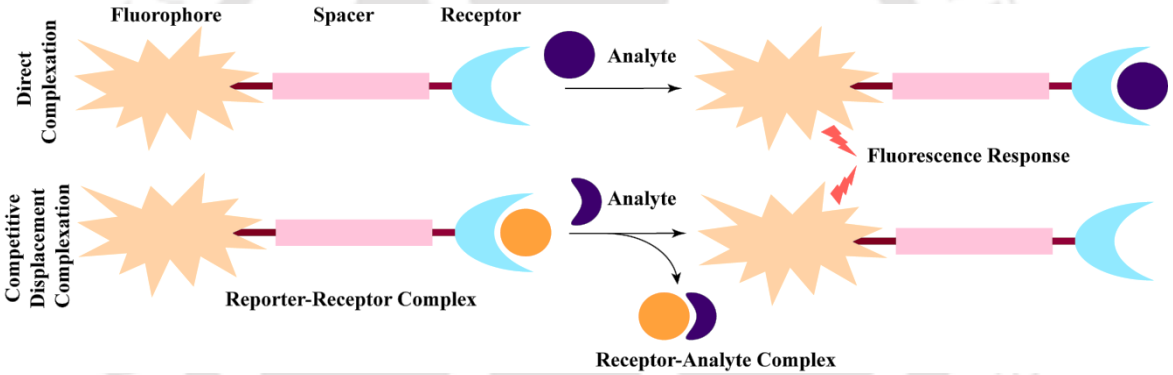

Scheme 1.1 Types of complexation- based chromogenic and fluorogenic probes.

In the strategy of competitive displacement complexation, however, the receptor and the signalling unit (reporter) are not covalently linked; instead, they form a complex (molecular ensemble), which serves as a probe.[1.28,1.29] Upon addition of analyte into the solution of the receptor-reporter ensemble, the stronger complexation of analyte with the receptor leads to the release of the reporter, thereby causing the change of spectroscopic signal of the system. It is noteworthy that complexation-based probes are usually affected by pH influence because different protonation states of the electronegative atoms in the ligands have different coordinating ability. This is why a pH buffer is often required in the detection system. Moreover, many metal ions have similar reactivity and may interfere with each other (e.g., Mg^{2+} vs Ca^{2+}, Ag^{+} vs Hg^{2+}, and Cd^{2+} vs Zn^{2+}) which makes the designing of complexation based probes for these metal ions more challenging. Obviously, the key issue for designing complexation-based chromogenic and fluorogenic probes is

how to construct a specific receptor for analyte. Toward this end, different novel receptors and thereby the corresponding probes for analytes have been developed by combining various photophysical processes and modern coordination reactions, which will be discussed in detail below.

1.2.1. Direct Complexation

Direct complexation strategy is generally used for developing chromogenic and fluorogenic probes for metal ions (Ca^{2+}, Zn^{2+}, Cu^{2+}, Hg^{2+}, etc.) by virtue of their strong coordinating abilities with electronegative heteroatoms (N, O, S, etc.).[1.30] Common tactics for achieving this goal are based on: (1) matchable ring/cavity size for a given ion, such as crown ethers with different ring sizes for alkali and alkaline earth metal ions; (2) suitable ligands for convenient formation of five- and six-membered ring complexes with metal ions, like the probes with EGTA (ethylene glycol tetraacetic acid) moiety for Ca^{2+}; and (3) soft-hard acid-base principle, such as the soft sulfur-containing receptors with high affinity for soft metal ions (e.g., Ag^{+} and Hg^{2+}).

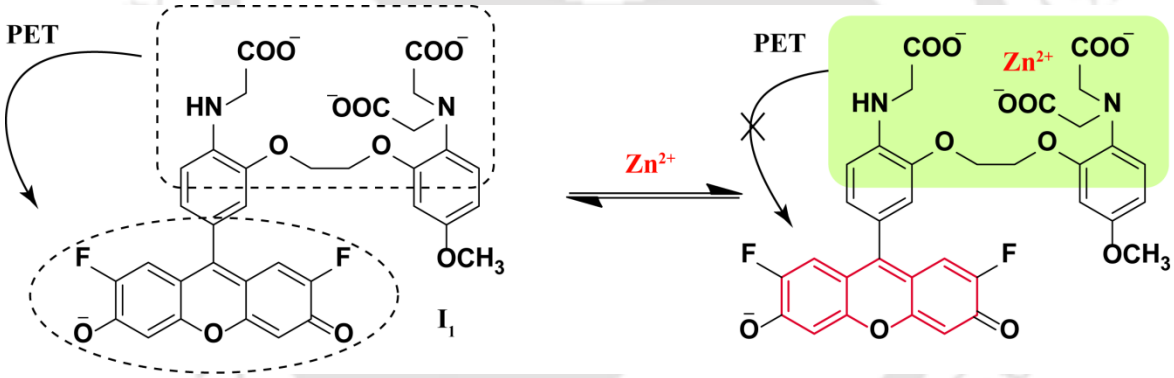

Figure 1.1 Response mechanism of a PET probe (**I_1**) to Zn^{2+}.

However, in the design of such probes, a photophysical process like photoinduced electron transfer (PET), internal charge transfer (ICT), or fluorescence resonance energy transfer (FRET) should be included to translate analyte binding into a spectroscopic signal change. In PET probes, a fluorochrome is usually connected via a spacer to a receptor, and the receptor containing electronegative atoms (e.g., nitrogen atom) has a relatively high energy nonbonding electron pair, which can transfer an electron to the excited fluorochrome, leading to the quenching of fluorescence. However, upon coordination to a metal cation, the reduction potential of the receptor is increased so that the corresponding highest occupied molecular orbital (HOMO) becomes lower in energy than that of the fluorochrome; consequently, the PET process from the receptor to the fluorochrome is

prohibited, and fluorescence intensity is enhanced.[1.31,1.32] The PET mechanism is repeatedly used in designing chromogenic and fluorogenic probes for metal ions. Figure 1.1 shows a typical example of PET based probes, FluoZin-3 (**I_1**),[1.33] which shows weak fluorescence intensiy due to the PET process from the receptor to the fluorochrome. However, the weak fluorescence can be sharply enhanced by inhibiting the PET process via complexation with Zn^{2+} of the tailor-made metal binding moiety containing N,N,N′-triacetic acid. As the process is also pertinent inside biological milieu, the probe has also been used in the selective imaging of Zn^{2+} in living cells.[1.33,1.34]

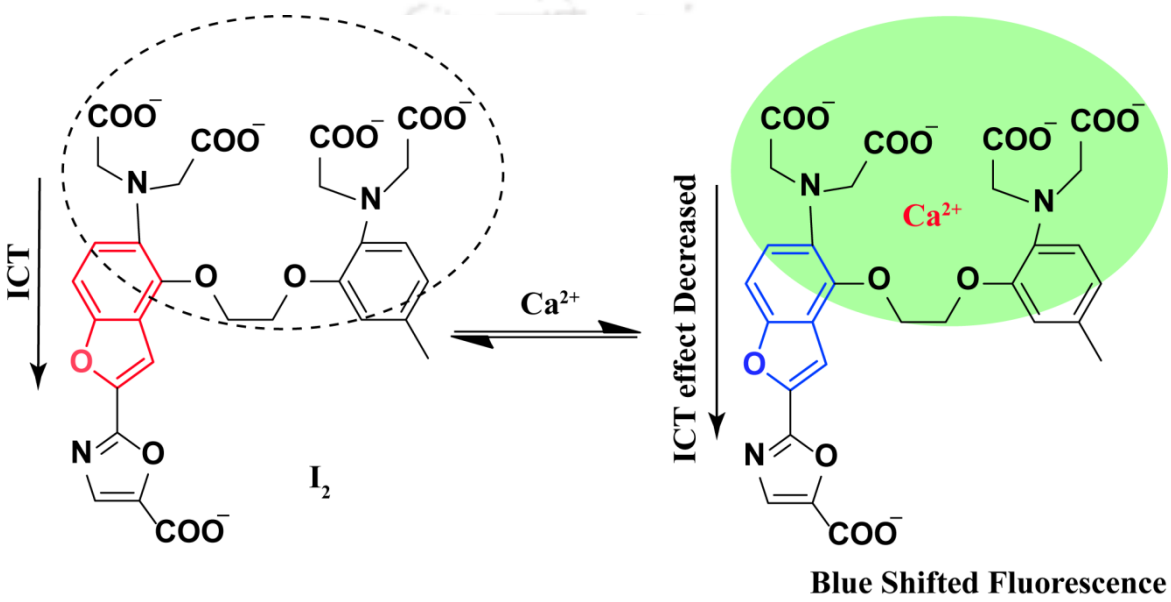

Figure 1.2 Response mechanism of an ICT probe (**I_2**) to Ca^{2+}.

In ICT probes, an electron-donating group in the receptor and the fluorochrome is bridged by a conjugated system; therefore, the nonbonding electron pair of the electrondonating group (metal binding sites) participates in the conjugation of the fluorochrome, which essentially differs from PET-based probes. In this case, the ICT process from the electron donor to the fluorochrome may occur upon excitation by light.[1.35,1.36] However, metal complexation with the receptor not only changes the energy gap between LUMO (lowest unoccupied molecular orbital) and HOMO but also the efficiency of ICT, causing changes in absorbance and fluorescence intensity with observable spectral shifts, which makes ratiometric measurements possible. Figure 1.2 represents a typical example of ICT probes, Fura 2 (**I_2**),[1.37,1.38] which binds with Ca^{2+} with a remarkable blue-shifted fluorescence. This enables intracellular determination of Ca^{2+} in a ratiometric mode, which effectively overcomes the influence of several variants like concentration and optical path length.

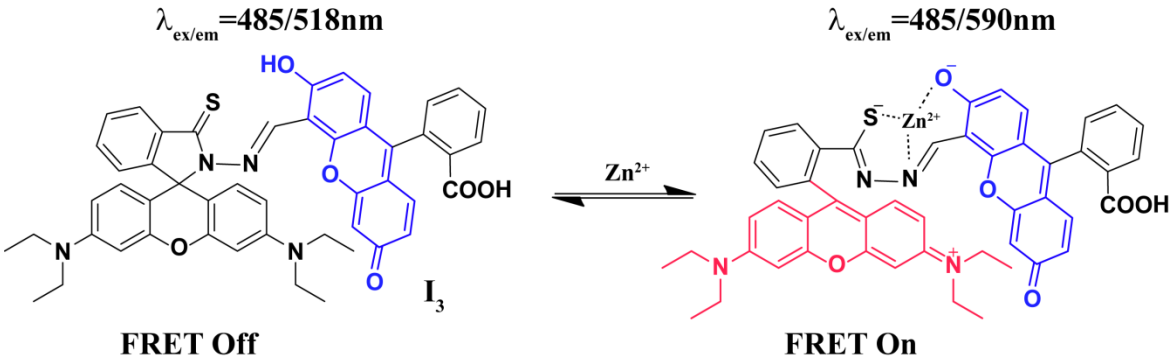

Figure 1.3 Response mechanism of a FRET probe (**I_3**) to Zn^{2+}.

FRET usually arises from interaction between a pair of different fluorophores, in which one acts as a fluorescence acceptor and the other as a donor. In the FRET process, the excited donor molecule passes its energy to the nearby acceptor at the ground state, and then the excited acceptor relaxes back to its ground state by emitting fluorescence. In some cases, the acceptor can be a quencher. FRET mainly depends on three factors: the distance between the donor and the acceptor, the extent of spectral overlap between the donor emission and acceptor absorption spectrum, and the relative orientation of the donor emission dipole moment and acceptor absorption moment.[1.39] Because of its distance-dependent efficiency, FRET has been widely used in the measurement of the distances between the two interacting fluorophores in macromolecules, especially biomacromolecules. On the other hand, when the acceptor is a fluorescent dye, FRET causes the relative change of fluorescence at two wavelengths, and this behavior can serve as an effective measure to design small molecular ratiometric probes by integrating the fluorescence donor and acceptor into one molecule. Figure 1.3 shows such a ratiometric probe,[1.40] in which fluorescein and rhodamine function as fluorescence donor and acceptor, respectively, because the fluorescence spectrum of fluorescein matches well with the absorption spectrum of rhodamine.[1.41] In the absence of Zn^{2+}, the rodamine moiety in **I_3** exists in a spirolactam form that has almost no absorption in the visible region, and thus cannot act as an acceptor; when excited at 485 nm, probe **I_3** shows only green emission at 518 nm characteristic of fluorescein. However, upon addition of Zn^{2+}, complexation of **I_3** with Zn^{2+} triggers the opening of spirolactam ring and the generation of an absorption peak at 560 nm, which leads to the occurrence of FRET and thus the change of fluorescence intensity ratio at 590/518 nm. It is noteworthy that the spiro-ring-opening of rhodamine has also been proved to be an efficient way for developing various spectroscopic off-on probes for metal ions.[1.42]

1.2.2. Competitive Displacement Complexation

In the strategy of competitive displacement complexation, a receptor-reporter ensemble is used as a probe, and the receptor selectively binds an analyte more strongly than the reporter, subsequent release of the reporter irreversibly changes the spectroscopic signal.[1.28,1.43,1.44] This strategy is similar to the classical complexiметric titration in analytical chemistry, where EDTA is often used as a titrant.[1.45,1.46] For example, the dye Eriochrome Black T binds Mg^{2+} forming a red complex at pH 10, and at the end point EDTA can extract Mg^{2+} from the complex, releasing blue coloured Eriochrome Black T.[1.47] Various chemosensing ensemble for detecting specific analytes are developed based on competitive displacement complexation strategy.[1.28,1.44] Anslyn et al. proposed the first colorimetric probe for detecting citrate in aqueous medium.[1.48] As shown in Figure 1.4 the probe was designed by assembling the receptor containing three guanidinium groups (**I_4**) and reporter (5-carboxyfluorescein). Binding between the receptor and reporter lowers the pKa of the phenol moiety of the reporter, causing its deprotonation. Upon reaction of the probe with citrate, the reporter is released as a phenol-protonated species via competitive displacement complexation, and a decrease in the reporter's fluorescence is observed, which allows the quantitative detection of citrate. The probe is selective for citrate over simple dicarboxylic and monocarboxylic acids in water and has been used to determine citrate concentration in commercial beverages.

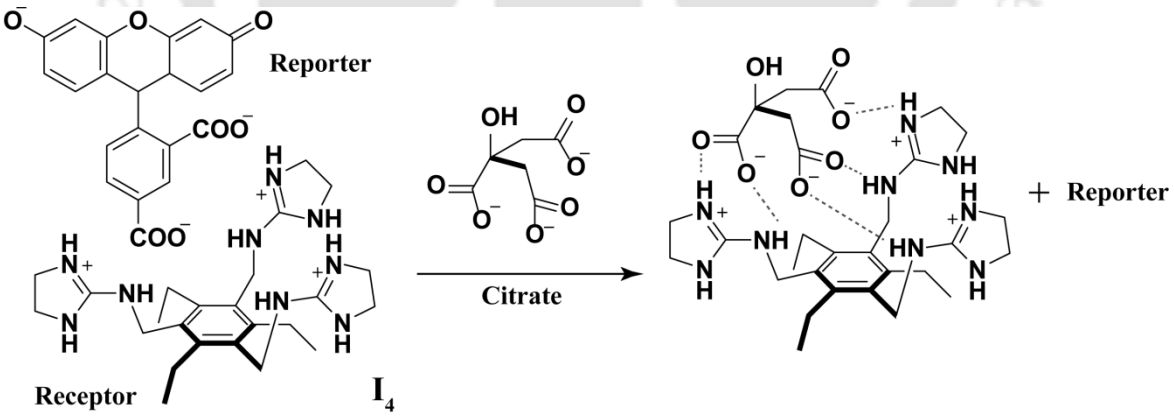

Figure 1.4 The chemosensing ensemble for the detection of citrate.

Later, other chemosensing ensembles for detecting various inorganic or organic substances, such as tartrate,[1.49] phosphate,[1.50] amino acids,[1.51,1.52] and carboxylates[1.53] has also been reported by them. Fabbrizzi and his co-workers has demonstrated the strategy of competitive displacement complexation by the application of metal complexes in the field

of chemosensing ensembles.[1.54] They utilized the Cu^{2+} complex **I_5** as the receptor and fluorescein derivatives as reporters to prepare chemosensing ensembles for PPi assays in neutral aqueous solution. The formation of the ensembles (K_a = 1.0 × 107 M^{-1}) completely quenched the fluorescence of fluorescein derivatives. However, reaction of the ensembles with PPi (K_a = 1.0 × 108 M^{-1}) restored the fluorescence, and no interference was observed from other anions including phosphate. Similar strategies have been employed by the same group for developing other chemosensing ensembles for amino acids,[1.55] dicarboxylates,[1.56] and guanosine monophosphate.[1.57]

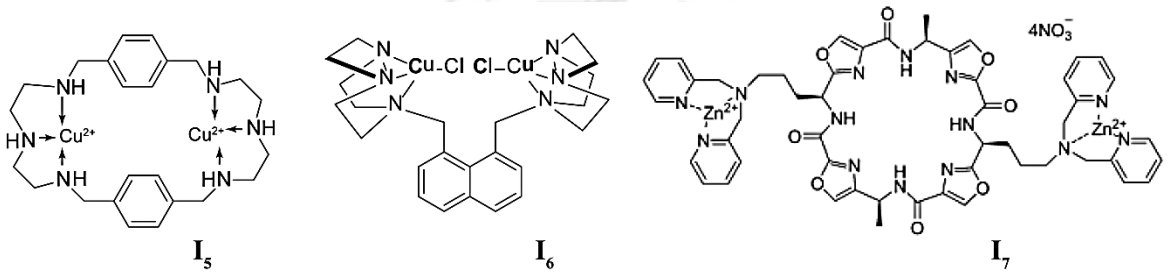

I_5 **I_6** **I_7**

Figure 1.5 Structures of compound **I_5**, **I_6** and **I_7**.

Another dinuclear Cu^{2+} compound **I_6** can complex with eosine Y yielding an ensemble (K_a = 5.6 × 104 M^{-1}), which has been used for the sensitive and selective fluorescence detection of oxalate (Ka = 1.3 × 105 M^{-1}) in neutral aqueous solution.[1.58] In some of the other example Zn^{2+}-DPA units have been used to build the corresponding ensembles for PPi assay.[1.59,1.60,1.61,1.62] *e.g.* introduction of two Zn^{2+}-DPA units into a cyclic peptide produces **I_7**,[1.63] and **I_7** complexes with 6,7-dihydroxy-4- (sulfomethyl)-coumarin forming an ensemble (Ka = 1 × 105 M^{-1}), which shows selective response in presence of PPi (K_a = 1 × 108 M^{-1}) in water.

There are also some examples where the spectroscopic responses in are based on anion-induced demetalation. A Cu^{2+} complex, Compound **I_8**, was designed for selective detection of sulfide anions.[1.64] In this case the fluorescence intensity of the tricarbocyanine skeleton is almost completely quenched by Cu^{2+}, and sulfide can bind with Cu^{2+} to form stable CuS precipitate (solubility product constant, K_{SP} = 1.27 × 10^{-36}), releasing the tricarbocyanine. Consequently, **I_8** showed a significant increase in fluorescence emission in the presence of sulfide in aqueous media. Compound **I_9** was reported as a fluorescent sensor for H_2S.[1.65] The binding of H_2S to Cu^{2+} in **I_9**, releases the fluorescein moiety resulting in fluorescence enhancement. High concentrations of reduced glutathione (GSH) do not interfere with the detection of H_2S, and the probe was also

applied for fluorescence imaging of H_2S in live cells. **I_{10}** is a water-soluble fluorescent probe, which can form a 2:1 ligand-metal complex with Cu^{2+} in HEPES buffer solution (pH 7.4)[1.66] and has been used for the sensitive and selective fluorescence detection of sulfide anion based on the same anion-induced demetalation. There are also many other similar examples where Cu^{2+} complexes have been employed for developing fluorescent probes for sulfide.[1.67-1.69]

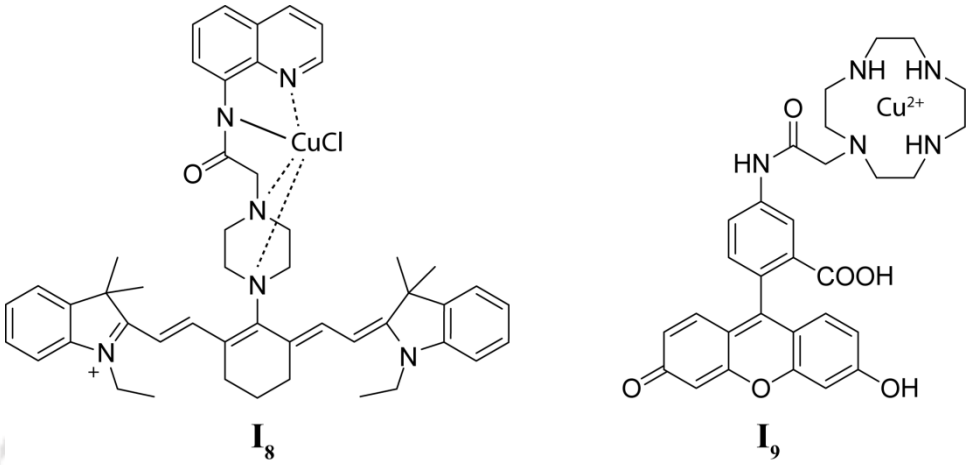

I_8 **I_9**

Figure 1.6 Structures of compound **I_8** and **I_9**.

The high affinity of CN^- for Cu^{2+} has been used to design chromogenic and fluorogenic probes for CN^- detection.[1.70-1.72] The metal-ligand complex formed between Cu^{2+} and **I_{11}** can further react with CN^- causing the removal of Cu^{2+} from the **I_{11}**-Cu^{2+} complex with a response in the NIR region of the fluorescence spectra.[1.71] This system has been also applied to detect CN^- produced by P. aeruginosa in C. elegans.

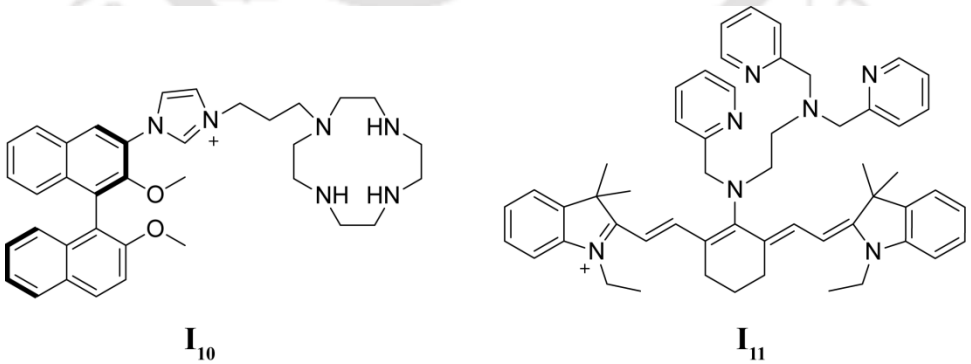

I_{10} **I_{11}**

Figure 1.7 Structures of compound **I_{10}** and **I_{11}**.

Similarly, other metal complexes have been used as chemosensing ensembles on the basis of the anion-induced demetalation, for the detection of cysteine (Cys),[1.73,1.74] I^-,[1.75,1.76] F^-,[1.77] PPi,[1.78-1.80] and amino acids.[1.81] The displacement of simple ligands (e.g., H_2O and Cl^-) in some of the metal complexes by an analyte could also produce spectral change.[1.82,1.83] Wolfbeis and co-workers reported the development of such a system based on a europium complex,[1.84] in which H_2O can be replaced by H_2O_2 to form a strongly luminescent complex without the occurrence of a redox reaction. This system can be applied for the detection of H_2O_2 produced in oxidase-catalyzed reactions. Similarly, **I_{12}** can serve as a colorimetric probe for CN^- via the substitution of H_2O.[1.85] Lippard et al. reported several NO probes, which are designed on the basis of iron cyclam,[1.86] ruthenium porphyrin,[1.87] and dirhodium tetracarboxylate complexes.[1.88] In these probes, the fluorescence of a fluorochrome is quenched by a paramagnetic transition metal ion, and reaction of the probes with NO forms a metal-NO adduct, causing the fluorochrome release and thus fluorescence enhancement (e.g., I_{13}[413] in Figure 1.9). However, these NO probes are not ideal for in vivo applications because of their low stability or poor water solubility.[1.89,1.90]

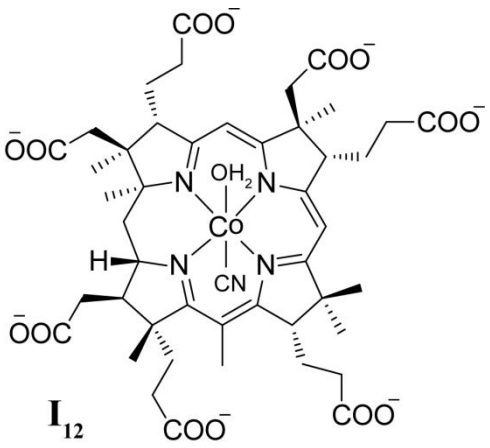

Figure 1.8 Structure of compound **I_{12}**

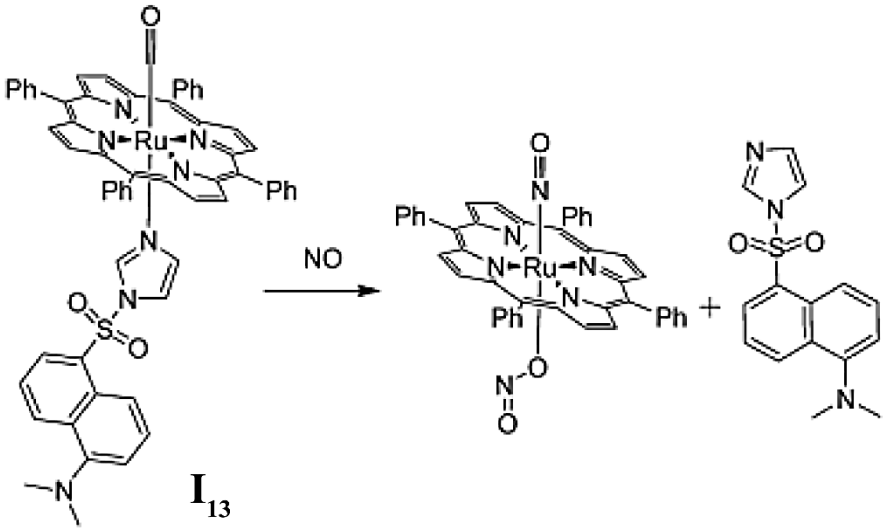

Figure 1.9 Reaction of **I_{13}** with NO.

On the basis of competitive displacement complexations, Anslyn et al. developed an array assay for small peptides and their phosphorylated analogues.[1.91] In this approach, five different receptors containing two tripeptide arms, three metal cations (Ni^{2+}, Co^{2+}, and Cu^{2+}), and three indicators (pyrocatechol violet, celestine blue, and gallocyanine) were used to create an array of 45 metal/receptor/indicator combinations that was used for pattern recognition of Pro-Ser-Glu, Ser-Glu-Glu, Pro-pSer-Glu, and pSer-Glu-Glu tripeptides.

1.3. Concluding Remarks and objective of thesis

From the above mentioned examples, it can be seen that in the last decade most of the chromogenic and fluorogenic probes were designed by using the fluorophores such as anthracene, benzofurazan, BODIPY, coumarin, cyanine, naphthalene, quinoline, squaraine, and xanthene, and a lot of them exhibit fluorescence off-on or ratiometric (wavelength shifts) responses to an analyte via the photophysical processes like PET, ICT, or FRET. Fluorescence off-on probes, as compared to on-off or ratiometric probes, have the advantage of the ease detection of low-concentration contrast relative to a "dark" background, which is rather suited for qualitative analysis due to the high sensitivity; whereas ratiometric probes, despite the disadvantage of time-consuming ratio calculation/measurement, can eliminate the influence of several variants (e.g., probe concentration, instrumental efficiency, and environmental conditions) by built-in correction of two emission bands, which is rather suited for accurate quantitative analysis. There is no doubt that the combination of the above reactions with a rationally functionalized fluorochrome will serve as effective strategies to design new chromogenic and fluorogenic probes. Moreover, the new probes with the following performances are desired. First, for practical applications of the probes in biochemical studies (especially for cell imaging studies), they should be soluble in purely aqueous or mixed aqueous-organic solvents because the usage of pure organic solvents usually destroys the normal function of biomolecules. Second, more probes with spectral response at longer wavelength region especially NIR region should be developed. Light in the longer wavelength region like far red or NIR region (650-900 nm) possesses the advantages such as good tissue penetration, low autofluorescence, and biological damage, and is thus favorable for in vivo imaging. Unfortunately, most of the existing NIR probes are derived from cyanine dyes, which suffer from poor stability. Therefore, chromogenic and fluorogenic probes with high

stability and good water solubility as well as spectral response in the far red or near Infra-red are still expected.

The focus of the thesis-work is 1) to design and synthesize simple, stable and water soluble (or soluble in mixed aqueous solvent) fluorogenic receptor molecules or chemosensor molecules for fluorescence as well as optical detection of ionic analytes, 2) application of the developed chemosensors in environmental or biological samples and 3) gradual development of the design of the sensor molecules to obtain spectral response in the longer wavelength region of the spectra.

References

[1.1] G. G. Stokes, *Philos. Trans. R. Soc. London*, 1852, **142**, 463.

[1.2] E. N. Harvey, *Science*, 1923, **57**, 501.

[1.3] L. R. Sousa and J. M. Larson, *J. Am. Chem. Soc.*, 1977, **99**, 307.

[1.4] A. W. Czarnik, *Acc. Chem. Res.*, 1994, **27**, 302.

[1.5] A. P. De Silva, H. Q. N. Gunaratne, T. Gunnlaugsson, A. J. M. Huxley, C. McCoy, J. T. Rademacher and T. E. Rice, *Chem. Rev.*, 1997, **97**, 1515.

[1.6] M. E. Germain and M. J. Knapp, *Chem. Soc. Rev.*, 2009, **38**, 2543.

[1.7] C. Bazzicalupi, A. Bencini, S. Biagini, A. Bianchi, E. Faggi, C. Giorgi, M. Marchetta, F. Totti and B. Valtancoli, *Chem.–Eur. J.*, 2009, **15**, 8049.

[1.8] L. Prodi, F. Bolleta, M. Montalti and N. Zaccheroni, *Coord. Chem. Rev.*, 2000, **205**, 59.

[1.9] F. Pina, M. A. Bernardo and E. Garcia-Espana, *Eur. J. Inorg. Chem.*, 2000, 2143.

[1.10] V. Amendola, L. Fabbrizzi, F. Foti, M. Licchelli, C. Mangano, P. Pallavicini, A. Poggi, D. Sacchi and A. Taglietti, *Coord. Chem. Rev.*, 2006, **250**, 273.

[1.11] G. Astray, C. Gonzalez-Barreiro, J. C. Mejuto, R. Rial-Otero and J. Simal-Ga´ ndara, *Food Hydrocolloids*, 2009, **23**, 1631.

[1.12] T. W. Bell and N. M. Hext, *Chem. Soc. Rev.*, 2004, **33**, 589.

[1.13] L. Basabe-Desmonts, D. N. Reinhoudt and M. Crego-Calama, *Chem. Soc. Rev.*, 2007, **36**, 993.

[1.14] V. Balzani, A. Credi and M. Venturi, Molecular Devices and Machines: Concepts and Perspectives for the Nanoworld, Wiley-VCH, Weinheim, DE, 2nd edn, 2008.

[1.15] V. Balzani, A. Credi and M. Venturi, *Chem. Soc. Rev.*, 2009, **38**, 1542.

[1.16] *Chem. Rev.* 2000; 100 (7), special issue on Chemosensors.

[1.17] Comprehensive Supramolecular Chemistry, ed. J. M. Lehn, J. L. Atwood, J. E. D. Davies, D. D. MacNicol, F. Vogtle and D. N. Reinhoudt, Pergamon, Oxford, UK, 1996, vol. 10.

[1.18] F. Mancin, E. Rampazzo, P. Tecilla and U. Tonellato, *Chem.–Eur. J.*, 2006, **12**, 1844.

[1.19] J. F. Callan, A. P. De Silva and D. C. Magri, *Tetrahedron*, 2005, **61**, 8551.

[1.20] H. N. Kim, M. H. Lee, H. J. Kim, J. S. Kim and J. Yoon, *Chem. Soc. Rev.*, 2008, **37**, 1465.

[1.21] C. Lodeiro and F. Pina, *Coord. Chem. Rev.*, 2009, **253**, 1353.

[1.22] G. Accorsi, A. Listorti, K. Yoosaf and N. Armaroli, *Chem. Soc. Rev.*, 2009, **38**, 1690.

[1.23] R. Martinez-Manez and F. Sancenon, *Chem. Rev.*, 2003, **103**, 4419.

[1.24] T. Gunnlaugsson, H. D. Paduka, M. Glynn, P. E. Kruger, G. M. Hussey, F. M. Pfeffer, C. M. Dos Santos and J. Tierney, J. *Fluoresc.*, 2005, **15**, 287.

[1.25] E. J. O'Neil and B. D. Smith, *Coord. Chem. Rev.*, 2006, **250**, 3068.

[1.26] V. Amendola and L. Fabbrizzi, *Chem. Commun.*, 2009, 513.

[1.27] L. Prodi, *New J. Chem.*, 2005, **29**, 20.

[1.28] S. L. Wiskur, H. Ait-Haddou, J. J. Lavigne and E. V. Anslyn, *Acc. Chem. Res.* 2001, **34**, 963.

[1.29] R. Martinez-Manez and F. Sancenon, *Chem. Rev.* 2003, **103**, 4419.

[1.30] J. F. Callan, A. P. de Silva and D. C. Magri, *Tetrahedron* 2005, **61**, 8551.

[1.31] E. M. Nolan and S. J. Lippard, *Acc. Chem. Res.* 2009, **42**, 193.

[1.32] A. E. Majzoub, C. Cadiou, I. Dechamps-Olivier, B. Tinant and F. Chuburu, *Inorg. Chem.* 2011, **50**, 4029.

[1.33] K. R. Gee, Z.-L. Zhou, W.-J. Qian and R. Kennedy, *J. Am. Chem. Soc.* 2002, **124**, 776.

[1.34] J. Zhao, B. A. Bertoglio, K. R. Gee and A. R. Kay, *Cell Calcium* 2008, **44**, 422.

[1.35] B. Valeur and I. Leray, *Coord. Chem. Rev.* 2000, **205**, 3.

[1.36] K. Komatsu, Y. Urano, H. Kojima and T. Nagano, *J. Am. Chem. Soc.* 2007, **129**, 13447.

[1.37] R. Y. Tsien, *J. Biol. Chem.* 1985, **260**, 3440.

[1.38] R. Y. Tsien, *Trends Neurosci.* 1988, **11**, 419.

[1.39] J. R. Lakowicz, Ed. Principles of Fluorescence Spectroscopy, 3rd ed.; Springer-Verlag: Berlin, 2006.

[1.40] Y. Ueno, J. Jose, A. Loudet, C. Perez-Bolivar, Jr. P. Anzenbacher and K. Burgess, *J. Am. Chem. Soc.* 2011, **133**, 51.

[1.41] Z.-X. Han, X.-B. Zhang, Z. Li, Y.-J. Gong, X.-Y. Wu, Z. Jin, C.-M. He, L.-X. Jian, J. Zhang, G.-L. Shen and R.-Q. Yu, *Anal. Chem.* 2010, **82**, 3108.

[1.42] M. Beija, C. A. M. Afonso and J. M. G. Martinho, *Chem. Soc. Rev.* 2009, **38**, 2410.

[1.43] M. E. Moragues, R. Martinez-Manez and F. Sancenon, *Chem. Soc. Rev.* 2011, **40**, 2593.

[1.44] B. T. Nguyen and E. V. Anslyn, *Coord. Chem. Rev.* 2006, **250**, 3118.

[1.45] G. Schwarzenbach and H. Ackermann, *Helv. Chim. Acta* 1947, **30**, 1798.

[1.46] K. L. Cheng, T. Kurtz and R. H. Bray, *Anal. Chem.* 1952, **24**, 1640.

[1.47] I. M. Kolthoff, E. B. Sandell, E. J. Meehan and S. Bruckenstein, Quantitative Chemical Analysis, 4th ed.; Macmillan: London, 1969; p803.

[1.48] A. Metzger and E. V. Anslyn, Angew. Chem., Int. Ed. 1998, 37, 649.

[1.49] J. J. Lavigne and E. V. Anslyn, *Angew. Chem., Int. Ed.* 1999, **38**, 3666.

[1.50] S. L. Tobey, B. D. Jones and E. V. Anslyn, *J. Am. Chem. Soc.* 2003, **125**, 4026.

[1.51] D. Leung, J. F. Folmer-Andersen, V. M. Lynch and E. V. Anslyn, *J. Am. Chem. Soc.* 2008, **130**, 12318.

[1.52] D. Leung and E. V. Anslyn, *J. Am. Chem. Soc.* 2008, **130**, 12328.

[1.53] L. Zhu, Z. L. Zhong and E. V. Anslyn, *J. Am. Chem. Soc.* 2005, **127**, 4260.

[1.54] L. Fabbrizzi, N. Marcotte, F. Stomeo and A. Taglietti, *Angew. Chem., Int. Ed.* 2002, **41**, 3811.

[1.55] M. A. Hortala, L. Fabbrizzi, N. Marcotte, F. Stomeo and A. Taglietti, *J. Am. Chem. Soc.* 2003, **125**, 20.

[1.56] M. Boiocchi, M. Bonizzoni, L. Fabbrizzi, G. Piovani and A. Taglietti, *Angew. Chem., Int. Ed.* 2004, **43**, 3487.

[1.57] V. Amendola, G. Bergamaschi, A. Buttafava, L. Fabbrizzi and E. Monzani, *J. Am. Chem. Soc.* 2010, **132**, 147.

[1.58] L. Tang, J. Park, H.-J. Kim, Y. Kim, S. J. Kim, J. Chin and K. M. Kim, *J. Am. Chem. Soc.* 2008, **130**, 12606.

[1.59] E. Hargrove, S. Nieto, T. Zhang and J. L. Sessler, Anslyn, E. V. *Chem. Rev.* 2011, **111**, 6603.

[1.60] C. Spangler, M. Schaeferling and O. S. Wolfbeis, *Microchim. Acta* 2008, **161**, 1.

[1.61] S. K. Kim, D. H. Lee, J.-I. Hong and J. Yoon, *Acc. Chem. Res.* 2009, **42**, 23.

[1.62] T. Sakamoto, A. Ojida and I. Hamachi, *Chem. Commun.* 2009, 141.

[1.63] M. J. McDonough, A. J. Reynolds, W. Y. G. Lee and K. A. Jolliffe, *Chem. Commun.* 2006, 2971.

[1.64] X. W. Cao, W. Lin and L. He, *Org. Lett.* 2011, **13**, 4716.

[1.65] K. Sasakura, K. Hanaoka, N. Shibuya, Y. Mikami, Y. Kimura, T. Komatsu, T. Ueno, T. Terai, H. Kimura and T. Nagano, *J. Am. Chem. Soc.* 2011, **133**, 18003.

[1.66] M. Q. Wang, K. Li, J. T. Hou, M. Y. Wu, Z. Huang and X. Q. Yu, *J. Org. Chem.* 2012, 77, 8350.

[1.67] W. Hao, A. McBride, S. McBride, J. P. Gao and Z. Y. Wang, *J. Mater. Chem.* 2011, **21**, 1040.

[1.68] F. Hou, L. Huang, P. Xi, J. Cheng, X. Zhao, G. Xie, Y. Shi, F. Cheng, X. Yao, D. Bai and Z. Zeng, *Inorg. Chem.* 2012, **51**, 2454.

[1.69] M. G. Choi, S. Y. Cha, H. K. Lee, H. L. Jeon and S. K. Chang, *Chem. Commun.* 2009, 7390.

[1.70] Lou, X.; Zhang, L.; Qin, J.; Li, Z. *Chem. Commun.* 2008, 5848.

[1.71] X. Chen, S.-W. Nam, G.-H. Kim, N. Song, Y. Jeong, I. Shin, S. K. Kim, J. Kim, S. Park and J. Yoon, *Chem. Commun.* 2010, **46**, 8953.

[1.72] R. G. Upendar, D. Priyadip, S. Sukdeb, B. Mithu, K. G. Sudip and D. Amitava, *Chem. Commun.* 2013, **49**, 255.

[1.73] J. Wu, R. Sheng, W. Liu, P. Wang, J. Ma, H. Zhang and X. Zhuang, *Inorg. Chem.* 2011, **50**, 6543.

[1.74] K. P. Rakesh, K. H. Vijaya, M. Kandula, R. Ankit, P. Dulal and P. R. Chebrolu, *Anal. Chem.* 2012, **84**, 6907.

[1.75] H. Wang, L. Xue and H. Jiang, *Org. Lett.* 2011, **13**, 3844.

[1.76] K. M. Ajit, R. Jagannath, S. Prithidipa, K. M. Subhra and C. Amarnath, *Org. Biomol. Chem.* 2012, **10**, 2231.

[1.77] S. Rochat and K. Severin, *Chem. Commun.* 2011, **47**, 4391.

[1.78] C. R. Lohani, J. M. Kim, S.-Y. Chung, J. Yoon and K.-H. Lee, *Analyst* 2010, **135**, 2079.

[1.79] K. Ghosh, A. R. Sarkar, A. Samadder and A. R. Khuda, *Org. Lett.* 2012, **14**, 4314.

[1.80] R. K. Pathak, K. Tabbasum, A. Rai, D. Panda and C. P. Rao, *Anal. Chem.* 2012, **84**, 5117.

[1.81] R. K. Pathak, J. Dessingou and C. P. Rao, *Anal. Chem.* 2012, **84**, 8294.

[1.82] S. Li, Y. Zhou, C. Yu, F. Chen and J. Xu, *New J. Chem.* 2009, **33**, 1462.

[1.83] C. Mannel-Croise, B. Probst and F. Zelder, *Anal. Chem.* 2009, **81**, 9493.

[1.84] O. S. Wolfbeis, A. Duerkop, M. Wu and Z. Lin, *Angew. Chem., Int. Ed.* 2002, **41**, 4495.

[1.85] C. Mannel-Croise and F. Zelder, *Inorg. Chem.* 2009, **48**, 1272.

[1.86] S. A. Hilderbrand, M. H. Lim and S. J. Lippard, In Topics in Fluorescence Spectroscopy; Geddes, C. D., Lakowicz, J. R., Eds.; Springer: Berlin, 2005; p 163 and references cited therein.

[1.87] M. H. Lim and S. J. Lippard, *Inorg. Chem.* 2004, **43**, 6366.

[1.88] S. A. Hilderbrand, M. H. Lim and S. J. Lippard, *J. Am. Chem. Soc.* 2004, **126**, 4972.

[1.89] M. H. Lim and S. J. Lippard,b*Acc. Chem. Res.* 2007, **40**, 41.

[1.90] X. Chen, X. Tian, I. Shin, J. Yoon, *Chem. Soc. Rev.* 2011, **40**, 4783.

[1.91] T. Zhang, N. Y. Edwards, M. Bonizzoni and E. V. Anslyn, *J. Am. Chem. Soc.* 2009, **131**, 11976.

Chapter 2

Experimental Section

Chapter 2

2.1 General Information and Materials.

All the materials for synthesis were purchased from commercial suppliers and used without further purification. The absorption spectra were recorded on a Perkin-Elmer Lamda-25 UV-visible spectrophotometer using 10 mm path length quartz cuvettes, while the fluorescence measurements were carried on a Horiba Fluoromax-4 spectrofluorometer using 10 mm path length quartz cuvettes with a slit width of 5 nm at 298 K. The mass spectra were obtained using Agilent Technologies 6520 Accurate mass spectrometer. NMR spectra were recorded on a Varian FT-400 MHz instrument and Bruker 600 MHz instrument. The chemical shifts were recorded in parts per million (ppm) on the scale. The following abbreviations are used to describe spin multiplicities in ^{1}H NMR spectra: s = singlet; d = doublet; t = triplet; m= multiplet. Elemental analyses were performed with a Perkin Elmer 2400 elemental analyser.

2.2. Detection of the Fe^{3+} in fetal blood serum by L_1

For determination of Fe^{3+} in fetal bovine serum, the serum was firstly treated with trichloroacetic acid (TCA) to release Fe^{3+} from protein according to a reported procedure.[2.1] 4 mL of 20% TCA was added to 4 mL serum, and then the mixture was stirred and heated to 90°C for 15 min. After cooling, the mixture was sonicated for 2 min. The protein precipitate was removed by centrifugation at 10000 rpm for 10 min. The supernatant was used for the Fe^{3+} assay. Aliquots of the above deproteined serum sample (0 µL, 10 µL, 20 µL, 30 µL, 40 µL, 50 µL, g = 60 µL, 70 µL, 80 µL, 90 µL, 100 µL) were added to 1 mL solution of **L_1** in CH_3CN/aqueous HEPES buffer (1 mM, pH 7.3; 1:4 v/v). After that the resulting solution is incubated at room temperature for 30 min, and then the fluorescence experiments with the following samples are performed.

2.3. Imaging of banana pith by using L_1

The freshly collected banana pith was sectioned and washed carefully with HEPES buffer (pH 7.3). Then the sections were treated with ligand solution (25 μM), washed and then photographed. Another set of sections were treated first with EDTA to chelate the iron present in the pith and then with ligand, and finally photographed.

2.4. UV−Vis and fluorescence spectral studies by L_1

Stock solutions of various ions (1 mM) were prepared in deionized water. A stock solution of **L_1** (1 mM) was prepared in DMSO. The solution of **L_1** was then diluted to 10 μM with CH_3CN/aqueous HEPES buffer (1 mM, pH 7.3; 1:4 v/v). The FBS (Fetal bovine serum) samples were kept at low temperature (-20 °C) for storage. 50 μL of serum was dissolved in 1.5 mL of de-ionized water and used as stock solution. The stock solution for HSA (Human Serum Albumin) protein was prepared at a concentration of 1 mg mL^{-1} in de-ionized water. Experiments could not be performed beyond this concentration with either the serum or HSA protein due to their precipitation. During titration experiment with increasing amount of metHb, the concentration of metHb (*met*-haemoglobin) inside cuvette is maintained from 0 to 4 μM. In titration experiments with increasing amount of Fe^{3+}, each time a 1 mL solution of **L_1** (10 μM) was filled in a quartz optical cell of 1 cm optical path length, and the ion stock solutions were added into the quartz optical cell gradually by using a micro-pipet. Spectral data were recorded at 1 min after the addition of the ions. In selectivity experiments, the test samples were prepared by placing appropriate amounts of the anions/cations stock into 2 mL of solution of **L_1** (20 μM). For fluorescence measurements, excitation was provided at 405 nm and emission was collected from 420 to 600 nm.

2.5 Evaluation of the binding constant for the formation of L_1-Fe complex

Receptor **L_1** with an effective concentration of 10 μM in an acetonitrile/aqueous HEPES buffer (1 mM; 1:4, v/ v; pH 7.3) was used for the emission titration studies with a Fe^{3+} solution. A stock solution of $Fe(NO_3)_3$, having a concentration of 0.2 mM in an acetonitrile/aqueous HEPES buffer (1:4, v/v; pH 7.3) solution was used. The effective Fe^{3+} concentration was varied between 0 and 30 μM for this titration.

The solution pH was adjusted to 7.3 using an aqueous HEPES buffer solution having an effective concentration of 1 mM.

The binding constant for the formation of the respective complexes were evaluated using the Benesi−Hildebrand (B−H) plot (eq 1).[2.2]

$$1/(I-I_0)=1/\{K(I_{max}-I_0)C\}+1/(I_{max}-I_0) \quad (2.1)$$

I_0 is the emission intensity of **L_1** at emission maximum (λ = 472 nm), I is the observed emission intensity at that particular wavelength in the presence of a certain concentration of the metal ion (C), I_{max} is the maximum emission intensity value that was obtained at λ = 472 nm during titration with varying metal ion concentration, K is the binding constant (M^{-1}) and was determined from the slope of the linear plot, and C is the concentration of the Fe^{3+} ion added during titration studies.

2.6. Detection limit of L_1

The detection limit was calculated based on the fluorescence titration. The fluorescence emission spectrum of **L_1** was measured independently for ten times and the standard deviation of blank measurement was achieved. To gain the slope, the ratio of the emission intensity at 472 nm was plotted as a concentration of Fe^{3+}.

The detection limit was calculated using the following equation:

$$\text{Detection limit} = 3\sigma/k \quad (2.2)$$

where σ is the standard deviation of blank measurement, k is the slope between the ratio of emission intensity versus [Fe^{3+}].

2.7. Cytotoxic effect on HeLa cells by L_1

The cytotoxic effect of compound **L_1** and **L_1-Fe** complex was determined by performing a standard MTT assay following the manufacturer instruction (Sigma-Aldrich, MO, USA). HeLa cells (human cervical carcinoma cell line) were initially cultured in a 25 cm^2 tissue culture flask in Dulbecco's Modified Eagle Medium (DMEM) supplemented with 10% (v/v) fetal bovine serum (FBS), penicillin (100 μg/mL) and streptomycin (100 μg/mL) in a CO_2 incubator. For MTT assay, cells

were seeded into 96-well plates (approximately 10^4 cells per well) and various concentrations of compound **L_1** and **L_1-Fe** complex (15, 30, 45 and 60 μM) made in DMEM were added to the cells and incubated for 24 h. Solvent control samples (cells treated with DMSO alone) and cells treated with $Fe(NO_3)_3$ alone were also included in parallel sets. Following incubation, the growth media was carefully aspirated and fresh DMEM containing MTT solution was added. The plate was further incubated for 3-4 h at 37°C. Subsequently, the supernatant was removed and the insoluble colored formazan product was solubilized in DMSO and its absorbance was measured in a microtitre plate reader (Infinite M200, TECAN, Switzerland) at 550 nm. The assay was performed in six sets for each concentration of compound **L_1** and **L_1-Fe** complex. Data analysis and calculation of standard deviation was performed with Microsoft Excel 2010 (Microsoft Corporation, USA).

2.8. Cell imaging studies by L_1

HeLa cells were propagated in Dulbecco's Modified Eagle Medium (DMEM) supplemented with 10% (v/v) fetal bovine serum, penicillin (100 μg/mL), and streptomycin (100 μg/mL). Cells were maintained under a humidified atmosphere of 5% CO_2 and at 37 °C incubator as mentioned before. For imaging studies, cells were seeded into a 6 well plate and incubated at 37^0 C in a CO_2 incubator for 3 days. Subsequently, cells were washed thrice with sterile phosphate buffered saline (pH 7.4) and incubated with 10 μM **L_1** in DMEM at 37 °C for 1 hr in a CO_2 incubator and observed under an epifluorescence microscope (Nikon eclipse Ti). The cells were again washed thrice with sterile PBS (pH 7.4) to remove the free **L_1**, and then incubated in the same with 20 μM $Fe(NO_3)_3$ for 1 hr and again the cell images were recorded using an epifluorescence microscope. The cells were then treated with 30 μM of KF solution and after incubation for 1hr the cells were washed with sterile PBS thrice to remove free compound and ions and then fluorescence microscopic images were recorded.

2.9. UV−Vis and fluorescence spectroscopic studies with L_2

Stock solutions of various ions (1 mM) were prepared in deionized water. A stock solution of **L_2** (5 mM) was prepared in DMSO. The solution of **L_2** was then diluted to 10 μM with CH_3CN/aqueous HEPES buffer (1 mM, pH 7.3; 1:4 v/v). In titration experiments, a quartz optical cell of 1 cm optical path length was filled with a 1 mL

solution of **L_2** (diluted from a stock of 5 mM) to which the ion stock solutions were gradually added using a micropipette. Spectral data were recorded within 1 min after addition of the ions. In selectivity experiments, the test samples were prepared by placing appropriate amounts of the cations stock into 1 mL of **L_2** solution (10 μM). For fluorescence measurements, excitation was provided at 380 nm, and emission was acquired from 400 nm to 700 nm.

2.10. Evaluation of the binding constant for the formation of L_2-Cu complex

Receptor **L_2** with an effective concentration of 10 μM in an acetonitrile/aqueous HEPES buffer (1 mM; 1:4, v/ v; pH 7.3) was used for the emission titration studies with a Cu^{2+} solution. A stock solution of $Cu(ClO_4)_2$, having a concentration of 0.2 mM in an acetonitrile/aqueous HEPES buffer (1:4, v/v; pH 7.3) solution was used. The effective Cu^{2+} concentration was varied between 0 and 60 μM for this titration. The solution pH was adjusted to 7.3 using an aqueous HEPES buffer solution having an effective concentration of 1 mM.

The basic equation (2.3) for determination of the ligand-metal complexation is:

$$D + nM = C \qquad (2.3)$$

Where D is the ligand molecule; M is the metal ion, and C is the complex.

The binding constant K of the metal complex was determined by equation (2.4), assuming the concentration of free metal is about equal to its total concentration ($[M] \approx [M]_t$),[2.2-2.4]

$$(F-F_0)/(F-F_m) = [C]/[D] = K[M]^n \qquad (2.4)$$

Where F_0, F, and F_m are the corrected fluorescence emission intensity (λ = 441 nm) of the complex at initial, interval t, and the final state at which the complex was fully formed upon addition of metal ion, respectively. The binding constant K was determined from the plot of the linear regression of $\log[(F-F_0)/(F_m-F)]$ vs. $\log[M]$ in equation (2.5), derived from equation (2.4), to obtain the intercept as log K and the slope as n.

$$\text{Log } [(F-F_0)/(F-F_m)] = \log K + n \log[M] \qquad (2.5)$$

2.11. Detection limit of L_2

The detection limit was calculated based on the fluorescence titration. The fluorescence emission spectrum of **L_2** was measured for multiple samples and the standard deviations of blank measurement were determined. To gain the slope, the ratio of the fluorescence intensity at 441 nm was plotted as a concentration of Cu^{2+}. The detection limit was calculated with the help of equation 2.2.

2.12. Cytotoxic effect on HeLa cells by L_2 and L_2-Cu Complex

The cytotoxic effect exerted by compound **L_2** and **L_2-Cu** complex on cultured HeLa cells was ascertained by a standard MTT assay. HeLa cells were initially cultured in 25 cm^2 tissue culture flask in Dulbecco's Modified Eagle Medium (DMEM) supplemented with 10% (v/v) fetal bovine serum (FBS), penicillin (100 μg/mL) and streptomycin (100 μg/mL) at 37°C in a CO_2 incubator. Prior to MTT assay, cells were seeded onto 96-well tissue culture plates (approximately 10^4 cells per well) and incubated with various concentrations of compound **L_2** and **L_2-Cu** complex (10, 20 and 40 μM) made in DMEM for a period of 24 h. As control samples, cells treated with DMSO or $Cu(ClO_4)_2$ alone were also included in parallel sets. Following 24 h incubation, the growth media was removed and fresh DMEM containing MTT solution was added to the cells and incubated for 3-4 h at 37°C. Subsequently, the MTT solution was removed and the insoluble colored formazan product was solubilized in DMSO and its absorbance was measured in a microtitre plate reader (Infinite M200, TECAN, Switzerland) at 550 nm. For every concentration of compound **L_2** and **L_2-Cu** complex, MTT assay was performed in six sets. Data analysis and calculation of standard deviation was performed with Microsoft Excel 2010 (Microsoft Corporation, USA). For statistical analysis, a one way analysis of variance (ANOVA) was performed using Sigma plot version 11.0.

2.13. Cell imaging studies by L_2

HeLa cells were initially propagated in a 25 cm^2 tissue culture flask containing DMEM medium as mentioned before. For the detection of intracellular Cu^{2+}, HeLa cells were seeded into a 6 well plate and grown in DMEM medium at 37^0C for 3 days in a CO_2 incubator. Subsequently, the cells were washed thrice with sterile phosphate buffered saline (PBS), incubated with 10 μM **L_2** in DMEM at 37°C for 1

hr in a CO_2 incubator and their images were acquired using a fluorescence microscope (Eclipse Ti-U, Nikon, USA) with a filter that allowed blue light excitation. The cells were further washed with sterile PBS in order to remove free **L_2**, and then incubated for 1 hr with 20 μM $Cu(ClO_4)_2$ made in sterile PBS. The images of the cells were again acquired with a fluorescence microscope as mentioned earlier.

2.14. UV−Vis and fluorescence spectral studies with L_3

Stock solutions of various ions (1 mM) were prepared in deionized water. A stock solution of **L_3** (1 mM) was prepared in DMSO. The solution of **L_3** was then diluted to 10 μM with CH_3OH/aqueous HEPES buffer (1 mM, pH 7.3; 1:4 v/v). In each titration experiments a 1 mL solution of **L_3** (10 μM) was taken in a quartz optical cell of 1 cm optical path length, and then the ion stock solutions were added into the optical cell gradually by using a micropipette. Spectral data were recorded at 1 min after the addition of the ions. In selectivity experiments, the test samples were prepared by placing appropriate amounts of the cations stock into 2 mL of solution of **L_3** (20 μM). For fluorescence measurements, excitation was provided at 405 nm, and emission was collected from 420 to 750 nm.

2.15. Evaluation of the binding constant for the formation of L_3-Cd and L_3-Al complex

Receptor **L_3** with an effective concentration of 10 μM in a Methanol/aqueous HEPES buffer (1 mM; 1:4, v/ v; pH 7.3) was used for the spectroscopic titration studies with a Cd^{2+} or Al^{3+} solution. A stock solution of $Cd(NO_3)_2$ or $Al(NO_3)_3$, having a concentration of 0.2 mM in an Methanol/aqueous HEPES buffer (1:4, v/v; pH 7.3) solution was used. The effective Cd^{2+} or Al^{3+} concentration was varied between 0 and 50 μM for this titration. The solution pH was adjusted to 7.3 using an aqueous HEPES buffer solution having an effective concentration of 1 mM.

The binding constant for the formation of the respective complexes were evaluated using the Benesi-Hildebrand (B−H) plot (eq 2.6 and eq 2.1).[2.2]

$$1/(A-A_0)=1/\{K(A_{max}-A_0)C\}+1/(A_{max}-A_0) \quad (2.6)$$

$$1/(I-I_0)=1/\{K(I_{max}-I_0)C\}+1/(I_{max}-I_0) \quad (2.1)$$

A_0 is the absorbance of **L_3** at absorbance maximum (λ = 510 nm), A is the observed absorbance at that particular wavelength in the presence of a certain concentration of the metal ion (C), A_{max} is the maximum absorbance value that was obtained at λ = 510 nm during titration with varying metal ion concentration, K is the binding constant (M^{-1}) and was determined from the slope of the linear plot, and C is the concentration of the Al^{3+} ion added during titration studies.

I_0 is the emission intensity of **L_3** at emission maximum (λ = 578 nm), I is the observed emission intensity at that particular wavelength in the presence of a certain concentration of the metal ion (C), I_{max} is the maximum emission intensity value that was obtained at λ = 578 nm during titration with varying metal ion concentration, K is the binding constant (M^{-1}) and was determined from the slope of the linear plot, and C is the concentration of the Cd^{2+} ion added during titration studies.

2.16. Detection limit of L_3

The detection limit was calculated based on the UV-Vis titration for Cd^{2+} and fluorescence emission in case of Al^{3+}. The fluorescence emission spectrum of **L_3** was measured ten times and the standard deviation of blank measurement was achieved. To gain the slope, the UV-Vis absorbance (or fluorescence emission in case of Cd^{2+}) at 510 nm (or at 578 nm in case of Cd^{2+}) and was plotted as a concentration of the corresponding metal ion concentration. The detection limit was calculated with the help of equation 2.2.

2.17. X-ray Crystallography.

In each case, a crystal of suitable size was selected from the mother liquor and immersed in silicone oil, and it was mounted on the tip of a glass fibre and cemented using epoxy resin. The intensity data were collected using a Bruker SMART APEXII CCD diffractometer, equipped with a fine-focus 1.75 kW sealed-tube Mo Kα radiation (λ = 0.710 73 Å) at 298(3) K, with increasing ω (width of 0.3° $frame^{-1}$) at a scan speed of 5 s $frame^{-1}$. SMART software was used for data acquisition. Data integration and reduction were undertaken with SAINT and XPREP[2.5] software. Multiscan empirical absorption corrections were applied to the data using the program SADABS.[2.6] Structures were solved by direct methods using

SHELXS-97[2.7] and refined with full-matrix least squares on F^2 using SHELXL-97.[2.8] All non-hydrogen atoms were refined anisotropically. The hydrogen atoms were located from the difference Fourier maps and refined. Structural illustrations have been drawn with ORTEP-3 for Windows.[2.9]

2.18. Cytotoxic effect on HeLa cells by L_3 and L_3-Cd Complex

The cytotoxic potential of compound **L_3** and **L_3-Cd** complex was ascertained by an MTT assay following the manufacturer instruction (Sigma-Aldrich, MO, USA). HeLa cells were initially propagated in a 25 cm^2 tissue culture flask in Dulbecco's Modified Eagle Medium (DMEM) supplemented with 10% (v/v) fetal bovine serum (FBS), penicillin (100 μg/mL) and streptomycin (100 μg/mL) in a CO_2 incubator. Prior to MTT assay, cells were seeded into 96-well plates (approximately 10^4 cells per well) and various concentrations of compound **L_3** and **L_3-Cd** complex (15, 30, 45 and 60 μM) made in DMEM were added to the cells and incubated for 24 h. Solvent control samples (cells treated with DMSO alone) and cells treated with $Cd(NO_3)_2$ alone were also included in parallel sets. Following incubation, the growth media was removed and fresh DMEM containing MTT solution was added. The plate was incubated for 3-4 h at 37°C. Subsequently, the supernatant was removed and the insoluble colored formazan product was solubilized in DMSO and its absorbance was measured in a microtitre plate reader (Infinite M200, TECAN, Switzerland) at 550 nm. The assay was performed in six sets for each concentration of compound **L_3** and **L_3-Cd** complex. Data analysis and calculation of standard deviation was performed with Microsoft Excel 2010 (Microsoft Corporation, USA). For statistical analysis, a one way analysis of variance (ANOVA) was performed using Sigma plot.

2.19. Cell imaging studies with L_3

HeLa cells were initially propagated in a 25 cm^2 tissue culture flask as described earlier and then seeded into a 6 well plate and incubated at 37^0 C in a CO_2 incubator for 3 days. Subsequently the cells were washed three times with sterile phosphate buffered saline (pH 7.4) and incubated with 10 μM **L_3** in DMEM at 37 °C for 1 h in a CO_2 incubator. The image of the cells was then recorded using an epifluorescence microscope (Nikon Eclipse Ti). The cells were again washed thrice with sterile PBS (pH 7.4) to remove excess **L_3**, and then incubated in sterile PBS (pH 7.4) with 20

μM $Cd(NO_3)_2$ for 1 h and the image of the cells were again recorded using epifluorescence microscope.

2.20. UV−Vis and fluorescence spectral studies with L_4

Stock solutions of various ions (1 mM) were prepared in deionized water. A stock solution of **L_4** (1 mM) was prepared in DMSO. The solution of **L_4** was then diluted to 10 μM with CH_3CN/aqueous HEPES buffer (1 mM, pH 7.3; 1:4 v/v). In titration experiments, each time a 1 mL solution of **L_4** (10 μM) was filled in a quartz optical cell of 1 cm optical path length, and the ion stock solutions were added into the quartz optical cell gradually by using a micropipet. Spectral data were recorded at 1 min after the addition of the ions. In selectivity experiments, the test samples were prepared by placing appropriate amounts of the anions/cations stock into 2 mL of solution of **L_4** (20 μM). For fluorescence measurements, excitation was provided at 340 nm and 495 nm, and emission was collected from 390/500 to 650/700 nm.

2.21. Evaluation of the apparent binding constant for the formation of L_4-Cu complex

Receptor **L_4** with an effective concentration of 10 μM in an acetonitrile/aqueous HEPES buffer (1 mM; 1:4, v/ v; pH 7.3) was used for the emission titration studies with a Cu^{2+} solution. A stock solution of $Cu(NO_3)_2$, having a concentration of 0.2 mM in an acetonitrile/aqueous HEPES buffer (1:4, v/v; pH 7.3) solution was used. The effective Cu^{2+} concentration was varied between 0 and 100 μM for this titration. The solution pH was adjusted to 7.3 using an aqueous HEPES buffer solution having an effective concentration of 1 mM.

The apparent binding constant for the formation of the respective complexes were evaluated using the Benesi−Hildebrand (B−H) plot (eq 2.6). [2.2, 2.10-2.12]

$$1/(A-A_0)=1/\{K(A_{max}-A_0)C\}+1/(A_{max}-A_0) \qquad (2.6)$$

In this case A_0 is the absorbance of **L_4** at absorbance maximum (λ = 702 nm), A is the observed absorbance at that particular wavelength in the presence of a certain concentration of the metal ion (C), A_{max} is the maximum absorbance value that was obtained at λ = 702 nm during titration with varying metal ion concentration, K is

the apparent binding constant (M^{-1}) and was determined from the slope of the linear plot, and C is the concentration of the Cu^{2+} ion added during titration studies.

2.22. Detection limit of L_4

The detection limit was calculated based on the UV-Vis titration. The UV-Vis absorbance spectrum of **L_4** was measured for ten times and the standard deviation of blank measurement was achieved. To gain the slope, the ratio of the UV-Vis absorbance at 702 nm was plotted as a concentration of Cu^{2+}. The detection limit was calculated with the help of equation 2.2.

2.23. Evaluation of different parameters for FRET process in L_4-Cu complex

The Förster distance R_0 was calculated using the expression shown in eq 2.9,

$$R_0=0.211[(J)Q(n^{-4})(\kappa^2)] \qquad (2.9)$$

where, n is the refractive index of the medium in between donor and acceptor and was taken approximately to be equal to 1.4. κ^2 is the dipole orientation factor. Depending upon the relative orientation of donor and acceptor, the value ranges from 0-4, and it is often assumed to be 2/3. Q is the fluorescence quantum yield of the donor in the absence of acceptor. J is the spectral overlap integral between the emission spectrum of the donor and the absorption spectrum of the acceptor and is shown in the following eq 2.10,

$$J=\int f_D(\lambda)\varepsilon(\lambda)\lambda^4 d\lambda \qquad (2.10)$$

where $f_D(\lambda)$ is the normalized emission of the donor and $\varepsilon(\lambda)$ is the molar absorption coefficient (M^{-1} cm^{-1}) of the donor. Energy transfer efficiency (Φ_{ET}) was evaluated using the expression shown in eq 2.11,

$$\Phi_{ET}=1-(F'_D/F_D) \qquad (2.11)$$

where F'_D and F_D denote the donor fluorescence intensity with and without an acceptor, respectively.

Energy transfer rate constant (K_{ET}) was calculated using eq 2.12,

$$\Phi_{ET}=K_{ET}/(1/\tau_D+K_{ET}) \qquad (2.12)$$

where τ_D denotes the fluorescence lifetime of the donor fragment in the absence of acceptor.

2.24. Cytotoxic effect of L_4 and L_4-Cu complex on HeLa cells

The cytotoxic effect of compound **L_4** and **L_4-Cu** complex was determined by an MTT assay following the manufacturer instruction (Sigma-Aldrich, MO, USA). HeLa cells were initially propagated in a 25 cm^2 tissue culture flask in Dulbecco's Modified Eagle Medium (DMEM) supplemented with 10% (v/v) fetal bovine serum (FBS), penicillin (100 μg/mL) and streptomycin (100 μg/mL) in a CO_2 incubator. For cytotoxicity assay, cells were seeded into 96-well plates (approximately 10^4 cells per well) and various concentrations of compound **L_4** and **L_4-Cu** complex (15, 25, 50, 75 and 100 μM) made in DMEM were added to the cells and incubated for 24 h. Solvent control samples (cells treated with DMSO alone) and cells treated with $Cu(ClO_4)_2$ alone were also included in parallel sets. Following incubation, the growth media was removed and fresh DMEM containing MTT solution was added. The plate was incubated for 3-4 h at 37°C. Subsequently, the supernatant was removed and the insoluble colored formazan product was solubilized in DMSO and its absorbance was measured in a microtitre plate reader (Infinite M200, TECAN, Switzerland) at 550 nm. The assay was performed in six sets for each concentration of compound **L_4** and **L_4-Cu** complex. Data analysis and calculation of standard deviation was performed with Microsoft Excel 2010 (Microsoft Corporation, USA). For statistical analysis, a one way analysis of variance (ANOVA) was performed using Sigma plot.

2.25. Cell imaging studies with L_4

HELA cells were procured from National Center for Cell Sciences (NCCS), Pune, India. The cells were propagated in Dulbecco's Modified Eagle Medium (DMEM) supplemented with 10% (v/v) fetal bovine serum, penicillin (100 μg/mL), and streptomycin (100 μg/mL). Cells were maintained under a humidified atmosphere of 5% CO_2 and at 37 °C incubator as mentioned before. For cell imaging studies, cells were seeded into a 6 well plate and incubated at 37^0 C in a CO_2 incubator for 3 days. After 3 days cells were washed three times with phosphate buffered saline (pH 7.4) and incubated with 10 μM **L_4** in DMEM at 37 °C for 1 hr in a CO_2 incubator and observed under epifluorescence microscope (Nikon eclipse Ti). The

cells were again washed thrice with PBS (pH 7.4) to remove the free **L_4**, and then incubated in phosphate buffered saline with 20 μM $Cu(ClO_4)_2$ for 1 hr and again images were taken using epifluorescence microscope. The cells are then treated with 30 μM of Na_2S solution, after incubation for 1hr; the cells were washed with PBS three times to remove free compound and ions before analysis. Then fluorescence microscopic images were acquired.

2.26. Synthesis and characterization of the compounds

2.26.1. Synthesis of L_1

Quinoline 2-carboxaldehyde (471 mg, 3 mmol) and 2-amino benzimidazole (400 mg, 3 mmol) were dissolved in 20 mL of methanol. To this was added approximately 2 drops of acetic acid, and the resulting solution was refluxed for 10 h. An yellowish precipitate was found. The reaction mixture was allowed to attain room temperature, and then the precipitate was collected through filtration. The residue was washed thoroughly with methanol to isolate **L_1** in pure form with 43% yield. ^{1}H NMR [400 MHz, DMSO-d_6, J (Hz), δ (ppm)]: 9.52 (1H, s), 8.53 (1H, d, J=9.2), 8.42 (1H, d, J=8.4), 8.34 (1H, d, J=8.4), 8.19 (1H, m), 8.09 (1H, t, J=6.8), 7.99 (1H, d, J=8.4), 7.72-7.93 (3H, m), 7.62 (1H, t, J=7.2), 6.153 (1H, s). ^{13}C NMR [100 MHz, DMSO-d_6, δ (ppm)]: 165.12, 157.91, 155.36, 154.76, 138.62, 138.13, 137.49, 130.69, 130.15, 129.48, 128.84, 128.05, 127.66, 119.94, 119.31, 112.30, 111.70. ESI-MS (positive mode, m/z). Calcd for $C_{17}H_{12}N_4$: 272.106. Found: 273.1128 ($M + H^+$). Anal. Calcd. for $C_{17}H_{12}N_4$ (272.106): C 74.98, H 4.44, N 20.58; found C 74.89, H 4.35, N 20.65.

2.26.2. Synthesis of L_1C

L_1C was synthesized following a method previously reported in literature.[2.13]

2.26.3. Synthesis of L_2

2,6-Diformyl-4-methylphenol was prepared by previously reported procedure.[2.14] A 250 mL round bottom flask with stirrer bar was charged with 4-methylphenol (8.65 g, 80.0 mmol) and hexamethylenetetramine (22.43 g, 160 mmol). To this was added trifluoroacetic acid (90 mL, 1.21 mol) and the yellow solution became hot. A reflux condenser was fitted and the solution was heated to 145°C for 18 h, during which

time it turned dark brown/black. The hot solution was poured into 4N HCl (aq) (200 mL) and stirred for 2 h, during which time a solid was formed. The mixture was placed in a refrigerator overnight and was subsequently filtered and washed with the supernatant, ice cold water (2 x 100 mL) and methanol (2 x 50 mL). The off-white solid was then air dried (8.47 g, 65 %). ^{1}H NMR (400 MHz, $CDCl_3$) δ ppm: 11.43 (s, 1H), 10.19 (s, 2H), 7.75 (s, 2H), 2.37 (s, 3H). ^{13}C NMR (100 MHz, CDCl3) δ ppm: 192.1 (br), 161.7, 137.9, 129.5, 122.8, 20.0. MS (EI) *m/*z 164 [M]+ (75 %), 136 [MCO]+ (100 %), 107 (33 %). Elem. Anal. Found (Calculated for $C_9H_8O_3$) % C 65.95 (65.85), H 4.91 (4.91).

2,6-Diformyl-4-methylphenol (164.16 mg, 1 mmol) and 1-amino-2-naphthol hydrochloride (195.65 mg, 1 mmol) were dissolved in 20 mL of methanol. To this was added approximately 2 drops of acetic acid, and the resulting solution was refluxed for 10 h. A reddish precipitate was found. The reaction mixture was allowed to attain room temperature, and then the precipitate was collected through filtration. The residue was washed thoroughly with methanol to isolate **L_2** in pure form with 52% yield (the yield was calculated based on the starting reagents). ^{1}H NMR [400 MHz, DMSO-d_6, J (Hz), δ (ppm)]: 9.27 (2H, s), 8.00 (2H, d, J=8.4), 7.93 (2H, s), 7.81 (2H, d, J=8.0), 7.55 (2H, d, J=8.8), 7.47 (2H, t, J=8.0), 7.33 (4H, q, J=7.6, J=8.8), 2.42 (3H, s). ^{13}C NMR [100 MHz, DMSO-d_6, δ (ppm)]: 188.82, 167.27, 144.57, 127.83, 126.26, 123.83, 123.27, 122.30, 121.98, 121.38, 119.12, 117.63, 116.21, 19.70. ESI-MS (negetive mode, m/z).Calcd for $C_{29}H_{19}N_2O_3$: 443.14. Found: 443.14 (M - $3H^+$). Anal.Calcd. for $C_{29}H_{22}N_2O_3$ (446.16): C 78.01, H 4.97, N 6.27; found C 77.96, H 4.95, N 6.31.

2.26.4. Synthesis of L_2C

L_2C was synthesized following previously reported literature.[2.15]

2.26.5. Synthesis of L_3

Picolinohydrazide was prepared following a literature method.[2.16] Picolinohydrazide (137 mg, 1 mmol) and 4-(Dimethylamino)cinnamaldehyde (175 mg, 1 mmol) were dissolved in 5 mL of methanol. To this was added approximately 2 drops of acetic acid, and the resulting solution was stirred at room temperature for 10 h. A yellow precipitate was obtained, which was collected through filtration. The residue was

washed thoroughly with methanol to isolate **L_3** in pure form with 68% yield (the yield was calculated based on the starting reagents). ^{1}H NMR [600 MHz, $CDCl_3$, $SiMe_4$, J (Hz), δ (ppm)]: 10.81 (1H, s), 8.55 (1H, d, j=4.2), 8.29 (1H, d, J=8.4), 7.98 (1H, d, J=9), 7.86-7.89 (1H, m), 7.45-7.47 (1H, m), 7.36 (2H, d, J=9), 6.96 (1H, q, J=9, J=15.6), 6.85 (1H, d, J=15.6), 6.67 (2H, d, J=8.4), 2.99 (6H, s,). ^{13}C NMR [150 MHz, $CDCl_3$, $SiMe_4$, δ (ppm)]: 159.99, 151.51, 151.21, 149.41, 148.17, 141.22, 137.71, 128.78, 126.72, 124.08, 123.02, 120.54, 112.24, 40.36. ESI-MS (positive mode, m/z). Calcd for $C_{17}H_{18}N_4O$: 294.148. Found: 295.155 ($M + H^+$). Anal. Calcd. for $C_{17}H_{18}N_4O$ (294.15): C 69.13, H 6.48, N 18.97, O 5.42; found C 69.10, H 6.45, N 19.08, O 5.37.

2.26.6. Synthesis of L_3C_1.

Benzohydrazide was prepared following a literature method.[2.17] Benzohydrazide (136 mg, 1 mmol) and 4-(Dimethylamino)cinnamaldehyde (175 mg, 1 mmol) were dissolved in 5 mL of methanol. To this was added approximately 2 drops of acetic acid, and the resulting solution was stirred at room temperature for 10 h. A yellow precipitate was obtained, which was collected through filtration. The residue was washed thoroughly with methanol to isolate **L_3C_1** in pure form with 82% yield (the yield was calculated based on the starting reagents). ^{1}H NMR [400 MHz, DMSO-d_6, J (Hz), δ (ppm)]: 11.61 (1H, s), 8.18 (1H, d, j=8.8), 7.89 (2H, d, j=7.6), 7.57 (1H, d, j=6.8), 7.51 (2H, t, j=6.8), 7.45 (2H, d, j=8.4), 6.91 (1H, d, j=16), 6.78 (1H, q, j=9.2, j=15.6), 6.70 (2H, d, j=8), 2.94 (6H, s). ^{13}C NMR [100 MHz, DMSO-d_6, δ (ppm)]: 162.75, 150.74, 139.87, 133.67, 131.56, 128.44, 127.57, 123.68, 120.56, 112.03, 40.20. ESI-MS (positive mode, m/z). Calcd for $C_{18}H_{19}N_3O$: 293.153. Found: 294.164 ($M + H^+$). Anal. Calcd. for $C_{18}H_{19}N_3O$ (293.153): C 73.44, H 6.85, N 14.27, O 5.44; found C 73.40, H 6.83, N 14.40, O 5.37.

2.26.7. Synthesis of L_3C_2

Picolinohydrazide (137 mg, 1 mmol) and 4-(Dimethylamino)benzaldehyde (149 mg, 1 mmol) were dissolved in 5 mL of methanol. To this was added approximately 2 drops of acetic acid, and the resulting solution was stirred at room temperature for 10 h. A white precipitate was obtained, which was collected through filtration. The residue was washed thoroughly with methanol to isolate **L_3C_2** in pure form with 61% yield (the yield was calculated based on the starting reagents). ^{1}H NMR [600

MHz, $CDCl_3$, $SiMe_4$, J (Hz), δ (ppm)]: 10.81 (1H, s), 8.55 (1H, d, j=3.6), 8.30 (1H, d, J=4.2), 8.16 (1H, d, J=3.6), 7.86-7.89 (1H, m), 7.69-7.71 (2H, m), 7.44-7.46 (1H, m), 6.68-6.70 (2H, q, J=6.6), 3.02 (6H, s). ^{13}C NMR [150 MHz, $CDCl_3$, $SiMe_4$, δ (ppm)]: 159.83, 152.16, 149.90, 149.69, 148.15, 137.72, 129.60, 126.60, 122.92, 121.38, 111.83, 40.31. ESI-MS (positive mode, m/z). Calcd for $C_{15}H_{16}N_4O$: 268.1324. Found: 269.1404 ($M + H^+$).

2.26.8. Synthesis of L_4

Rhodamine B hydrazide were prepared following a literature method.[2.18] Rhodamine B hydrazide (456 mg, 1 mmol) and indole-3-carboxaldehyde (145 mg, 1 mmol) were dissolved in 20 mL of methanol. To this was added approximately 2 drops of acetic acid, and the resulting solution was refluxed for 10 h. An off-white precipitate was found. The reaction mixture was allowed to attain room temperature, and then the precipitate was collected through filtration. The residue was washed thoroughly with methanol to isolate **L_4** in pure form with 83% yield (the yield was calculated based on the starting reagents). ^1H NMR [400 MHz, $CDCl_3$, $SiMe_4$, J (Hz), δ (ppm)]: 9.26 (1H, s), 8.51 (1H, s), 7.96 (1H, d, J=8.4), 7.90 (1H, d, J=7.6), 7.49 (2H, t, J=3.6), 7.05-7.20 (7H, m), 6.54 (1H, d, J=8.8), 6.46 (1H, d, J=2.4), 6.24 (1H, d, J=2.4), 6.22 (1H, d, J=2.4), 3.28 (8H, q, J=7.2), 1.11 (12H, t, J=7.2). ^{13}C NMR [100 MHz, $CDCl_3$, $SiMe_4$, δ (ppm)]: 164.20, 153.85, 151.09, 148.90, 148.01, 136.78, 132.87, 131.39, 128.79, 128.50, 124.85, 124.16, 123.11, 122.91, 122.75, 120.88, 113.62, 111.31, 108.04, 106.94, 102.02, 98.01, 66.80, 44.47, 12.77. ESI-MS (positive mode, m/z). Calcd for $C_{37}H_{37}N_5O_2$: 583.29. Found: 584.30 ($M + H^+$). Anal. Calcd. for $C_{37}H_{37}N_5O_2$ (583.29): C 76.13, H 6.39, N 12.00, O 5.48; found C 76.06, H 6.34, N 12.08, O 5.45;

2.26.9. Synthesis of L_4C

1-Methyl indole-3-carboxaldehyde was prepared by the reported procedure.[37] Rhodamine B hydrazide (456 mg, 1 mmol) and 1-methyl indole-3-carboxaldehyde (159 mg, 1 mmol) were dissolved in 20 mL of methanol. To this was added approximately 2 drops of acetic acid, and the resulting solution was refluxed for 10 h. A white precipitate was found. The reaction mixture was allowed to attain room temperature, and then the precipitate was collected through filtration. The residue was washed thoroughly with methanol to isolate **L_4C** in pure form with 70% yield

(the yield was calculated based on the starting reagents). ^{1}H NMR [400 MHz, $CDCl_3$, $SiMe_4$, J (Hz), δ (ppm)]: 10.00 (1H, s), 8.12 (1H, d, J=7.2), 7.92 (1H, d, J=2.8), 7.44 (2H, t, J=2.8), 7.08-7.21 (7H, m), 6.47 (1H, d, J=9.2), 6.40 (1H, d, J=2.0), 6.25 (2H, q, J=2.4, J=4.0), 4.76 (3H, s), 3.32 (8H, q, J=7.2), 1.16 (12H, t, J=7.2). ^{13}C NMR [100 MHz, $CDCl_3$, $SiMe_4$, δ (ppm)]: 185.44, 168.99, 168.68, 157.34, 154.03, 153.51, 149.01, 137.30, 132.64, 131.17, 129.84, 129.98, 128.75, 128.21, 125.54, 124.74, 123.99, 122.95, 122.84, 121.74, 121.40, 121.11, 119.20, 114.96, 112.28, 111.82, 108.38, 108.31, 105.59, 98.08, 97.94, 65.46, 44.48, 41.87, 12.76. ESI-MS (positive mode, m/z). Calcd for $C_{38}H_{39}N_5O_2$: 597.31. Found: 598.3188 ($M + H^+$). Anal. Calcd. for $C_{38}H_{39}N_5O_2$ (597.31): C 76.35, H 6.58, N 11.72, O 5.35; found C 76.38, H 6.51, N 11.76, O 5.29;

References

[2.1] M. Kumar and A. Puri, *Indian J Occup Environ Med.*, 2012**, 16**, 40.

[2.2] H. A. Benesi and J. H. Hildebrand, *J. Am. Chem. Soc.*, 1949**, 71**, 2703.

[2.3] K. A. Connors, Binding Constants; John Wiley & Sons: New York; (1987) 339.

[2.4] B. Valeur, Molecular Fluorescence; Wiley-VCH: Weinheim; (2000) 339.

[2.5] SMART, SAINT, and XPREP; Siemens Analytical X-ray Instruments Inc.: Madison, WI, 1995.

[2.6] G. M. Sheldrick, SADABS: Software for Empirical Absorption Correction; Institute fur Anorganische Chemieder Universitat, University of Gottingen: Gottingen, Germany, 1999−2003.

[2.7] G. M. Sheldrick, SHELXS-97; University of Gottingen: Gottingen, Germany, 1997.

[2.8] G. M. Sheldrick, SHELXL-97: Program for Crystal Structure Refinement; University of Gottingen: Gottingen, Germany, 1997.

[2.9] L. J. Farrugia, *J. Appl. Crystallogr.*, 1997, **30**, 565.

[2.10] A. Basu and G. Das, *Inorg. Chem.* 2012, **51**, 882.

[2.11] P. Bose and P. Ghosh, *Chem. Commun.* 2010, **46**, 2962.

[2.12] F. Han, Y. Bao, Z. Yang, T. M. Fyles, J. Zhao, X. Peng, J. Fan, Y. Wu and S. Sun, *Chem. Eur. J.* 2007, **13**, 2880 –2892.

[2.13] C. G. Neochoritis, T. Zarganes-Tzitzikas, C. A. Tsoleridis, J. Stephanidou-Stephanatou, C. A. Kontogiorgis, D. J. Hadjipavlou-Litina and T. Choli-Papadopoulou, *Eur. J. Med. Chem.*, 2011, **46**, 297.

[2.14] L. F. Lindoy, G. V. Meehan and N. Svenstrup, *Synthesis*, 1998, **7**, 1029.

[2.15] W. Gu, Y. Shen, Y. Li, Y. Pan and C. Zhu, *Inorg. Chim. Acta*, 2006, **359**, 1339.

[2.16] S. Benhammadi, A. A. Othman, A. Derdour and A. Mami, *Asian Journal of Chemistry*, 2010, **22**, 5535.

[2.17] X. Q. Wang, Z. G. Zhao, X. L. Liu and W. J. Li, *Journal of Chemical Research*, 2010, **34**, 307.

[2.18] W. Y. Liu, H. Y. Li, B. X. Zhao and J. Y. Miao, *Org. Biomol. Chem.*, 2011, **9**, 4802.

Appendix

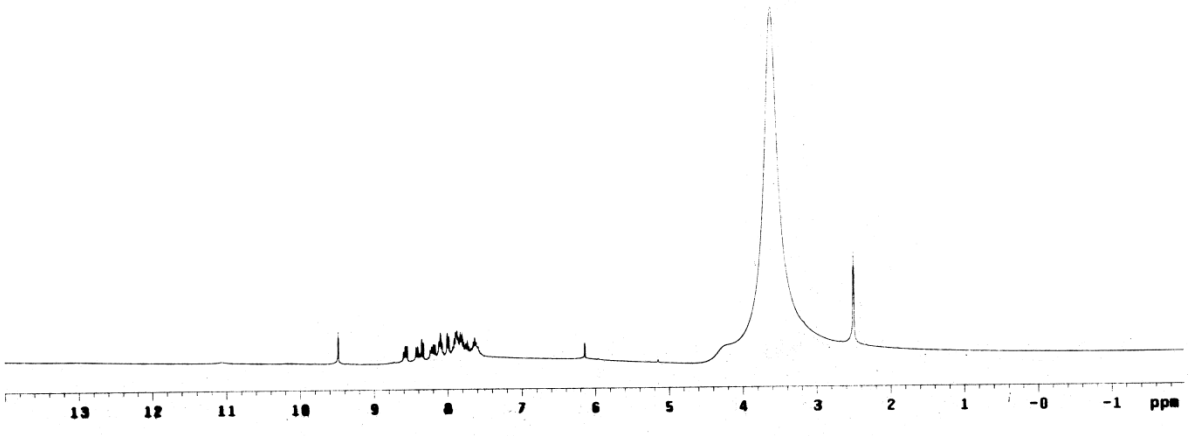

Figure A2.1 ^{1}H NMR spectrum of $\mathbf{L_1}$ in DMSO-d_6 solution.

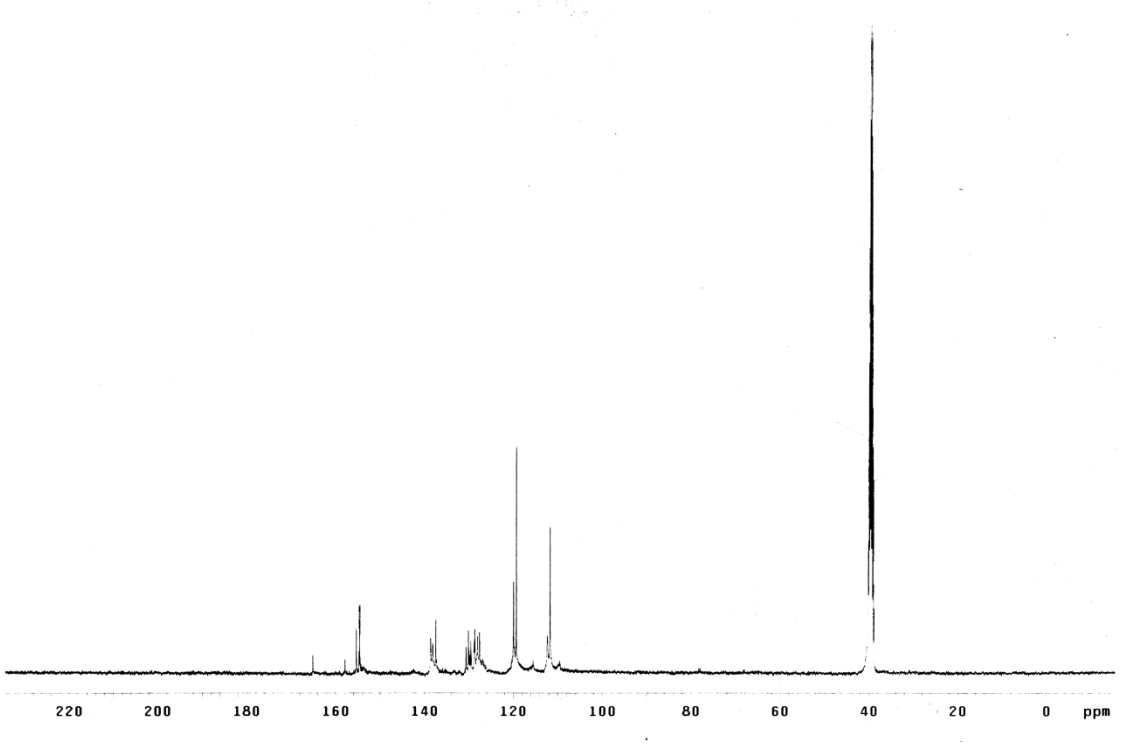

Figure A2.2 ^{13}C NMR spectrum of $\mathbf{L_1}$ in DMSO-d_6 solution.

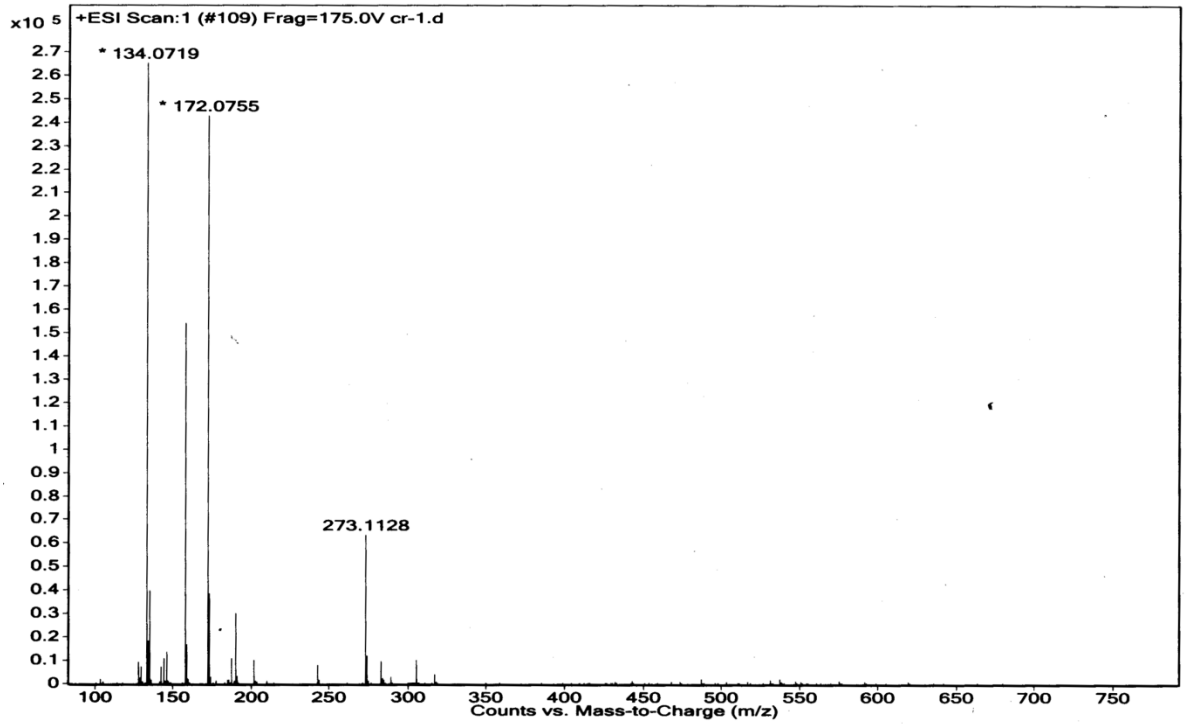

Figure A2.3 Mass spectrum of $\mathbf{L_1}$ (Mass spectrum obtained in positive mode)**.**

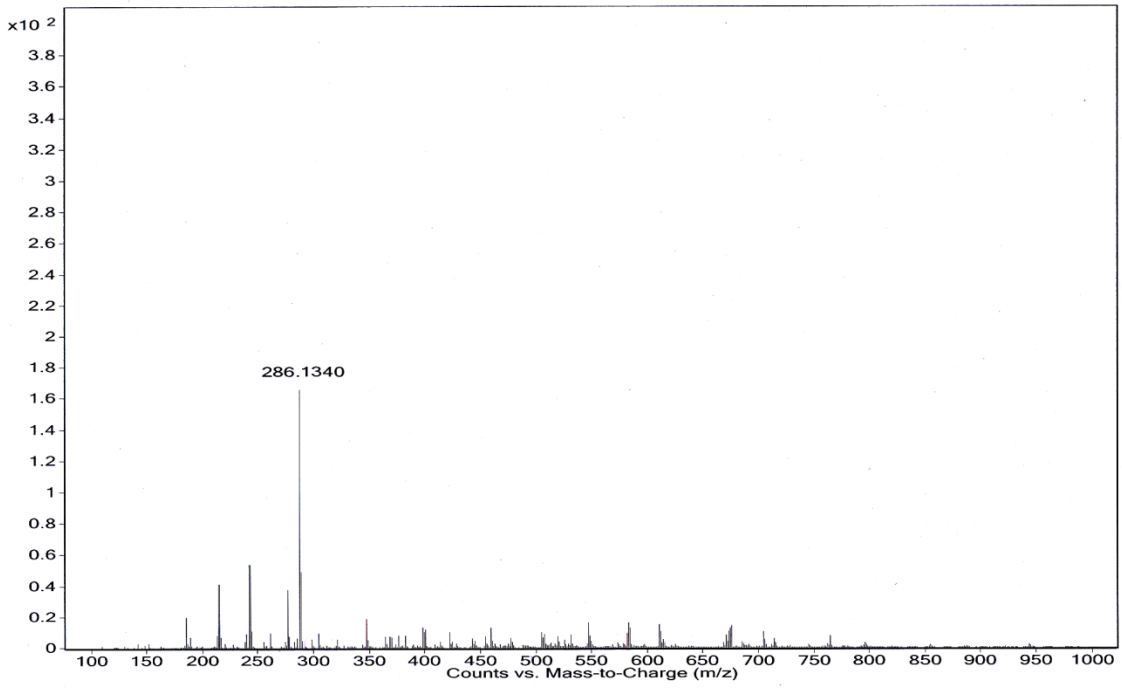

Figure A2.4 Mass spectrum of $\mathbf{L_1C}$ (Mass spectrum obtained in positive mode)**.**

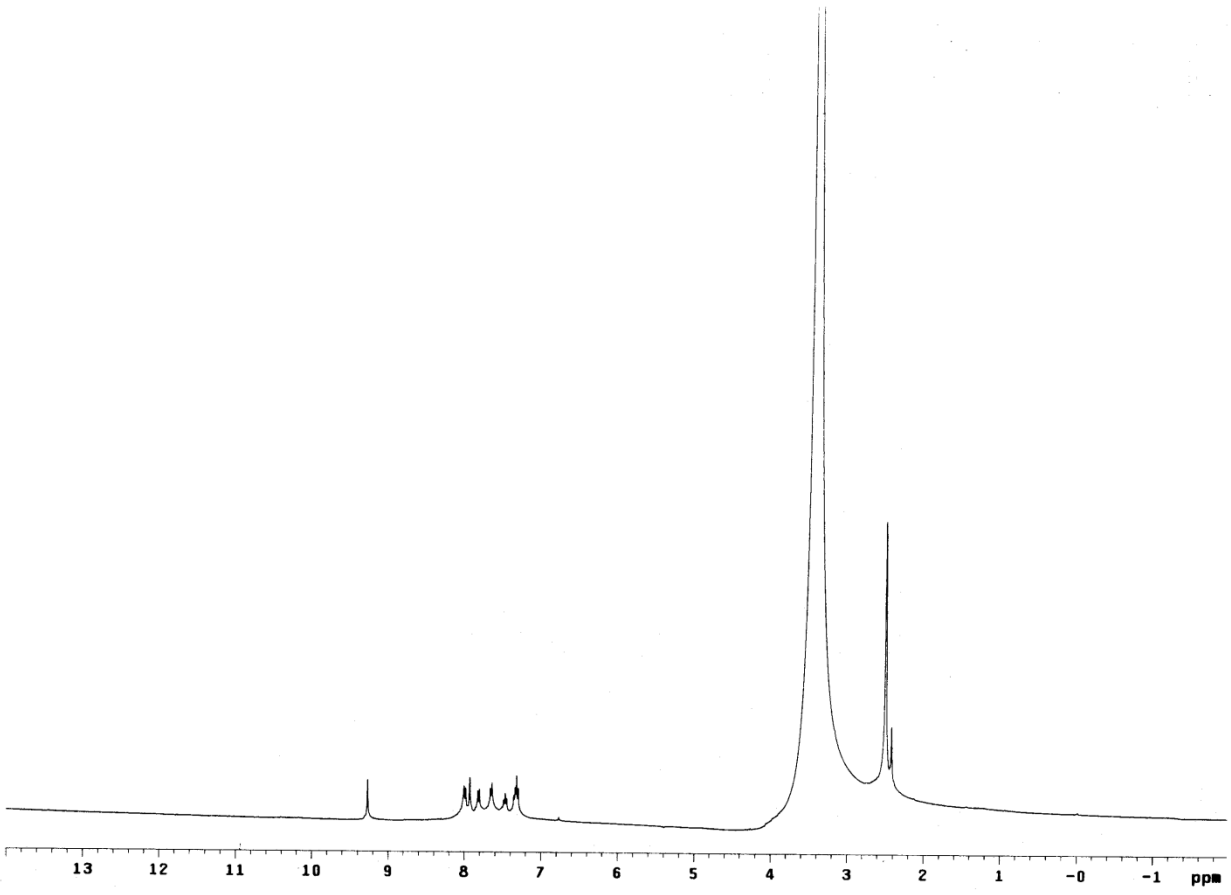

Figure A2.5 ^{1}H NMR spectrum of $\mathbf{L_2}$ in DMSO-d_6 solution.

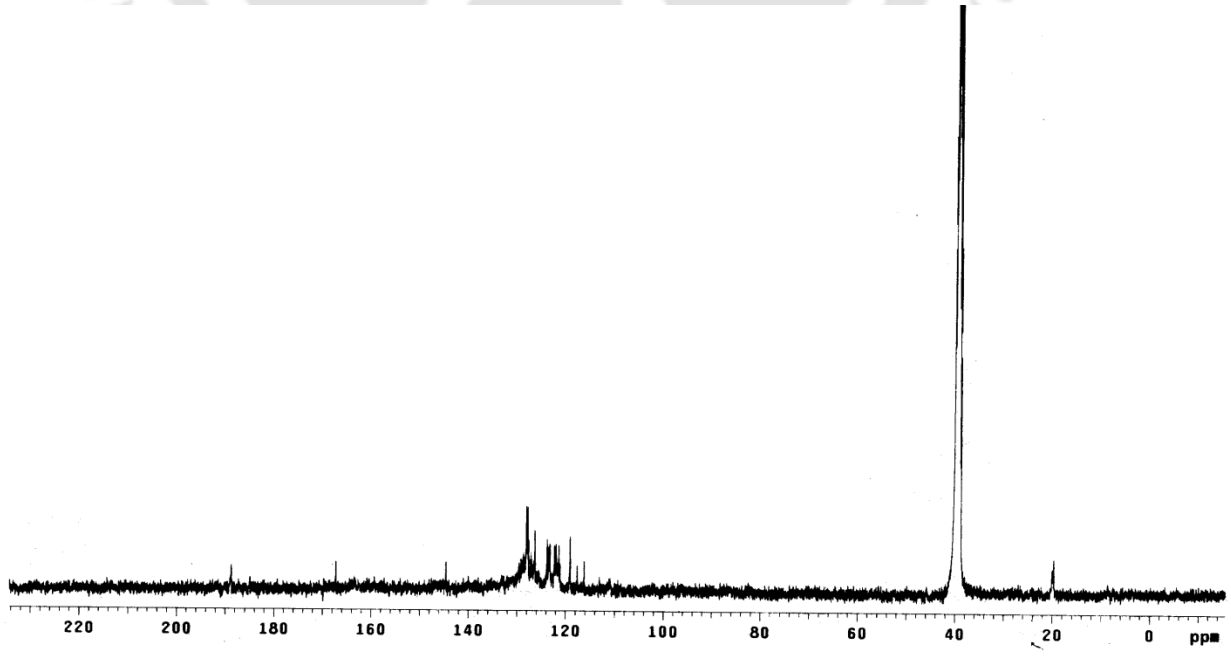

Figure A2.6 ^{13}C NMR spectrum of $\mathbf{L_2}$ in DMSO-d_6 solution.

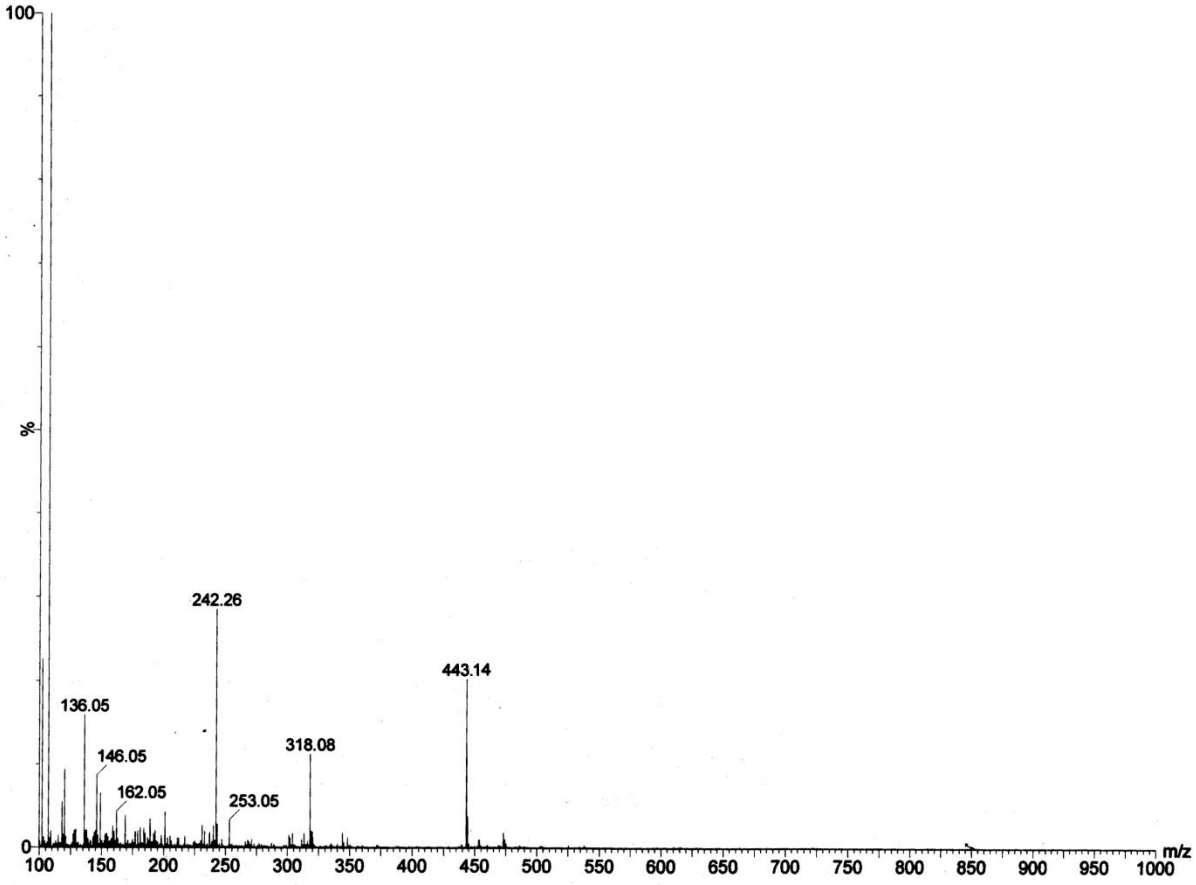

Figure A2.7 Mass spectrum of $\mathbf{L_2}$ (Mass spectrum obtained in negative mode)**.**

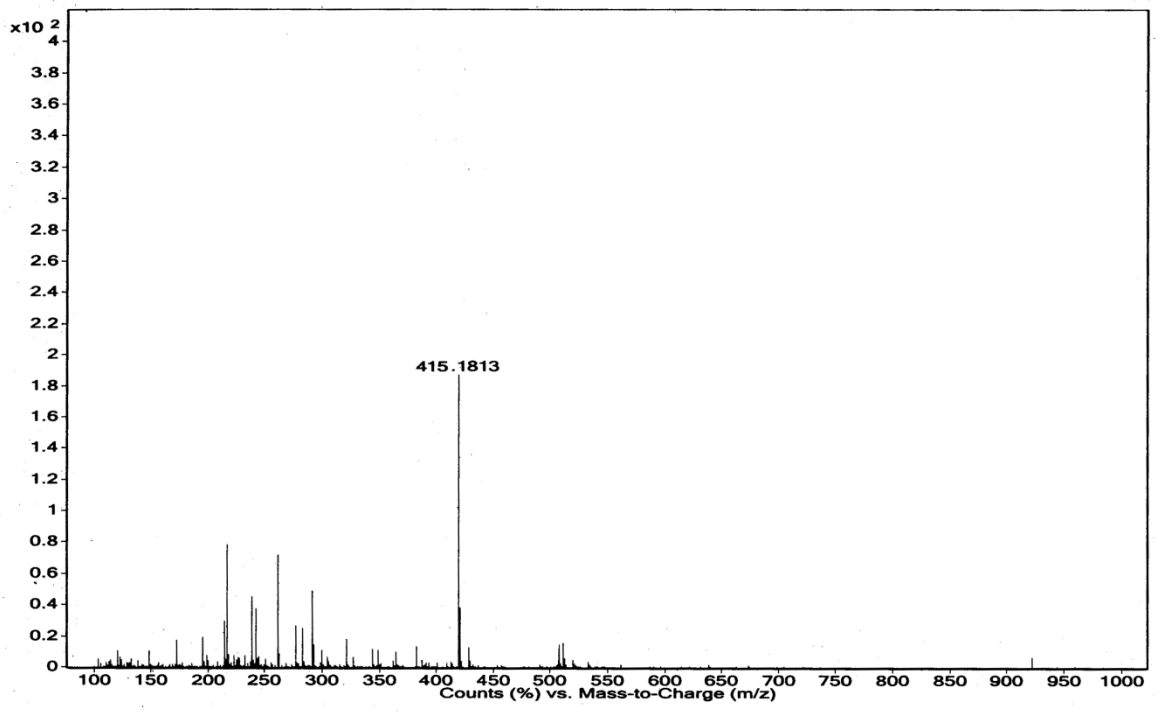

Figure A2.8 Mass spectrum of $\mathbf{L_2C}$ (Mass spectrum obtained in positive mode)**.**

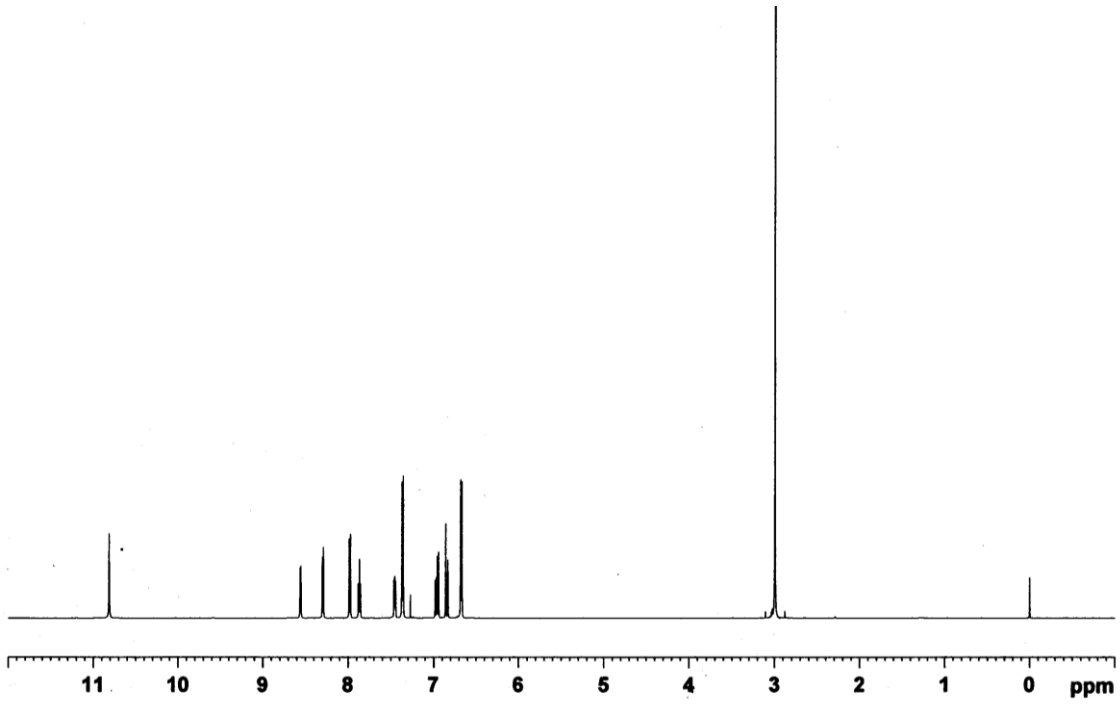

Figure A2.9 ^{1}H NMR spectrum of $\mathbf{L_3}$ in $CDCl_3$ solution.

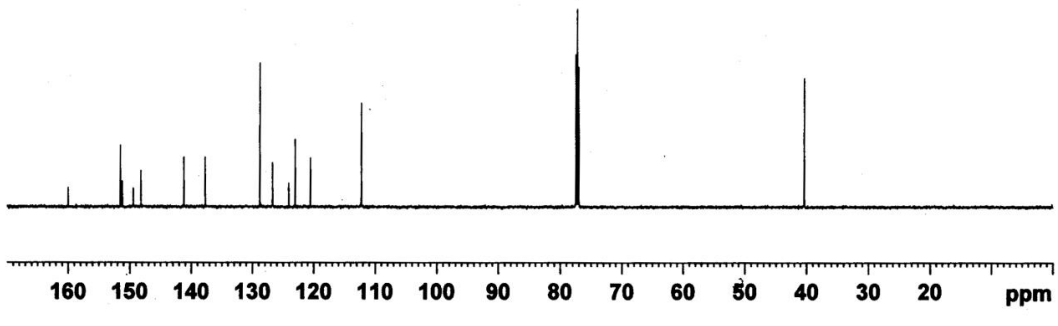

Figure A2.10 ^{13}C NMR spectrum of $\mathbf{L_3}$ in $CDCl_3$ solution.

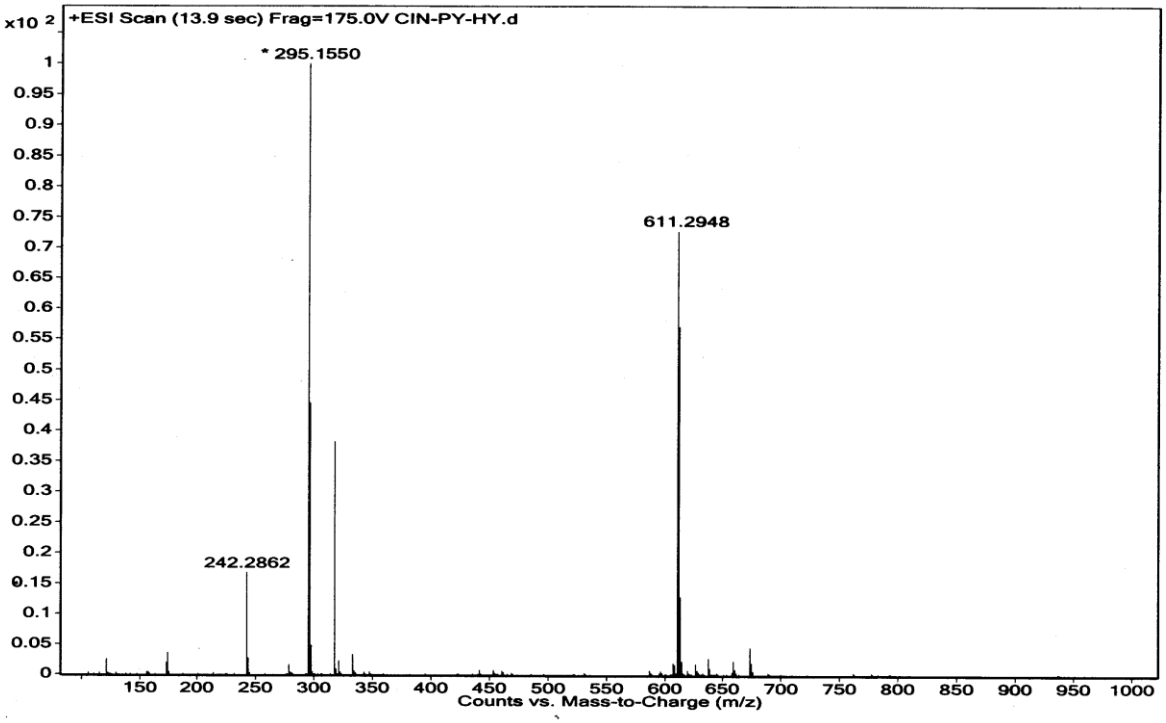

Figure A2.11 Mass spectrum of $\mathbf{L_3}$ (Mass spectrum obtained in positive mode)**.**

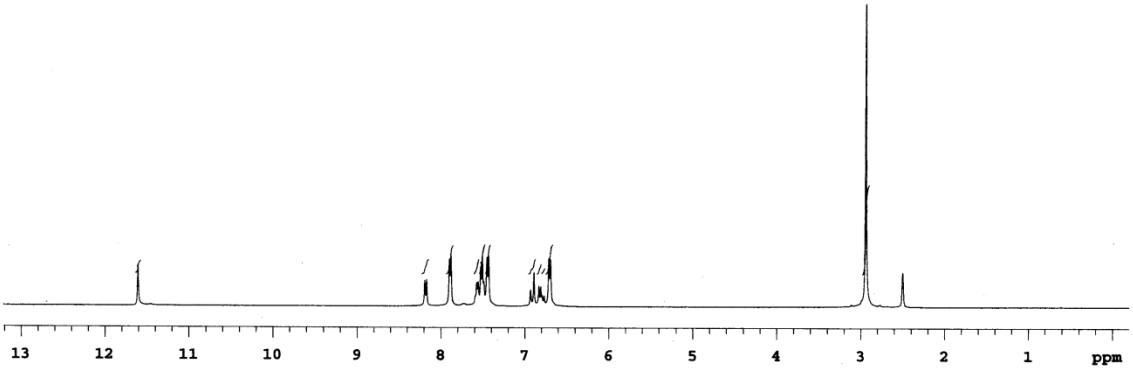

Figure A2.12 ^{1}H NMR spectrum of $\mathbf{L_3C_1}$ in DMSO-d_6 solution.

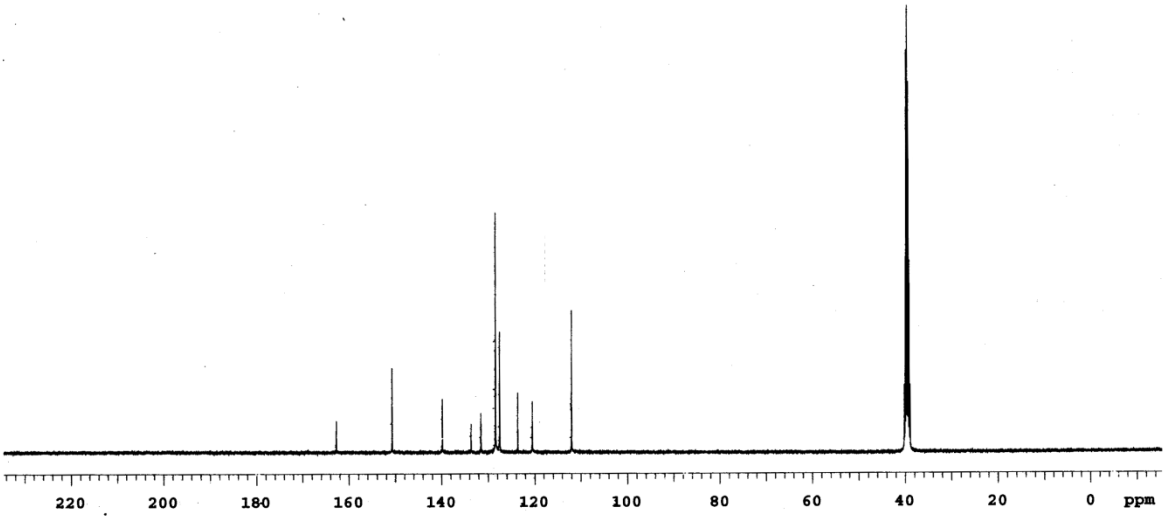

Figure A2.13 ^{13}C NMR spectrum of $\mathbf{L_3C_1}$ in DMSO-d_6 solution.

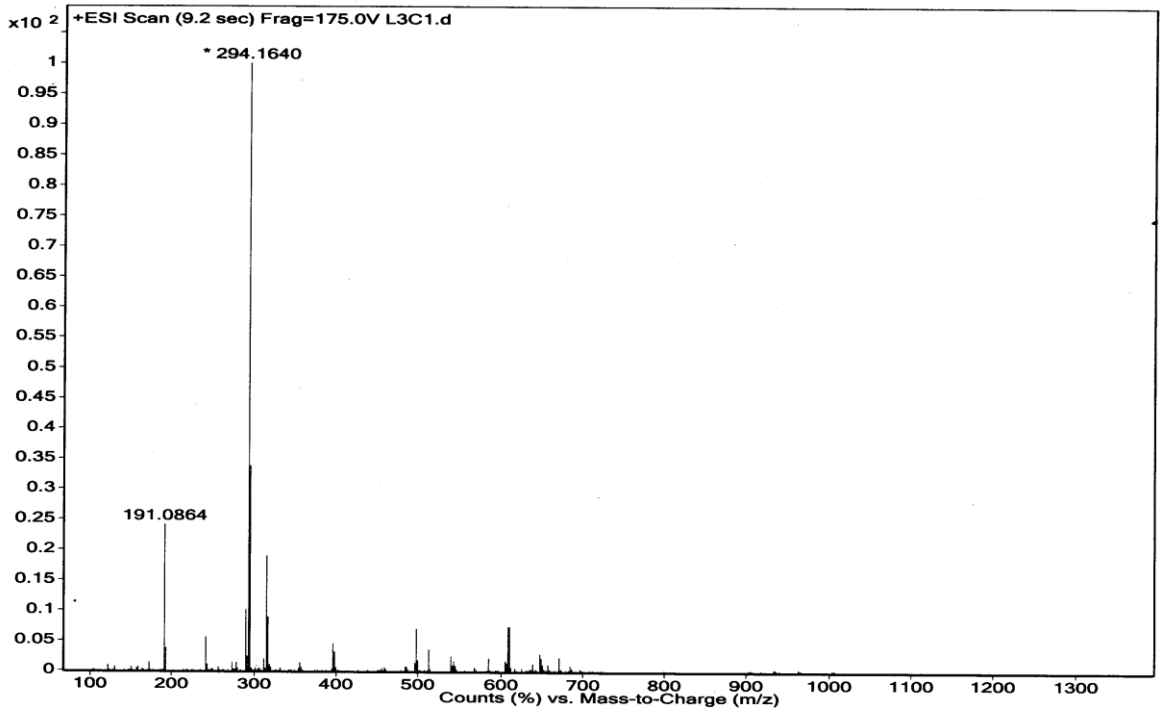

Figure A2.14 Mass spectrum of $\mathbf{L_3C_1}$ (Mass spectrum obtained in positive mode)**.**

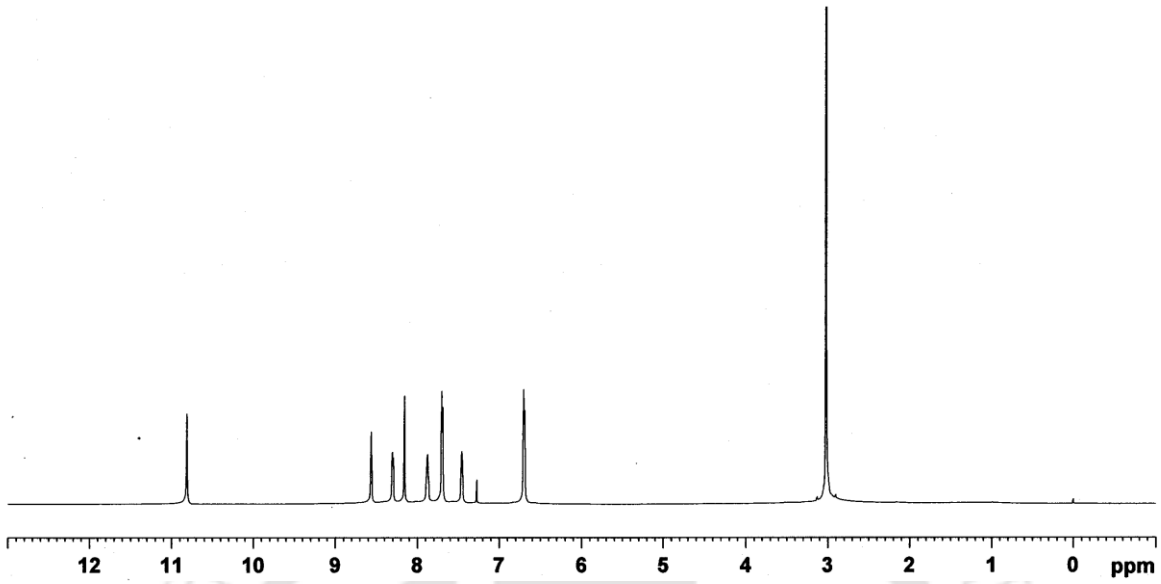

Figure A2.15 ^{1}H NMR spectrum of $\mathbf{L_3C_2}$ in $CDCl_3$ solution.

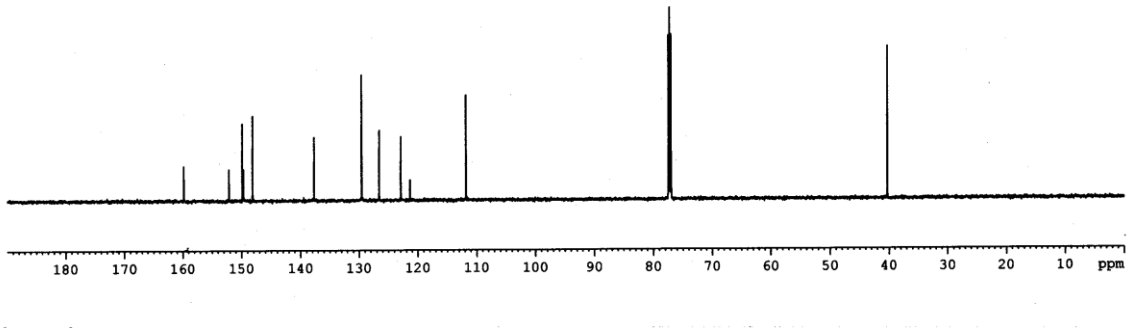

Figure A2.16 ^{13}C NMR spectrum of $\mathbf{L_3C_2}$ in $CDCl_3$ solution.

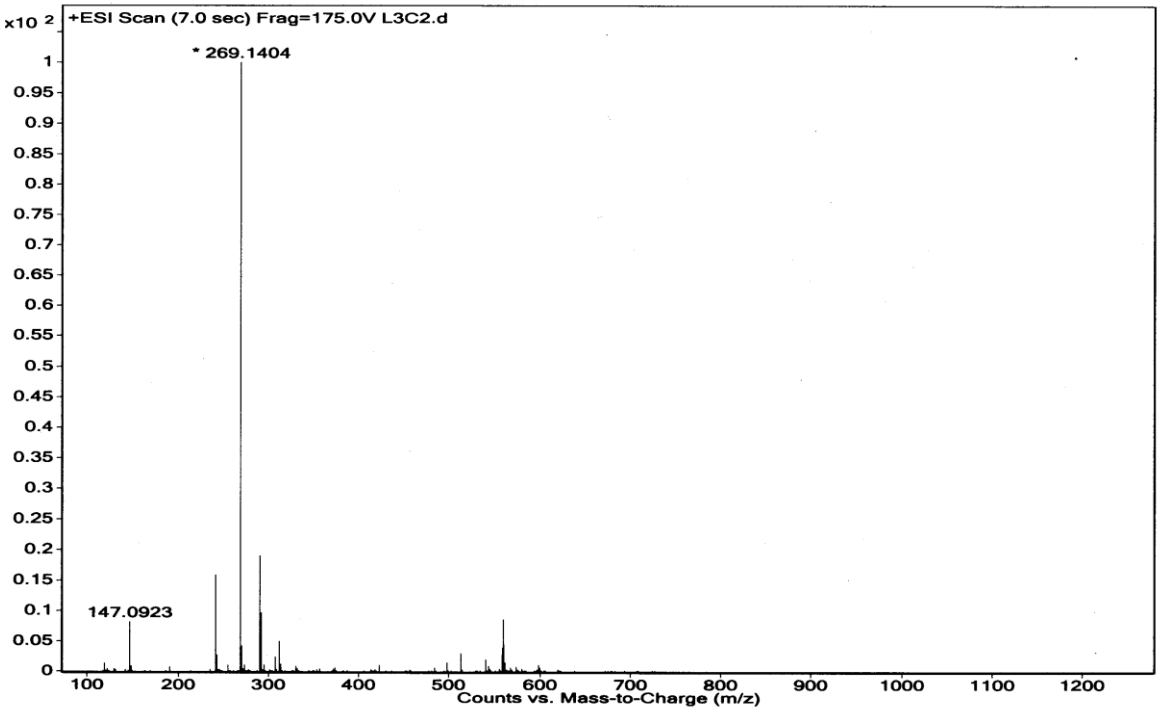

Figure A2.17 Mass spectrum of $\mathbf{L_3C_2}$ (Mass spectrum obtained in positive mode)**.**

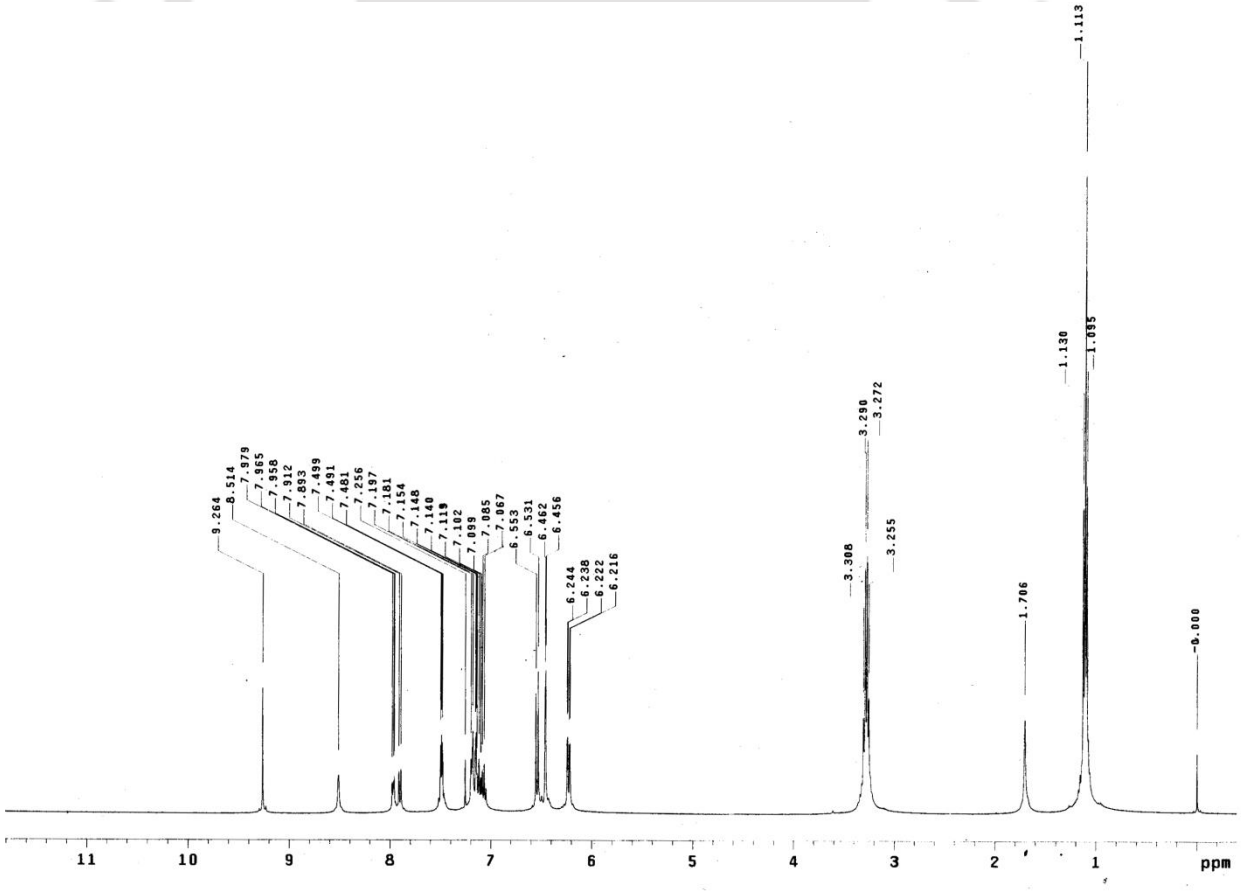

Figure A2.18 ^{1}H NMR spectrum of $\mathbf{L_4}$ in $CDCl_3$ solution.

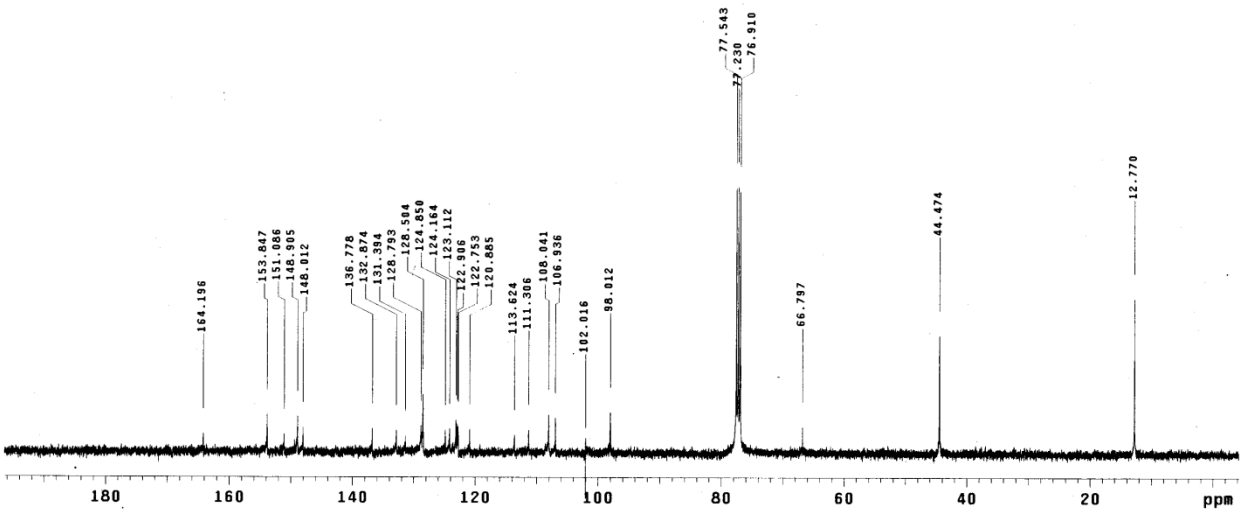

Figure A2.19 ^{13}C NMR spectrum of **L_4** in $CDCl_3$ solution.

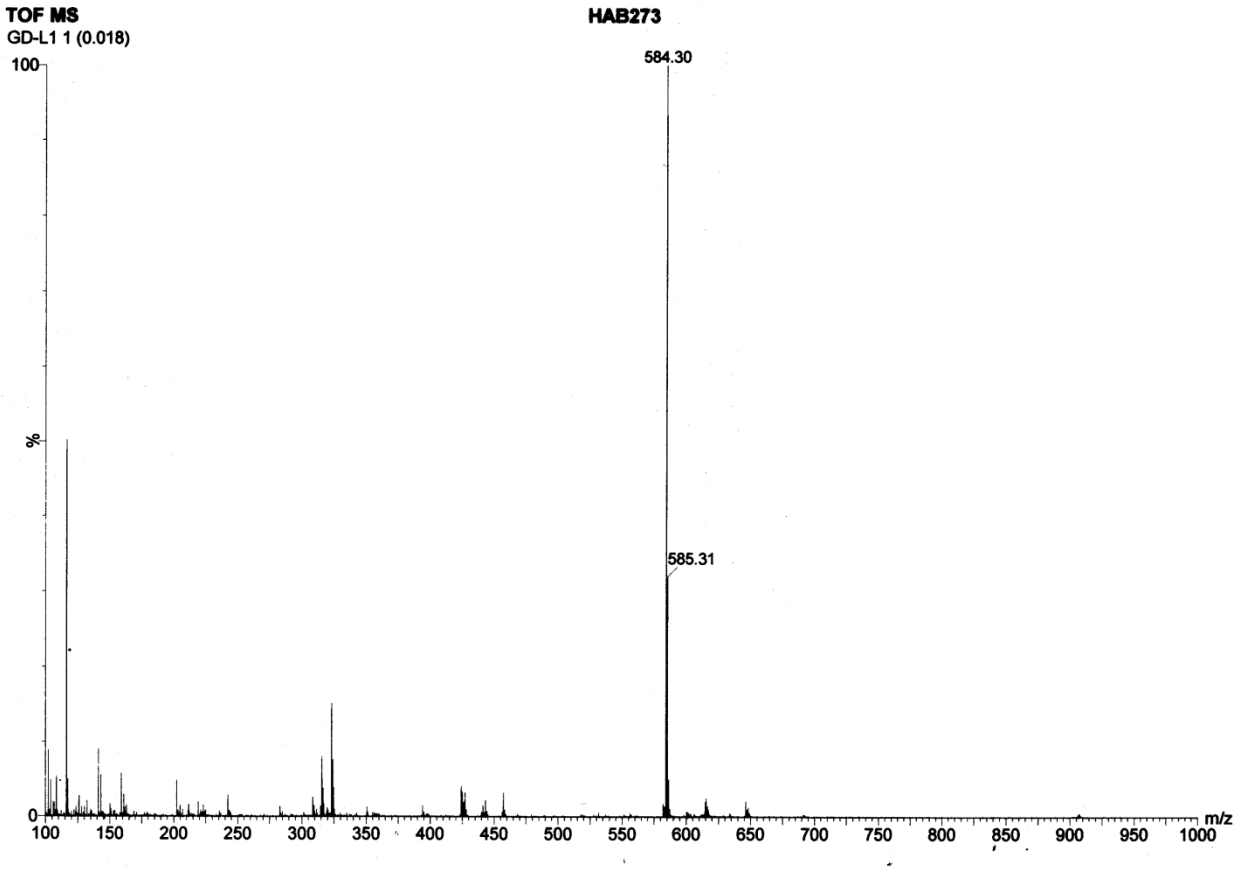

Figure A2.20 Mass spectrum of **L_4** (Mass spectrum obtained in positive mode**).**

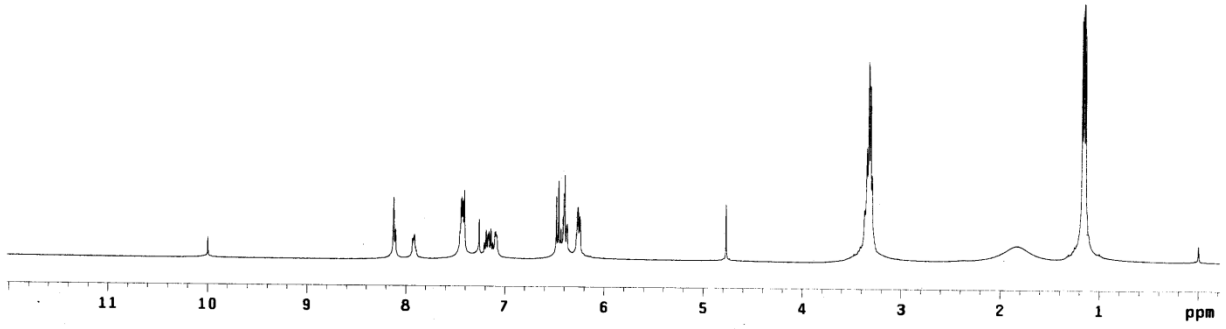

Figure A2.21 ^{1}H NMR spectrum of **L_4C** in $CDCl_3$ solution.

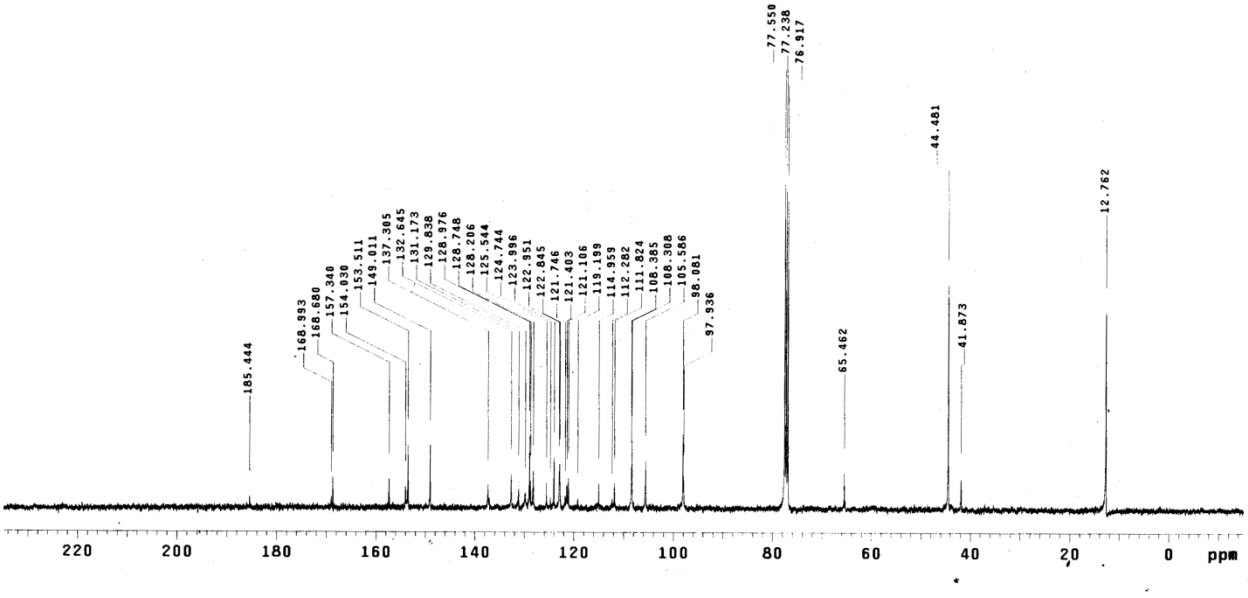

Figure A2.22 ^{13}C NMR spectrum of **L_4C** in $CDCl_3$ solution.

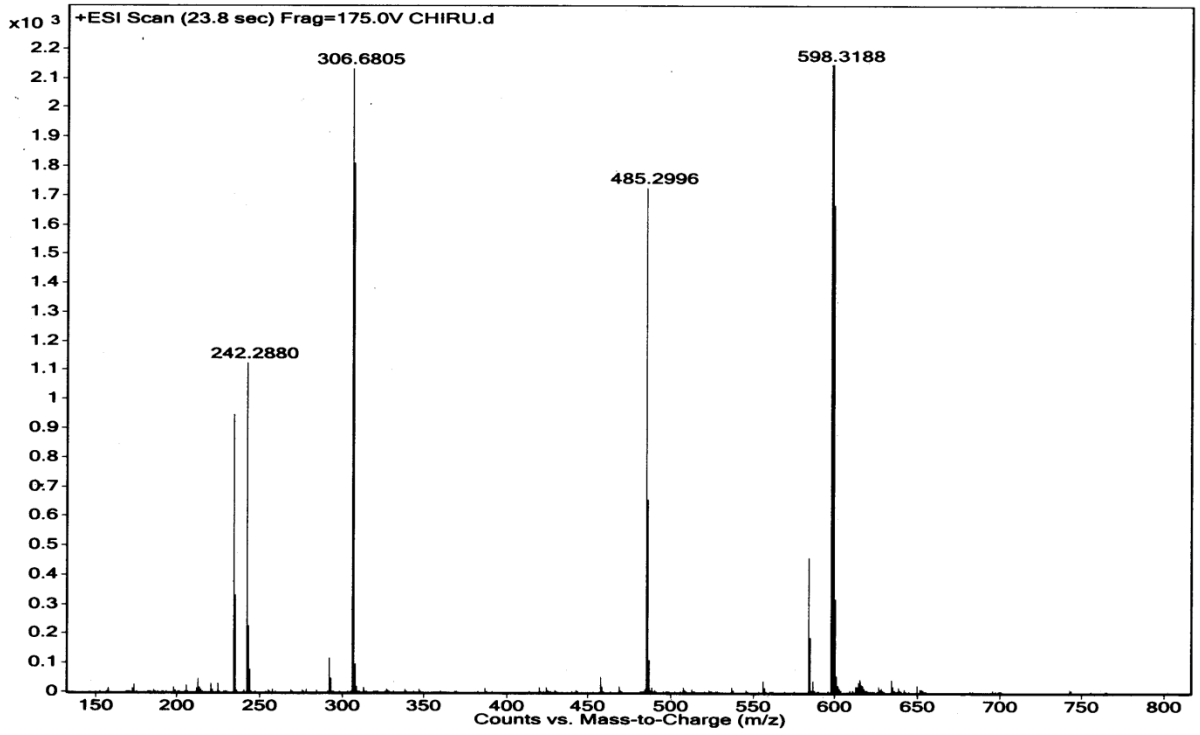

Figure A2.23 Mass spectrum of **L_4C** (Mass spectrum obtained in positive mode)**.**

Chapter 3

A Quinoline based Fluorophoric Probe for Sensing of Fe^{3+} ions by switch ON Green Fluorescence and Application of the Metal-Ligand Complex as a Selective Sensor for F^- Ions

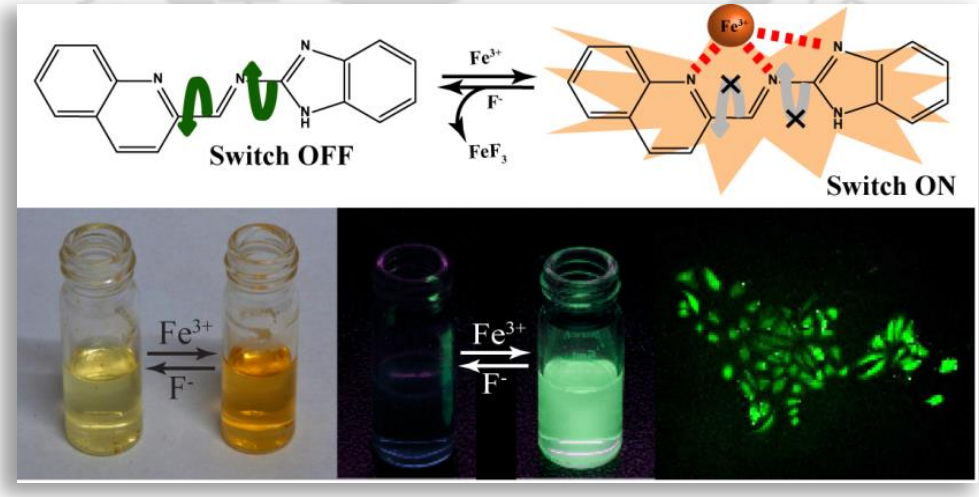

Chapter 3

3.1. Background and Focus of the Chapter

Among biologically important metals, iron is one of the most abundant essential elements found in human body and is critical to sustain important physiological processes.[3.1-3.5] Iron provides the oxygen-carrying capacity of heme and acts as a cofactor in many enzymatic reactions. It plays key roles in numerous biological processes at cellular level ranging from oxygen metabolism and electron-transfer processes to DNA and RNA synthesis.[3.6,3.7] Iron is indispensable for most organisms, and its deficiency as well as overload can lead to detrimental consequences.[3.8-3.11] Given the physiological implications of iron, its detection assumes considerable significance. It is generally believed that probes with a fluorescence enhancement signal upon interaction with analyte are desirable. However, Fe^{3+} ion is well-known as a fluorescence quencher due to its paramagnetic nature, and most of the reported Fe^{3+} receptors, such as analogues of ferrichromes or siderophores, undergo a fluorescence quenching when bound with Fe^{3+}.[3.12-3.14] Therefore, the development of new fluorescent Fe^{3+} indicators, especially those that exhibit selective Fe^{3+}-amplified emission, is still a challenge.[3.15,3.16]

Development of selective and efficient signaling units for detection of various chemically and biologically important anions has also attained significant interest.[3.17,3.18] In this context, the role of fluoride in human health is well recognized. While at low concentration fluoride plays a beneficial role in treating osteoporosis and protecting dental health, it is apparently toxic at higher doses.[3.19] Over the years, high concentration of fluoride anion in the environment and in drinking water has been related to the occurrence of several types of ailment in humans.[3.19-3.21] Hence there is a growing need of developing systems capable of recognition, binding and/or sensing of fluoride in a competitive and aqueous environment. Although, the significance of fluoride anion has led to efforts to develop fluoride sensors over the past decade,[3.22-3.29] but due to its high enthalpy of hydration fluoride sensing in aqueous solution has proved to be very difficult and molecular systems that can sense fluoride anions in aqueous systems are scarce.[3.30,3.31]

In conjunction with visible absorbance signals, a fluorescence response in the visible region would be an added advantage with regard to sensitivity, specificity, and fast

response real-time monitoring[3.32-3.34] of cations and anions over the methods which are based on a single kind of optical response. From the recent literature it is apparent that considerable efforts have been made for selective sensing of Iron[3.1-3.5] and fluoride[3.22-3.29] ions with absorbance and emission in the visible region. However, the optical detection of these analytes in aqueous/mixed aqueous media is still rare. Together with their high sensitivity and efficiency, fluorescent receptors which are soluble in aqueous/mixed solvent offer an added advantage in cellular analysis.[3.35,3.36] In addition, the optical detection of analytes inside living organisms helps to probe their site of action and physiological functions.[3.37,3.38]

Schiff bases are well known as ion carriers and for the formation of stable complexes with transition metal ions. The structure of Schiff bases render geometric and cavity control of host-guest complexation and produce exceptional selectivity, sensitivity and stability for a specific ion. Consequently, Schiff base complexes have attracted increasing attention in the area of ionic binding. Quinoline aldehyde based Schiff base are noteworthy and their transition metal complexes are extensively studied for their proteasome inhibiting activity in human cancer cells.[3.39] The quinoline scaffold having a formyl/acetyl group adjacent to heterocyclic nitrogen can be easily appended with other fluorophore bearing amino groups to yield Schiff base compounds, which can form complexes with a wide range of transition metal ions. Several studies have demonstrated the use of rationally designed Schiff base ligands for optical sensing of transition metal ions.[3.40-3.45]

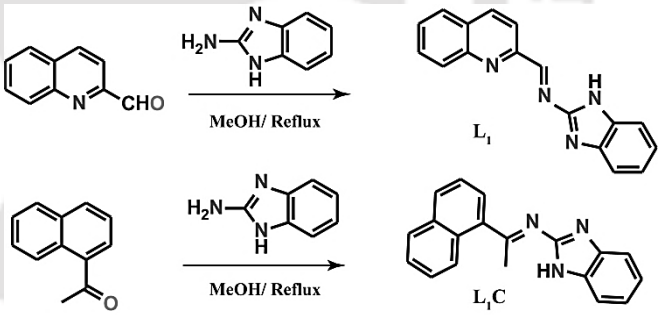

Scheme 3.1 Synthesis of $\mathbf{L_1}$ and $\mathbf{L_1C}$

In view of the biological importance of Fe^{3+} and F^- ions, the advantage of the characteristics of an UV-Vis response has been combined with the sensitivity of a fluorophoric response for the construction of a chemosensor probe (Scheme 1), that may be potentially useful for the detection of Fe^{3+} as well as F^- ions in physiological pH. This chapter describes the metal and anion sensing capabilities of a quinoline functionalized fluorophoric Schiff base ligand $\mathbf{L_1}$ (Scheme 1) and the absorption and fluorescence behaviour of $\mathbf{L_1}$ upon metal complexation, both in solution as well as in live cells.[3.46]

3.2. UV-Vis spectroscopic studies of L_1 in presence of Fe^{3+}

The interaction of **L_1** with various guest species was ascertained by UV-Vis absorption spectroscopic analysis. As observed in Figure 3.1A, ligand **L_1** in CH_3CN/aqueous HEPES buffer (1 mM, pH 7.3; 1:4 v/v**)** shows an absorption maximum at 283 nm, which may be ascribed to intra-molecular π-π* charge transfer (CT) transition. Addition of increasing amounts of Fe^{3+} ions resulted in an increase in absorption (figure 3.1B), with a visual change in color from yellowish to reddish (Figure 3.1A inset). This may be accounted by the change in the orientation of the aromatic fluorophoric units in the ligand. To appropriately determine the selectivity of **L_1** towards Fe^{3+}, we examined the absorption behaviour of **L_1** in presence of various metal ions (Na^+, K^+, Ca^{2+}, Mg^{2+}, Cr^{3+}, Hg^{2+}, Cu^{2+}, Pb^{2+}, Zn^{2+}, Fe^{2+}, Al^{3+}, Ni^{2+}, Co^{2+}, Cd^{2+}, and Ag^+) as their perchlorate or nitrate salts. However, no change in absorption band of compound **L_1** in the presence of other metal ions was observed.

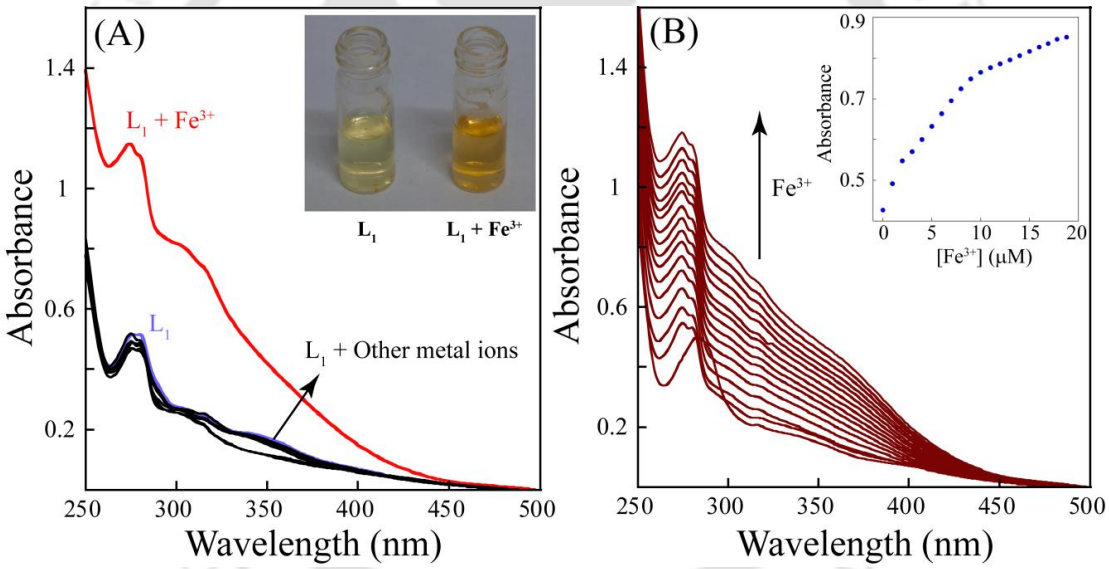

Figure 3.1 (A) Changes of the UV-Vis spectra of ligand **L_1** (10 μM) observed upon addition of Fe^{3+} (1 equivalent) and other metal ions (perchlorate or nitrate salts of Na^+, K^+, Ca^{2+}, Mg^{2+}, Cr^{3+}, Hg^{2+}, Cu^{2+}, Pb^{2+}, Zn^{2+}, Fe^{2+}, Al^{3+}, Ni^{2+}, Co^{2+}, Cd^{2+}, and Ag^+) (10 equivalent) in mixed solvent system. **Inset**: Visual change in color of **L_1** after addition of Fe^{3+} (B) UV-Vis titration spectra of **L_1** (10 μM) upon incremental addition of $Fe(NO_3)_3$. **Inset:** Changes in the UV-Vis absorbance at 274 nm with incremental addition of Fe^{3+}.

3.3. Fluorescence spectroscopic studies of L_1 in presence of Fe^{3+}

The selectivity of **L_1** for Fe^{3+} was also studied by fluorescence emission spectroscopy. As evident from Figure 3.2A, a solution of **L_1** (10.0×10^{-6} M) exhibited a low intensity emission maxima at 472 nm when excited at 405 nm. Addition of Fe^{3+} to this receptor

solution induced a significant increase in the fluorescence response with a redshift of the emission maxima to 478 nm. The spectral change is also accompanied by a visual change of the fluorescence emission from colorless to green (Figure 3.2A inset)**.** It can also be observed from Figure 3.2A that the metal-ligand binding induced fluorescence intensity enhancement of **L_1** was significantly selective towards Fe^{3+} ions. The fluorescence response of **L_1** to other metal ions such as Na^{+}, K^{+}, Ca^{2+}, Mg^{2+}, Cr^{3+}, Hg^{2+}, Cu^{2+}, Pb^{2+}, Zn^{2+}, Fe^{2+}, Al^{3+}, Ni^{2+}, Co^{2+}, Cd^{2+}, and Ag^{+} was also tested under the same conditions as used above for Fe^{3+}. No significant fluorescence change of **L_1** occurred even in the presence of excess of these metal ions.

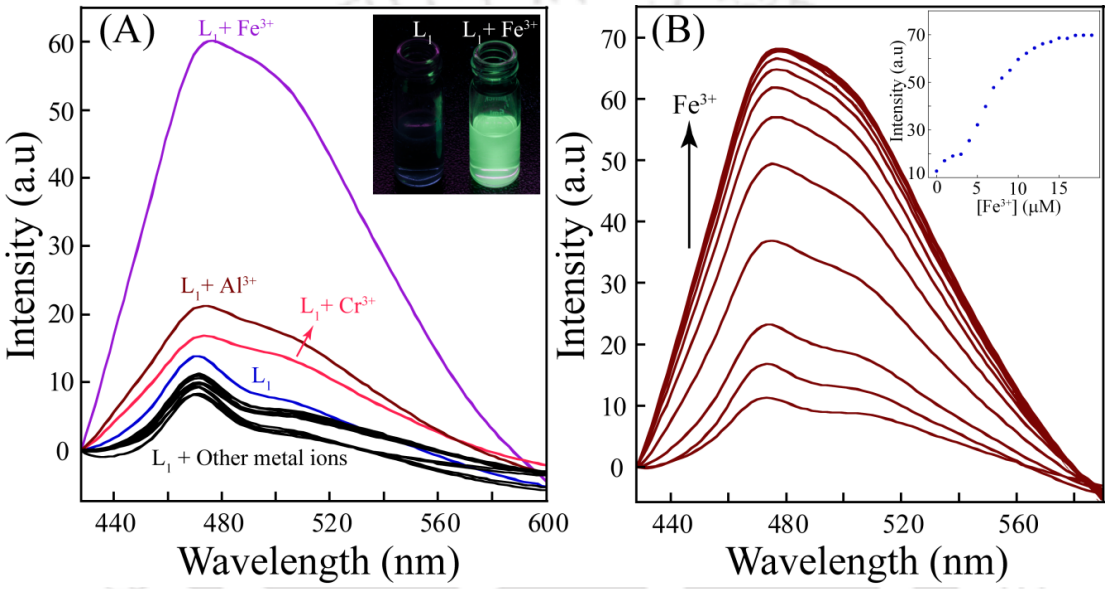

Figure 3.2 (A) Changes of the fluorescence emission of receptor **L_1** (10 μM) observed upon addition of Fe^{3+} (1 equivalent) and other metal ions (perchlorate or nitrate salts of Na^{+}, K^{+}, Ca^{2+}, Mg^{2+}, Cr^{3+}, Hg^{2+}, Cu^{2+}, Pb^{2+}, Zn^{2+}, Fe^{2+}, Al^{3+}, Ni^{2+}, Co^{2+}, Cd^{2+}, and Ag^{+}) (10 equivalent) in mixed solvent system. **Inset:** Visual change in fluorescenc emission of **L_1** after addition of Fe^{3+} (B) Fluorescence titration spectra of **L_1** (10 μM) upon incremental addition of 2 equiv. of Fe^{3+} (λ_{ex}= 405 nm). **Inset:** Changes in the fluorescence intensity at 472 nm with incremental addition of Fe^{3+}.

To gain an insight of the properties of **L_1** as a receptor for Fe^{3+}, a titration of the receptor was performed with increasing concentration of Fe^{3+}. As evident in Figure 3.2B the fluorescence intensity of a 10 μM solution of **L_1** was enhanced with gradual addition of Fe^{3+} ions, which also confirmed that receptor **L_1** exhibited a high sensitivity toward Fe^{3+}, with near about 6 fold increase of its fluorescence intensity upon addition of only 2.0 equiv of Fe^{3+} ions. The 1:1 stoichiometry of the **L_1**-Fe^{3+} was established from the measurements of emission intensity as a function of Fe^{3+} concentration (inset in Figure 3.2B), where a clear bend of the curve can be observed at 1 equivalent of added Fe^{3+}.

This stoichiometry was also confirmed with the help of job's plot (Appendix, Figure A3.1) and further corroborated by ESI-MS studies (Appendix, Figure A3.2), which indicated the presence of molecular-ion peaks at m/z 542.069 and 199.5372 corresponding to the mass of $[L_1+Fe+5H_2O+2NO_3]^+$ and $[L_1+Fe+3H_2O+OH]^{2+}$ respectively. The binding constant for the formation of **L_1-Fe** complex was calculated on the basis of change in emission at 472 nm by considering a 1:1 binding stoichiometry (Appendix, Figure A3.3A). The binding constant (*K*) determined by the B-H method was found to be 2.6×10^4 M^{-1}. It is significant to mention that the detection limit of **L_1** for Fe^{3+} ions was found to be in micro molar level, which was significantly lower than the U.S. EPA maximum allowable limit for Fe^{3+} ions (0.3 mg/L) in drinking water.

3.4. Rationalization of the results

The change in emission spectral behavior of **L_1** in presence of Fe^{3+} can be explained by chelation-enhanced fluorescence (CHEF). As **L_1** is a biheteroaryl system so the quinoline and the benzimidazole rings may not be perfectly planar, metal coordination helps the rings to become more planar and in turn enhance the resonance. When both the part of the ligand is in a non-planar orientation, the fluorescence is quenched due to lack of internal charge transfer throughout the system. But in presence of a suitable metal cation the lone pairs of electron from the imine, quinoline and benzimidazole nitrogen may participate in metal-ligand coordination bonding. Due to metal assisted planar structure of the metal-ligand coordination complex, the possibility of internal charge transfer throughout the π-system increases; leading to a highly conjugated geometry and a radical enhancement of the fluorescence intensity.

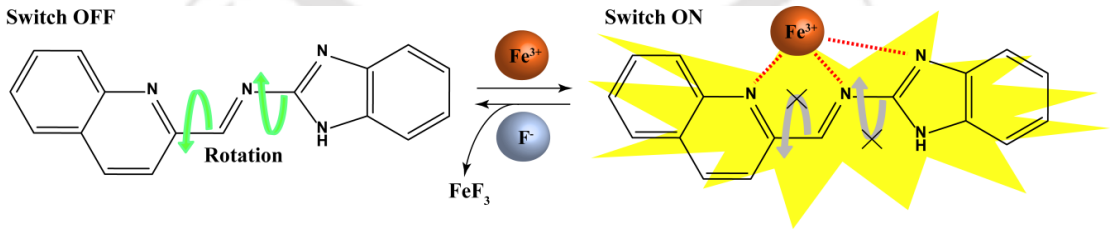

Scheme 3.2 Fe^{3+}-induced fluorescence switch OFF→ON of the receptor **L_1**.

To further verify the significance and involvement of the quinoline lone pair in Fe^{3+} sensing event, we have synthesized a control compound **L_1C**. **L_1C** has a similar structure to **L_1** but in place of a quinoline moiety in **L_1** a naphthalene moiety is present in **L_1C**. Fluorescence emission studies with **L_1C** revealed that there was no significant change in the emission intensity upon addition of an excess amount of Fe^{3+} to a solution containing

L_1C (Appendix, Figure A3.3B), which suggested that in absence of quinoline moiety, Fe^{3+} binding event did not occur. Based on these findings, it can be presumed that the chelating mode of binding to Fe^{3+} by **L_1** restrict the molecule in a planar geometry which extends the conjugation of the π-electron throughout the molecule, which in turn trigger a switch ON response in the fluorescence spectra via chelation-enhanced fluorescence (CHEF) mechanism (Scheme 3.2).

To further understand the relationship between the structural changes from **L_1** to it's complex with Fe^{3+} and the optical response of **L_1** to Fe^{3+} we carried out density functional theory (DFT) calculations with B3LYP/631+G(d,p) method basis set using the Gaussian 03 program. The optimized geometry and the highest occupied molecular orbital (HOMO) and the lowest unoccupied molecular orbital (LUMO) of **L_1** and its Fe^{3+} complex are presented in Figure 3.3. The slight lowering in the HOMO to LUMO energy gap in **L_1-Fe** complex compared to free **L_1** probably causing the small red shift in the emission spectra of **L_1** when $Fe^{3+}$was added to it. Selected orbitals and their corresponding energies were provided in Appendix which might have been playing vital role in the optical spectral outcome (Figure A3.5). The substantial decrease in the total energy (From -23784.90 eV of **L_1** to -66459.76 eV of **L_1-Fe** complex) of **L_1** on complexation with Fe^{3+} suggests that the formed **L_1-Fe** complex is highly stable which is probably initiating the spectral out come through CHEF mechanism.

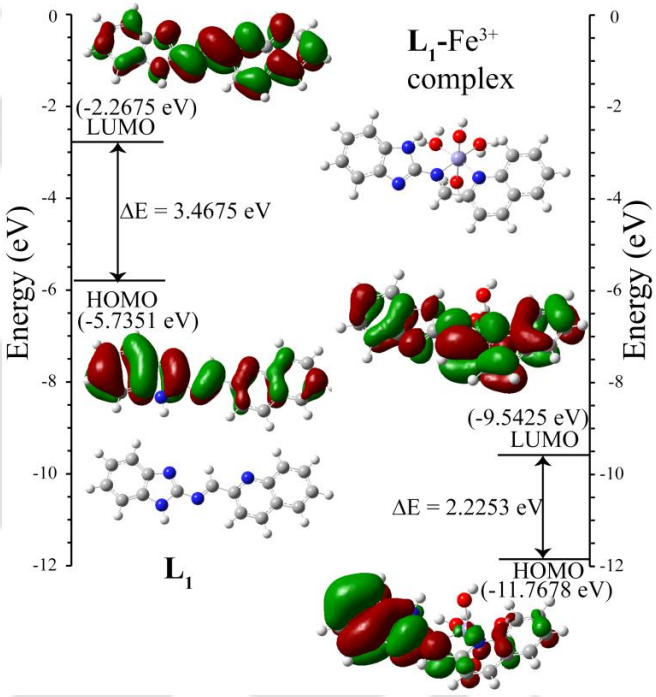

Figure 3.3 Energy diagrams of HOMO and LUMO orbitals of **L_1** and the **L_1–Fe** complex calculated at the DFT level using a B3LYP/6-31+G(d,p) basis set.

3.5. Application of L_1 in Environmental samples

The potential utility of **L_1** in sensing Fe^{3+} ion was also checked in complex environmental as well as biological samples. Tap, lake and river water were collected from laboratory,

the pool of serpentine lake in IIT Guwahati, and Brahmaputra river (Kamrup district, Assam), respectively. Fe^{3+} (1-10 μM) were spiked into these samples before the addition of $\mathbf{L_1}$ (10 μM). The results of the fluorescence spectroscopic measurements observed from this study are depicted in Figure 3.4A The fluorescence intensities were also proportional to the concentrations of Fe^{3+} in the range of 1–10 μM (lower than current aquatic life standard in India, which is 1.0 mg/l based on toxic effects).[3.47] Therefore, the ligand $\mathbf{L_1}$ can be applied for detection of traces of Fe^{3+} in complex environmental systems.

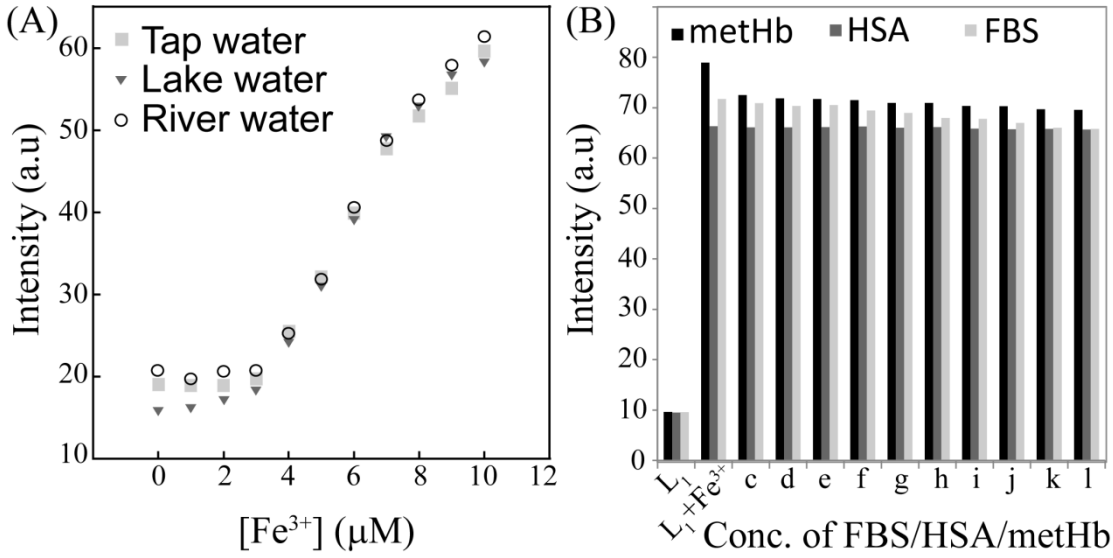

Figure 3.4 (A) Change in fluorescence intensities of $\mathbf{L_1}$ (10 μM) at 472 nm wavelength upon continuous addition of Fe^{3+} (0–10 μM) in three natural water samples. (B) Selectivity of $\mathbf{L_1}$ towards Fe^{3+} in the presence of different concentrations of HSA protein, blood serum (FBS) and *met*-Hemoglobin in mixed solvent system; **a** = $\mathbf{L_1}$ (10 μM) + 0 μL protein, **b** = $\mathbf{L_1}$ (10 μM) + Fe^{3+} (10 μM) + 0 μL protein, **c-l** = incremental addition of different proteins (10 μL -100 μL) to the solution **b**.

The involvement of peroxides and free radicals in the different reactions inside human body can enhance the oxidation of the oxyheme form, resulting in a breakdown of the heme ring and liberation of iron.[3.48-3.51] Humans do not have an active iron excretion mechanism, and levels of nontransferrin-bound-iron (NTBI) in excess of the regulated Fe^{3+} concentrations can generate reactive oxygen species (ROS) that can lead to dysfunction of the heart, liver, anterior pituitary, and pancreas. Thus excess iron inside living system is implicated in the etiology of several degenerative diseases.[3.52,3.53] Given the significant physiological impact of Fe^{3+} in living system, there is a considerable need of designing sensor probe which can detect Fe^{3+} ions in mammalian body fluid. In this regard we have verified the Fe^{3+} detecting capability of $\mathbf{L_1}$ in presence of plasma protein (HSA), globular protein (*Met*-haemoglobin) and fetal bovine serum (FBS). As evident

from figure 3.4B no change in the fluorescence emission of **L_1-Fe** complex was observed on addition of varying concentrations of *Met*-haemoglobin, Human serum albumin (HSA) and fetal bovine serum (FBS). This indicated the high binding efficiency of **L_1** with Fe^{3+} ions over the *met*-haemoglobin, Human serum albumin (HSA) protein and fetal bovine serum. On the other hand, when Fe^{3+} ions were added to the solution of ligand **L_1** and *met*-haemoglobin/Human serum albumin (HSA) protein/ fetal bovine serum, the characteristic fluorescence enhancement was observed in the emission intensity at 472nm of **L_1** (Appendix, Figure A3.9). These observations again reiterate the strong interactions of ligand **L_1** with Fe^{3+} ions over the biological guests.

The strong potential of **L_1** in sensing Fe^{3+} ions are further demonstrated by fluorescence microscope imaging of native iron pools inside plant system. The banana pith sections are chosen as an iron-rich part of banana plant. When these sections were treated with **L_1**, a strong green emission was observed indicating the presence of Fe^{3+} ions (Figure 3.5). A control experiment was also performed where the banana pith sections were treated with EDTA to chelate the iron present and then treated with **L_1**. The control experiment didn't show any increase in green fluorescence of the banana pith sections which concludes that the emergence of the green fluorescence is only due to the formation of **L_1-Fe** complex inside the biological system.

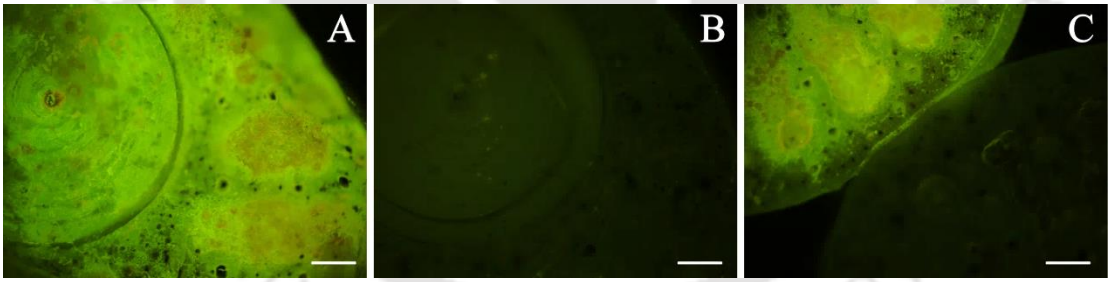

Figure 3.5 Fluorescence microscopic photograph of transverse section of (A) banana pith treated with **L_1**, (B) banana pith treated with EDTA first followed by **L_1**, (C) banana pith treated with **L_1** and banana pith treated with EDTA first followed by **L_1** attached together. Scale bar for the images is 200 μm.

3.6. UV-Vis spectroscopic studies of L_1-Fe complex in presence of anions

Hence from the above mentioned studies it was evident that **L_1** selectively binds with Fe^{3+} to form **L_1-Fe** complex with a distinct change in its optical as well as fluorescence properties. The next endeavor was to ascertain the influence of different anions on the disassembly/dissociation of this metal-ligand complex and their effect on the reversibility

of this complex to regenerate **L_1.** The UV-Vis spectroscopic study of the **L_1-Fe** complex was pursued in presence of different anions such as F^-, Cl^-, Br^-, I^-, CN^-, $H_2PO_4^-$, NO_3^-, NO_2^-, SO_4^{2-}, HSO_3^-, and S^{2-}. It is worth mentioning that the regeneration of compound **L_1** was observed only by adding F^- to the solution containing **L_1-Fe**, whereas other anions failed to demonstrate any significant spectral change. To obtain a comprehensive understanding of the properties of **L_1-Fe** complex in presence of F^- anion, a solution of **L_1** in mixed solvent containing 1 equiv. of Fe^{3+} was titrated in presence of increasing amount of fluoride anions. The UV-Vis spectral pattern of the titration spectra (Figure 3.6A) displayed a reverse trend to the titration curve obtained with Fe^{3+} (Figure 3.1B), which provided evidence that ligand **L_1** could be regenerated from the complex in presence of F^-.

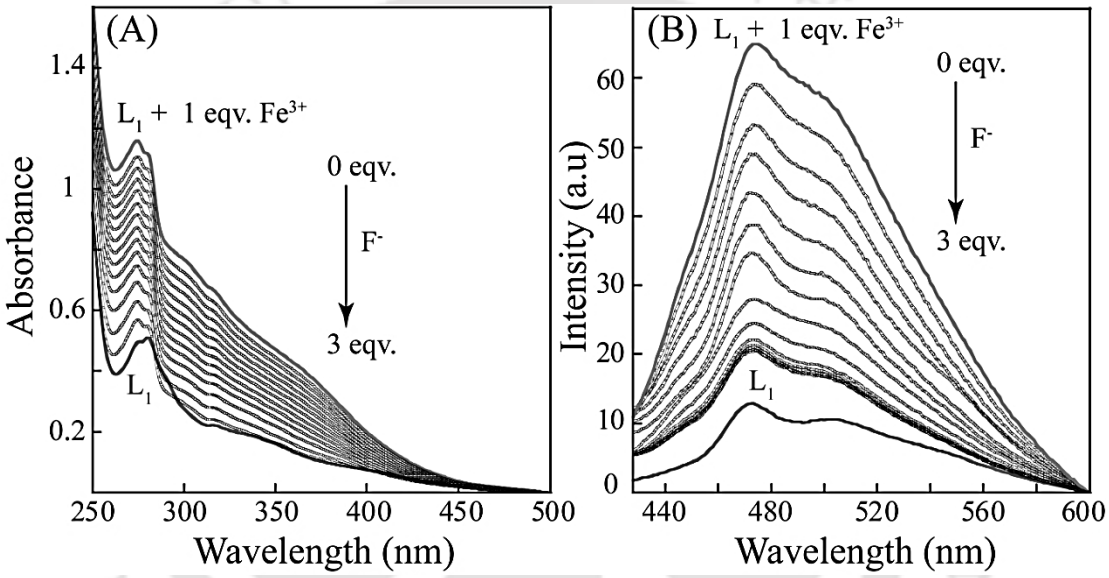

Figure 3.6 (A) UV-Vis titration spectra of **L_1** (10 μM) with 1 equiv of Fe^{3+} upon addition of sodium fluoride (30 μM) in mixed solvent system. (B) Fluorescence titration spectra (λ_{ex} = 405 nm) of **L_1** (10 μM) with 1 equiv of Fe^{3+} upon addition of fluoride (30 μM) ion.

3.7. Fluorescence spectroscopic studies of L_1-Fe complex in presence of anions

Fluorescence spectroscopy studies of **L_1-Fe** complex in presence of different anions were also pursued. Interestingly it was observed that the emission of **L_1-Fe** complex was completely restored to its native **L_1** state, selectively in presence of fluoride anions. To further verify the fluorescence "ON-OFF'' switching property of the sensor, fluorescence titration experiment was performed. Initially the fluorescence intensity of the compound **L_1** was enhanced to an adequate level in presence of 1 equiv. of Fe^{3+} ions, the resulting **L_1-Fe** complex was then titrated by addition of increasing amounts of fluoride ions. As evident from Figure 3.6B the fluorescence intensity of **L_1-Fe** complex decreased with

increasing concentration of fluoride anion and on addition of near about 3 equiv. of F^- anion both the intensity and overall pattern of emission spectrum closely resembled those of compound **L_1** (Figure 3.2B), so that the fluorescence intensity along with the maximum emission peak were fully regained. After addition of the F^- anion, the fluorescence emission response of the **L_1-Fe** complex was rapid (within 15 sec) and stable and thus the probe was robust and virtually rendered real-time monitoring of the target anion. Thus, the results of the spectroscopic studies indicated that the sensor **L_1** was regenerated during the detection procedure of fluoride anions.

In order to verify the reason of the fluorescence "off-on" property, the mass spectrum of the **L_1-Fe** system is also recorded in presence of F^-. The mass spectrum of the **L_1-Fe** system shows a molecular-ion peak at 542.069, corresponding to the mass of $[L_1 + Fe + 5H_2O + 2NO_3]^+$ (Appendix, Figure A3.2). While subsequent addition of F^- ions to the above solution gives a molecular ion peak at m/z 273.11 which confirmed the identity of free **L_1** and validated the mechanism of the sensing of fluoride anions (Appendix, Figure A3.10).

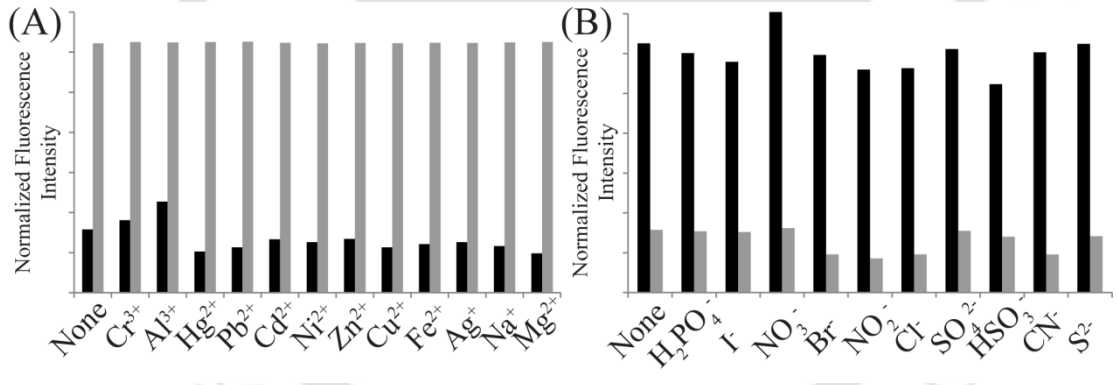

Figure 3.7 (A) Normalized fluorescence responses of **L_1** (10 μM) to various cations in mixed solvent system. The black bars represent the emission intensities of **L_1** in the presence of cations of interest (50 μM). The grey bars represent the change of the emission that occurs upon the subsequent addition of Fe^{3+} to the above solution; (B) Normalized fluorescence responses of **L_1-Fe** complex to various anions in mixed solvent system. The black bars represent the emission intensities of **L_1-Fe** in the presence of anions of interest (50 μM). The grey bars represent the change of the emission that occurs upon the subsequent addition of F^- to the above solution. The intensities were recorded at 472 nm.

The practical applicability of compound **L_1** and **L_1-Fe** complex as a Fe^{3+} and F^- selective fluorescent sensor was addressed by carrying out experiments in the presence of other competing cations and anions, which may interfere in estimation of iron and fluoride

(Figure 3.7). The receptor **L_1** and the **L_1-Fe** complex both exhibited exclusivity and were efficient in their sensing ability of the respective analytes from a competitive environment.

3.8. Biological studies of L_1 in presence of Fe^{3+} and F^-

The results obtained through solution-based fluorescence measurements with the ligand **L_1** were interesting and highlight the potential of the ligand to selectively detect Fe^{3+} at low levels. Given the relevance of iron in cellular physiology and its biomedical implications, it was conceived that that compound **L_1** could perhaps be explored for fluorescence-based detection of intracellular Fe^{3+}. In this regard, determination of cytotoxic effect of compound **L_1** and **L_1-Fe** complex on model human cells was pertinent, prior to pursuing sensing applications in cells. To this end, HeLa cells were treated with varying concentrations of compound **L_1** and **L_1-Fe** complex for a period of 24 h and the cytotoxic effect of the test compounds were ascertained by MTT assay. As evident from Figure 3.8, the essential observation was that compound **L_1** as well as **L_1-Fe** complex did not induce any pronounced effect on the viability of HeLa cells. With increase in the concentration of the tested compound, a marginal reduction in cell viability was observed and even at the highest tested concentration of both the compounds (60 µM), the cell viability was nearly 80%. The viability of HeLa cells was not influenced by neither the solvent (DMSO) nor the iron salt, substantiating that the observed cytotoxic effect could be attributed to the ligand **L_1** and **L_1-Fe** complex.

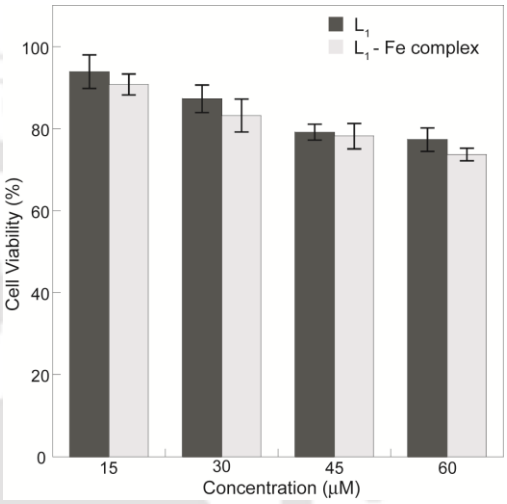

Figure 3.8 MTT assay to determine the cytotoxic effect of compound **L_1** and **L_1-Fe** complex on HeLa cells.

Based on the results obtained in the cytotoxic assay, it was conceived that compound **L_1** at a concentration below 15 µM could be used for fluorescence-based imaging studies in order to detect **L_1-Fe** complex in live cells. To pursue this goal, HeLa cells were treated with 10 µM **L_1** solution for 1 h followed by incubation with 10 µM $Fe(NO_3)_3$ to allow the formation of **L_1-Fe** complex. From our previous optical as well as mass spectroscopic studies, the binding stoichiometry between **L_1** and Fe^{3+} was found to be 1:1, and hence it can be reasonably presumed that the concentration of **L_1-Fe** complex formed in HeLa cells

would be much lower than the concentration (15 μM) at which a marginal cytotoxic effect of the complex was manifested (Figure 3.8).

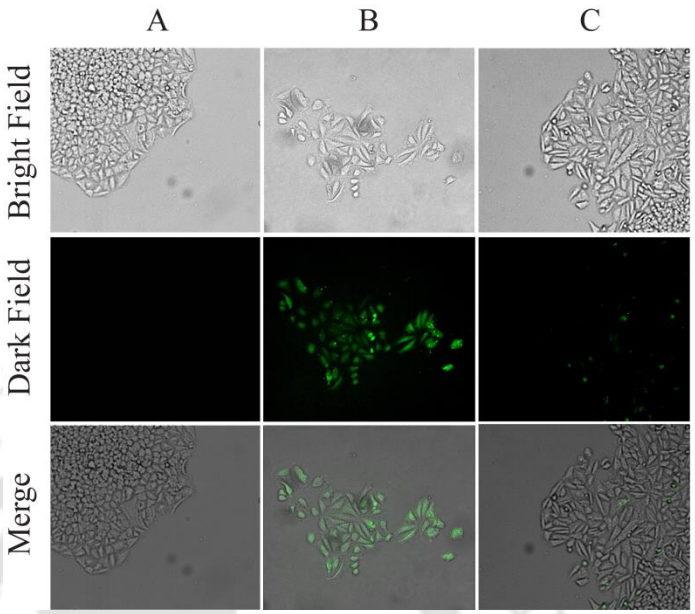

Figure 3.9 Fluorescence microscopic images of HeLa cells (A) after treating with 10 μM $\mathbf{L_1}$, (under blue light) (B) after adding 20 μM of Fe^{3+}, (under blue light) to the $\mathbf{L_1}$ treated cells (C) after adding 30 μM F^-, (under green light) to the ($\mathbf{L_1}$ + Fe^{3+}) treated cells. Scale bar for the images is 50 μm.

Fluorescence microscope analysis revealed that HeLa cells treated with compound $\mathbf{L_1}$ alone failed to exhibit any fluorescence emission (Figure 3.9, Panel A). Interestingly, on incubation with $Fe(NO_3)_3$, a switch-ON fluorescence was conspicuous inside HeLa cells, which indicated the formation of $\mathbf{L_1}$**-Fe** complex, as observed earlier in solution studies. It may also be mentioned here that the fluorescence was spread across the cell (Figure 3.9, Panel B). Fluoride sensing inside HeLa cells by $\mathbf{L_1}$**-Fe** complex could also be pursued as evident from the notable switch-OFF of the green fluorescence emission inside cells following incubation with KF solution (Figure 3.9, Panel C). Collectively, the result obtained from fluorescence microscopic analysis indicated that compound $\mathbf{L_1}$ could cross the membrane barrier, infuse into HeLa cells and efficiently sense intracellular Fe^{3+} and F^- even in the complex cellular milieu. Bright field images of HeLa cells indicated that the treated cells exhibited the characteristic morphological traits, which also suggested that the cells were viable. Collectively the results reflect interesting prospect for future *in vivo* biomedical applications of the sensor.

3.9. Conclusion

In conclusion, the work in this chapter describes the design and application of a fluorophoric receptor $\mathbf{L_1}$ which selectively binds with Fe^{3+} ions and triggers a switch ON response in optical and fluorescence spectra in the visible region. The recognition behaviour of $\mathbf{L_1}$ is evaluated in presence of various competitive metal ions in mixed aqueous media. The detection limit for Fe^{3+} was found to be much lower than the

permissible Fe^{3+} concentration in drinking water as per standard norms. Further, evaluation of the **L_1-Fe** complex prepared *in situ* demonstrated great promise for the detection of the Fe^{3+} ion in the presence of globular protein, serum and human serum albumin (HSA) solution. Anion dependent studies with **L_1-Fe** complex revealed that dissociation of the complex is possible selectively in presence of fluoride anion, which makes the **L_1-Fe** complex an efficient sensor for fluoride anions. The receptor **L_1** shows intense change in its fluorescence emission when bound to Fe^{3+} in physiological conditions. Hence, the effectiveness of compound **L_1** as a sensor for intracellular detection of Fe^{3+} by fluorescence microscopy was also studied. Moreover, the fluorescence microscopic analysis strongly suggested that compound **L_1** could readily permeate into HeLa cells and rapidly sense intracellular Fe^{3+} and F^-.

References

[3.1] B. Wang, J. Hai, Z. Liu, Q. Wang, Z. Yang and S. Sun, *Angew. Chem., Int. Ed.* 2010, **49**, 4576.

[3.2] O. Oter, K. Ertekin, C. Kirilmis, M. Koca and M. Ahmedzade, *Sens. Actuators, B,* 2007, **122**, 450.

[3.3] L. J. Fan and W. E. Jones, *J. Am. Chem. Soc.*, 2006, **128**, 6784.

[3.4] J. Mao, L. N. Wang, W. Dou, X. L. Tang, Y. Yan and W. S. Liu, *Org. Lett.*, 2007, **9**, 4567.

[3.5] C. R. Lohani and K. H. Lee, *Sens. Actuators, B*, 2010, **143**, 649.

[3.6] R. S. Eisenstein, *Annu. Rev. Nutr.*, 2000, **20**, 627.

[3.7] B. F. Matzanke, G. Muller-Matzanke and K. N. Raymond, Iron Carriers and Iron Proteins, VCH Publishers, New York, 1989, Vol. 5.

[3.8] N. C. Andrews, *N. Engl. J. Med.*, 1999, **341**, 1986.

[3.9] D. Touati, *Arch. Biochem. Biophys.*, 2000, **373**, 1.

[3.10] E. Beutler, V. Felitti, T. Gelbart and N. Ho, *Drug Metab. Dispos.*, 2001, **29**, 495.

[3.11] R. R. Crichton, Inorganic Biochemistry of Iron Metabolism: From Molecular Mechanisms to Clinical Consequences, 2nd ed., John Wiley & Sons, Chichester, 2001.

[3.12] L. Ma, W. Luo, P. J. Quinn, Z. Liu and R. C. Hider, *J. Med. Chem.*, 2004, **47**, 6349.

[3.13] R. Nudelman, O. Ardon, Y. Hadar, Y. Chen, J. Libman and A. Shanzer, *J. Med. Chem.*, 1998, **41**, 1671.

[3.14] H. Weizman, O. Ardon, B. Mester, J. Libman, O. Dwir, Y. Hadar, Y. Chen and A. Shanzer, *J. Am. Chem. Soc.*, 1996, **118**, 12368.

[3.15] D. P. Murale, S. T. Manjare, Y. S. Lee and D. G. Churchill, *Chem. Commun.*, 2014, **50**, 359.

[3.16] D. P. Murale, A. P. Singh, J. Lavoie, H. Liew, J. Cho, H. I. Lee, Y. H. Suh, D. G. Churchill, *Sensors and Actuators B*, 2013, **185**, 755.

[3.17] P. D. Beer and P. A. Gale, *Angew. Chem., Int. Ed.*, 2001, **40**, 486.

[3.18] R. Martinez-Manez and F. Sancenon, *Chem. Rev.*, 2003, **103**, 4419.

[3.19] E. Gazzano, L. Bergandi, C. Riganti, E. Aldieri, S. Doublier, C. Costamagna, A. Bosia and Ghigo, *Curr. Med. Chem.*, 2010, **17**, 2431.

[3.20] B. Spittle, Neurotoxic effects of fluoride, *Fluoride*, 2011, **44**, 117.

[3.21] P. Grandjean and P. J. Landrigan, *Lancet*, 2006, **368**, 2167.

[3.22] M. Cametti and K. Rissanen, *Chem. Commun.*, 2009, 2809.

[3.23] S.-D. Jeong, A. Nowak-Krol, Y. Kim, S.-J. Kim, D. T. Gryko and C.-H. Lee, *Chem. Commun.*, 2010, **46**, 8737.

[3.24] T. Mizuno, W.-H. Wei, L. R. Eller and J. L. Sessler, J. Am. Chem. Soc., 2002, **124**, 1134.

[3.25] J. Ren, Z. Wu, Y. Zhou, Y. Li and Z. Xu, *Dyes Pigm*., 2011, **91**, 442.

[3.26] P. Sokkalingam and C.-H. Lee, *J. Org. Chem.*, 2011, **76**, 3820.

[3.27] Y. Qu, J. Hua and H. Tian, *Org. Lett*., 2010, **12**, 3320.

[3.28] J. Wang, L. Yang, C. Hou and H. Cao, *Org. Biomol. Chem*., 2012, **10**, 6271.

[3.29] I.-S. Ke, M. Myahkostupov, F. N. Castellano and F. P. Gabbai, *J. Am. Chem. Soc.*, 2012, **134**, 15309.

[3.30] C. R. Cooper, N. Spencer and T. D. *Chem. Commun*., 1998, 1365.

[3.31] T. W. Hudnall and F. P. Gabbai, *J. Am. Chem. Soc*., 2007, **129**, 11978.

[3.32] H. N. Kim, M. H. Lee, H. J. Kim, J. S. Kim and J. Yoon, *Chem. Soc. Rev.*, 2008, **37**, 1465.

[3.33] R. McRae, P. Bagchi, S. Sumalekshmy and C. J. Fahrni, *Chem. Rev*. 2009, **109**, 4780.

[3.34] Z. Xu, J. Yoon and D. R. Spring, Fluorescent chemosensors for Zn2+, *Chem. Soc. Rev*., 2010, **39**, 1996.

[3.35] R. P. Haugland, Handbook of Fluorescent Probes and Research Chemicals, 9th ed., Molecular Probes, Eugene, OR, 2002.

[3.36] E. L. Que, D. W. Domaille and C. J. Chang, *Chem. Rev.*, 2008, **108**, 4328.

[3.37] B. Valeur and I. Leray, *Chem. Rev.*, 2000, **205**, 3.

[3.38] X. Peng, J. Du, J. Fan, J. Wang, Y. Wu, J. Zhao, S. Sun and T. Xu, *J. Am. Chem. Soc.*, 2007, **129**, 1500.

[3.39] S. Adsule, V. Barve, D. Chen, F. Ahmed, Q. P. Dou, S. Padhye and F. H. Sarkar, *J. Med. Chem.*, 2006, **49**, 7242.

[3.40] N. Aksuner, E. Henden, I. Yilmaz and A. Cukurovali, *Sensors and Actuators B,* 2008, **134**, 510.

[3.41] N. Aksuner, E. Henden, I. Yilmaz and A. Cukurovali, *Dyes and Pigments,* 2009, **83**, 211.

[3.42] Z. Yang, M. She, J. Zhang, X. Chen, Y. Huang, H. Zhu, P. Liu, J. Li and Z. Shi, *Sensors and Actuators B*, 2013, **176**, 482.

[3.43] L. Yang, W. Zhu, M. Fang, Q. Zhang and C. Li, *Spectrochimica Acta Part A: Molecular and Biomolecular Spectroscopy*, 2013, **109**, 186.

[3.44] M. Kumar, J. N. Babu and V. Bhalla, *J Incl Phenom Macrocycl Chem*., 2010, **66**, 139.

[3.45] L. Tang, F. Li, M. Liu and R. Nandhakumar, *Spectrochimica Acta Part A*, 2011, **78**, 1168.

[3.46] C. Kar, S. Samanta, S. Mukherjee, B. K. Datta, A. Ramesh and G. Das, *New J. Chem.*, 2014, **DOI:** 10.1039/C4NJ00239C

[3.47] M. Kumar and A. Puri, *Indian J Occup Environ Med.*, 2012**, 16**, 40.

[3.48] J. Kanner, J. B. German and J. E. Kinsella, *CRC Crit. Rev. Food Nutr.*, 1987, **25**, 317.

[3.49] R. E. Brantley, S. J. Smerdson, A. J. Wilkinson, E. W. Singleton and S. O. Otson, *J. Biol. Chem.*, 1993, **268**, 6995.

[3.50] P. Brown, O. Shalev and R. P. Hebbel, *Free Radical Biol. Med.*, 1998, **24**, 1040.

[3.51] S. R. Riberov and P. G. Bochev, Biochemistry and Biophysics, 1982, **213**, 288.

[3.52] H. Nick, *Curr. Opin. Chem. Biol.*, 2007**, 11**, 419.

[3.53] C. Hershko, G. Link and A. M. Konijn, Iron Chelation. In Molecular and Cellular Iron Transport; Templeton, D. M., Ed.; Marcel Dekker, Inc.: New York, 2002; 787.

Appendix

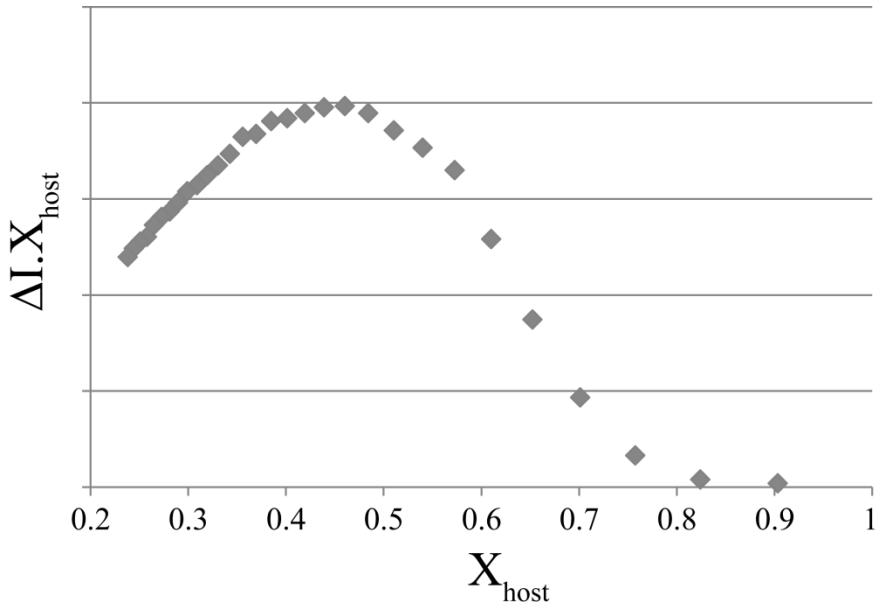

Figure A3.1: Job's plot between $\mathbf{L_1}$ and Fe^{3+} ions. Where X_{host} = the mole fraction of $\mathbf{L_1}$ and ΔI is the change $(I-I_0)$ in the intensity of the emission spectra in presence of guest.

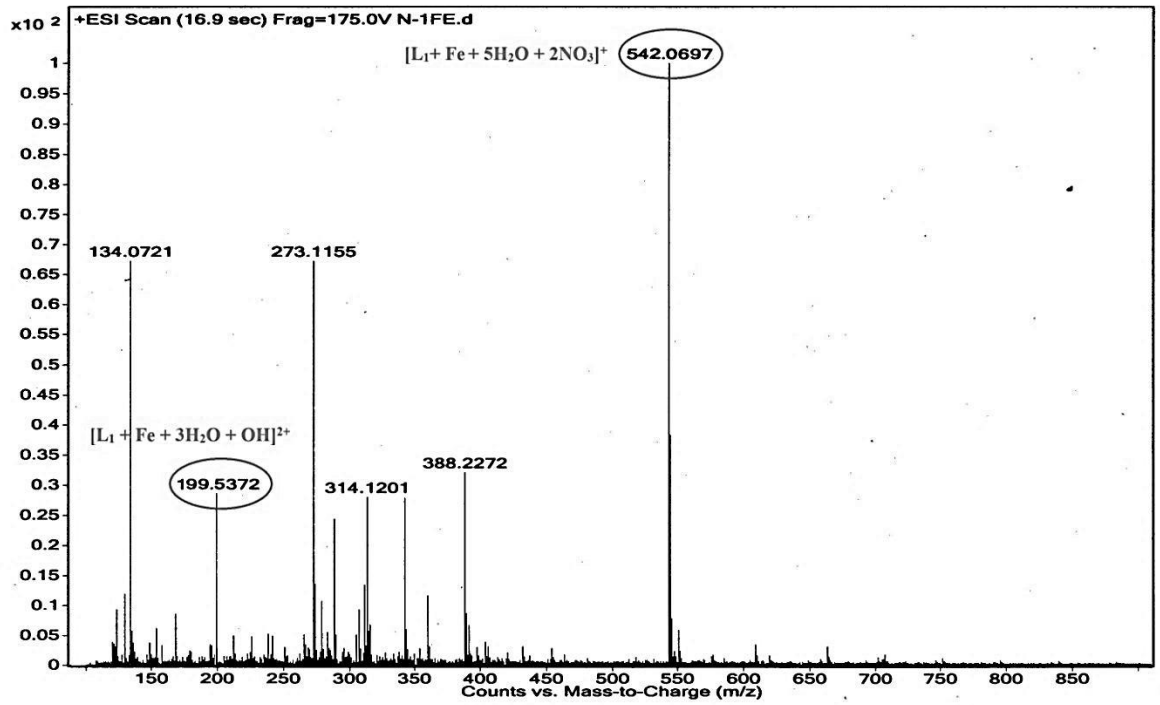

Figure A3.2: Mass spectrum of $\mathbf{L_1}$-Fe complex.

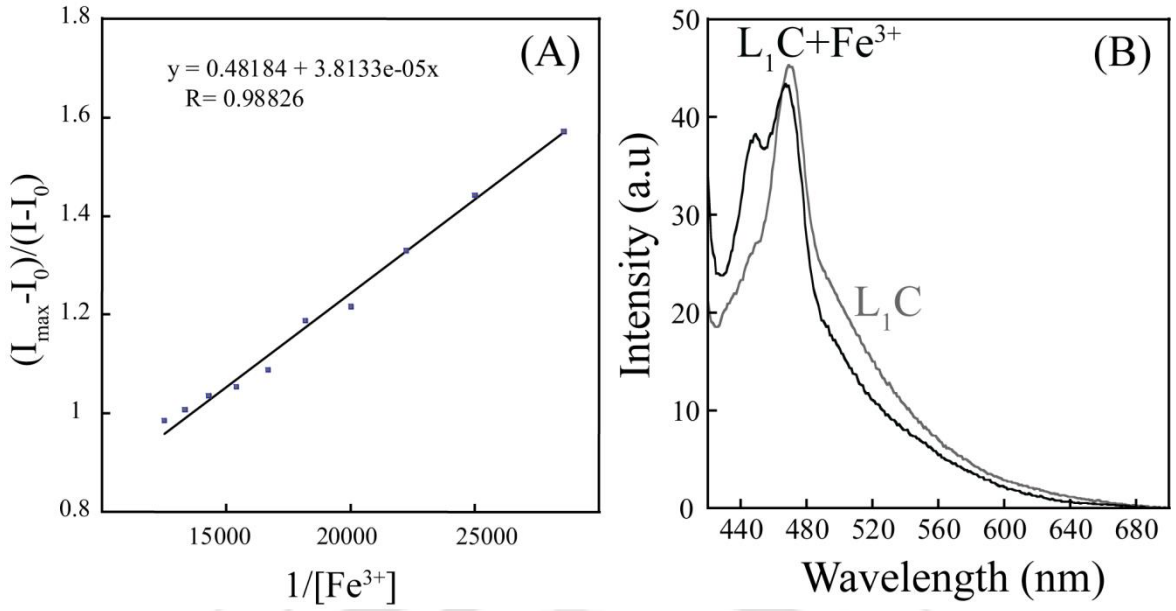

Figure A3.3: (A) Bensei-Hildebrand plot obtained from the fluorescence emission (calculated at λ_{em}) studies. (B) Changes of the of fluorescence emission of compound **L_1C** (10 μM) observed upon addition of 10 eqv. of Fe^{3+} ions.

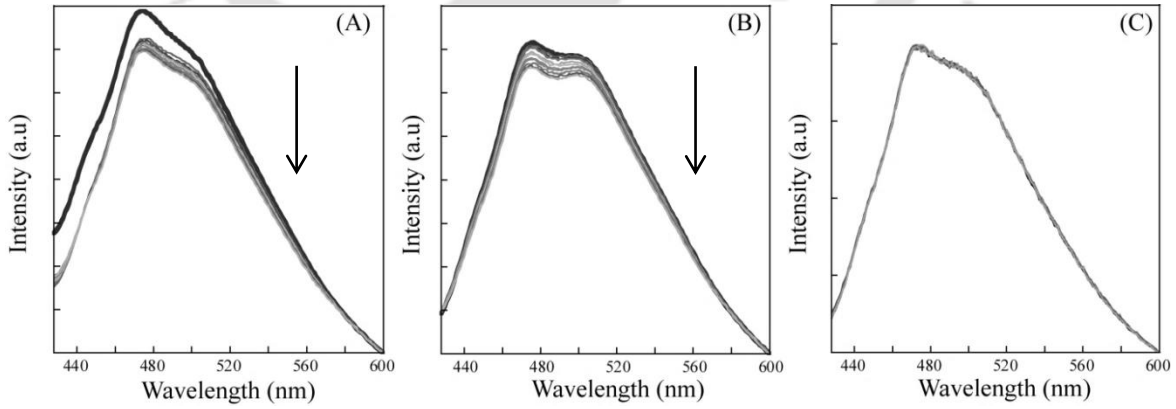

Figure A3.4: Changes in fluorescence intensity of **L_1-Fe** complex in present of different amounts of proteins. A) metHb B) FBS C)HSA

Occupied Orbitals	Energy (eV)	Vacant Orbitals	Energy (eV)
HOMO -2 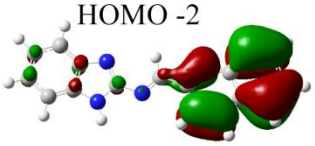	-6.5079	LUMO 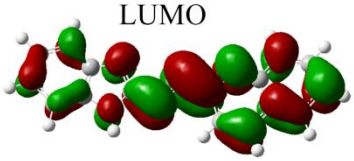	-2.2675
HOMO -1 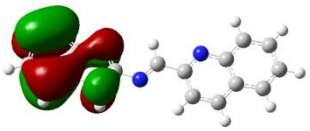	-6.1375	LUMO+1 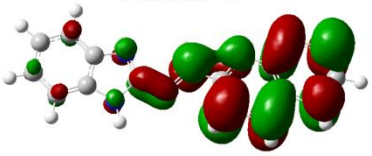	-1.2215
HOMO 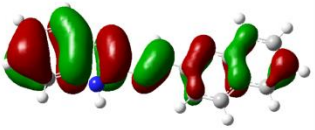	-5.7351	LUMO+2 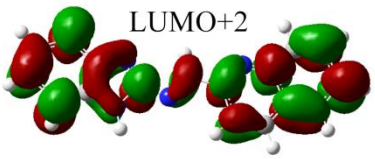	-0.1913

Figure A3.5: Selected orbitals and their energies for $\mathbf{L_1}$ at B3LYP/6-31G(d,p).

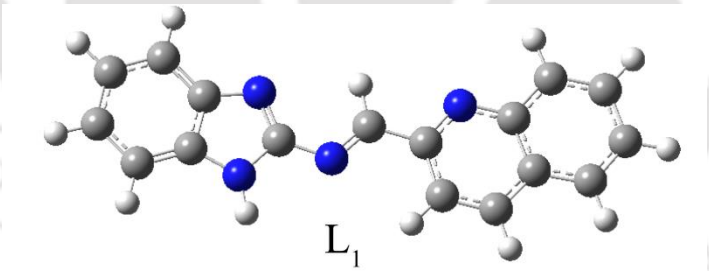

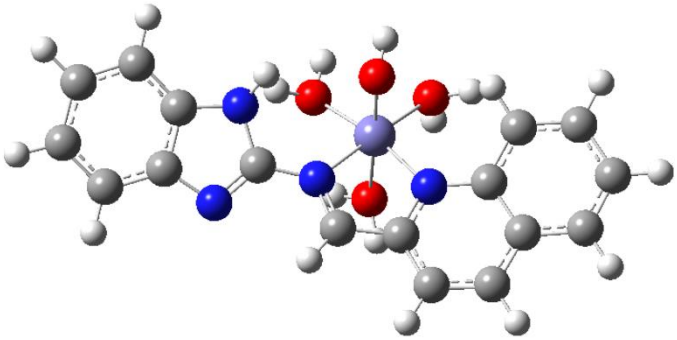

$[Fe\ (L_1)(H_2O)_3(OH)]^{2+}$

Figure A3.6: Optimized proposed structures of $\mathbf{L_1}$ and $\mathbf{L_1}$-**Fe** complex

Center Number	Atomic Number	Atomic Type	Coordinates (Angstroms) X	Y	Z
1	6	0	-3.94656	0.720773	-4.1E-05
2	6	0	-4.26671	-0.66523	0.000053
3	6	0	-5.58285	-1.13174	0.00014
4	6	0	-6.5881	-0.16937	0.000128
5	6	0	-6.29064	1.209949	0.000036
6	6	0	-4.97959	1.669673	-4.6E-05
7	6	0	-2.0726	-0.3138	-8.3E-05
8	1	0	-5.81569	-2.19214	0.000212
9	1	0	-7.62619	-0.48772	0.000194
10	1	0	-7.10828	1.924401	0.000029
11	1	0	-4.7455	2.729038	-0.00013
12	6	0	0.163272	0.188487	-0.0001
13	1	0	-0.06494	1.257634	-0.00014
14	6	0	1.587802	-0.16135	-6.5E-05
15	6	0	2.016518	-1.52101	-7.5E-05
16	6	0	3.76025	0.615636	0.000009
17	6	0	3.359969	-1.78914	-4.2E-05
18	1	0	1.267398	-2.30379	-0.00011
19	6	0	4.659107	1.716218	0.000063
20	6	0	4.290985	-0.71599	0.000003
21	1	0	3.726522	-2.8126	-4.2E-05
22	6	0	6.018967	1.504142	0.000097
23	1	0	4.233042	2.713918	0.000069
24	6	0	5.696156	-0.90023	0.000038
25	6	0	6.542237	0.187224	0.000083
26	1	0	6.70068	2.349384	0.000132
27	1	0	6.094457	-1.9115	0.000031
28	1	0	7.61787	0.038469	0.000111
29	7	0	2.423765	0.87028	-2.1E-05
30	7	0	-0.75155	-0.71853	-9.6E-05
31	7	0	-2.57876	0.904484	-0.00013
32	7	0	-3.04233	-1.29691	0.000017
33	1	0	-2.8465	-2.28576	0.000079

Rotational constants (GHZ): 1.505329 0.101277 0.094893

Figure A3.7: Coordinates for optimized geometry of $\mathbf{L_1}$ at B3LYP/6-31G(d,p).

Center Number	Atomic Number	Atomic Type	Coordinates (Angstroms) X	Y	Z
1	6	0	-4.15873	0.96518	0.058624
2	6	0	-4.04387	-0.2774	-0.62417
3	6	0	-5.14743	-0.95835	-1.12573
4	6	0	-6.38741	-0.35979	-0.90749
5	6	0	-6.52185	0.864597	-0.21098
6	6	0	-5.41918	1.54183	0.284585
7	6	0	-2.06922	0.548694	-0.0468
8	1	0	-5.06158	-1.89875	-1.65914
9	1	0	-7.28006	-0.85098	-1.28042
10	1	0	-7.51399	1.279179	-0.06941
11	1	0	-5.50995	2.483883	0.812994
12	6	0	-0.05761	1.74934	0.110683
13	1	0	-0.59263	2.695979	0.089735
14	6	0	1.384047	1.66554	0.110088
15	6	0	2.233869	2.785824	0.172073
16	6	0	3.176221	0.203706	-0.34455
17	6	0	3.594758	2.588729	0.053589
18	1	0	1.812779	3.774741	0.315311
19	6	0	3.646756	-1.04959	-0.81591
20	6	0	4.102871	1.300644	-0.23385
21	1	0	4.280507	3.426766	0.134536
22	6	0	4.990783	-1.22873	-1.07129
23	1	0	2.925221	-1.8003	-1.12181
24	6	0	5.482954	1.063142	-0.47188
25	6	0	5.922759	-0.18125	-0.86094
26	1	0	5.339208	-2.17593	-1.47089
27	1	0	6.179902	1.888831	-0.36782
28	1	0	6.976091	-0.354	-1.05275
29	7	0	1.853277	0.400553	-0.05177
30	7	0	-2.90799	1.44249	0.403666
31	1	0	-1.87089	-1.84777	0.677163
32	26	0	0.475353	-0.91925	0.375109
33	7	0	-0.69042	0.608062	0.051899
34	8	0	-1.01151	-2.05733	1.112838
35	1	0	-0.91034	-3.02223	1.139648
36	8	0	0.614449	-0.39574	2.390773
37	1	0	0.92487	0.462841	2.717628
38	1	0	-0.17004	-0.6339	2.911741
39	8	0	1.634875	-2.45562	0.987627
40	1	0	2.510655	-2.55784	0.574844
41	1	0	1.791403	-2.43868	1.946752
42	8	0	0.286139	-1.51757	-1.27376
43	1	0	0.351014	-2.48657	-1.32608
44	7	0	-2.66958	-0.58337	-0.62034
45	1	0	-2.2084	-1.04158	-1.40522

Rotational constants (GHZ): 0.490834 0.103481 0.094098

Figure A3.8: Coordinates for optimized geometry of $\mathbf{L_1}$ at B3LYP/6-31G(d,p)

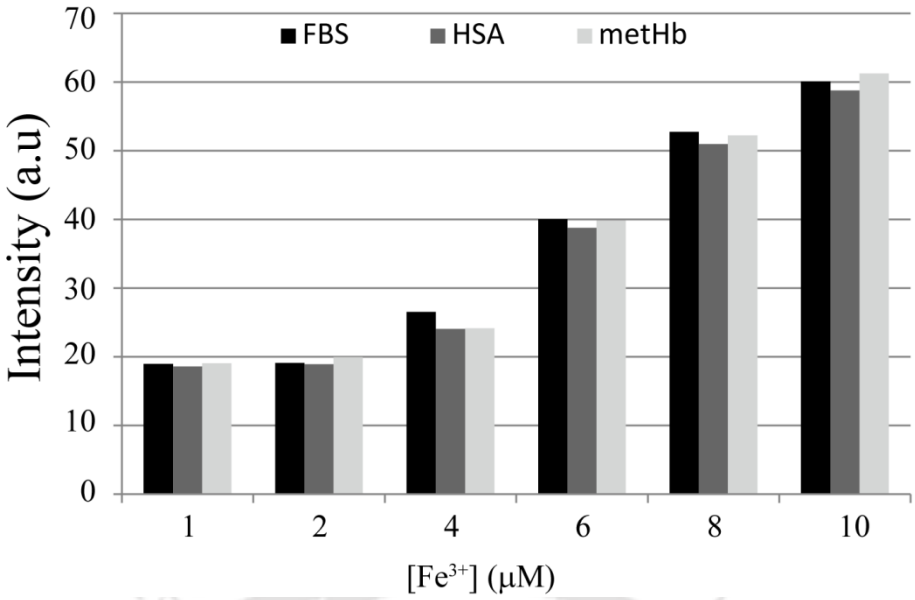

Figure A3.9: fluorescence emission (calculated at λ_{em}) of **L_1** on addition of increasing concentration of Fe^{3+} in different protein environment.

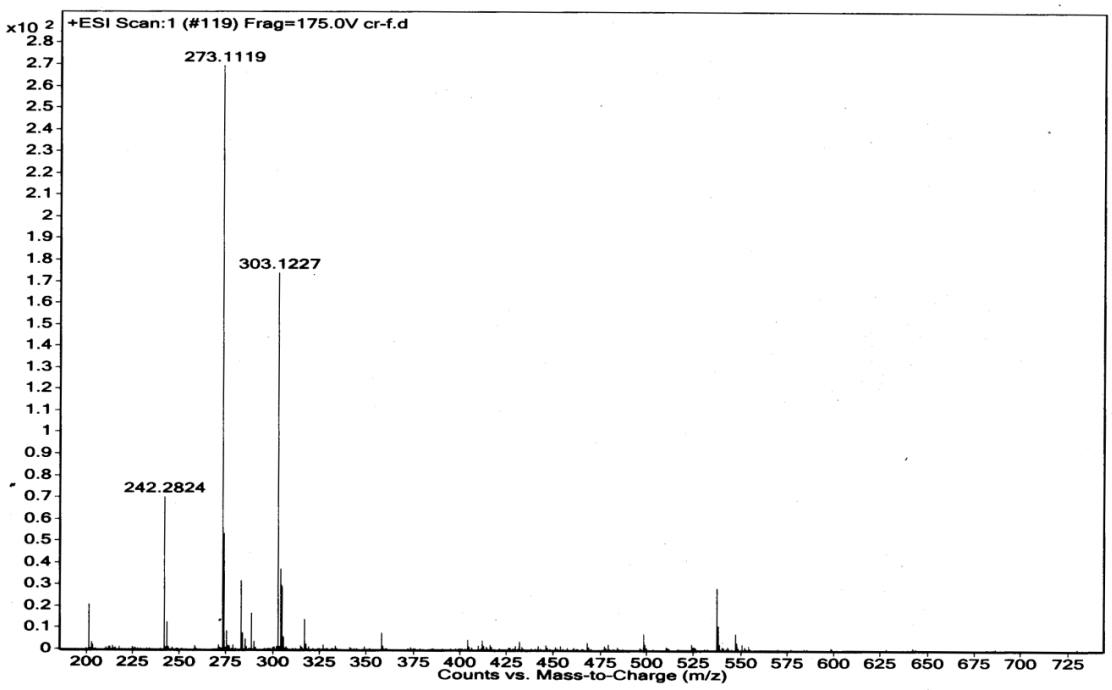

Figure A3.10: Mass spectrum of **L_1-Fe**+Fluoride

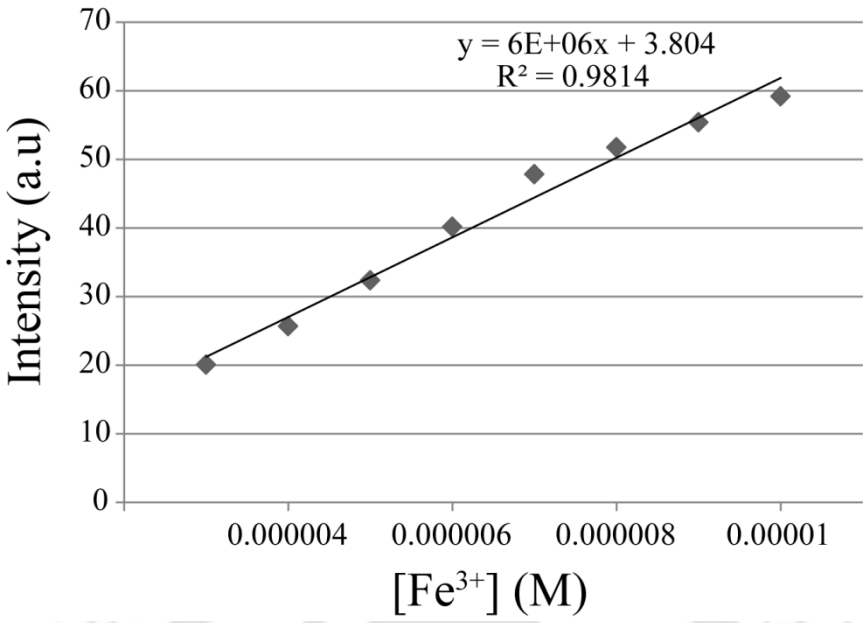

Figure A3.11 (A) Intensity versus Concentration plot for measuring the detection limit (3σ/k, here σ=0.99172) of Fe^{3+} by $\mathbf{L_1}$.

Table A3.1 selectivity coefficient of Fe^{3+} over other metal ions

Metal Ions	Selectivity Coefficient
$\mathbf{Al^{3+}}$	2.75
$\mathbf{Cu^{2+}}$	5.65
$\mathbf{Cr^{3+}}$	3.45
$\mathbf{Hg^{2+}}$	6.69
$\mathbf{Pb^{2+}}$	5.57
$\mathbf{Cd^{2+}}$	4.71
$\mathbf{Zn^{2+}}$	4.69
$\mathbf{Ni^{2+}}$	4.94
$\mathbf{Ag^{+}}$	5.22
$\mathbf{Na^{+}}$	5.36
$\mathbf{Mg^{2+}}$	6.36
$\mathbf{Fe^{2+}}$	4.94

Chapter 4

A CHEF based Ratiometric Sensor for Selective Detection of Cu^{2+} ions by Switch ON Yellow Fluorescence

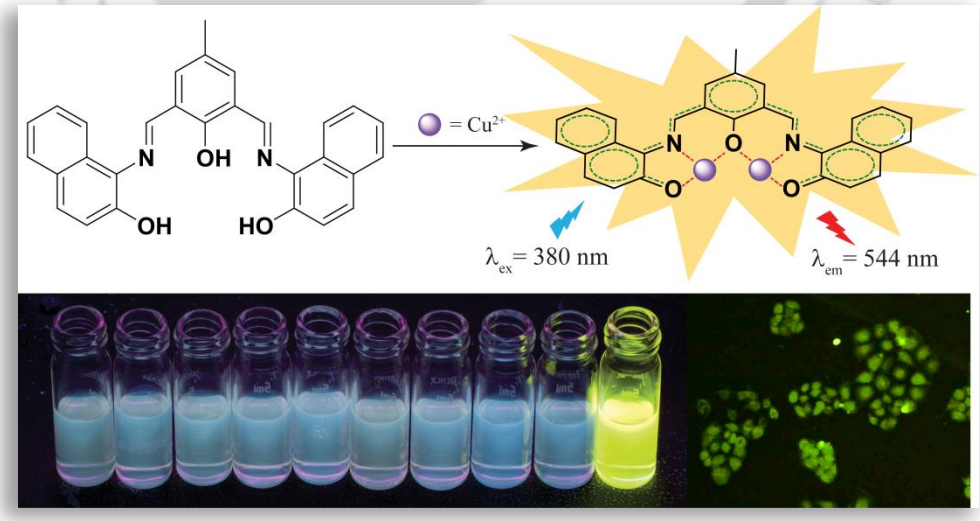

Chapter 4

4.1. Background and Focus of the Chapter

Copper is a critical element, whose regulation, efflux and homeostasis at the cellular level has significant implications on normal cellular physiology.[4.1-4.4] Additionally, Cu^{2+} is among the essential micronutrients for all known life forms.[4.5] Copper-containing enzymes play a significant role in different catalytic processes starting from providing energy for biochemical reactions to assisting the formation of cross-links in collagen and elastin, and thereby maintaining and repairing connective tissues related to heart and arteries.[4.6-4.11] Recently, it has been suggested that copper deficiency can increase the risk of developing coronary heart disease.[4.12-4.15] In addition to these crucial roles, Cu^{2+} could also behave as an ecological pollutant and could be potentially toxic to living cells if present in large concentrations. Excessive amounts of Cu^{2+} could lead to detrimental effects by causing oxidative stress and disorders associated with neurodegenerative diseases including Alzheimer's, Parkinson's, Menkes, Wilson's, prion diseases, hypoglycemia, dyslexia and infant liver damage.[4.16-4.28] Owing to the significant physiological relevance and associated biomedical implications, there is considerable interest in developing selective and sensitive copper sensors. However, the challenge is in the development of sensors which are biocompatible and functional in the complex biological environment.

For open-shell metal ions, such as copper (II), multiple nonemissive de-excitation pathways involving electron transfer or excited-state energy transfer are typically available to quench fluorescence.[4.29] Thus most of the techniques for accurate and selective detection of Cu^{2+} are based on chemosensors that undergo a fluorescence intensity quenching (turn-OFF) in presence of the analyte.[4.30-4.34] But in practical analysis turn ON methods are preferred over the turn OFF phenomena because other organic substances presence in the system may interfere with the detection of the analytes by quenching the fluorescence of the chemosensor. Moreover, Cu^{2+} ions are known to be extensively solvated in an aqueous medium, so the unfavorably high enthalpy of solvation poses a challenge to chemists in developing a suitable receptor for sensing of this ion in an aqueous environment. Although a number of chemosensors have been reported for Cu^{2+}

that show fluorescence enhancement,[4.35-4.42] but there are still only a few examples of "OFF-ON" type sensors available in aqueous systems.[4.43-4.49] Given this background, it is necessary to develop newer sensor molecules, which can be used for the efficient and selective detection of Cu^{2+} ions inside living system, even when present in trace quantities.

Fluorescence sensors that sense analyte by showing change in emission intensity at two different wavelengths has an added advantage because one can quantitively measure the analyte concentration by using the ratio of intensities of the well separated fluorescence peaks with rational intensities at two different wavelengths for free probe and analyte bound probe. A ratiometric probe allows a calibration curve to be determined *in vitro* that is independent of the sample conditions (e.g. concentration of the probe, sample thickness, intensity of illumination) and hence can be used to quantitate microscopy studies *in vivo*.[4.50] It can also be employed to rectify the systematic error introduced by interference of environmental conditions and background disturbances compared to a monosignal system.[4.51-4.54]

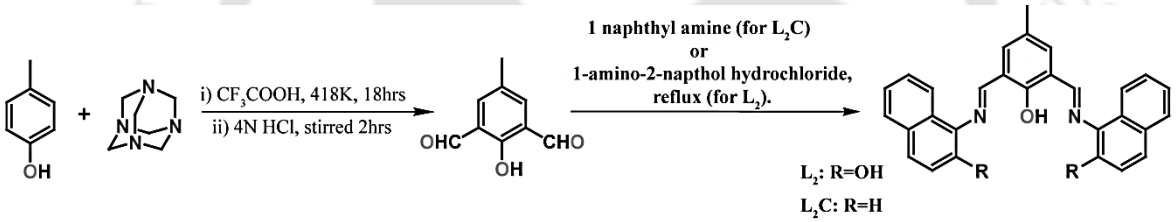

Scheme 4.1 Synthetic scheme for $\mathbf{L_2}$ and $\mathbf{L_2C}$

This chapter discuss the copper sensing capabilities of a 1-amino-2-naphthol functionalized conjugated fluorophoric Schiff base ligand $\mathbf{L_2}$ and the absorption and fluorescence behavior of $\mathbf{L_2}$ upon metal complexation.[4.55] We have reasonably chosen a conjugated system containing two naphthalene moieties as the fluorophore for designing the receptor $\mathbf{L_2}$; this compound display dual luminescence with two clearly resolved emission bands in the visible region from the locally excited (LE) state and a strongly red shifted long wavelength emitted by an internal charge-transfer (ICT) state. Three hydroxyl groups along with two imine nitrogen present in $\mathbf{L_2}$ offers excellent coordination sites for the binding of transition metal ions. Chelating mode of binding to Cu^{2+} by $\mathbf{L_2}$ restrict the molecule in a planar geometry which extends the conjugation of the π-electron throughout the molecule, which in turn triggers a switch ON yellow fluorescence response via chelation-enhanced fluorescence (CHEF) mechanism.

4.2. UV-Vis spectroscopic studies of L_2 in presence of Cu^{2+}

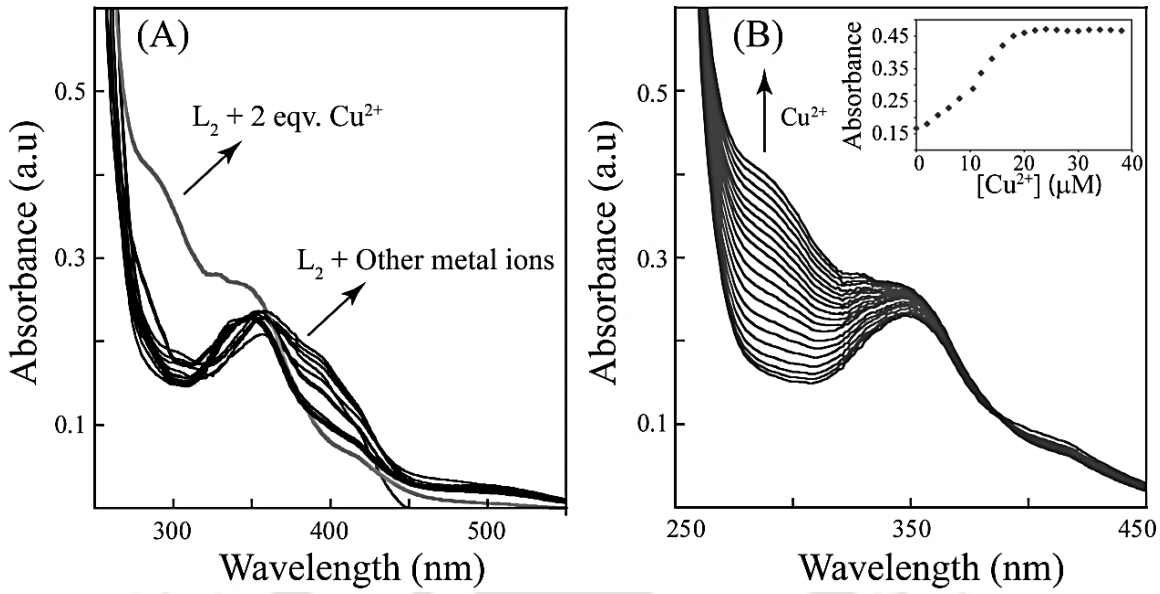

Figure 4.1 (A) UV/Vis absorption spectra of receptor $\mathbf{L_2}$ (10 μM) observed upon addition of 10 equivalent metal ions (perchlorate or nitrate salts of Na^+, K^+, Ca^{2+}, Mg^{2+}, Cr^{3+}, Hg^{2+}, Cu^{2+}, Pb^{2+}, Zn^{2+}, Fe^{3+}, Al^{3+}, Co^{2+}, Ni^{2+}, Cd^{2+}, and Ag^+) in a CH_3CN/aqueous HEPES buffer (1 mM, pH 7.3; 1:4 v/v). (B) UV/Vis titration spectra of $\mathbf{L_2}$ (10 μM) upon incremental addition of $Cu(ClO_4)_2$ in CH_3CN/aqueous HEPES buffer (1 mM, pH 7.3; 1:4 v/v).

The interaction of $\mathbf{L_2}$ with various metal ions was pursued through UV-visible absorption spectroscopy. As evident from Figure 4.1A, in case of the ligand $\mathbf{L_2}$ in CH_3CN/aqueous HEPES buffer (1 mM, pH 7.3; 1:4, v/v), an absorption maximum at 350 nm was recognized, which may be ascribed to intra-molecular π-π* charge transfer (CT) transition. Addition of Cu^{2+} to a solution of $\mathbf{L_2}$ led to the emergence of a hump near 290 nm. This may be accounted by the change in the orientation of the aromatic fluorophoric units in the ligand. It was pertinent to ascertain the selectivity of $\mathbf{L_2}$ for which perchlorate or nitrate salts of Na^+, K^+, Ca^{2+}, Mg^{2+}, Cr^{3+}, Hg^{2+}, Cu^{2+}, Pb^{2+}, Zn^{2+}, Fe^{2+}, Co^{2+}, Ni^{2+}, Cd^{2+}, and Ag^+ in CH_3CN/aqueous HEPES buffer (1 mM, pH 7.3; 1:4 v/v) were selected. As evident from Figure 4.1A, a conspicuous change in UV-vis spectral pattern was manifested only in presence of Cu^{2+}, while interaction with other metal ions failed to reveal any significant change in the absorption spectra of $\mathbf{L_2}$. In order to gain a quantitative insight of the specific interaction of Cu^{2+} and $\mathbf{L_2}$, a sequential titration of $\mathbf{L_2}$ with increasing Cu^{2+} (0 eqv. to 6 eqv. of Cu^{2+}) was pursued. As evident from Figure 4.1B, an absorption band appeared around 290 nm, which became prominent with incremental addition of Cu^{2+}. It may be mentioned that application of the ligand $\mathbf{L_2}$ rendered sensitive detection of Cu^{2+} in solution, with the detection limit of Cu^{2+} obtained from absorption measurements being

3.0 ppb. This level of detection was significant and considerably lower than the U.S. EPA maximum allowable limit for Cu^{2+} ions (1.3 ppm) in drinking water.

4.3. Fluorescence spectroscopic studies of L_2 in presence of Cu^{2+}

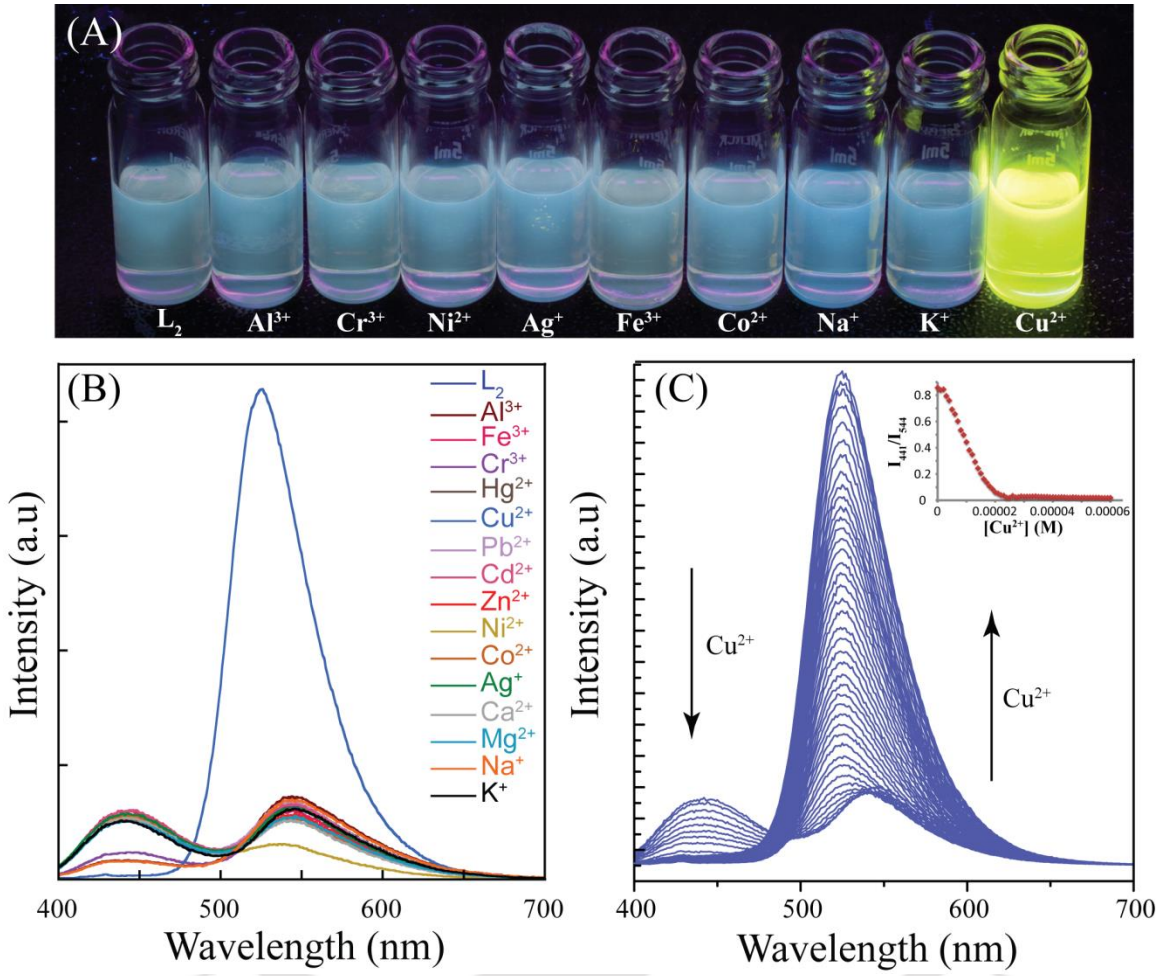

Figure 4.2 (A) Visual change in the fluorescence of $\mathbf{L_2}$ in presence of various metal ions (B) Changes in the fluorescence emission of receptor $\mathbf{L_2}$ (10 μM) observed upon addition of metal ions (10 equivalent). (C) Fluorescence titration spectra of $\mathbf{L_2}$ (10 μM) upon incremental addition of 6 equiv. of $Cu(ClO_4)_2$. **Inset:** Changes in the fluorescence intensity ratio (I_{441}/I_{544}) with incremental addition of Cu^{2+}.

The selectivity of $\mathbf{L_2}$ for Cu^{2+} was also studied by fluorescence emission spectroscopy of a solution of $\mathbf{L_2}$ (10 μM) in the absence and presence of an excess (10 equiv) of various metal ions in CH_3CN/aqueous HEPES buffer (1 mM, pH 7.3; 1:4 v/v). As evident from Figure 4.2B, two distinct emission maxima at 441 nm and 544 nm were discernible when a solution consisting of the ligand $\mathbf{L_2}$ was excited at 380 nm. These two clearly resolved emission bands in the visible region originated from the locally excited (LE) state and a strongly red shifted long wavelength emitted by an internal charge-transfer (ICT) state,

respectively. It was also observed that the emission bands displayed low intensity, which suggested lack of any highly conjugated system. Addition of Cu^{2+} to this receptor solution induced a significant switch ON fluorescence response near 544 nm, with a visual display of yellow fluorescence (Figure 4.2A). As evident from Figure 4.2B, the strong selectivity of **L_2** for Cu^{2+} captured through the prominent switch ON fluorescence was also substantiated by the fact that the ligand failed to reveal any noticeable spectral change following interaction with other metal ions (Na^+, K^+, Ca^{2+}, Mg^{2+}, Cr^{3+}, Hg^{2+}, Pb^{2+}, Zn^{2+}, Fe^{3+}, Co^{2+}, Ni^{2+}, Cd^{2+}, Al^{3+} and Ag^+). To obtain a nuanced understanding of the properties of **L_2** as a receptor for Cu^{2+}, a titration of the receptor was performed with increasing concentration of Cu^{2+}. As observed in Figure 4.2C, incremental addition of Cu^{2+} ions resulted in a striking ratiometric change in the emission signal of **L_2**. The fluorescence emission titration studies indicated that the receptor **L_2** rendered a broad dynamic range for quantitative estimation of Cu^{2+} with near about 10 fold increase of its fluorescence intensity at 544 nm and a simultaneous decrease in the lower wavelength emission band (441 nm) upon addition of only 6.0 eqv of Cu^{2+} ions. It is worth mentioning that the increment in the fluorescence intensity near 544 nm was also accompanied by minor blue shift of the peak (upto 20 nm) which was perhaps due to the change of the charge-transfer character of the emissive species.

Under the optimum conditions, the change in the fluorescence intensity of **L_2** at 441 nm wavelength had a linear relationship with the concentration of Cu^{2+} over the range of 1 to 24 µM whereas the intensity at 544 nm exhibited a prominent linear relationship with increasing concentration of Cu^{2+} over the range of 22 to 60 µM. Thus **L_2** (10 µM) can act as an efficient sensor for an overall range of 1 to 60 µM. The individual linear calibration curves are indicated in Figure A4.2.

The inset in Figure 4.2C indicates the correlation of the intensity ratios of emission at 441 nm to that at 544 nm (I_{441}/I_{544}) to the concentration of Cu^{2+}. It is evident that ratiometric measurements of the fluorescence emission intensity of **L_2** provided a linear window of estimation of Cu^{2+} and afforded ultrasensitive detection of the metal ion. Further, the ratiometric assay can be used to generate a calibration curve for sensitive detection of Cu^{2+} concentration, independent of the ligand concentration. This feature enhances the merit of the ligand as an analytical tool and augers well for quantitative estimation of Cu^{2+} in an unknown sample. Further, from the inset in Figure 4.2C, a bend of the curve at 2 equivalent of added Cu^{2+} was evident, which suggested a 1:2 stoichiometry of the **L_2** /Cu^{2+}

adduct. This stoichiometry was also established with the help of job's plot (Appendix, Figure A4.3) and further corroborated by ESI-MS studies (Appendix, Figure A4.4), which indicated the presence of a molecular-ion peak at m/z 623.04, corresponding to the mass of $[(L_2\text{-}3H) + 2Cu^{2+} + 3H_2O]^+$. The Benesi–Hildebrand (B–H) plot of $1/ [I- I_0]$ vs. $1/[Cu^{2+}]^2$ for the titration of $\mathbf{L_2}$ and Cu^{2+} ion provided a straight line (Appendix, Figure A4.5), indicating 1: 2 complex formation with association constant (K) being 9.13 X 10^8 M^{-1}. It is significant to mention that the detection limit of $\mathbf{L_2}$ for Cu^{2+} ions was found to be 10^{-8} M level, which was significantly lower than the U.S. EPA maximum allowable limit for Cu^{2+} ions (1.3 ppm) in drinking water. Although all the fluorescence experiments were performed at room temperature (25°C) but temperature dependent studies (Appendix, Figure A4.6) with $\mathbf{L_2}$ shows that the system retains its sensing property even at 60°C.

The precision of the process was tested by individually preparing ten solutions, all in CH_3CN/aqueous HEPES buffer (1 mM, pH 7.3; 1:4 v/v) and each containing the same quantity of ligand and metal ions. The precision were expressed in terms of the coefficient of variation, for solutions containing 1 ppm and 10 ppm of Cu^{2+} ions. The solutions containing 1 ppm and 10 ppm of Cu^{2+} ions were shaken for one minute and allowed to stand for 10 minutes. The precision for the 1 ppm solution was found to be 0.024 and for the 10 ppm solution it was 0.011.

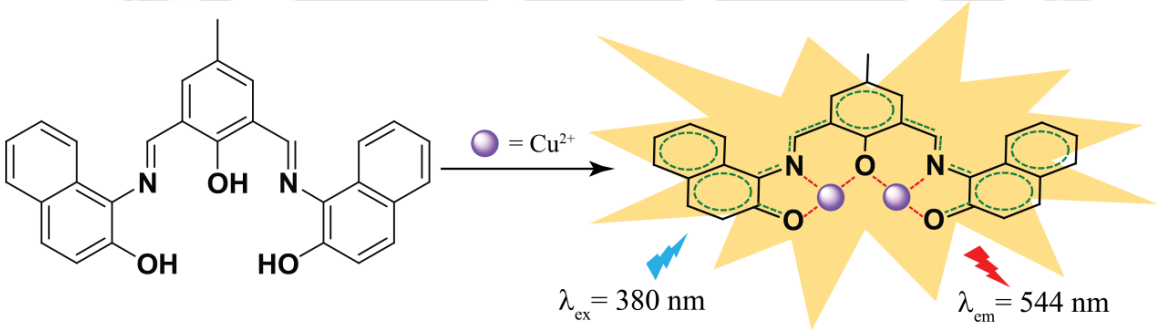

Scheme 4.2 Schematic representation of Cu^{2+} binding and sensing event by receptor $\mathbf{L_2}$.

In the context of Cu^{2+} binding by receptor $\mathbf{L_2}$ it may be construed that the OH groups of $\mathbf{L_2}$ undergo deprotonation in presence of Cu^{2+} ions and strengthen the interaction between coordinated Cu^{2+} and the fluorophore $\mathbf{L_2}$. It is well documented in the literature that receptor like $\mathbf{L_2}$ forms binuclear metal complexes by a phenoxy bridged linkage.[4.56,4.57] Due to the formation of Cu^{2+} coordinated complex (see appendix Figure A4.5), the molecule has a propensity to attain a planar geometry. The subsequent charge transfer throughout the π-system is thus facilitated, leading to a highly conjugated geometry and a

radical enhancement of the fluorescence intensity, which enables colorimetric and ratiometric detection of Cu^{2+} ions (Scheme 4.2).

To further establish the significance of the –OH groups of the naphthalene units as effective binding sites for Cu^{2+} and to probe their role in maintaining planar configuration of $\mathbf{L_2}$-Cu^{2+} complex, a control compound $\mathbf{L_2C}$ was synthesized, devoid of the hydroxyl groups in the naphthalene units. Metal dependent fluorescence studies with $\mathbf{L_2C}$ failed to reveal any observable increment in the emission spectra even in presence of large amount of Cu^{2+} ions (Appendix, Figure A4.7), which suggested that the presence of the hydroxyl groups in the naphthalene units are critical for achieving the planar geometry and sensing Cu^{2+} ions.

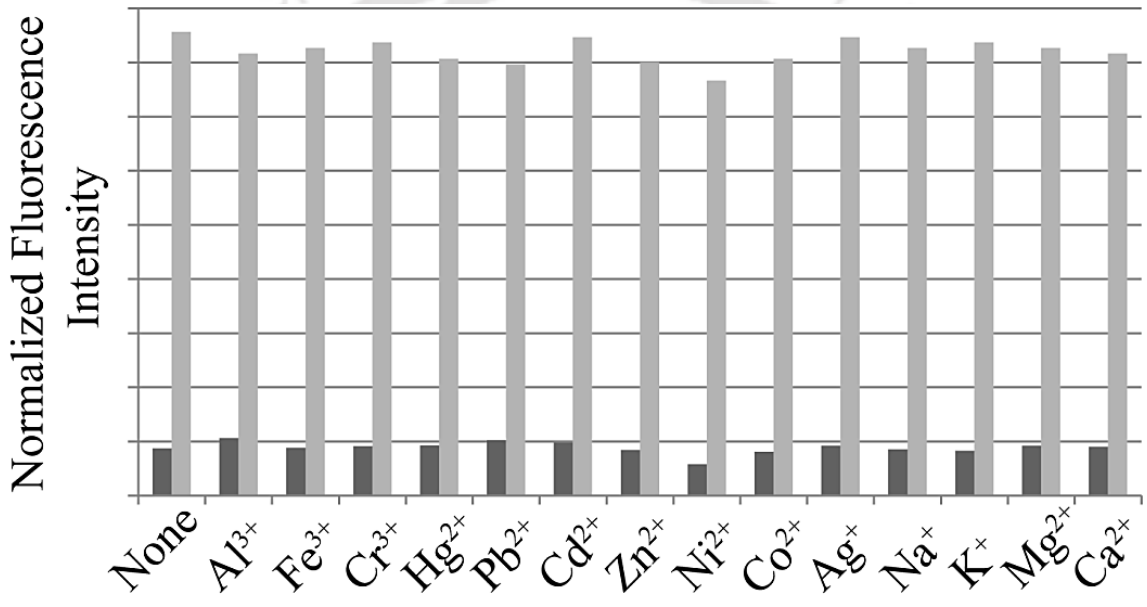

Figure 4.3 Normalized fluorescence responses of $\mathbf{L_2}$ (10 μM) to various cations in CH_3CN/aqueous HEPES buffer (1 mM, pH 7.3; 1:4 v/v). The black bars represent the emission intensities of $\mathbf{L_2}$ in the presence of cations of interest (50 μM). The grey bars represent the change of the emission that occurs upon the subsequent addition of Cu^{2+} to the above solution.

The sensitive detection of Cu^{2+} in aqueous solution afforded with $\mathbf{L_2}$ was encouraging and the results suggested that the ligand can perhaps be deployed for selective probing of Cu^{2+} in complex samples. To validate this hypothesis, the selectivity of $\mathbf{L_2}$ was further tested in presence of other competing cations, which may interfere with the estimation of Cu^{2+} (The selectivity coefficients of Cu^{2+} over other metal ions are shown in Table A1 of the Appendix). Interestingly, even in the presence of various interfering cationic species, interaction of Cu^{2+} with $\mathbf{L_2}$ resulted in a ratiometric change in the fluorescence signal of the ligand, which was unequivocally observed for every cation and the magnitude of the

normalized fluorescence intensity was nearly equivalent for all the samples (Figure 4.3). This result clearly reflects the excellent discrimination of Cu^{2+} rendered by the ligand even in the presence of competing metal ions and presents an exciting prospect of using the ligand for selective probing of Cu^{2+} in biological samples. As the system is intended for potential application in biological system, the influence of some biological coexisting species was also ascertained (*viz*. Bovine serum albumin and fetal bovine serum) in the sensing behaviour of the metal ion (Appendix, Figure A4.8).

4.4. Potential applicability of L_2 in the analysis of Cu^{2+}.

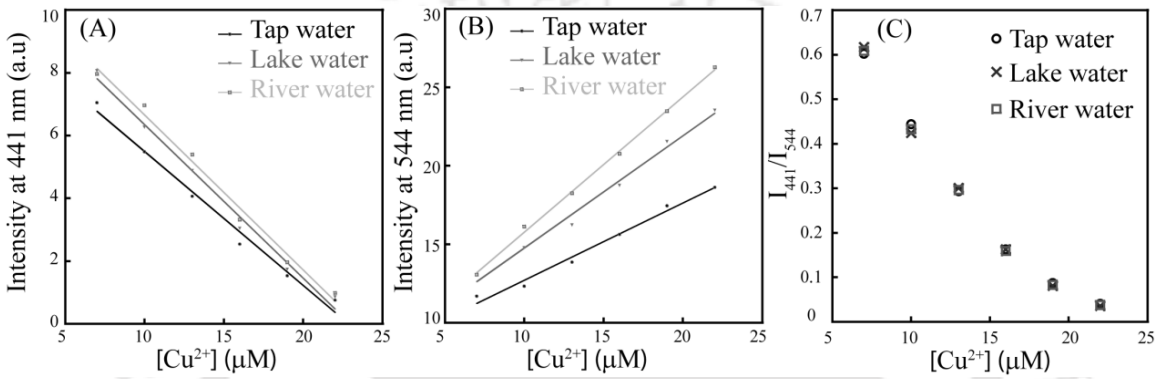

Figure 4.4 (A) Linear fluorescence intensities of $\mathbf{L_2}$ (10 μM) at 441 nm wavelength upon addition of Cu^{2+} (7–21 M) in three natural water samples. (B) Linear fluorescence intensities of $\mathbf{L_2}$ (10 μM) at 544 nm wavelength upon addition of Cu^{2+} (7–21 M) in three natural water samples. (C) The ratio (I_{441}/I_{544}) of fluorescence intensities of $\mathbf{L_2}$ (10 μM) upon addition of Cu^{2+} (7–21 M) in three natural water samples.

The potential utility of $\mathbf{L_2}$ in sensing Cu^{2+} was also checked using complex environmental samples. Tap, lake and river water were collected from laboratory, the pool of serpentine lake in IIT Guwahati, and Brahmaputra river (Kamrup district, Assam), respectively. Cu^{2+} (7-21 μM) were spiked into these samples before the addition of $\mathbf{L_2}$ (10 μM). The results of the fluorescence spectroscopic measurements observed from this study are depicted in Figure 4.4. The changes in fluorescence intensities corresponding to both the wavelengths (441 nm and 544 nm) were proportional to the concentrations of Cu^{2+} in the range of 7-21 μM. From figure 4.4A and figure 4.4B the drawback of the individual calibration curves to determine the concentration of the analyte in water from different sources can be easily understood. Although the presence of Cu^{2+} ions in different sources can be easily detected from the characteristic changes in the fluorescence intensity but the quantitative estimation of the analytes are not possible from the above mentioned curves. However, the ratios of the intensities at two different wavelength (441 nm/544 nm) are constant for a definite

concentration of added Cu^{2+} ion, and thus from the ratiometric calibration curve indicated in figure 4.4C we can easily determine the quantity of the analyte, which also endorses the advantage of ratiometric calibration curve over the individual calibration curves.

4. 5. Biological studies of L_2 in presence of Cu^{2+}.

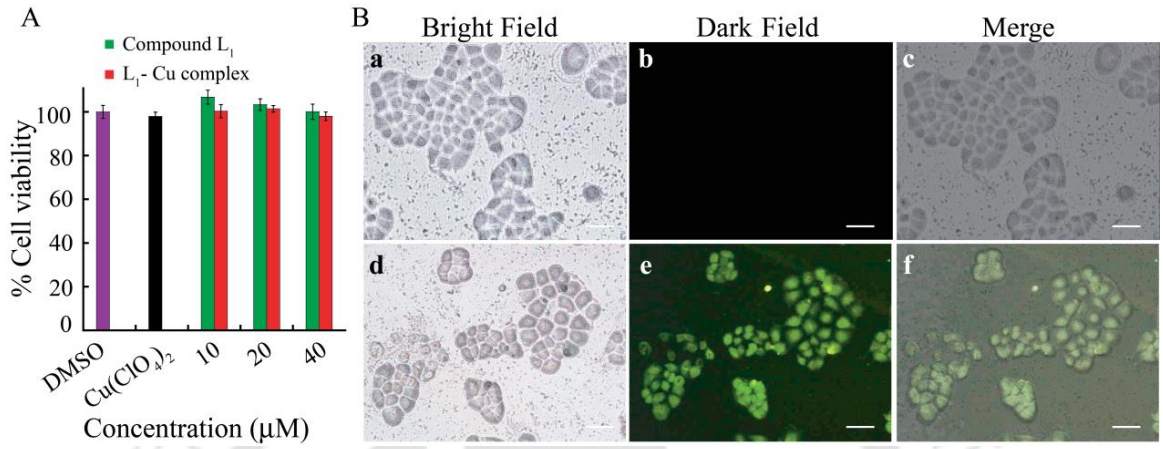

Figure 4.5 (A) MTT assay to determine the cytotoxic effect of compound $\mathbf{L_2}$ and $\mathbf{L_2}$ **-Cu** complex on HeLa cells. (B) Fluorescence microscopic images of HeLa cells after adding 10 μM of $\mathbf{L_2}$ (panel a-c) and after subsequent treatment with 20 μM Cu^{2+}, (panel d-f).

Given the profound physiological implications of cellular copper pool, there is considerable motivation in developing novel probes for detecting intracellular levels of copper. Considering the fact that biological samples constitute a complex milieu, the selectivity and sensitivity of the probe would be critical. An additional challenge is to design a sensor, which is biocompatible and can detect target analyte at low levels. In our study, the results obtained through solution-based fluorescence measurements with the ligand $\mathbf{L_2}$ were encouraging as they clearly demonstrated the prospect of the ligand to selectively detect Cu^{2+} at low levels. To ascertain the true potential of the ligand $\mathbf{L_2}$ for sensing intracellular Cu^{2+} levels and to have a rational measure of its biocompatibility, it was pertinent to initially determine the cytotoxic effect of $\mathbf{L_2}$ as well as the $\mathbf{L_2}$**-Cu** complex. A standard MTT assay revealed that both $\mathbf{L_2}$ and $\mathbf{L_2}$**-Cu** complex failed to exert any adverse effect on the viability of cultured HeLa cells, even upto a tested concentration of 40 μM (Figure 4.5A). The non-cytotoxic nature of the ligand $\mathbf{L_2}$ is a favorable attribute in the context of bio-sensing, since the developed sensor is not only selective for Cu^{2+} but is also amenable to non-destructive analysis of cellular levels of the metal ion. Encouraged by the biocompatibility of $\mathbf{L_2}$, we evaluated its potential as a sensor for intracellular detection of Cu^{2+} through fluorescence microscopy. When HeLa cells were treated with 10

μM **L_2**, the cells failed to display any fluorescence (Figure 4.5B, Panel b). Interestingly, when the cells were subsequently exposed to 20 μM $Cu(ClO_4)_2$, a dramatic switch-ON yellowish green fluorescence was conspicuous (Figure 4.5B, Panel e), indicating selective sensing of Cu^{2+} in cells. It was also observed that the fluorescence was distributed across the cell and not spatially restricted. This suggested that the ligand **L_2** could readily pervade through the membrane and suffuse HeLa cells, and upon subsequent addition of $Cu(ClO_4)_2$, formation of **L_2-Cu** complex ensued throughout the cell. It is also worthwhile to mention that HeLa cells retained their characteristic morphological traits during treatment with the ligand and $Cu(ClO_4)_2$ as evident from the bright field images of treated cells (Figure 4.5B, Panels a and d). This was an indication that the ligand **L_2** as well as **L_2-Cu** complex were not cytotoxic to HeLa cells, reiterating earlier results of the MTT assay.

Collectively, the findings of the cytotoxicity assay and fluorescence-based cell imaging are encouraging for future diagnostic applications of the sensor. Given the fact that exogenously added ligand **L_2** and **L_2-Cu** complex were found to be non-cytotoxic to HeLa cells even after 24 h interaction period, the copper probe **L_2** developed in the present study holds interesting prospect in specific biomedical domain applications which demand prolonged analysis time.

4. 6. Conclusion

In summary, this chapter discuss the development of a Cu^{2+} sensitive receptor probe **L_2** which selectively binds with Cu^{2+} ions and impels a switch ON response in optical and fluorescence spectra in the visible region, which makes it a dual probe for naked eye detection of analyte through change in color and fluorescence. Apart from the changes in the UV-Vis spectra the fluorescence response at two different wavelengths makes it an efficient ratiometric sensor for the detection of Cu^{2+} ions. The detection limit for Cu^{2+} was found to be much lower than the permissible Cu^{2+} concentration in drinking water as per standard norms. The receptor **L_2** shows intense change in its fluorescence emission when bound to Cu^{2+} in physiological conditions. Hence, the effectiveness of compound **L_2** as a probe for intracellular detection of Cu^{2+} by fluorescence microscopy was also studied. Moreover, the fluorescence microscopic analysis strongly suggested that compound **L_2** could readily cross the membrane barrier, permeate into HeLa cells and rapidly sense intracellular Cu^{2+}. Thus, with regard to analogous studies related to Cu(II) signaling systems, our work presents the added advantages of high detection limit, quantitive measurement of the analyte concentration by using the ratio of intensities of the well

separated fluorescence peaks and the non-cytotoxic character of the ligand and the metal-ligand complex. In future, it is envisaged that the biocompatible feature of the developed sensor may be exploited to monitor intracellular flux of Cu^{2+} *in vivo* for extended periods in order to achieve a better understanding of the patho-physiological implications of copper homeostasis.

References

[4.1] M. L. Turski and D. J. Thiele, *J. Biol. Chem.*, 2009, **284**, 717.

[4.2] L. Banci, I. Bertini, S. Ciofi-Baffoni, T. Kozyreva, K. Zovo and P. Paulmaa, *Nature*, 2010, **465**, 645.

[4.3] E. L. Que, D. W. Domaille and C. J. Chang, *Chem. Rev.*, 2008, **108**, 1517.

[4.4] H. Kozlowski, A. Janicka Klos, J. Brasun, E. Gaggelli, D. Valensin and G. Valensin, *Coord. Chem. Rev.*, 2009, **253**, 2665.

[4.5] S. J. Lippard and J. M. Berg, Principles of Bioinorganic Chemistry; University Science Books: Mill Valley, CA, 1994.

[4.6] E. Gaggelli, H. Kozlowski, D. Valensin and G. Valensin, *Chem. Rev.*, 2006, **106**, 1995.

[4.7] T. V. O. Halloran and V. C. Culotta, *J. Biol. Chem.*, 2000, **275**, 25057.

[4.8] A. C. Rosenzweig and T. V. O. Halloran, *Curr. Opin. Chem. Biol.* 2000, **4**, 140.

[4.9] A. Singh, Q. Yao, L. Tong, W. C. Still and D. Sames, *Tetrahedron Lett.*, 2000, **41**, 9601.

[4.10] S. Puig and D. J. Thiele, *Curr. Opin. Chem. Biol.*, 2002, **6**, 171.

[4.11] F. Arnesano, L. Banci, I. Bertini and S. Ciofi-Baffoni, *Eur. J. Inorg. Chem.*, 2004, 1583.

[4.12] D. Y. Sasaki, D. R. Shnek, D. W. Pack and F. H. Arnold, *Angew. Chem., Int. Ed.*, 1995, **34**, 905.

[4.13] R. Kramer, *Angew. Chem. Int. Ed.*, 1998, **37**, 772.

[4.14] A. Torrado, G. K. Walkup and B. Imperiali, *J. Am. Chem. Soc.*, 1998, **120**, 609.

[4.15] P. Grandini, F. Mancin,; P. Tecilla, P. Scrimin and U. Tonellato, *Angew. Chem. Int. Ed.*, 1999, **38**, 3061.

[4.16] C. Vulpe, B. Levinson, S. Whitney, S. Packman and J. Gitschier, *Nat. Genet.*, 1993, **3**, 7.

[4.17] D. J. Waggoner, T. B. Bartnikas and J. D. Gitlin, *Neurobiol. Dis.*, 1999, **6**, 221.

[4.18] J. S. Valentine and P. J. Hart, *Proc. Natl. Acad. Sci. USA*, 2003, **100**, 3617.

[4.19] D. R. Brown and H. Kozlowski, *Dalton Trans.*, 2004, 1907.

[4.20] K. J. Barnham, C. L. Masters and A. I. Bush, *Nat. Rev. Drug Discov.*, 2004, **3**, 205.

[4.21] B. E. Kim, T. Nevitt and D. J. Thiele, *Nat. Chem. Biol.*, 2008, **4**, 176.

[4.22] G. J. Brewer, *Curr. Opin. Chem. Biol.*, 2003, **7**, 207.

[4.23] G. L. Millhauser, *Acc. Chem. Res.*, 2004, **37**, 79.

[4.24] S. P. Leach, M. D. Salman and D. Hamar, *Anim. Health Res. Rev.*, 2006, **7**, 97.

[4.25] K. J. Barnham and A. I. Bush, *Curr. Opin. Chem. Biol*., 2008, **12**, 222.

[4.26] R. R. Crichton, D. T. Dexter and R. J. Ward, *Coord. Chem. Rev.*, 2008, **252**, 1189.

[4.27] M. C. Linder and M. Hazegh-Azam, *Am. J. Clim. Nutr*., 1996, **63**, 797S.

[4.28] R. Uauy, M. Olivares and M. Gonzalez, *Am. J. Clim. Nutr*., 1998, **67**, 952S.

[4.29] R. Bergonzi, L. Fabbrizzi, M. Licchelli and C. Mangano, *Coord. Chem. Rev.*, 1998, **170**, 31.

[4.30] Z. C. Liu, Z. Y. Yang, T. R. Li, B. D. Wang, Y. Li, D. D. Qin, M. F. Wang and M. H. Yan, *Dalton Trans.*, 2011, **40**, 9370.

[4.31] S. H. Kim, J. S. Kim, S. M. Park and S. K. Chang, *Org. Lett.*, 2006, **8**, 371.

[4.32] H. S. Jung, , P. S. Kwon, J. W. Lee, J. I. Kim, C. S. Hong, J. W. Kim, S. H. Yan, J. Y. Lee, J. H. Lee, T. H. Joo and J. S. Kim, *J. Am. Chem. Soc.*, 2009, **131**, 2008.

[4.33] S. Khatua, S. H. Choi, J. Lee, J. O. Huh, Y. Do and D. G. Churchill, *Inorg. Chem.*, 2009, **48**, 1799.

[4.34] V. Chandrasekhar, S. Das, R. Yadav, S. Hossain, R. Parihar, G. Subramaniam and P. Sen, *Inorg. Chem.*, 2012, **51**, 8664.

[4.35] Z. C. Weng, R. Yang, H. He and Y. B. Jiang, *Chem. Commun.*, 2006, 106.

[4.36] X. Qi, E. J. Jun, L. Xu, S. J. Kim, J. S. J. Hong, Y. J. Yoon and J. Yoon, *J. Org. Chem.*, 2006, **71**, 2881.

[4.37] M. Suresh, A. Ghosh and A. Das, *Chem. Commun.*, 2008, 3906.

[4.38] H. J. Kim, J. Hong, A. Hong, S. Ham, J. H. Lee and J. S. Kim, *Org. Lett.*, 2008, **10**, 1963.

[4.39] S. Yan, V. Leen, S. V. Snick, N. Boens and W. Dehaen, *Chem. Commun.*, 2010, **46**, 6329.

[4.40] H. S. Jung, M. Park, D. Y. Han, E. Kim, C. Lee, S. Ham and J. S. Kim, *Org. Lett.*, 2009, **11**, 3378.

[4.41] Z. Xu, X. Yi, X. Qian, J. Cui and D. Cui, *Org. Lett.*, 2005, **7**, 889.

[4.42] M. Royzen, Z. Dai and J. W. Canary, *J. Am. Chem. Soc.*, 2005, **127**, 1612.

[4.43] V. Dujols, F. Ford and A. W. Czarnik, *J. Am. Chem. Soc.*, 1997, **119**, 7386.

[4.44] J. Liu and Y. Lu, *J. Am. Chem. Soc.*, 2007, **129**, 9838.

[4.45] Y. Xiang, A. Tong, P. Jin and Y. Ju, *Org. Lett.*, 2006, **8**, 2863.

[4.46] K. W. K. Swamy, S. K. Ko, S. Kwon, H. Lee, C. Mao, J.-M. Kim, K.-H. Lee, J. Kim, I. Shin and J. Yoon, *Chem. Commun.*, 2008, 5915.

[4.47] X. Chen, M. Jou, H. Lee, S. Kou, J. Lim, S. W. Nam, S. Park, K. M. Kim and J. Yoon, *Sensors and Actuators B*, 2009, **137**, 597.

[4.48] Z. C. Wen, R. Yang, H. He and Y. B. Jiang, *Chem. Commun.*, 2006, 106.

[4.49] Q. Wu and E. V. Anslyn, *J. Am. Chem.Soc.*, 2004, **126**, 14682.

[4.50] S. Deo and H. A. Godwin, *J. Am. Chem. Soc.*, 2000, **122**, 174.

[4.51] E. M. Nolan and S. J. Lippard, *Chem. Rev.*, 2008, **108**, 3443.

[4.52] X. J. Peng, Y. K. Wu, J. L. Fan, M. Z. Tian and K. Han, *J. Org. Chem*., 2005, **70**, 10524.

[4.53] Y. Qu, J. L. Hua and H. Tian, *Org. Lett*., 2010, **12**, 3320.

[4.54] L. M. Yao, J. Zhou, J. L. Liu, W. Feng and F. Y. Li, *Adv. Funct. Mater*, 2012, **22**, 2667.

[4.55] C. Kar, M. D. Adhikari, B. K. Datta, A. Ramesh and G. Das, *Sensors and Actuators B*, 2013, **188**, 1132.

[4.56] S. Mandal, V. Balamurugan, F. Lloret and R. Mukherjee, *Inorg. Chem.* 2009, **48,** 7544.

[4.57] A. Mukherjee, F. Lloret and R. Mukherjee, *Inorg. Chem.*, 2008, **47**, 4471.

Appendix

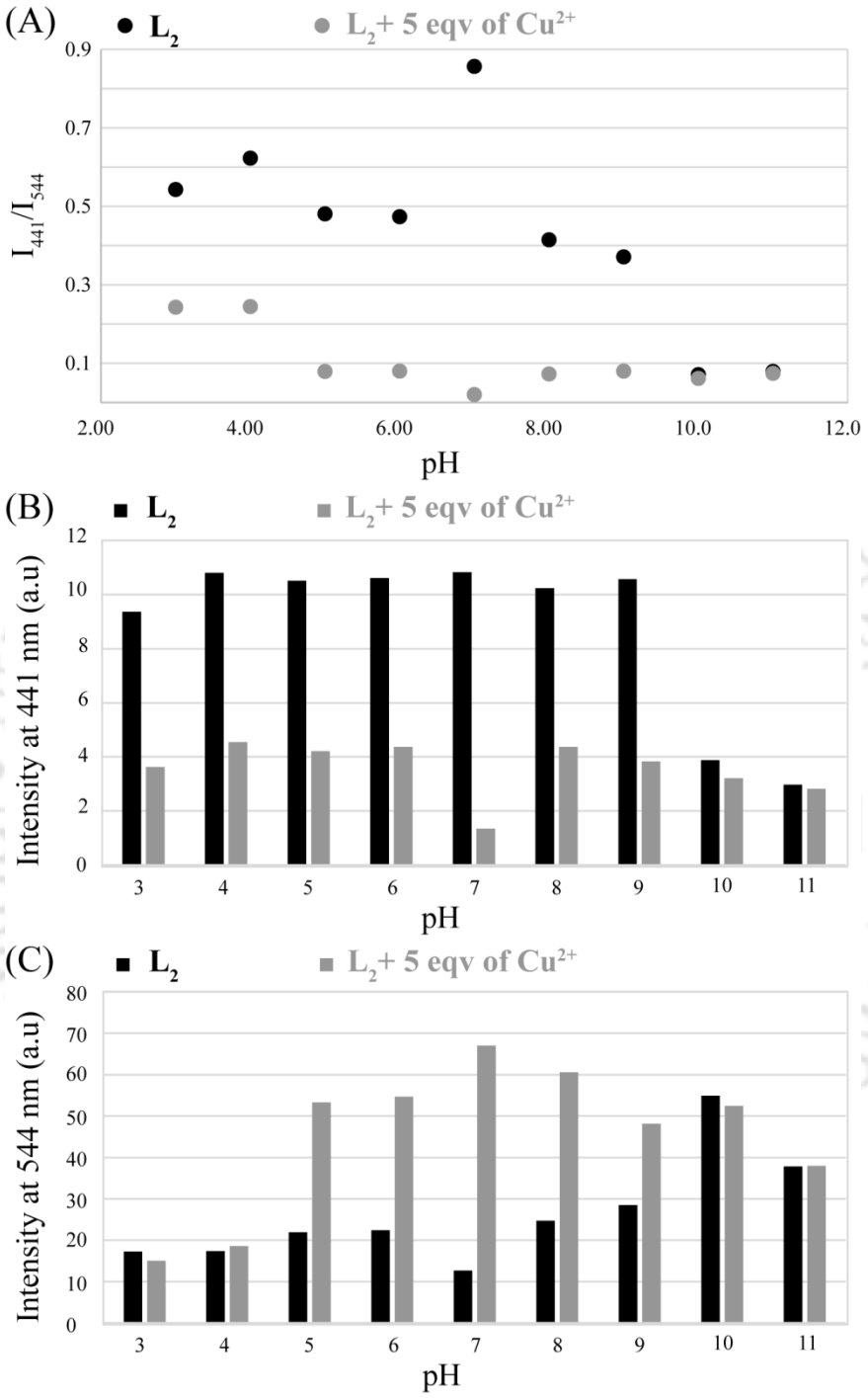

Figure A4.1 (A) Fluorescence intensity ratio of $\mathbf{L_2}$ (I_{441}/I_{544}) at different pH of the solution. (B) Fluorescence intensity of $\mathbf{L_2}$ at 441 nm wavelength against varying pH of the solution. (C) Fluorescence intensity of $\mathbf{L_2}$ at 544 nm wavelength against varying pH of the solution

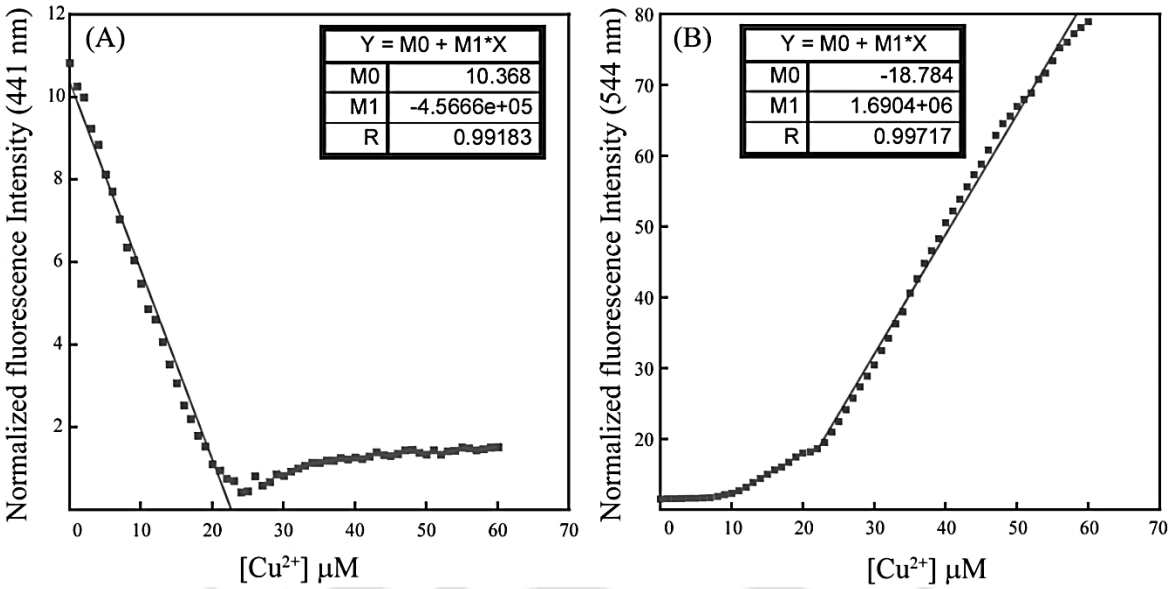

Figure A4.2 (A) Change in fluorescence intensity of $\mathbf{L_2}$ at 441 nm with continuous addition of Cu^{2+}. (B) Change in fluorescence intensity of $\mathbf{L_2}$ at 544 nm with continuous addition of Cu^{2+}.

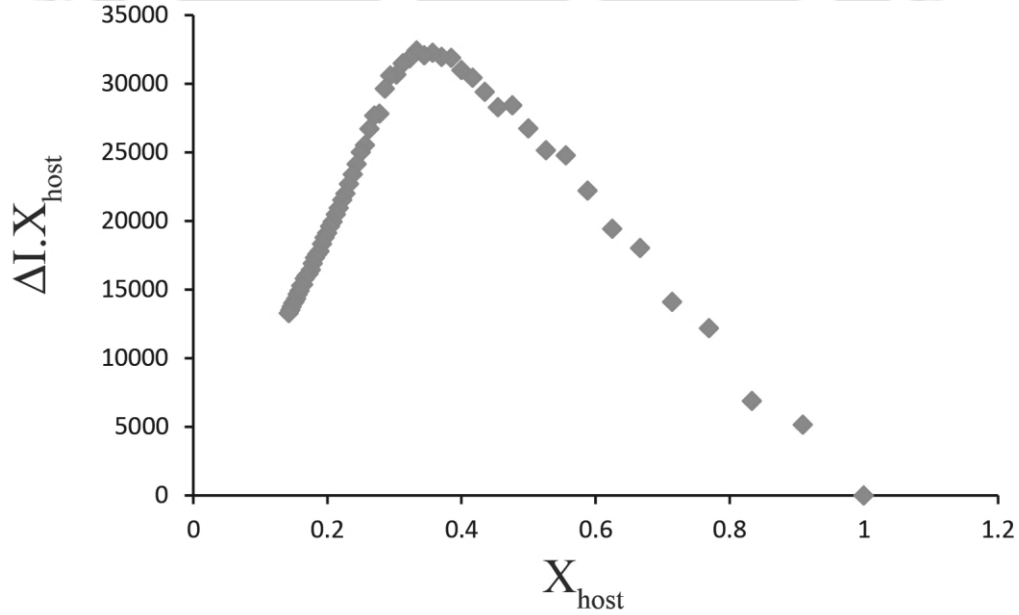

Figure A4.3 Job's plot between $\mathbf{L_2}$ and Cu^{2+} ions. Where X_{host} = the mole fraction of $\mathbf{L_2}$ and ΔI is the change ($I-I_0$) in the intensity of the emission spectra in presence of guest.

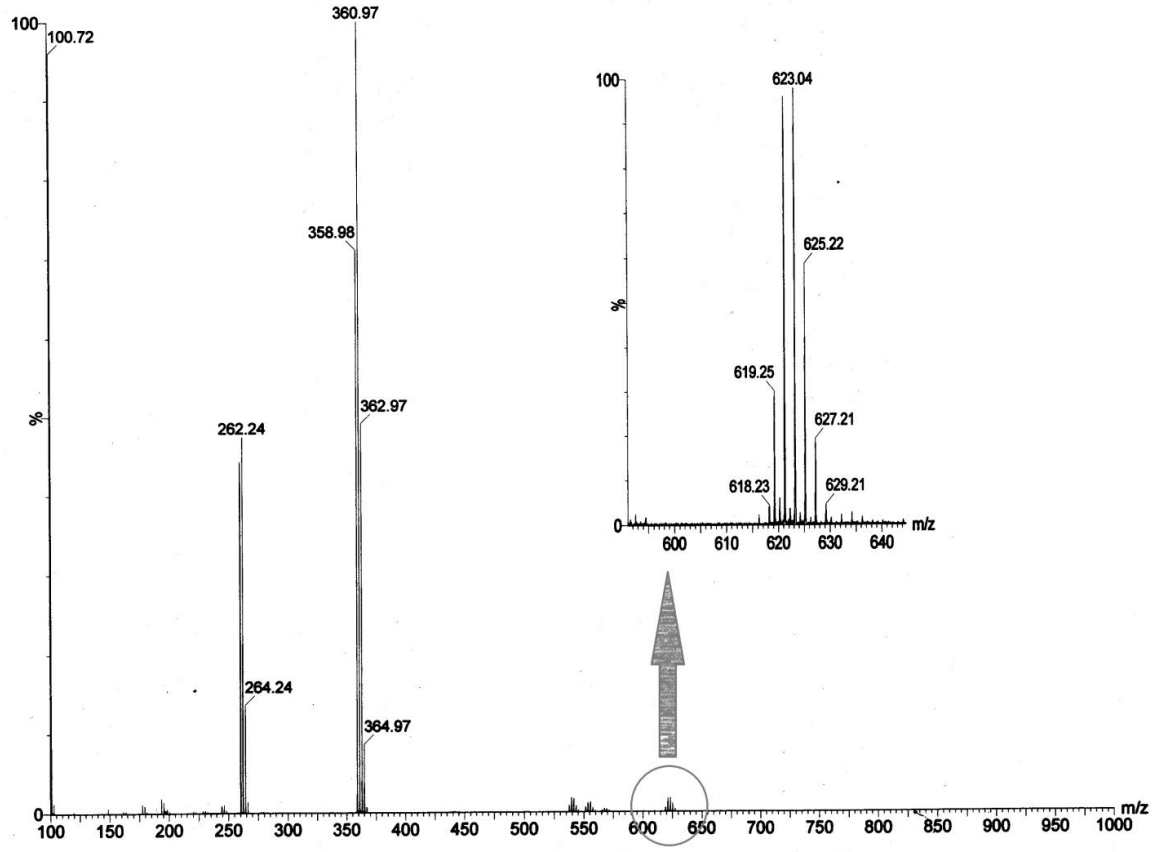

Figure A4.4 Mass spectrum of **L_2-Cu** complex (Mass spectrum obtained in positive mode).

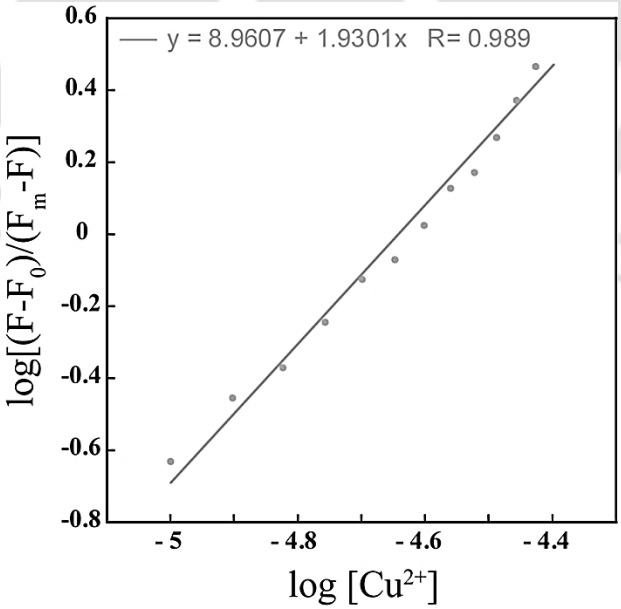

Figure A4.5 Benesi-Hildebrand plot (linear plot) of relative fluorescence intensity log[([F-F_0]/[Fm-F])] vs concentration of Cu^{2+} cation log[Cu^{2+}] added during fluorescence titration.

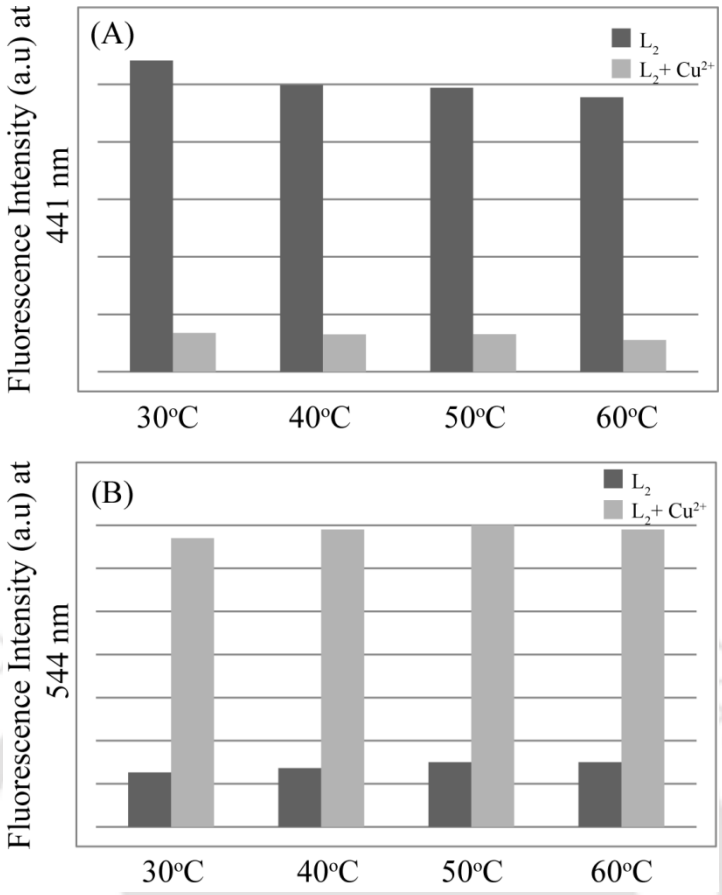

Figure A4.6 Sensing efficiency of the Ligand $\mathbf{L_2}$ at different temperature. (A) Change in fluorescence intensity at 441 nm (B) change in fluorescence intensity at 544 nm.

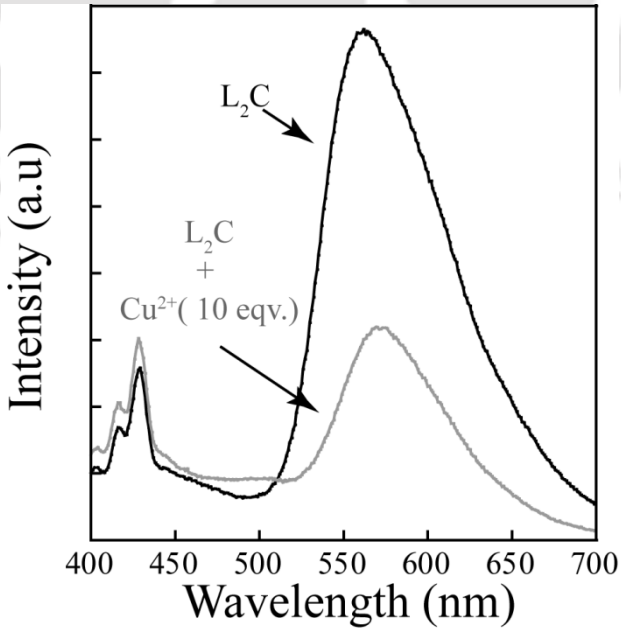

Figure A4.7 Fluorescence spectra of $\mathbf{L_2}$ in presence and absence of an excess amount of Cu^{2+}.

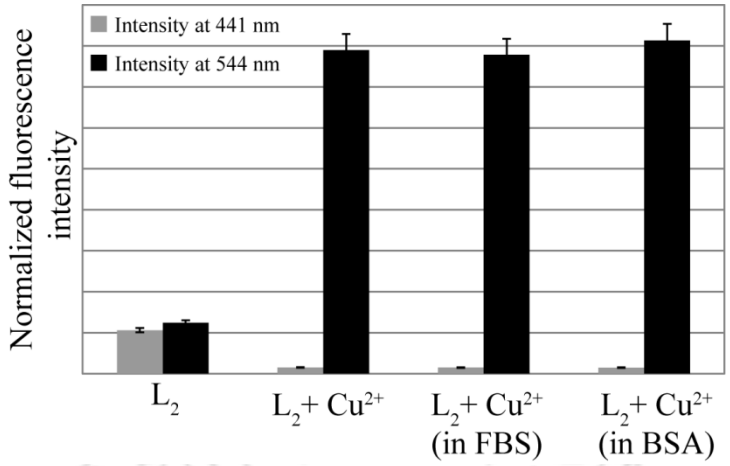

Figure A4.8 Sensing behavior of $\mathbf{L_2}$ upon addition of 6 equivalent of Cu^{2+} in presence of FBS (100 µL) and BSA (100 µL).50 mL of serum was dissolved in 1.5 mL of de-ionized water and used as stock solution. The bulk solution for BSA protein was made by using 1 mg mL^{-1}.

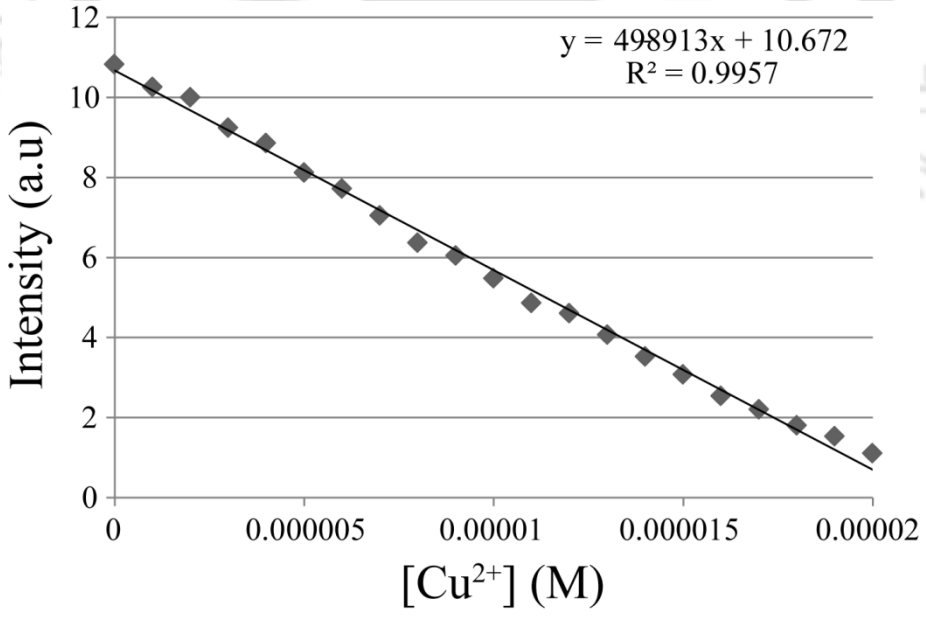

Figure A4.9 (A) Intensity (441 nm) versus Concentration plot for measuring the detection limit (3σ/k, here σ=0.004025) of Cu^{2+} by $\mathbf{L_2}$.

Table A1 selectivity coefficient of Cu^{2+} over other metal ions

Metal Ions	Selectivity Coefficient
Al^{3+}	7.650019
Fe^{3+}	9.366542
Cr^{3+}	9.152095
Hg^{2+}	8.696323
Pb^{2+}	7.779721
Cd^{2+}	8.7133
Zn^{2+}	9.469753
Ni^{2+}	13.26428
Co^{2+}	9.898245
Ag^{+}	9.220153
Na^{+}	9.708764
K^{+}	10.06389
Mg^{2+}	8.972964
Ca^{2+}	9.021105

Chapter 5

A Single Probe to Sense Al^{3+} Colorimetrically and Cd^{2+} by Turn-ON Orange Fluorescence

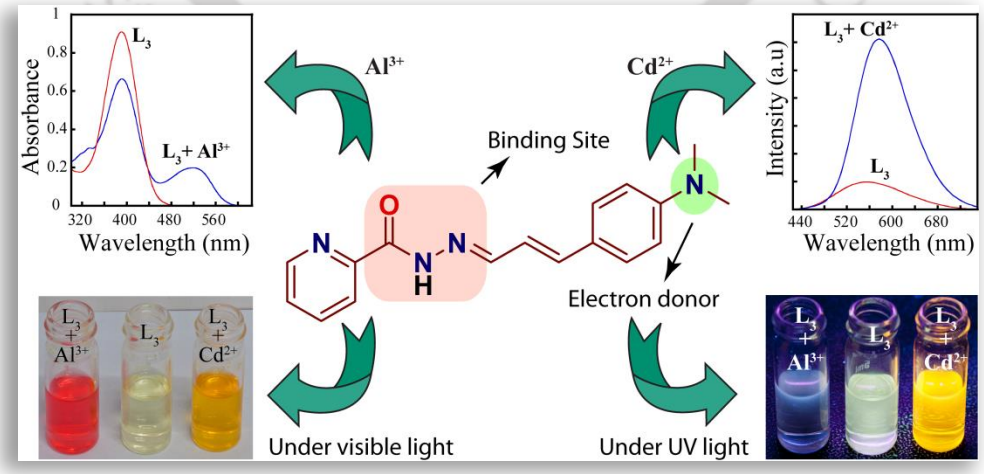

Chapter 5

5.1. Background and Focus of the Chapter

Among various heavy metal ions cadmium ions are banned in electrical and electronic equipment by the European Union's Restriction on Hazardous Substances (RoHS) directive due to their adverse effect to human health.[5.1] Cadmium metal ion is also not biodegradable, thus can be easily accumulated in the environment, resulting in contaminated food and water.[5.2] Cadmium is also an extremely toxic and carcinogenic metal.[5.3] Although intake of cadmium may also take place through smoking and food, but inhalation of cadmium-containing dust is the major route. Cadmium is generally found in electric batteries, pigments in plastics, electroplated steel, and so on.[5.4] A high exposure level of cadmium is related to damage of liver and kidneys, increased risks of cardiovascular diseases, and cancer mortality. Therefore, cadmium was listed as number 7 on ATSDR's "CERCLA Priority List of Hazardous Substances"[5.5] and may cause acute and chronic toxicity.

In fact, there are some fluorescent sensors that have been recently reported for detection and analysis of cadmium metal ions.[5.6-5.12] However, there are only a few fluorescent sensors that can detect cadmium with a fluorescence signal at higher wavelength (orange or red) region of the spectra,[5.13-5.16] and even rare examples are available in living cells.[5.13] So far, the greatest challenge for detecting Cd^{2+} comes from the interference of other transition metal ions like Zn^{2+}, as they are in the same group of the periodic table and hence exhibit similar chemical properties. This sensing impediment underscores the need for developing Cd^{2+}-selective sensors that can distinguish Cd^{2+} from Zn^{2+} with high sensitivity and selectivity under physiological conditions.

Along with cadmium, aluminium is also one of the most biologically and environmentally relevant metal. Aluminium is the third most abundant element (after oxygen and silicon), and the most abundant metal, in the Earth's crust. Aluminium is generally found in most animal and plant tissues and in natural waters in its ionic form Al^{3+}. Frequent use of aluminium in water treatment, food additive, pharmaceutical products, occupational dusts

and cooking utensils results in moderate increase in the Al^{3+} concentration in food. Tolerable weekly aluminium dietary intake in the human body is estimated to be 7 mg/kg body weight.[5.17-5.19] After absorption, Al^{3+} is carried by the plasma proteins and distributed in all tissues of human and animals and eventually accumulate in bone, causing softening of the bone, atrophy, and even aberrance.[5.20-5.24] The presence of Al^{3+} ions have been implicated in the damage of the central nervous system and is also thought to be involved in neurodegenerative ailments such as Alzheimer's disease and Parkinson's syndrome.[5.20-5.24] Considering the physiological relevance and biomedical implications of Al^{3+}, there is significant interest in developing selective and sensitive Al^{3+} sensors. Until recently, only a few fluorescent chemosensors have been developed for detection of Al^{3+}.[5.25-5.31]

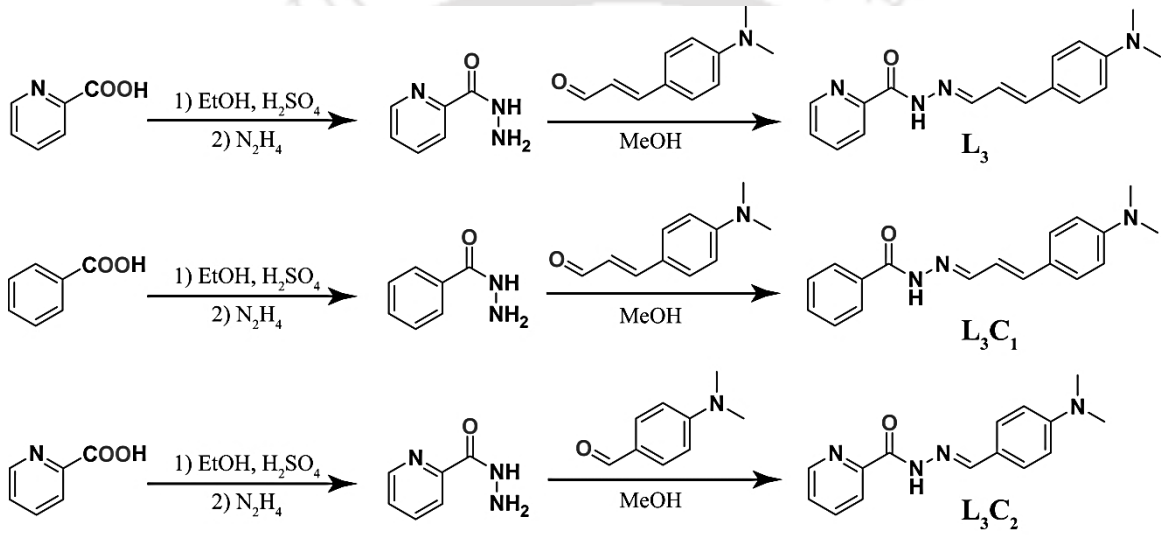

Scheme 5.1 Synthetic scheme for the ligands $\mathbf{L_3}$, $\mathbf{L_3C_1}$ and $\mathbf{L_3C_2}$.

In recent years, fluorescent chemosensors have attracted significant interest because of their potential use in medicinal and environmental research. The most commonly employed method used for metal ion detection is the designing of ligand molecule containing an electron donating group at one end and a metal coordination site at the other end, bridged by conjugated π-electron system. Binding of metal ions with the ligand, initiate the internal charge transfer through the conjugated π-electron system, which induces an observable change in the electronic or fluorescence spectra of the ligand.

Most fluorescent sensors for Al^{3+} as well as Cd^{2+} possess good selectivity, but demonstration of these sensor for in-field device application are scarcely reported. This chapter demonstrate the cadmium and aluminium sensing capabilities of a pyridine-2-carbohydrazide functionalized conjugated fluorophoric Schiff base ligand $\mathbf{L_3}$ (Scheme 5.1)

and the absorption and fluorescence behaviour of **L_3** upon metal complexation. The lone pair of electron over the Nitrogen atom of N,N-dimethyl moiety of **L_3** act as an electron donor and the imine nitrogen along with the carbonyl oxygen serves as the metal binding site. Binding of specific metal ions with **L_3** generates intramolecular charge transfer through the conjugated π-electron bridge and induce a spectroscopic response in the near red region of the spectra. The strong selectivity and in-field application possibility of the developed sensor is verified by using it in paper strips. It is also demonstrated that the developed sensor as well as the ligand-cadmium complex was non-toxic and the ligand **L_3** could readily detect the presence of intracellular Cd^{2+} ions in live HeLa cells via a characteristic fluorescence switch ON mechanism.

5.2. UV-Vis spectroscopic studies of L_3 in presence of metal ions.

UV−Vis spectra recorded for **L_3** in CH_3OH/aqueous HEPES buffer (1 mM, pH 7.3; 1:4, v/v) indicated an absorption maximum at 390 nm, which may have originated due to the intra-molecular π-π* charge transfer (CT) transition. The selectivity of **L_3** was verified with perchlorate or nitrate salts of Na^+, Mg^{2+}, Cr^{3+}, Hg^{2+}, Cu^{2+}, Pb^{2+}, Zn^{2+}, Fe^{3+}, Co^{2+}, Ni^{2+}, Cd^{2+}, and Al^{3+} in CH_3OH/aqueous HEPES buffer (1 mM, pH 7.3; 1:4 v/v). Although other metal ions like Cd, Ni, Zn, Pb and Co exhibit some binding interaction with the receptor **L_3** which is accompanied by 40 nm red shift of the absorption maxima but a significant change in UV-Vis spectral pattern was observed only in presence of Al^{3+}, among all the other metal ions used (Figure 5.1A). Upon addition of Al^{3+}, the intensity of the absorption bands of **L_3** at 390 nm decreased with a concomitant appearance of two new bands at 330 nm and at 510 nm. The change in the UV-Vis spectra is also well supported by a visual change of the receptor solution from light yellow to dark red on addition of nearly 1.0 equivalent of Al^{3+} ions (Figure 5.1B inset). The UV-Vis titration experiment was also performed with incremental amount of Al^{3+} ions, wherein two well-defined isosbestic points at 348 and 445 nm were observed (Figure 5.1B), which clearly suggested a prominent conversion of **L_3** into the **L_3-Al** complex. The complex formed between **L_3** and Al^{3+} was observed to be 1:1 in stoichiometry, which was established with the help of job's plot (Appendix, Figure A5.1) based on the changes in absorbance at 510 nm. This stoichiometry in the solution state was also supported by ESI-MS studies (Appendix, Figure A5.2), which indicated the presence of a molecular-ion peak at m/z 445.05, corresponds to the mass of $[\mathbf{L_3}+Al+3Cl+H_2O+H]^+$. The binding constant for the formation of **L_3-Al** complex was also calculated on the basis of change in absorbance at

510 nm by considering a 1:1 binding stoichiometry (Appendix, Figure A5.3). The binding constant (*K*) determined by the B-H method was found to be 5×10^4 M^{-1}. It is significant to mention that the detection limit of **L_3** for Al^{3+} ions was found to be 8.7 µM (Appendix, Figure A5.4) which is lower than tolerable weekly aluminium dietary intake in an average human body.[5.17-5.19] The selective change in the absorbance spectra of **L_3** can be attributed to the high positive charge of the metal ion. On complexion with **L_3**, Al^{3+} significantly attracts the electron cloud from the N,N-dimethyl moiety via conjugated π-electron bridge and the probability of ligand to metal charge transfer (LMCT) also increases resulting in formation of a red shifted new band in the spectra.

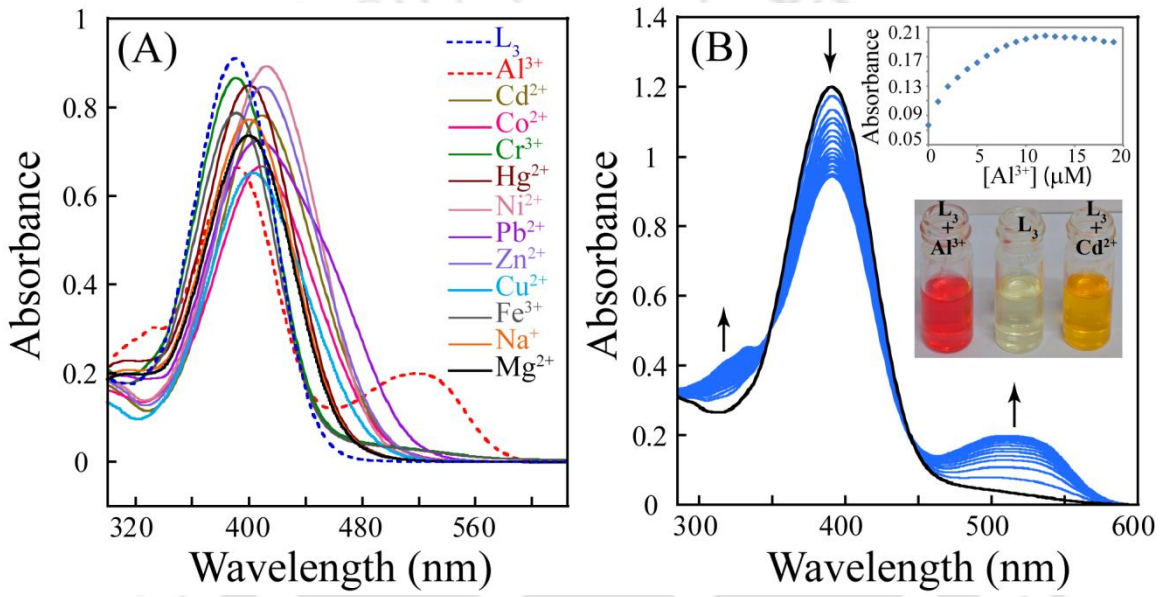

Figure 5.1 (A) UV-Vis absorption spectra of receptor **L_3** (10 µM) observed upon addition of 5 equivalent metal ions (perchlorate or nitrate salts of Na^+, Mg^{2+}, Cr^{3+}, Hg^{2+}, Cu^{2+}, Pb^{2+}, Zn^{2+}, Fe^{3+}, Co^{2+}, Ni^{2+}, Cd^{2+}, and Al^{3+}) in a CH_3OH/aqueous HEPES buffer (1 mM, pH 7.3; 1:4 v/v). (B) UV-Vis titration spectra of **L_3** (10 µM) upon incremental addition of $Al(NO_3)_3$ in CH_3OH/aqueous HEPES buffer (1 mM, pH 7.3; 1:4 v/v). **Inset:** Changes in the absorbance at 510 nm with incremental addition of Al^{3+} and visual change in the solution colour after addition of metal ions.

For a theoretical appraisal on the selective chromogenic response of **L_3** toward Al^{3+}, the Density Functional Theory Calculation (DFT) of **L_3** and its Aluminium complex were carried out. The electronic spectrum of **L_3** alone showing absorbance maximum at 390 nm is mainly generated from the transition of HOMO to LUMO. However as both the Job's plot and mass spectrum indicated formation of a 1:1 **L_3-Al** complex, the structure optimization of **L_3-Al** complex was also performed to explore the most suitable binding mode between **L_3** and Al^{3+}. As for Al^{3+} two probable coordination sites are available, the first one involving the pyridine nitrogen (Structure **i** in figure 5.2A) and the second one

involving the carbonyl oxygen (structure **ii** in figure 5.2A), theoretical calculations were done for both the possibility. Structure 'ii' was found to be 8.01 Kcal more stable than structure 'i' (Appendix, Table A5.1). Thus it can be argued here that chelation of Al^{3+} with $\mathbf{L_3}$ involving the carbonyl oxygen and the imine nitrogen led to the formation of a highly stable complex. The DFT calculation revealed that there is a reasonable decrease in the HOMO to LUMO energy gap from $\mathbf{L_3}$ to its Aluminium complex (figure 5.2B) which is in agreement with the subsequent generation of the red shifted new absorbance peak on addition of Al^{3+} to $\mathbf{L_3}$. The comparison between the structure of $\mathbf{L_3}$ and $\mathbf{L_3}$**-Al** complex clearly revealed that on chelation with the Al^{3+}, ligand $\mathbf{L_3}$ gained perfect planarity with an extended conjugation (Appendix, Figure A5.6). Thus, undoubtedly the formation of the highly stable $\mathbf{L_3}$**-Al** complex followed by extension in the conjugation and increases in the probability of charge transfer initiated this unusual colorimetric response. Selected orbitals and their corresponding energies for both $\mathbf{L_3}$ and $\mathbf{L_3}$**-Al** complex, which are likely to be critical in the spectral outcome are provided in supporting information (Appendix, Table A5.2 and Table A5.3).

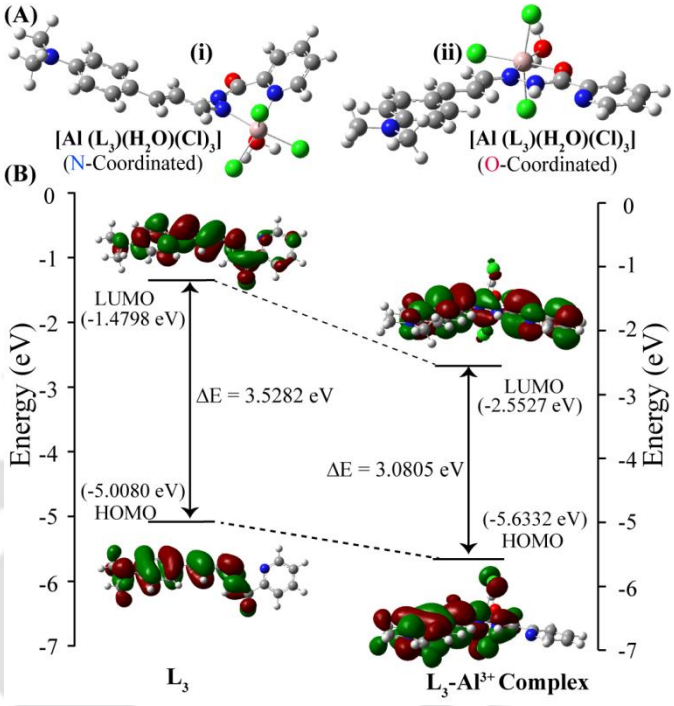

Figure 5.2 (A) Optimized structures of $\mathbf{L_3}$**–Al** complex with two different possible binding modes. (B) Energy diagrams of HOMO and LUMO orbitals of $\mathbf{L_3}$ and the $\mathbf{L_3}$**–Al** complex (structure **i**) calculated at the DFT level using a B3LYP/6-31+G(d,p) basis set.

5.3. Fluorescence spectroscopic studies of L_3 in presence of metal ions.

The selectivity of $\mathbf{L_3}$ for different metal ions (Na^+, Mg^{2+}, Cr^{3+}, Hg^{2+}, Cu^{2+}, Pb^{2+}, Zn^{2+}, Fe^{3+}, Co^{2+}, Ni^{2+}, Cd^{2+}, and Al^{3+} in CH_3OH/aqueous HEPES buffer) was also studied by fluorescence emission spectroscopy. As evident from Figure 5.3A, a solution of $\mathbf{L_3}$ (10.0×10^{-6} M) exhibited a low intensity emission maxima at 554 nm when excited at 405 nm. Addition of Cd^{2+} to this receptor solution induced a dramatic increase in the fluorescence

intensity along with a significant red shift of the emission maxima to 578 nm. The increase in fluorescence was also observed under an UV lamp wherein there was a sharp change in the solution fluorescence from colorless to orange in presence of Cd^{2+} ions (Figure 5.3A inset). It can also be observed from Figure 5.3A that the metal-ligand binding induced switch-ON fluorescence of **L_3** was entirely selective towards Cd^{2+} ions, as no significant fluorescence change of **L_3** occurred even in the presence of excess of other metal ions. To further understand the properties of **L_3** as a receptor for Cd^{2+}, a titration of the receptor was performed with increasing concentration of Cd^{2+}. As evident in Figure 5.3B the fluorescence intensity of a 10 μM solution of **L_3** was enhanced systematically with incremental addition of Cd^{2+} ions, which also confirmed that receptor **L_3** exhibited a high sensitivity toward Cd^{2+}. The 1:1 stoichiometry of the **L_3-Cd** was established from the measurements of emission intensity as a function of Cd^{2+} concentration (inset in Figure 5.3B), where a clear bend of the curve was observed at 1.0 equivalent of added Cd^{2+}.

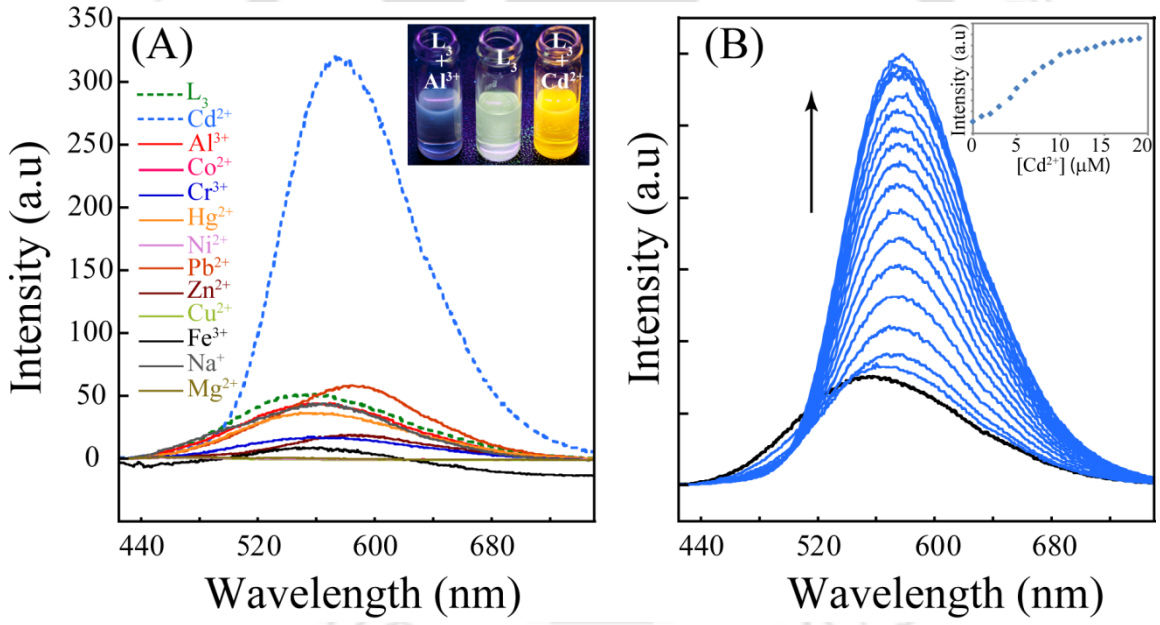

Figure 5.3 (A) Changes of the fluorescence emission of receptor **L_3** (10 μM) observed upon addition of 5 equivalent metal ions (perchlorate or nitrate salts of Na^+, Mg^{2+}, Cr^{3+}, Hg^{2+}, Cu^{2+}, Pb^{2+}, Zn^{2+}, Fe^{3+}, Co^{2+}, Ni^{2+}, Cd^{2+}, and Al^{3+}) in a CH_3OH/aqueous HEPES buffer (1 mM, pH 7.3; 1:4 v/v). **Inset:** Visual change in the solution fluorescence after addition of metal ions. (B) Fluorescence titration spectra of **L_3** (10 μM) upon incremental addition of $Cd(NO_3)_2$ in CH_3OH/aqueous HEPES buffer (1 mM, pH 7.3; 1:4 v/v). **Inset:** Changes in the emission intensity at 578 nm with incremental addition of Cd^{2+}.

This stoichiometry in the solution state was also confirmed with the help of job's plot (Appendix, Figure A5.1) and further supported by ESI-MS studies (Appendix, Figure A5.10), which indicated the presence of a molecular-ion peak at m/z 443.02, corresponds

to the mass of [$\mathbf{L_3}$ + Cd^{2+} + Cl^-]$^+$. The binding constant for the formation of **L_3-Cd** complex was calculated on the basis of change in emission at 578 nm by considering a 1:1 binding stoichiometry (Appendix, Figure A5.2). The binding constant (*K*) determined by the B-H method was found to be 3.3×10^5 M^{-1}. The detection limit of $\mathbf{L_3}$ for Cd^{2+} ions was found to be 1.2 μM (Appendix, Figure A5.4).

The change in emission spectral behavior of $\mathbf{L_3}$ in presence of Cd^{2+} can be explained by chelation-enhanced fluorescence (CHEF). Although $\mathbf{L_3}$ is a conjugated system but the metal binding site and the N,N-dimethyl ring of $\mathbf{L_3}$ may not be perfectly planar in the free ligand. Metal coordination renders the system more planar and in turn enhances the internal charge transfer from the N,N-Dimethyl moiety to the metal binding site. In absence of the metal ions there is no sufficient pull for the electronic charge over the N,N-Dimethyl substituted benzene ring and thus the fluorescence is quenched due to lack of internal charge transfer throughout the system. But binding of a suitable metal cation by the imine nitrogen and the amide oxygen may drag the electronic charge from the N,N-Dimethyl substituted benzene ring. Due to the metal ion assisted electron pull and the N,N-Dimethyl inducted electron push, the possibility of internal charge transfer throughout the π-system increases; leading to a highly conjugated geometry and a radical enhancement of the fluorescence intensity. To further verify the significance of the conjugated chain length and the pyridine unit in the sensing event of metal ions, we have synthesized two control compounds $\mathbf{L_3C_1}$ and $\mathbf{L_3C_2}$. $\mathbf{L_3C_1}$ has a similar structure to $\mathbf{L_3}$ but in place of a pyridine moiety in $\mathbf{L_3}$ a benzene moiety is present. In case of $\mathbf{L_3C_2}$ we had chosen N,N-dimethyl carboxaldehyde in place of the cinnamaldehyde (Scheme 5.1). Fluorescence emission and UV-Vis spectroscopic studies with $\mathbf{L_3C_1}$ and $\mathbf{L_3C_2}$ revealed some interesting facts, which help us to further understand the beauty of the ligand designing. From fluorescence emission spectra of $\mathbf{L_3C_1}$ we found that there was no significant increase in the emission intensity with the tested metal ions, similarly UV-Vis absorbance was also almost unchanged upon addition of an excess amount of Cd^{2+}/Al^{3+} to a solution containing $\mathbf{L_3C_1}$ (Appendix, Figure A5.8 and Figure A5.9). whereas in case of $\mathbf{L_3C_2}$ there was a significant increase in the emission intensity (at 520 nm) in presence of Cd^{2+}, although the response towards Zn^{2+} ions is much more pronounced but perceivable change in presence of Cd^{2+} is sufficient enough to understand the significance of the pyridine moiety to control the optical response of the ligand towards specific cations. Similar to the result obtained from the fluorescence spectroscopy, UV-Vis absorbance

shows formation of a new peak (near 450 nm) in presence of Al^{3+} ions. Thus, from the above mentioned results it can be concluded that the presence of both, the long conjugated geometry as well as the pyridine moiety are significant prerequisites for the metal sensing ability of **L_3**. The pyridine ring basically controls the selective optical response for the metal ions and the extended conjugation assists to shift the optical response to longer wavelength region of the spectrum. Further proof of the metal binding modes of the ligand was obtained from the X-ray crystallographic studies of **L_3-Cd** complex.

5.4. X-ray Crystallographic Analysis.

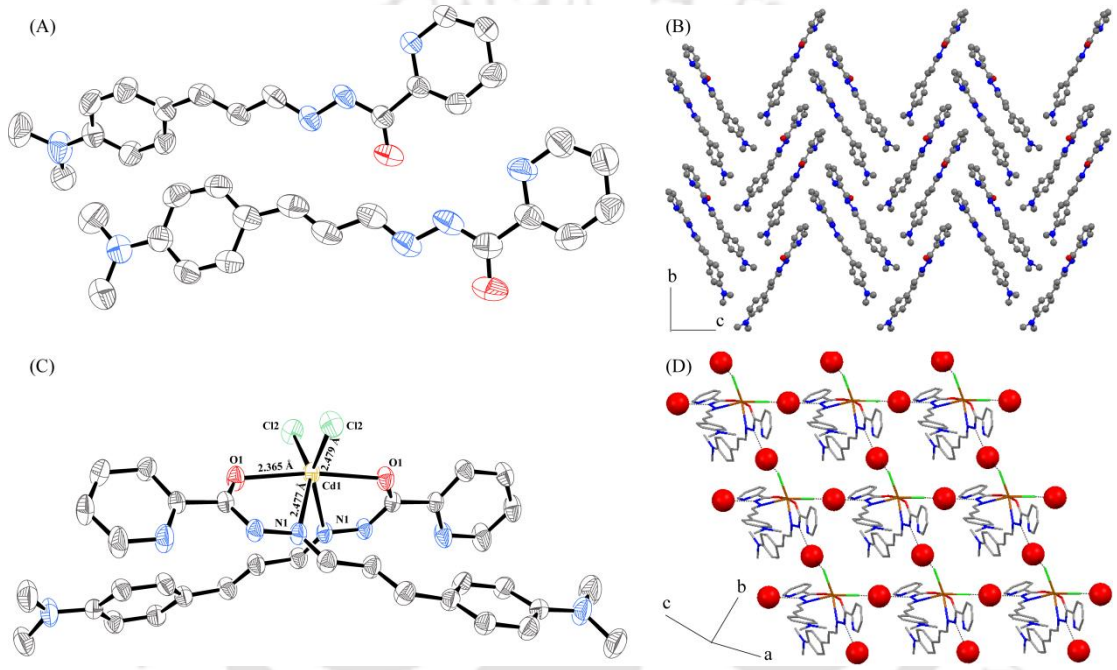

Figure 5.4 (A) Thermal ellipsoid plot (50% probability level) of **L_3** (B) Packing diagram of **L_3** (C) Thermal ellipsoid plot (50% probability level) of the **L_3-Cd** complex. (D) Packing diagram of **L_3-Cd** complex. All hydrogen atoms were deleted for clarity.

Single crystals of **L_3** suitable for XRD analysis were obtained from methanol, which crystallizes in monoclinic space group P21 with Z = 4. The asymmetric unit contains two symmetry-independent **L_3** molecules (Z' = 2), which differ considerably in their torsions involving the conjugated aliphatic -CH=CH-CH=N- chain (Figure 5.4A). The solid-state structure of the metal complex **L_3-Cd** was also investigated by X-ray crystallography. Initially, we attempted to crystallize various metal salts [Chloride and nitrate salts of Cd^{2+} and Al^{3+}] with **L_3** in a variety of solvents. Indeed, the crystals suitable for crystallographic analysis were obtained in DMF/methanol mixture. The crystal structures of the ligand and the complex are shown in Figure 5.4. In the Cd complex **L_3-Cd**, each asymmetric unit

contains one coordinating ligand, where Cd^{2+} is chelated by imine nitrogen, carbohydrazide oxygen, and chloride anion. Two ligand molecules along with chloride ions form disordered octahedral coordination geometry. The Cd^{2+}–N bond distance is 2.477 Å, the Cd^{2+}-Cl^{-} bond distance is 2.479 Å and the distance between O and Cd^{2+} is of 2.365 Å. These data demonstrate that the hydrazide moiety is mainly involved in the capture of metal ions, while the cinnamaldehyde moiety is responsible for the optical response of the sensor.

5.5. Metal-Ion Competition Studies.

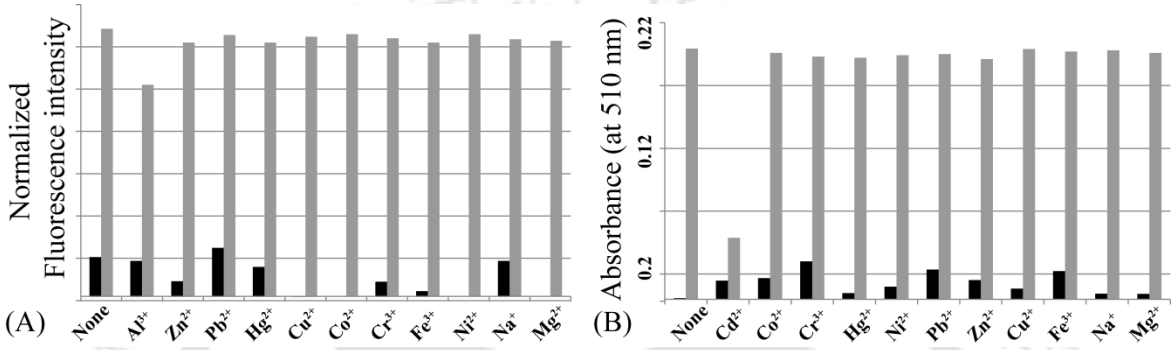

Figure 5.5. (A) Normalized fluorescence responses of $\mathbf{L_3}$ (10 μM) to various cations in CH_3OH/aqueous HEPES buffer (1 mM, pH 7.3; 1:4 v/v). The black bars represent the emission intensities of $\mathbf{L_3}$ in the presence of cations of interest (50 μM). The grey bars represent the change of the emission that occurs upon the subsequent addition of Cd^{2+} to the above solution; the intensities were recorded at 578 nm. (B) Absorbance of $\mathbf{L_3}$ (10 μM) at the wavelength 510 nm in presence of various cations in CH_3OH/aqueous HEPES buffer (1 mM, pH 7.3; 1:4 v/v). The black bars represent the absorbance of $\mathbf{L_3}$ in the presence of cations of interest (50 μM). The grey bars represent the change of the absorbance that occurs upon the subsequent addition of Al^{3+} to the above solution.

The individual emission and UV-Vis response of $\mathbf{L_3}$ in presence of different transition-metal ions had revealed a notable selectivity for Cd^{2+} and Al^{3+} ions (Figure 5.3). However, the most important criterion for a selective cation probe is the ability to detect a specific cation in a complex milieu of other competing ions. To validate this hypothesis, the selectivity of $\mathbf{L_3}$ was further tested in presence of other competing cations, which may interfere with the estimation of Cd^{2+} or Al^{3+} (Figure 5.5A). The emission intensity of Cd^{2+}-bound $\mathbf{L_3}$ was nearly unaltered in the presence of 5 equiv of Na^{+}, Mg^{2+}, Cr^{3+}, Hg^{2+}, Cu^{2+}, Pb^{2+}, Zn^{2+}, Fe^{3+}, Co^{2+}, Ni^{2+} and Al^{3+}, indicating excellent selectivity for Cd^{2+} over these competing cations. The response of $\mathbf{L_3}$ for Al^{3+} over other competing metals ions was evaluated based on UV-Visible absorbance at 510 nm. It was observed that, although the Cd^{2+} sensing ability of $\mathbf{L_3}$ is not hindered by any of the metal cation but sensitivity of $\mathbf{L_3}$

towards Al^{3+} was relatively low in the presence of Cd^{2+} ions, which is due to the greater preference of **L_3** towards Cd^{2+} ions over Al^{3+} ions.

5.6. Application of L_3 in Paper strips.

The strong sensing potential of **L_3** for Al^{3+} and Cd^{2+} ions are further verified by incorporation in paper strips. Sensing paper strips were prepared by coating the **L_3** solution (in chloroform) on a filter paper to demonstrate the in-field device application. As evident from figure 5.6 paper strips coated with only **L_3** exhibited a moderate yellow emission under a hand held UV lamp. However, after dipping it into an aqueous solution of cadmium nitrate an intense orange fluorescence was observed. The aluminium sensing behaviour of **L_3** was also displayed with a sharp change in colour of the paper strip from yellow to red under visible white light. Thus, the paper strips dipped in a solution of **L_3** showed a turn on response similar to the result obtained from the spectroscopic studies and was selective to Cd^{2+} and Al^{3+}. Although zinc is known to be analogous to cadmium in spectroscopic behavior, it was interesting to observe that zinc failed to promote any turn ON response neither with the paper strips, nor in the fluorescence emission studies. To the best of our knowledge this is the first report where a monomeric sensor molecule is used to demonstrate the paper strip model that can efficiently sense Cd^{2+} in presence of other metals including Zn^{2+}.

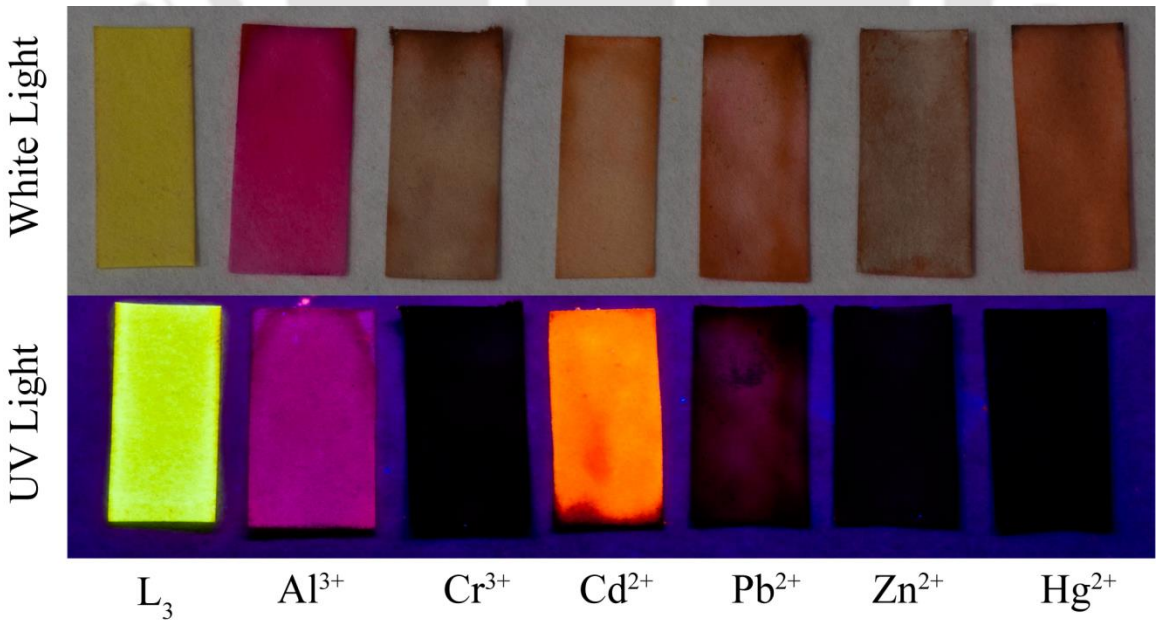

Figure 5.6 Demonstration of the Al^{3+} and Cd^{2+} sensing by **L_3** coated paper strips**.**

5.7. Intracellular sensing of Cd^{2+} by imaging studies.

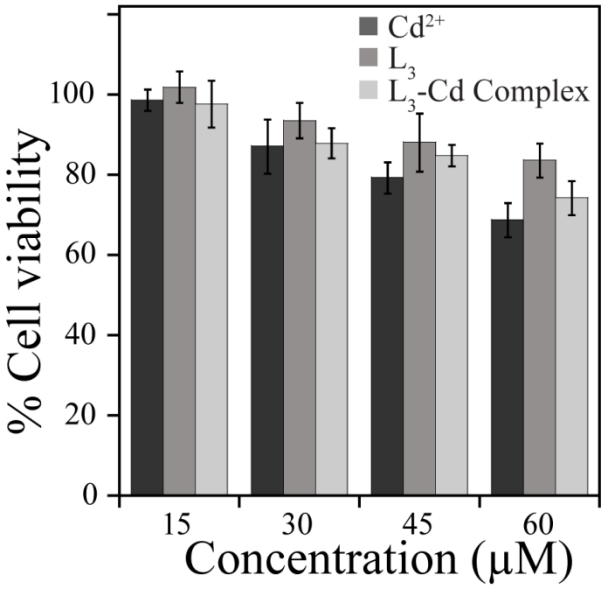

Figure 5.7 MTT assay to determine the cytotoxic effect of compound **L_3** and **L_3-Cd** complex on HeLa cells.

Given the significant physiological and toxicological implications of cellular cadmium pool, there is considerable motivation in developing probes for detecting intracellular levels of cadmium. In our study, the results obtained in solution-based fluorescence measurements with the ligand **L_3** demonstrated the potential of the ligand to selectively detect Cd^{2+} at low levels. However, to harness the potential of the ligand **L_3** for sensing intracellular Cd^{2+} levels, it was pertinent to initially determine the cytotoxic effect of **L_3** as well as the **L_3-Cd** complex. A standard *in vitro* MTT assay suggested that at low concentrations (upto 30μM) both **L_3** and **L_3-Cd** complex failed to exert any detrimental effect on the viability of HeLa cells (Figure 5.7). The non-toxic nature of the ligand **L_3** holds significant implications in the context of sensing and suggested that the developed sensor was not only selective for Cd^{2+} but also amicable to non-destructive intracellular sensing of the metal ion. Encouraged by the non-toxic attribute of **L_3**, our subsequent endeavor was to ascertain the sensing potential of **L_3** for intracellular detection of Cd^{2+} through fluorescence microscopy.

When HeLa cells were treated with 10 μM **L_3**, the cells failed to exhibit any fluorescence (Figure 5.8B, Panel b). Interestingly, when the cells were subsequently exposed to 15 μM $Cd(NO_3)_2$, a dramatic switch-ON orange fluorescence manifested (Figure 5.8B, Panel e), indicating selective sensing of Cd^{2+} in cells. The evenly distributed intracellular fluorescence observed across HeLa cells suggested that the ligand **L_3** could transit through the membrane and pervade the cells and upon subsequent addition of $Cd(NO_3)_2$, formation of the highly fluorescent **L_3-Cd** complex resulted throughout the cell. It was also observed that HeLa cells retained their typical morphological trait during treatment with the ligand and $Cd(NO_3)_2$ as evident from the bright field images of treated cells (Figure 5.8B, Panels a and d). This observation also suggested that the ligand **L_3** as well as **L_3-Cd^{2+}** complex were not cytotoxic to HeLa cells, corroborating earlier results of the MTT assay.

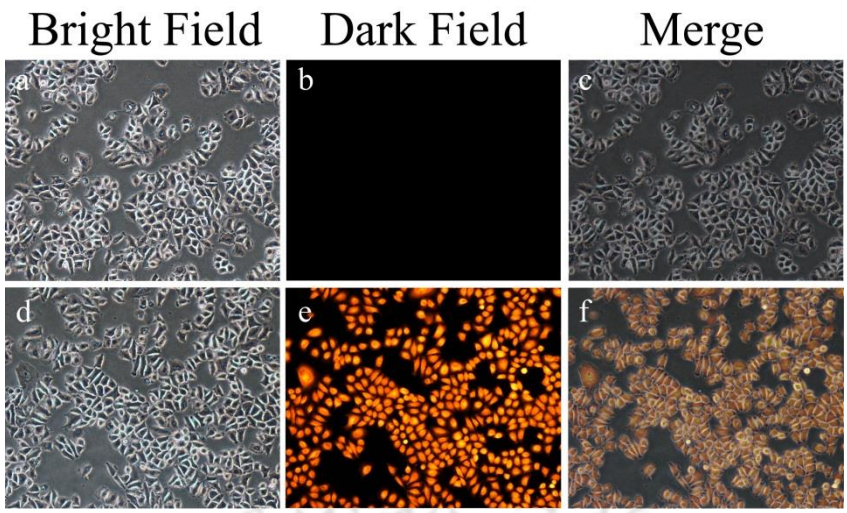

Figure 5.8 Fluorescence microscopic images of HeLa cells after adding 10 μM of $\mathbf{L_3}$ (panel a-c) and after subsequent treatment with 15 μM Cd^{2+}, (panel d-f).

5.8. Conclusion

In summary, this chapter reports the design and application of a receptor molecule $\mathbf{L_3}$ which selectively sense Al^{3+} and Cd^{2+} ions with a switch ON response respectively in optical and fluorescence spectra in the visual region. Apart from the visible changes, an in-field device application was further demonstrated by sensing Al^{3+} and Cd^{2+} ions in paper strips coated with $\mathbf{L_3}$. The structure of the complex formed between $\mathbf{L_3}$ and Cd^{2+} was studied by X-Ray diffraction techniques, which also proves strong interaction between the ligand and Cd^{2+} ions in the solid state. The fluorescence spectroscopic studies revealed that $\mathbf{L_3}$ displayed strong preference for Cd^{2+} ions over other interfering ions including Zn^{2+}. The observations of the cytotoxicity assay and fluorescence-based cell imaging are encouraging for future diagnostic applications of the sensor. Given the fact that the ligand $\mathbf{L_3}$ and $\mathbf{L_3}$-$\mathbf{Cd^{2+}}$ complex were found to be non-toxic to cultured HeLa cells even after 24 h interaction period, the cadmium probe $\mathbf{L_3}$ developed in the present study holds interesting prospect in analytical and biomedical domain applications.

References

[5.1] The European Parliament and the Council of the European Union, "Directive on the Restriction of the Use of Certain Hazardous Substances in Electrical and Electronic Equipment". 2002/95/EC.

[5.2] W. De Vries, P. F. Romkens and G. Schutze, *Rev. Environ. Contam. Toxicol.*, 2007, **191**, 91.

[5.3] R. R. Lauwerys, A. M. Bernard, H. A. Reels and J.-P. Buchet, *Clin. Chem. (Washington, D. C.)*, 1994, **40**, 1391.

[5.4] G. F. Nordberg, R. F. M. Herber and L. Alessio, Cadmium in the Human Environment, Oxford University Press, Oxford, UK, 1992.

[5.5] Agency for Toxic Substances and Disease Registry, 4770 Buford Hwy NE, Atlanta,GA 30341. http://www.atsdr.cdc.gov/cercla/07list.html.

[5.6] M. E. Huston, C. Engleman and A. W. Czarnik, *J. Am. Chem. Soc.*, 1990, **112**, 7054.

[5.7] C. Lu, Z. Xu, J. Cui, R. Zhang and X. Qian, *J. Org. Chem.*, 2007, **72**, 3554.

[5.8] M. Choi, M. Kim, K. D. Lee, K.-N. Han, I.-A. Yoon, H.-J. Chung and J. Yoon, *Org. Lett.*, 2001, **3**, 3455.

[5.9] T. Gunnlaugsson, T. C. Lee and R. Parkesh, *Org. Lett.*, 2003, **5**, 4065.

[5.10] R. T. Bronson, D. J. Michaelis, R. D. Lamb, G. A. Husseini, P. B. Farnsworth, M. R. Linford, R. M. Izatt, J. S. Bradshaw and P. B. Savage, *Org. Lett.*, 2005, **7**, 1105.

[5.11] X. Tang, X. Peng, W. Dou, J. Mao, J. Zheng, W. Qin, W. Liu, J. Chang and X. Yao, *Org. Lett.*, 2008, **10**, 3653.

[5.12] L. Prodi, M. Montalti, N. Zaccheroni, J. S. Bradshaw, R. M. Izatt and P. B. Savage, *Tetrahedron Lett.*, 2001, **42**, 2941.

[5.13] T. Cheng, Y. Xu, S. Zhang, W. Zhu, X. Qian and L. Duan, *J. Am. Chem. Soc.*, 2008, **130**, 16160.

[5.14] T. Cheng, T. Wang, W. Zhu, X. Chen, Y. Yang, Y. Xu and X. Qian, *Org. Lett.*, 2011, **13**, 3656.

[5.15] M. Taki, M. Desaki, A. Ojida, S. Iyoshi, T. Hirayama, I. Hamachi and Y. Yamamoto, *J. Am. Chem. Soc.*, 2008, **130**, 12564.

[5.16] W. Liu, L. Xu, R. Sheng, P. Wang, H. Li and S. Wu, *Org. Lett.*, 2007, **9**, 3829.

[5.17] J. Barcelo and C. Poschenrieder, *Environ. Exp. Bot.*, 2002, **48**, 75.

[5.18] B. Valeur and I. Leray, *Coord. Chem. Rev.*, 2000, **205**, 3.

[5.19] Z. Krejpcio and R. W. P. J. Wojciak, *Environ. Studies*, 2002, **11**, 251.

[5.20] G. D. Fasman, Coord. *Chem. Rev.*, 1996, **149**, 125.

[5.21] P. Nayak, *Environ. Res.*, 2002, **89**, 111.

[5.22] C. S. Cronan and W. J. Walker, P. R. Bloom, *Nature*, 1986, **324**, 140.

[5.23] G. Berthon, *Coord. Chem.Rev.*, 2002, **228**, 319.

[5.24] D. R. Burwen, S. M. Olsen, L. A. Bland, M. J. Arduino, M. H. Reid, W. R. Jarvis, *Kidney Int.*, 1995, **48**, 469.

[5.25] H. M. Park, B. N. Oh, J. H. Kim, W. Qiong, I. H. Hwang, K.-D. Jung, C. Kim and J. Kim, *Tetrahedron Lett.*, 2011, **52**, 5581.

[5.26] D. Maity and T. Govindaraju, *Chem. Commun.*, 2010, 4499.

[4.27] D. Maity and T. Govindaraju, *Inorg. Chem.*, 2010, **49**, 7229.

[5.28] C. R. Lohani, J.-M. Kim, S.-Y. Chung, J. Yoon and K.-H. Lee, *Analyst*, 2010, *135*, 2079.

[5.29] H. O. Jang, K. Nakamura, S.-S. Yi, J. S. Kim, J. R. Go and J. J. Yoon, *Inclusion Phenom. Macrocycl. Chem.*, 2001, **40**, 313.

[5.30] J. L. Ren, J. Zhang, J. Q. Luo, X. K. Pei and Z. X. Jiang, *Analyst*, 2001, **126**, 698.

[5.31] Y.-W. Wang, M.-X. Yu, Y.-H. Yu, Z.-P. Bai, Z. Shen, F.-Y. Li and X.-Z. You, *Tetrahedron Lett.*, 2009, **50**, 6169.

Appendix

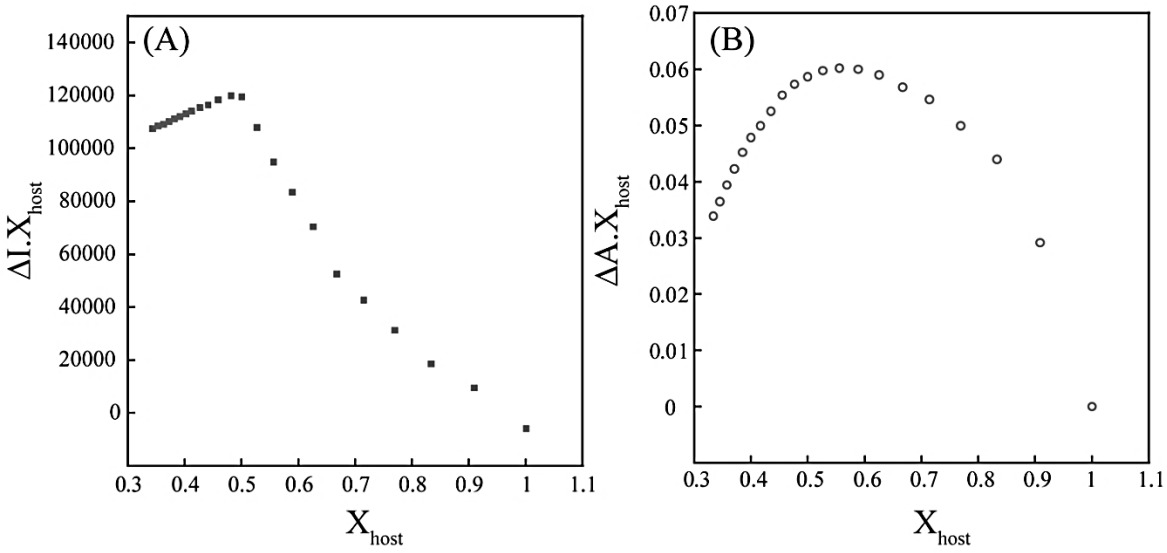

Figure A5.1 (A) Job's plot between $\mathbf{L_3}$ and Cd^{2+} ions. Where X_{host} = the mole fraction of $\mathbf{L_3}$ and ΔI is the change $(I-I_0)$ in the intensity of the emission spectra in presence of guest. (B) Job's plot between $\mathbf{L_3}$ and Al^{3+} ions. Where X_{host} = the mole fraction of $\mathbf{L_3}$ and ΔA is the change $(A-A_0)$ in the absorbance at 510 nm of the UV-Vis spectra in presence of guest.

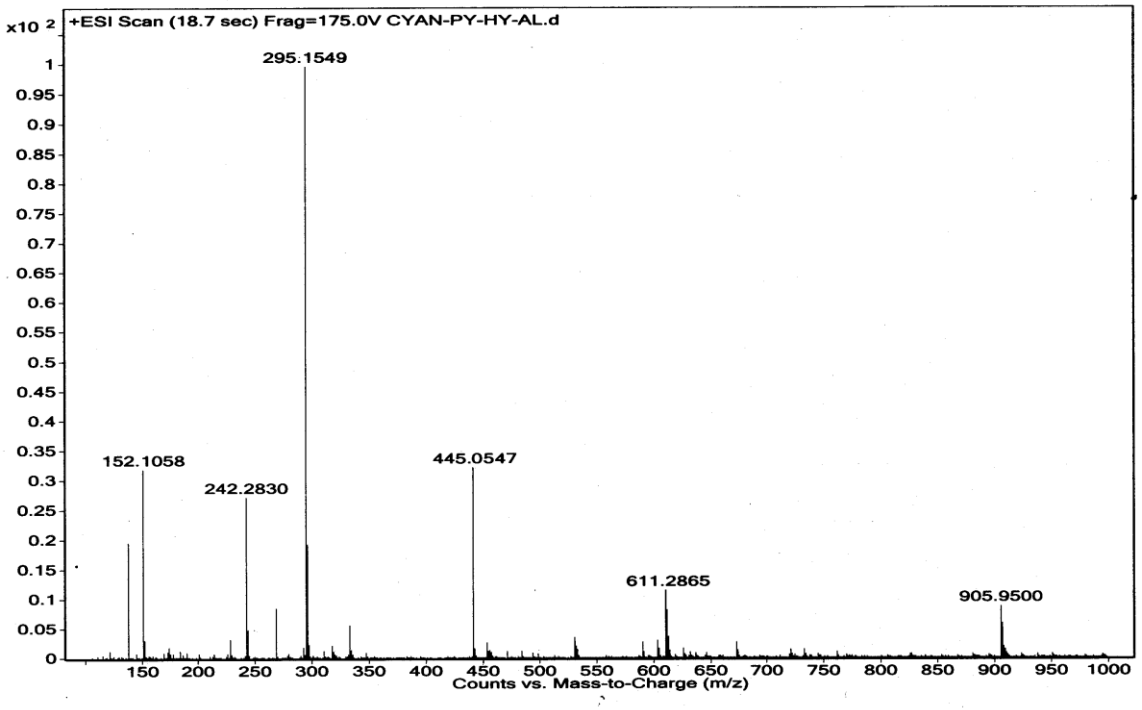

Figure A5.2 Mass spectrum of $\mathbf{L_3}$**-Al** complex.

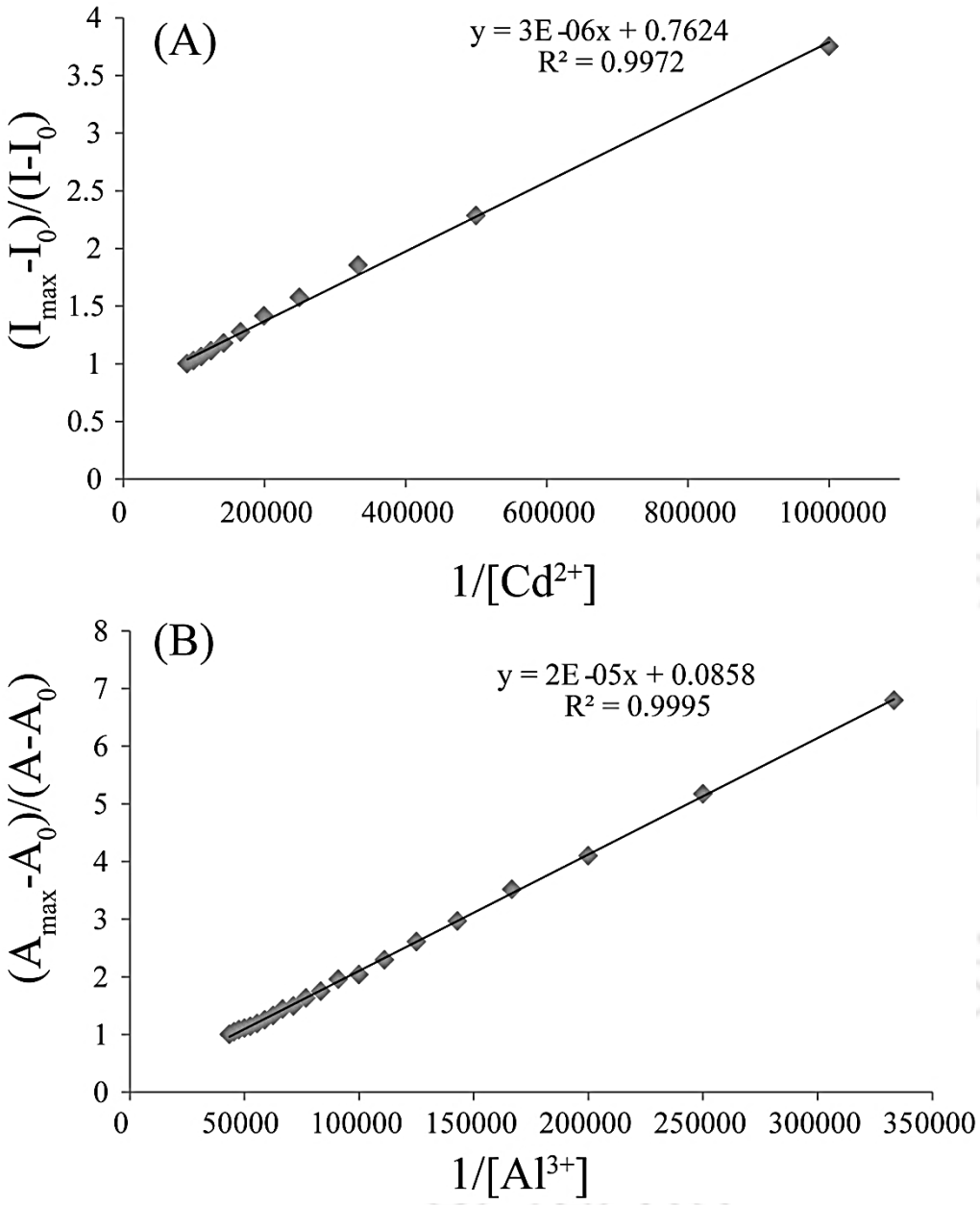

Figure A5.3 (A) Bensei-Hildebrand plot for **L_3-Cd** complex obtained from the fluorescence emission (calculated at λ_{em}) studies. (B) Bensei-Hildebrand plot for **L_3-Al** complex obtained from the UV-Vis studies (calculated at λ= 510nm) studies.

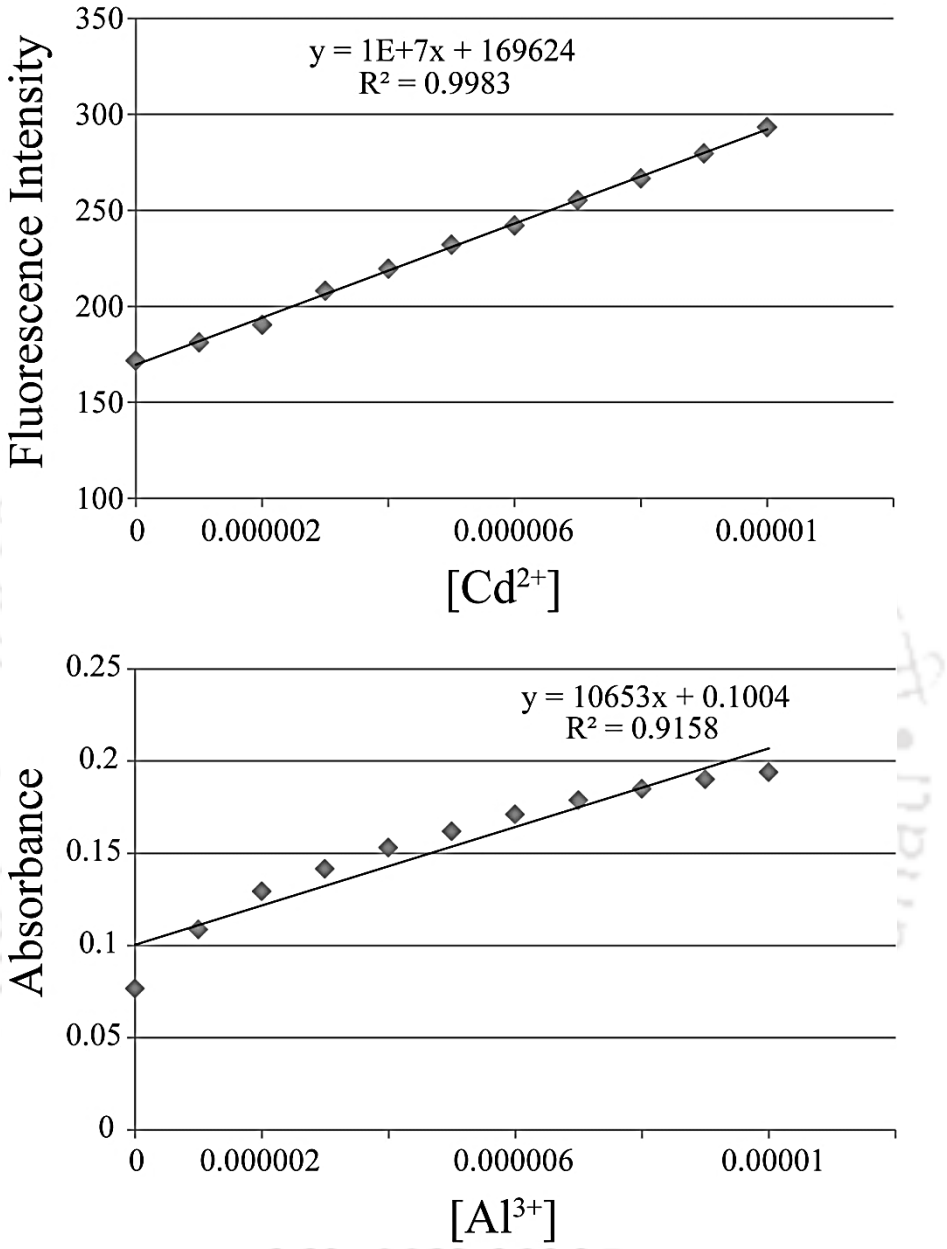

Figure A5.4 (A) Intensity versus Concentration plot for measuring the detection limit (3σ/k, here σ=11.657) of Cd^{2+} by $\mathbf{L_3}$. (B) Absorbance versus Concentration plot for measuring the detection limit (3σ/k, here σ=0.030888) of Al^{3+} by $\mathbf{L_3}$.

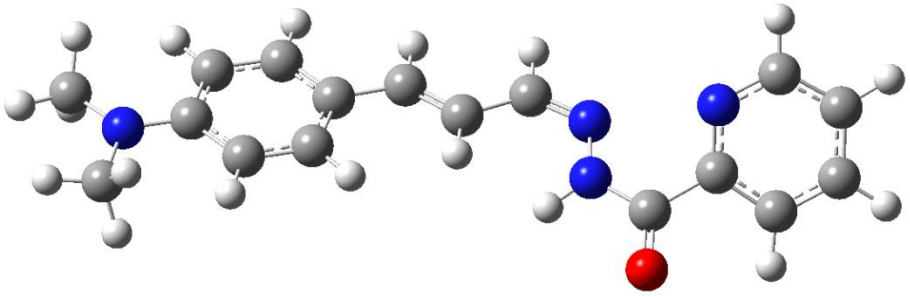

Figure A5.5 Optimized structure of $\mathbf{L_3}$ at B3LYP/6-31+ G(d,p).

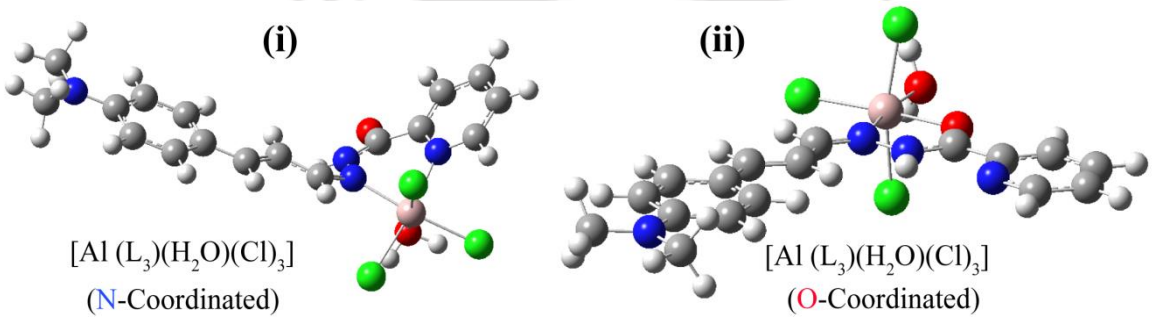

Figure A5.6 Optimized proposed structures of $\mathbf{L_3}$**-Al** complex at B3LYP/6-31+ G(d,p) (i) coordination through pyridine-N (ii) coordination through carbonyl-O.

Table A5.1. Calculated total energies of $\mathbf{L_3}$ and $\mathbf{L_3}$**-Al** complex at B3LYP/6-31+ G(d,p)

Molecule	Total Energy (a.u)
$\mathbf{L_3}$	-952.85647086
$\mathbf{L_3}$**-Al** Complex (N-Coordinated) [Structure (i)]	-2652.59357349
$\mathbf{L_3}$**-Al** Complex (O-Coordinated) [Structure (ii)]	-2652.60637327

Structure **(ii)** is more stable by 8.01 kcal/mole than the structure **(i)**

Table A5.2 Coordinates for optimized geometry of $\mathbf{L_3}$ at B3LYP/6-31+ G(d,p).

Centre number	Atomic Number	Atomic Type	Coordinates (Angstoms)		
			x	y	z
1	6	0	3.723277	-1.65778	-0.42072
2	6	0	2.634455	-0.788824	-0.21742
3	6	0	2.946128	0.534725	0.155113
4	6	0	4.252358	0.961667	0.318962
5	6	0	5.344118	0.077511	0.122704
6	6	0	5.038689	-1.249353	-0.26274
7	1	0	3.527721	-2.68612	-0.71511
8	1	0	2.147965	1.252222	0.320253
9	1	0	4.42959	1.991895	0.601117
10	1	0	5.831694	-1.964763	-0.43996
11	6	0	1.279979	-1.283328	-0.40033
12	6	0	0.112177	-0.609468	-0.25955
13	1	0	1.212517	-2.33374	-0.6869
14	1	0	0.129867	0.435694	0.038527
15	6	0	-1.16664	-1.261673	-0.45062
16	1	0	-1.14548	-2.337525	-0.62321
17	6	0	-4.95118	0.467229	0.03199
18	6	0	-6.13227	0.89006	-0.58919
19	6	0	-7.31574	0.222221	-0.28839
20	1	0	-6.10072	1.725077	-1.27934
21	6	0	-6.05261	-1.141963	1.22462
22	6	0	-7.27818	-0.818878	0.638056
23	1	0	-8.24925	0.512389	-0.76152
24	1	0	-5.99156	-1.93543	1.967308
25	1	0	-8.1758	-1.365736	0.909196
26	7	0	6.647714	0.494555	0.304648
27	7	0	-4.90414	-0.525092	0.931702
28	6	0	-3.69682	1.244029	-0.26855
29	8	0	-3.73534	2.45431	-0.46955
30	7	0	-2.48692	0.587926	-0.28473
31	1	0	-1.70409	1.212181	-0.46516
32	7	0	-2.3609	-0.764307	-0.44021
33	6	0	6.931766	1.889364	0.598148
34	1	0	8.006038	2.014215	0.737087
35	1	0	6.611828	2.563436	-0.20978
36	1	0	6.437781	2.211094	1.522882
37	6	0	7.746312	-0.402532	-0.011
38	1	0	8.690432	0.092268	0.218714

39	1	0	7.697437	-1.320154	0.58806
40	1	0	7.76154	-0.691091	-1.07217

Rotational constants (GHZ): 1.0804546 0.0699011 0.0670133

Table A5.3 Coordinates for optimized geometry of **L_3-Al** complex at B3LYP/6-31+ G(d,p),

Structure **i**

Centre number	Atomic Number	Atomic Type	Coordinates (Angstroms)		
			x	y	z
1	6	0	-4.78031	-1.413635	0.620151
2	6	0	-3.81109	-0.483185	0.186705
3	6	0	-4.28723	0.765794	-0.27251
4	6	0	-5.63395	1.066849	-0.29756
5	6	0	-6.60543	0.124319	0.13982
6	6	0	-6.1332	-1.131358	0.601734
7	1	0	-4.45227	-2.385332	0.980087
8	1	0	-3.5847	1.518903	-0.61581
9	1	0	-5.94365	2.039659	-0.65731
10	1	0	-6.82923	-1.885159	0.946092
11	6	0	-2.4175	-0.844641	0.233085
12	6	0	-1.33503	-0.103639	-0.14705
13	1	0	-2.21344	-1.843211	0.619467
14	1	0	-1.45493	0.902126	-0.53648
15	6	0	-0.02244	-0.641236	0.007953
16	1	0	0.092025	-1.603802	0.497466
17	6	0	3.075936	2.027147	-0.08401
18	6	0	3.584921	3.278196	0.269193
19	6	0	4.539321	3.361929	1.277392
20	1	0	3.215266	4.148928	-0.25741
21	6	0	4.432866	0.9747	1.468391
22	6	0	4.959223	2.188403	1.897696
23	1	0	4.943189	4.324771	1.574493

24	1	0	4.7485	0.034382	1.901261
25	1	0	5.69249	2.197897	2.696085
26	7	0	-7.9449	0.419838	0.115405
27	6	0	2.002475	2.028954	-1.14263
28	8	0	1.919186	2.947945	-1.94784
29	7	0	1.037019	1.059076	-1.10727
30	1	0	0.370756	1.103046	-1.87162
31	7	0	1.111918	-0.123477	-0.37874
32	6	0	-8.40351	1.716907	-0.36137
33	1	0	-9.49154	1.751402	-0.31263
34	1	0	-8.01111	2.538624	0.251411
35	1	0	-8.10657	1.894397	-1.40267
36	6	0	-8.9189	-0.558481	0.578276
37	1	0	-9.92023	-0.139376	0.483087
38	1	0	-8.88043	-1.481153	-0.01456
39	1	0	-8.76059	-0.821954	1.631801
40	7	0	3.511756	0.88525	0.490104
41	17	0	5.160098	-1.675435	-0.19211
42	17	0	2.448881	-1.691459	1.974907
43	17	0	2.11337	-2.896918	-1.28484
44	8	0	3.361292	-0.368296	-2.05384
45	1	0	2.961807	-1.111043	-2.54913
46	1	0	4.319617	-0.563987	-2.04697
47	13	0	2.945671	-1.122958	-0.11205

Rotational constants (GHZ): 0.2758046 0.0556066 0.0510078

Structure **ii**

Centre number	Atomic Number	Atomic Type	Coordinates (Angstroms)		
			x	y	z
1	6	0	-4.77121	-1.653961	-0.000178
2	6	0	-3.71267	-0.720827	-0.00016
3	6	0	-4.06959	0.645907	-0.000074
4	6	0	-5.38865	1.054419	-0.000014
5	6	0	-6.45032	0.108787	-0.00004
6	6	0	-6.09816	-1.265002	-0.000114
7	1	0	-4.53639	-2.715177	-0.000236
8	1	0	-3.29592	1.40767	-0.000054
9	1	0	-5.60533	2.11501	0.000056
10	1	0	-6.86651	-2.027389	-0.000116
11	6	0	-2.35205	-1.2001	-0.000217
12	6	0	-1.19576	-0.4773	-0.000153
13	1	0	-2.24625	-2.284794	-0.000315
14	1	0	-1.23383	0.608426	-0.000034
15	6	0	0.062593	-1.155452	-0.000201
16	1	0	0.076181	-2.242855	-0.000287
17	6	0	2.934039	2.602926	0.000153
18	6	0	4.227788	3.125094	0.000335
19	6	0	4.368224	4.511613	0.000361
20	1	0	5.07619	2.451227	0.000448
21	6	0	1.971226	4.679328	0.000026
22	6	0	3.22197	5.304401	0.000204
23	1	0	5.354857	4.963922	0.000501
24	1	0	1.057957	5.269572	-0.000101
25	1	0	3.287531	6.387301	0.000217
26	7	0	-7.76305	0.511356	0
27	7	0	1.81946	3.353689	0
28	6	0	2.727983	1.132328	0.000111
29	8	0	3.671672	0.318194	0.000216
30	7	0	1.450417	0.707413	-0.000048

31	1	0	0.701578	1.390773	-0.0002
32	6	0	-8.09809	1.927682	0.000234
33	1	0	-9.18216	2.038567	0.000195
34	1	0	-7.70635	2.438743	0.889127
35	1	0	-7.70628	2.439025	-0.888458
36	6	0	-8.83051	-0.478041	0.000118
37	1	0	-9.79286	0.033162	0.000063
38	1	0	-8.78892	-1.12094	-0.888455
39	1	0	-8.78892	-1.120777	0.888815
40	7	0	1.261316	-0.65048	-0.000146
41	17	0	3.327584	-1.492274	2.266072
42	17	0	3.32818	-1.491854	-2.266047
43	17	0	2.238202	-3.712901	-0.00034
44	8	0	5.025555	-2.260014	0.000193
45	1	0	5.147516	-2.806892	-0.793398
46	1	0	5.147293	-2.806882	0.793826
47	13	0	3.112891	-1.641408	-0.00004

Rotational constants (GHZ): 0.1862056 0.0603920 0.0488042

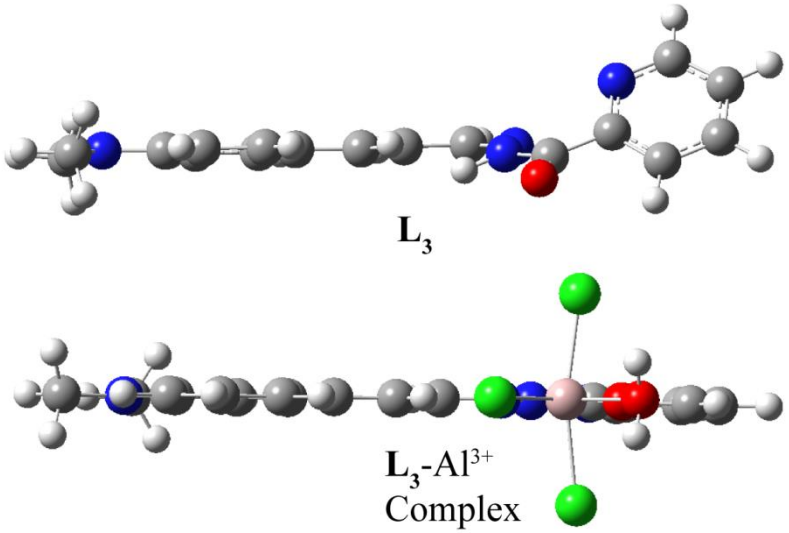

Figure A5.7 Comparison of the planarity between $\mathbf{L_3}$ and its Al-complex (structure **i**)

Table A5.4 Selected orbitals and their energies for $\mathbf{L_3}$ at B3LYP/6-31+ G(d,p).

Occupied Orbitals	Energy (eV)	Vacant Orbitals	Energy (eV)
HOMO -2 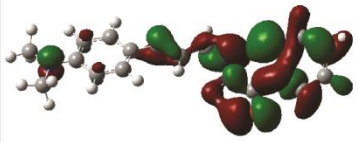	-6.4341	LUMO 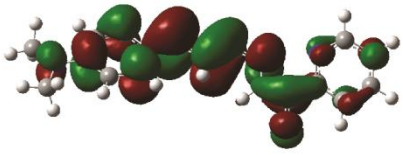	-1.4798
HOMO -1 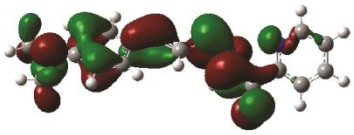	-6.0915	LUMO+1 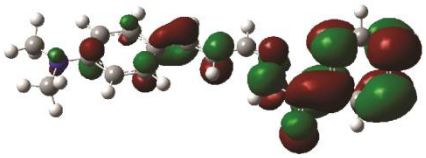	-0.8923
HOMO 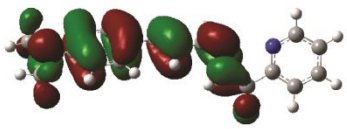	-5.0080	LUMO+2 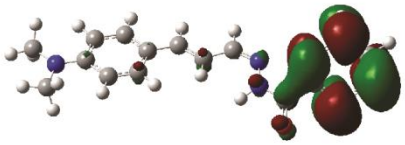	-0.3510

Table A5.5 Selected orbitals and their energies for L_3-Al complex (structure **ii**) at B3LYP/6-31+ G(d,p).

Occupied Orbitals	Energy (eV)	Vacant Orbitals	Energy (eV)
HOMO -2 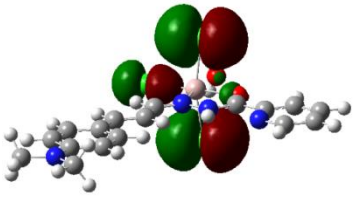	-6.2757	LUMO 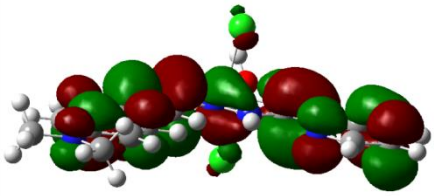	-2.5527
HOMO -1 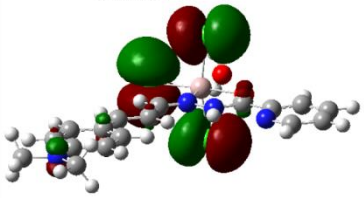	-5.8417	LUMO+1 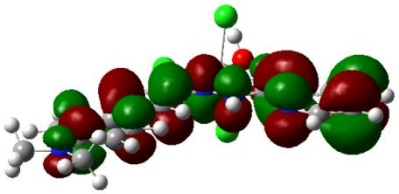	-1.9257
HOMO 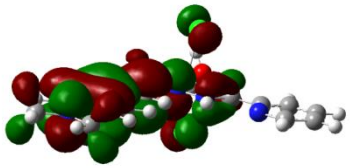	-5.6332	LUMO+2 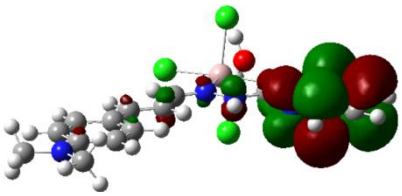	-1.3108

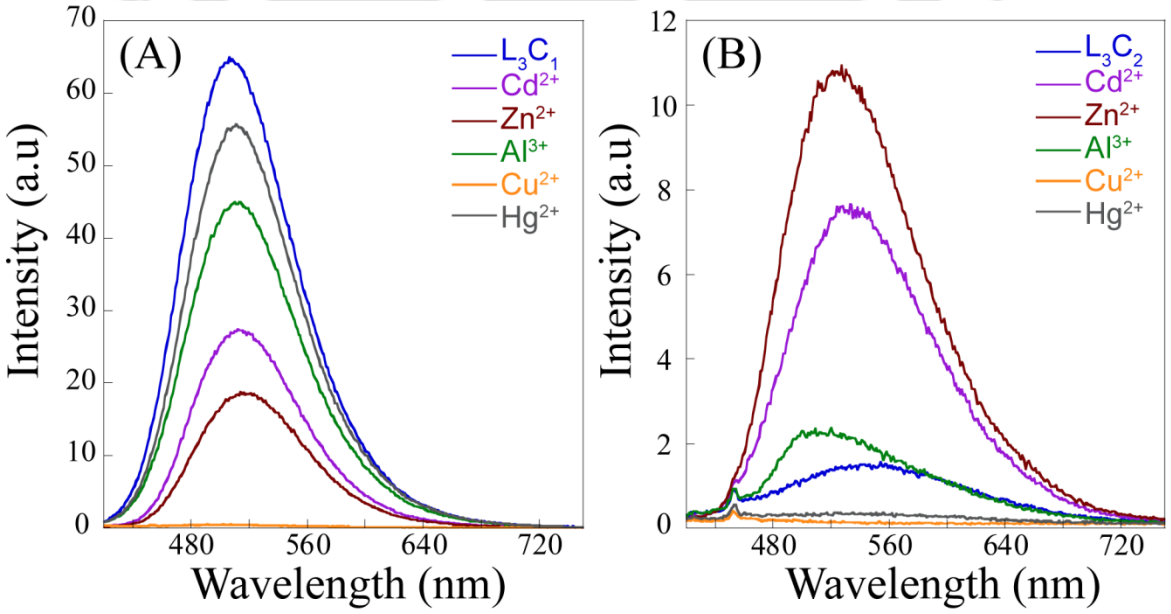

Figure A5.8 Fluorescence spectra of L_3C_1 and L_3C_2 in presence of various cations.

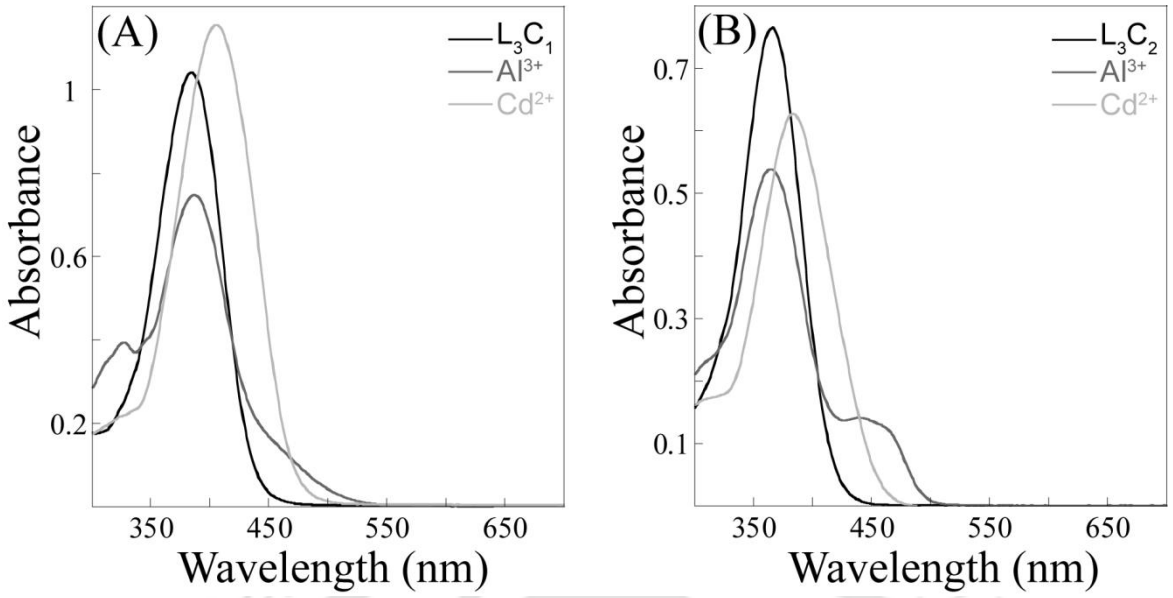

Figure A5.9: UV-Vis spectra of $\mathbf{L_3C_1}$ and $\mathbf{L_3C_2}$ in presence of Al^{3+} and Cd^{2+}.

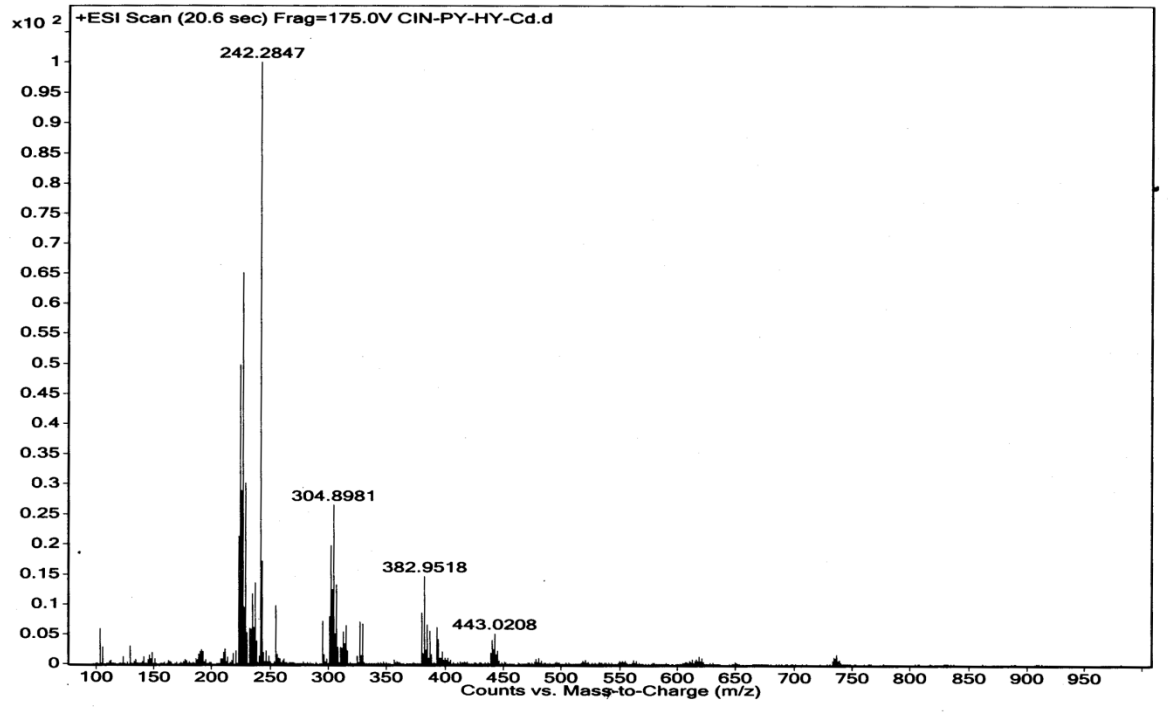

Figure A5.10: Mass spectrum of $\mathbf{L_3}$**-Cd** complex.

Table A5.6 Selectivity coefficient of Cd^{2+} over other metal ions

Metal ions	Selectivity Coefficient
Al^{3+}	5.98
Zn^{2+}	14.44
Pb^{2+}	4.34
Hg^{2+}	7.79
Co^{2+}	1533.33
Cr^{3+}	13.97
Fe^{3+}	48.23
Na^{+}	6.68
Mg^{2+}	1469.32

Table 2.1 Crystallographic Parameters and Refinement Details of **L_3** and **L_3-Cd** Complex.

Parameters	L_1	L_1-Cd
Formula	$C_{17}H_{18}N_4O$	$C_{34}H_{40}CdCl_2N_8O_4$
Formula weight	294.35	808.05
Crystal system	Monoclinic	Monoclinic
Space group	P21	C2/c
a (Å)	5.9895(4)	18.0309(4)
b (Å)	14.7978(8)	10.7197(4)
c (Å)	17.8142(14)	20.3059(6)
β (deg)	96.481(6)	111.574(2)
V (Å)	1568.81(18)	3649.88(19)
Z	4	4
T (K)	298(2)	298(2)
μ (cm^{-1})	0.081	0.793
dcal (g cm^{-3})	1.246	1.470
crystal dimens (mm^3)	0.25×0.16×0.14	0.26×0.20×0.16
no. of reflns collected	2513	3086
no. of unique reflns	5103	4158
no. of params	401	236
R1; wR2 (I>2σ(I))	0.0776; 0.2489	0.0308;0.0958
R1; wR2(all)	0.1564; 0.3180	0.0422; 0.1066
GOF (F2)	0.932	0.783
CCDC No.	989403	989402

Chapter 6

A Rhodamine based Fluorophoric Probe for Sensing of Cu^{2+} Ions by Switch ON Red Fluorescence and Application of the Metal-Ligand Complex as a Selective Sensor for S^{2-} Ions

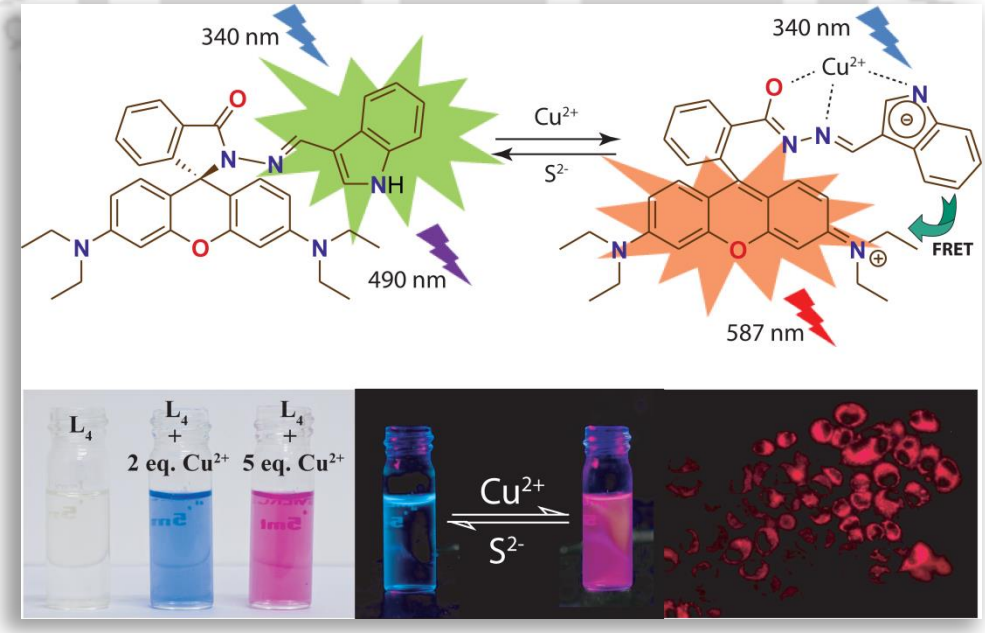

Chapter 6

6.1. Background and Focus of the Chapter

As discussed in section 4.1 Copper is one of the most abundant essential trace elements found in human body and has a fundamental role to sustain important physiological processes.[6.1-6.5] Owing to its significant physiological relevance and associated biomedical implications, there is considerable interest in developing selective and sensitive copper sensors. Along with specific sensors for biologically important cations development of selective and efficient signaling units for detection of various chemically and biologically important anions has also attained significant interest.[6.6,6.7] Being one of the biologically and environmentally important anions, sulfide is largely used in industrial processes, for instances, conversion into sulfur, preparation of sulfuric acid and dyes, cosmetic manufacturing, production of wood pulp, etc.[6.8] Apart from industrial processes sulfide anions can also be generated due to microbial reduction of sulfate by anaerobic bacteria or formed from the sulfur-containing amino acids in meat proteins.[6.8] Consequently there are enough risks for the sulfide ions to be exposed to drinking water. Sulfide can damage mucous membranes and can cause unconsciousness and respiratory problems.[6.8-6.10] The protonated forms HS^- or H_2S are even more toxic than the sulfide itself. At a low concentration, H_2S can produce dizziness, while at a higher concentration it can result in loss of consciousness, permanent damage of brain tissues, or even death through suffocation.[6.11] Therefore, development of quick and sensitive method for immediate sulfide detection in aqueous media and in biological systems is of high interest.

In the recent literature, a large number of colorimetric and fluorescent chemosensors have been reported for selective sensing of copper and sulfide ions with absorbance and emission in the visible region.[6.12–6.45] Although chemosensors with spectroscopic responses (absorbance/emission) at visible region have important roles in various research areas, recently molecular probes with near-infrared (NIR, 700–1000 nm) optical responses are particularly gaining special interest.[6.46-6.48] As for NIR radiation the possibility of scattering is minimized, so unlike UV-Vis radiation, NIR radiation provides high sample penetration. Additionally, the autofluorescence generated from the chromophores and

macromolecules present in the analytic samples are less likely to interfere. This phenomenon enables the assessment of molecular and physiological events in several layers deep inside the analyte samples and tissues.[6.49-6.51] There have been few reports on UV-Vis–NIR sensing of cation and anions.[6.52-6.65] Together with visible and NIR absorbance signals, a fluorescence response at a visible region would be an added advantage to the sensing of cations and anions over the methods involving just one kind of optical response. Commonly one of the three different photoinduced processes are involved for the signaling event of luminescence based chemosensors, namely, PET (photoinduced electron transfer),[6.66-6.68] PCT (photoinduced charge transfer),[6.69] and RET (resonance energy transfer).[6.70-6.74] RET is a nonradiative energy transfer process in which the excitation energy of the donor is transferred to the nearby acceptor via long-range dipole-dipole interaction and/or short-range multipolar interaction. RET-based probes are particularly favorable for biological applications than single dye-based probes, as the RET-based process is not dependent on the concentration of a single emissive probe and one can quantitively measure the analyte concentration by using the ratio of intensities of the well separated fluorescence peaks with rational intensities at two different wavelengths for free probe and analyte bound probe.[6.75-6.79]

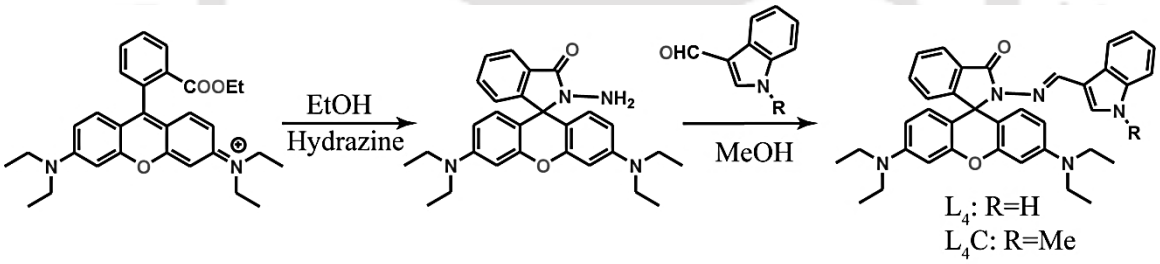

Scheme 6.1 Synthetic scheme for the ligand **L_4** and **L_4C**.

Encouraged by the biological importance of Cu^{2+} and S^{2-} ions, in this chapter[6.80] we envisioned to combine the advantage of the characteristics of an NIR optical response with the sensitivity of a RET based fluorophoric response for the construction of a chemosensor probe (Scheme 6.1), that may be potentially useful for the detection of Cu^{2+} as well as S^{2-} ions at physiological pH. Herein, we discuss the metal and anion sensing capabilities of an indole functionalized rhodamine based fluorophoric ligand **L_4** and the absorption and fluorescence behaviour of **L_4** upon metal complexation. We have also demonstrated by fluorescence microscopic studies that ligand **L_4** could readily detect the presence of intracellular Cu^{2+} as well as S^{2-} ions in live HeLa cells via a characteristic fluorescence

switch ON/OFF mechanism. We have reasonably chosen rhodamine and indole derrivatives as the two fluorophores for designing the receptor **L_4**; the binding of Cu^{2+} with **L_4** trigger the opening of the spyrolactum ring of the rhodamine derivative, whose absorption spectra shows a significant spectral overlap with the emission spectra of the indole moiety and offers the chance of a RET process. In addition to the FRET signal, an increased absorbance in the NIR region of the UV-Vis spectra is also noticed. The 'switch ON' behavior of the receptor **L_4** is observed selectively in presence of Cu^{2+} ions. The formation of the **L_4-Cu** complex is reversible but the reversibility of the **L_4-Cu** system to regenerate **L_4** is noticeable only in presence of S^{2-} anions.

6.2. UV-Vis spectroscopic studies of L_4 in presence of Cu^{2+}

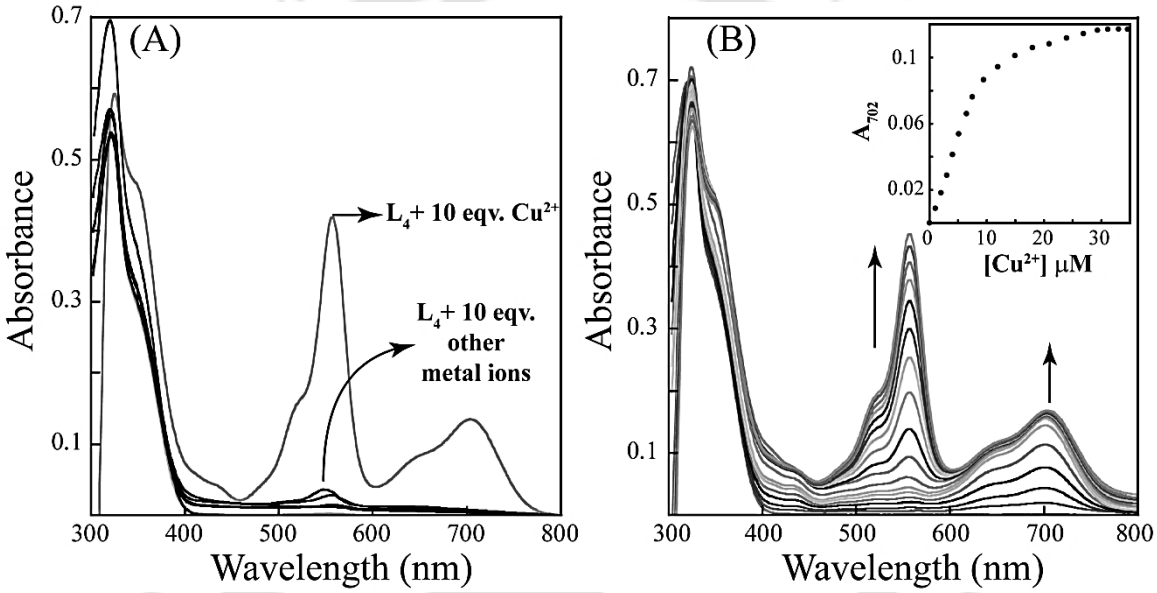

Figure 6.1 (A) UV-Vis absorption spectra of receptor **L_4** (10 μM) observed upon addition of 10 equivalent metal ions (perchlorate or nitrate salts of Na^+, K^+, Ca^{2+}, Mg^{2+}, Cr^{3+}, Hg^{2+}, Cu^{2+}, Pb^{2+}, Zn^{2+}, Fe^{2+}, Co^{2+}, Ni^{2+}, Cd^{2+}, and Ag^+) in a CH_3CN/aqueous HEPES buffer (1 mM, pH 7.3; 1:4 v/v). (B) UV-Vis titration spectra of **L_4** (10 μM) upon incremental addition of $Cu(ClO_4)_2$ in CH_3CN/aqueous HEPES buffer (1 mM, pH 7.3; 1:4 v/v). **Inset:** Changes in the absorbance at 702 nm with incremental addition of Cu^{2+}.

UV-Vis spectra recorded for **L_4** in CH_3CN/aqueous HEPES buffer (1 mM, pH 7.3; 1:4, v/v) indicated an absorption maximum at 324 nm, which may possibly be attributed to intra-molecular π-π* charge transfer (CT) transition. According to previous studies certain transition-metal ions bind selectively with suitable derivatives of rhodamine,[6.81] wherein metal-ligand binding induces opening of the spirolactam ring and generation of the xanthene form. This structural change is manifested in the electronic and fluorescence spectral patterns. Thus the selectivity of **L_4** was checked with perchlorate or nitrate salts of

Na^+, K^+, Ca^{2+}, Mg^{2+}, Cr^{3+}, Hg^{2+}, Cu^{2+}, Pb^{2+}, Zn^{2+}, Fe^{2+}, Co^{2+}, Ni^{2+}, Cd^{2+}, and Ag^+ in CH_3CN/aqueous HEPES buffer (1 mM, pH 7.3; 1:4 v/v). A significant change in UV-Vis spectral pattern was observed only in presence of Cu^{2+}, among all the other metal ions used (Figure 6.1A). During sequential titration (0 eqv. to 3 eqv. of Cu^{2+}) an NIR absorption band appeared around 702 nm along with a hump in the visible region near 557 nm (Figure 6.1B) and the solution turned from colorless to blue (Appendix, Figure A6.1). With further increase in the concentration of Cu^{2+} the color of the solution changed from blue to pink with the emergence of a sharp peak near 557 nm of the electronic spectra. It is significant to mention that the detection limit of **L_4** for Cu^{2+} ions was found to be 8.8 ppb, which is much lower than the U.S. EPA maximum allowable limit for Cu^{2+} ions (1.3 ppm) in drinking water.

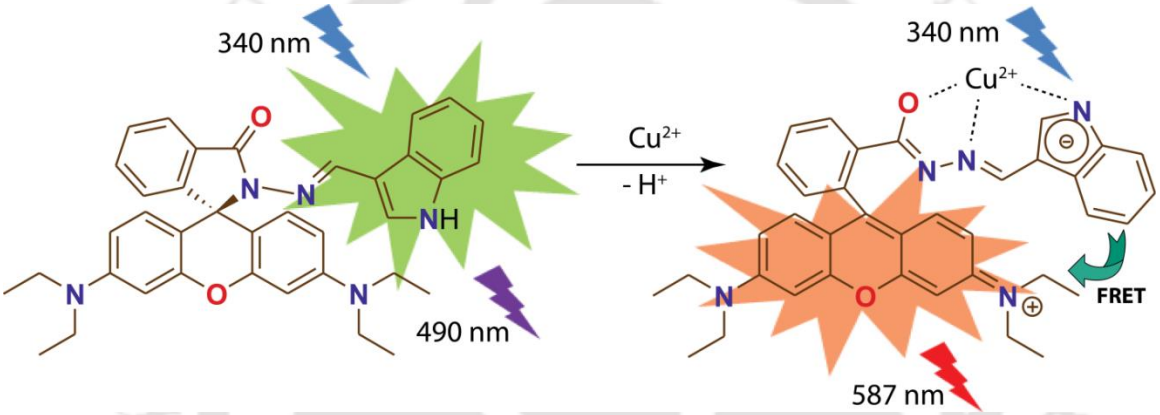

Scheme 6.2 Cu^{2+}-induced FRET OFF→ON of the receptor **L_4**.

In the recent literature deprotonation induced NIR sensing by indole moiety was reported by P. Ghosh and co-workers.[6.82] In the present study, visual color change of the solution from colorless to blue is a consequence of the ratiometric deprotonation of the NH proton of indole moiety in presence of the metal cation. Such a huge shift of absorption spectra could be attributed to the high conjugation and planarity of the indole moiety of **L_4** with the binding site of the receptor (Scheme 6.2) which favors maximum distribution of the negative charge of the deprotonated receptor in the presence of the guest metal ion. Regardless of the deprotonation of indole moiety, the formation of the peak near 557 nm is mostly due to the breakage of the spirolactum ring structure of **L_4** and subsequent formation of the xanthene form. The spectral changes due to formation of the **L_4-Cu** complex and the deprotonation of the indole unit occur simultaneously with addition of Cu^{2+}. However, in the present case the individual steps cannot be analyzed in solution. Therefore, the apparent binding constant for the formation of **L_4-Cu** complex is calculated

on the basis of change in absorbance at 702 nm by considering a 1:1 binding stoichiometry. The apparent binding constant (*K*) determined by the B-H method was found to be 1.71×10^4 M^{-1} (Appendix, Figure A6.2).

To verify the significance of the deprotonation of indole –NH in generating the NIR peak, a new control compound **L_4C** was synthesized where the indole –NH proton was replaced by $–CH_3$. As expected the compound **L_4C** failed to show an NIR peak in presence of Cu^{2+}. The only change of the absorption spectra of **L_4C** in presence of Cu^{2+} ions was the formation of a sharp peak near 550 nm; predominantly due to the rupture of the spirolactum ring of rhodamine into the xanthene form (Appendix, Figure A6.3).

6.3. Fluorescence spectroscopic studies of L_4 in presence of Cu^{2+}

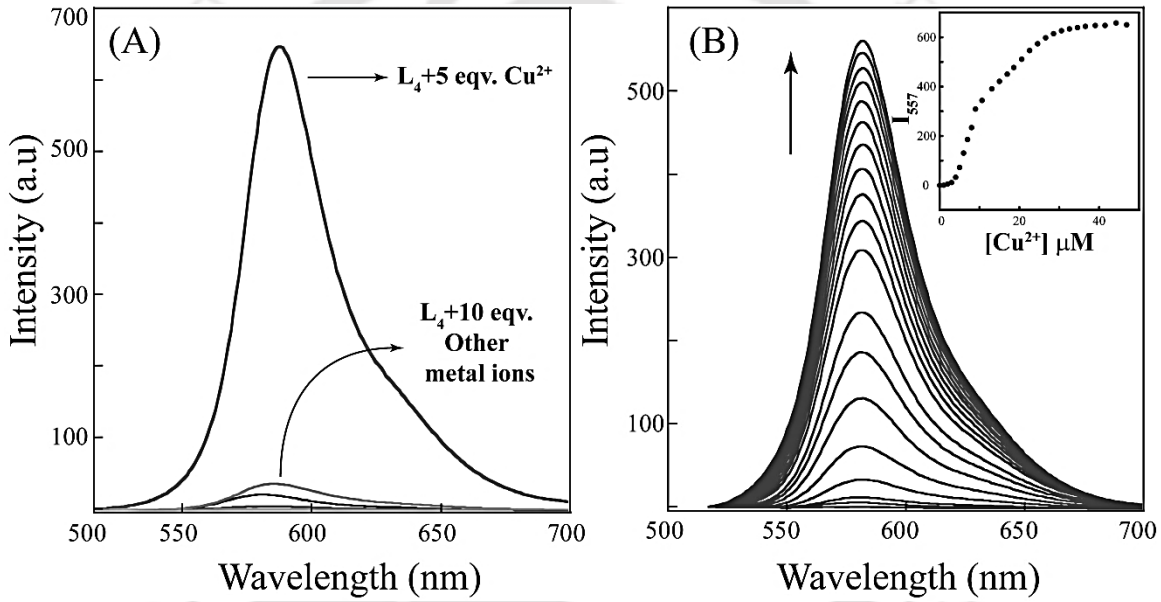

Figure 6.2 (A) Changes of the fluorescence emission of receptor **L_4** (10 μM) observed upon addition of metal ions (perchlorate or nitrate salts of Na^+, K^+, Ca^{2+}, Mg^{2+}, Cr^{3+}, Hg^{2+}, Cu^{2+}, Pb^{2+}, Zn^{2+}, Fe^{2+}, Co^{2+}, Ni^{2+}, Cd^{2+}, and Ag^+) (10 equivalent) in a CH_3CN/aqueous HEPES buffer (1 mM, pH 7.3; 1:4 v/v). (B) Fluorescence titration spectra of **L_4** (10 μM) upon incremental addition of 5 equiv. of $Cu(ClO_4)_2$ in CH_3CN/aqueous HEPES buffer (1 mM, pH 7.3; 1:4 v/v) λ_{ex}= 495 nm. **Inset:** Changes in the fluorescence intensity at 585 nm with incremental addition of Cu^{2+}.

The selective binding of **L_4** with Cu^{2+} among all other metal ions was also studied using the emission spectroscopy of the solution of **L_4** (10.0×10^{-6} M) in the absence and presence of an excess (10 equiv) of each of the metal ions in CH_3CN/aqueous HEPES buffer (1 mM, pH 7.3; 1:4 v/v) (Figure 6.2A). As the receptor **L_4** bears two different fluorophore units so we consider it to be appropriate to study the metal binding event of **L_4** at two different excitation wavelengths corresponding to the excitation wavelength of the

xanthene unit (495 nm) and the indole unit (340 nm) respectively. As evident from Figure 6.2B, excitation of the initial solution of receptor **L_4** at 495 nm wavelength did not show any significant emission over the range of 500 nm to 700 nm. This supports the facts that in absence of metal ions the receptor remains in the spirolactum form, and the nonexistence of the highly conjugated xanthene form results in the suppression of emission in the above mentioned region. Addition of Cu^{2+} to this receptor solution induces a significant switch ON fluorescence response near 585 nm, with a visual display of reddish-pink fluorescence. Switch ON responses for the absorption spectral band at 557 nm and the emission band near 585 nm on binding to Cu^{2+} suggest opening of the spirolactam ring in **L_4** on metal ion coordination. It can also be observed from Figure 6.2A that the metal-ligand binding induced ring opening of **L_4** and the generation of xanthene moiety is very much selective towards Cu^{2+} ions and does not reveal any noticeable spectral change for other tested metal ions (Na^+, K^+, Ca^{2+}, Mg^{2+}, Cr^{3+}, Hg^{2+}, Pb^{2+}, Zn^{2+}, Fe^{2+}, Co^{2+}, Ni^{2+}, Cd^{2+}, and Ag^+). To gain an insight of the properties of **L_4** as a receptor for Cu^{2+}, a titration of the receptor was performed with increasing concentration of Cu^{2+}. As described in Figure 6.2B the fluorescence intensity of a 10 μM solution of **L_4** was enhanced with incremental addition of Cu^{2+} ions, which also confirmed that receptor **L_4** exhibited a high sensitivity toward Cu^{2+}, with near about 600 fold increase of its fluorescence intensity upon addition of only 5.0 equiv of Cu^{2+} ions.

The binding of Cu^{2+} ion induces opening of the spirolactam ring in **L_4** with an associated switch on UV-Vis spectral response in the range 500−580 nm, which has a significant spectral overlap with the emission spectrum of the indole fragment and this fact unlocks a plausible route for nonradiative transfer of excitation energy between donor indole to acceptor xanthene moiety and initiates an intramolecular FRET process. In the free ligand **L_4** the FRET pathway is totally suppressed and only an emission maximum near 480 nm is observed when excited at 340 nm. Binding of the receptor to Cu^{2+} induces the FRET process to produce an intense rhodamine-based red emission i.e. energy transfer from indole to xanthene is due to the ring opening resulting in increase of overlap integral between indole and xanthene moiety.[6.78] Thus when titrated with increasing concentration of Cu^{2+} the emission band with a λ_{max} near 457 nm starts to decrease along with a concomitant generation of a new fluorescence band at 585 nm. This change in fluorescence was also observed visually and the color changed to reddish-pink as shown in the inset of Figure 6.3A.

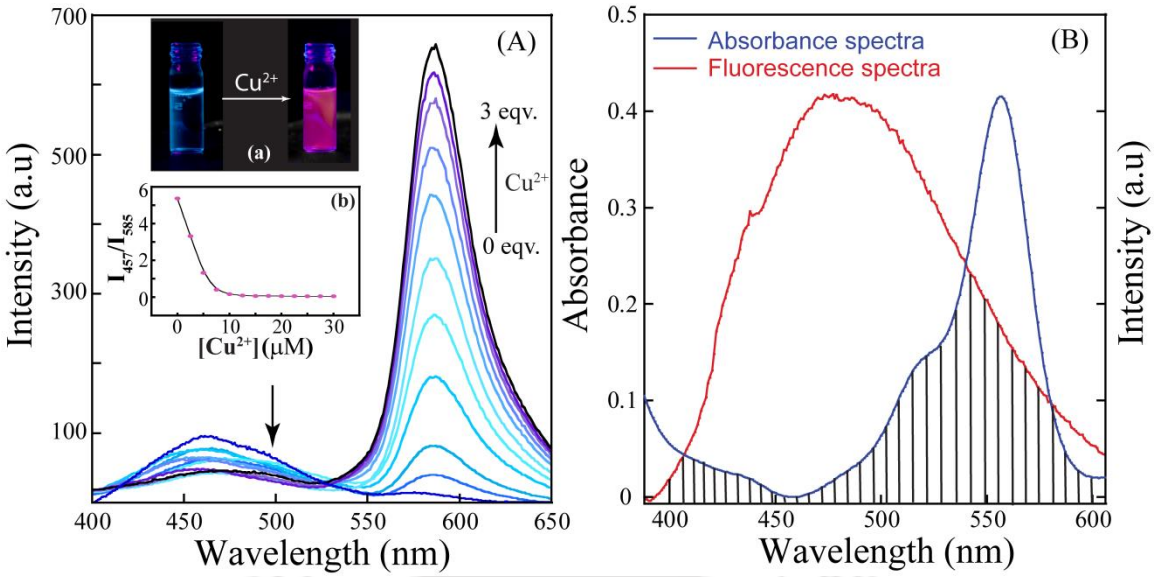

Figure 6.3 Fluorescence spectra (λ_{ex} = 340 nm) of (A) $\mathbf{L_4}$ (10 μM) with varying [Cu^{2+}] (0−3 eqv.), and (B) is the overlap (shown with vertical stripes) between emission and absorption spectra of the donor and acceptor, respectively. All studies were carried out in CH_3CN/aqueous HEPES buffer (1 mM, pH 7.3; 1:4 v/v) medium. **Inset:** (a) Visual change of the colour of the $\mathbf{L_4}$ solution in presence of Cu^{2+} under UV light; (b) The changes of fluorescent intensity ratios at 457 and 585 nm (I_{457}/I_{585}) with increasing concentration of Cu^{2+}.

The singlet−singlet excitation energy-transfer efficiency (Φ_{ET}) between donor and acceptor were evaluated from steady state fluorescence data. The value for Φ_{ET} was found to be 51.5% while the Förster critical distance (R_0) was calculated as 35.8 Å.

The complex formed between $\mathbf{L_4}$ and Cu^{2+} is found to be 1:1 in stoichiometry, which is established with the help of job's plot (Appendix, Figure A6.4) from fluorescence spectrometry. Further confirmation of 1:1 stoichiometry was obtained from the ESI-MS studies. The molecular-ion peak is observed at m/z 708.21 in the mass spectrum which is related to the mass of [$\mathbf{L_4}$ + Cu^{2+} + NO_3] (Appendix, Figure A6.5).

The role of the C=O amide bond on binding Cu^{2+} cations was examined using FTIR techniques. The FTIR spectra of $\mathbf{L_4}$ revealed that the peak at 1702 cm^{-1}, the characteristic stretching frequency for the C=O amide bond of the rhodamine unit, shifted to 1630 cm^{-1} in presence of 2 equiv of the Cu^{2+} ion (Appendix, Figure A6.6). Such shift in the stretching frequency of C=O amide bond of the rhodamine unit on binding to a metal ion has been reported earlier.[6.83] Thus FTIR studies suggest that the shift in the stretching frequency of C=O bond was due to its coordination with metal cation (Cu^{2+}).

6.4. UV-Vis spectroscopic studies of L_4-Cu complex in presence of S^{2-}

Hence from the above mentioned studies we can conclude that **L_4** selectively binds with Cu^{2+} to form **L_4-Cu** complex with considerable change in its spectral properties. We have further studied the influence of different anions on the rupture of this metal-ligand complex and their effect on the reversibility of this complex to regenerate **L_4.** The optical properties of the **L_4-Cu** complex was studied in presence of different anions such as F^-, Cl^-, Br^-, I^-, CN^-, $H_2PO_4^-$, NO_3^-, ClO_3^-, ClO_4^-, SO_4^{2-}, HSO_3^-, PO_4^{3-} and S^{2-}. It was worth mentioning that the regeneration of compound **L_4** is observed only by adding S^{2-} to the solution containing **L_4-Cu**, whereas other anions failed to produce any discernible spectral change (Figure 6.4A). For further understanding a solution of **L_4** in CH_3CN/aqueous HEPES buffer (1 mM, pH 7.3; 1:4 v/v) containing 2 equiv. of Cu^{2+} is titrated in presence of sulfide anions. The UV-Vis spectral pattern of the titration experiment (Figure 6.4B) was similar but in reverse direction to the titration curve obtained with Cu^{2+} (Figure 6.1B). This fact is an evidence that ligand **L_4** is regained from complex in presence of S^{2-}.

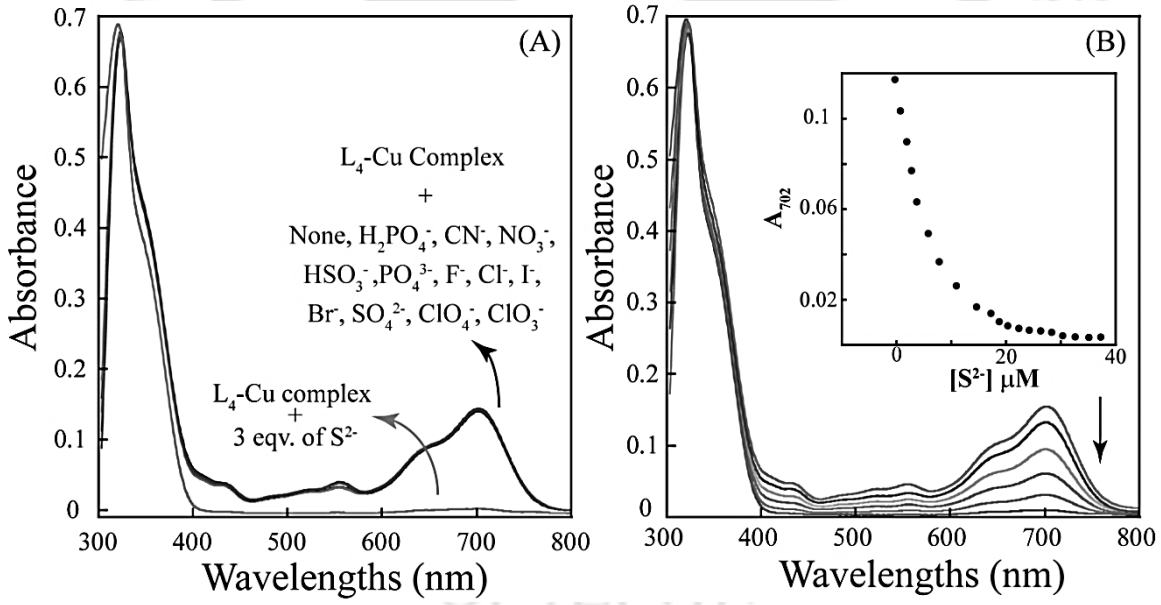

Figure 6.4 (A) Changes in the absorption spectra of **L_4-Cu** complex in presence of different anions. (B) UV-Vis titration spectra of **L_4** (10 µM) with 2 equiv of Cu^{2+} upon addition of sodium sulfide (30 µM) in CH_3CN/aqueous HEPES buffer (1 mM, pH 7.3; 1:4 v/v). **Inset:** Changes in the absorbance at 702 nm with incremental addition of S^{2-}.

6.5. Fluorescence spectroscopic studies of L_4-Cu complex in presence of S^{2-}

Apart from the results obtained from UV-Vis studies, the fluorescence spectroscopy also shows that the emission of the **L_4-Cu** complex returns to its native **L_4** state, selectively in presence of sulfide anions (Figure 6.5A). To further understand the fluorescence "ON-

OFF'' switching property of the sensor, we have performed fluorescence titration experiment. The fluorescence intensity of the compound **L_4** is enhanced to a moderate level in presence of 2 equiv. of Cu^{2+} ions, the resulting **L_4-Cu** complex is then titrated by the addition of various amounts of sulfide ions. Figure 6.5B shows that the intensity of the fluorescence emission decreases with increasing concentration of sulfide anion and on addition of near about 3 equiv. of S^{2-} anion both the intensity and overall pattern of emission spectrum closely matches those of compound **L_4** (Figure 6.2B), so the fluorescence intensity along with the maximum emission peak are totally regenerated. As the fluorescence spectrum was recorded within 15 sec after sulfide anion addition, and the intensity does not change with time, so the monitoring system is a virtually real-time and stable. The results of the spectroscopic studies indicated that the sensor **L_4** was recycled during the detection of sulfide anions.

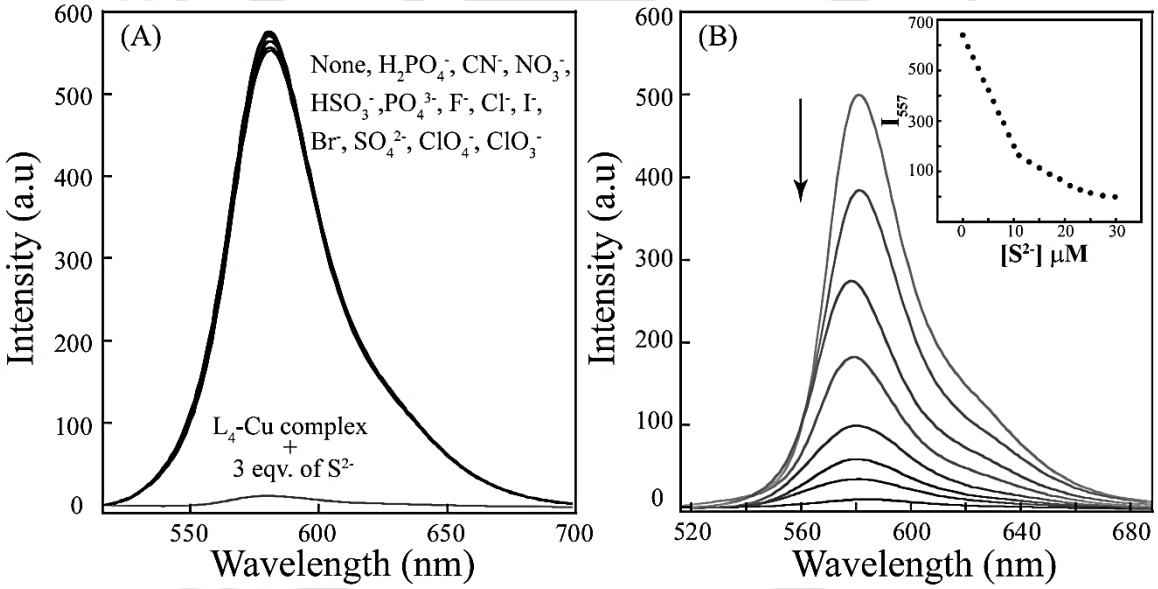

Figure 6.5 (A) Changes in the fluorescence spectra of **L_4-Cu** complex in presence of different anions (λ_{ex} = 495 nm). (B) Fluorescence titration spectra (λ_{ex} = 495 nm) of **L_4** (10 μM) with 2 equiv of Cu^{2+} upon addition of sodium sulfide (30 μM) in aqueous CH_3CN/aqueous HEPES buffer (1 mM, pH 7.3; 1:4 v/v). **Inset:** Changes in the fluorescence intensity at 585 nm with incremental addition of S^{2-}.

From our Cu^{2+} binding studies it was evident that the binding induced breakage of the spirolactum ring of **L_4** initiates the FRET pathway for efficient transfer of energy from indole moiety to the xanthene unit in the **L_4-Cu** complex. It is obvious that if the regeneration of **L_4** from **L_4-Cu** complex is possible in presence of sulfide anion then the removal of Cu^{2+} must affect the FRET process. Thus, continuous addition of sulfide ions to the **L_4-Cu** complex generates a spectrum (Figure 6.6) which is equivalent to the spectra

of **L_4** (when excited at 340 nm). The above mentioned fact provides strong evidence of the dissociation of **L_4-Cu** complex in presence of S^{2-} anions to restore the native structure of **L_4**.

In order to verify the reason of the fluorescence "off–on" property, the mass spectrum of the **L_4-Cu** system is also studied in presence of S^{2-}. The mass spectrum of the **L_4-Cu** system shows a molecular-ion peak at m/z 708.21, corresponding to [**L_4** + Cu+ NO_3]$^+$, while subsequent addition of S^{2-} ions to the above solution gives a molecular ion peak at m/z 584.30 (Appendix, Figure A6.7) which confirmed the identity of free **L_4** and substantiated the mechanism of the sensing of sulfide anions.

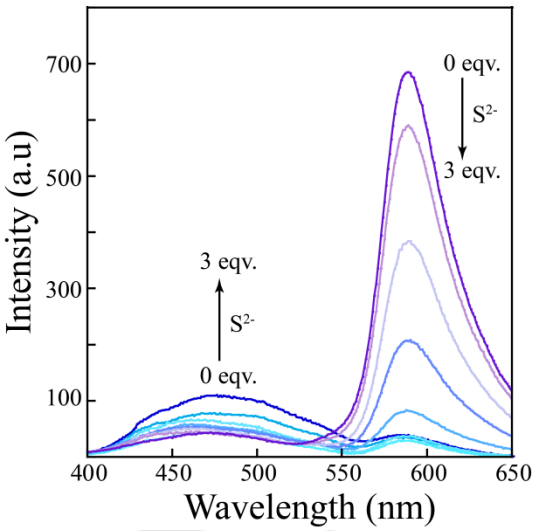

Figure 6.6 Fluorescence titration spectra (λ_{ex} = 340 nm) of **L_4** (10 μM) with 2 equiv of Cu^{2+} upon continuous addition of sodium sulfide in CH_3CN/aqueous HEPES buffer solution (1 mM, pH 7.3; 1:4 v/v).

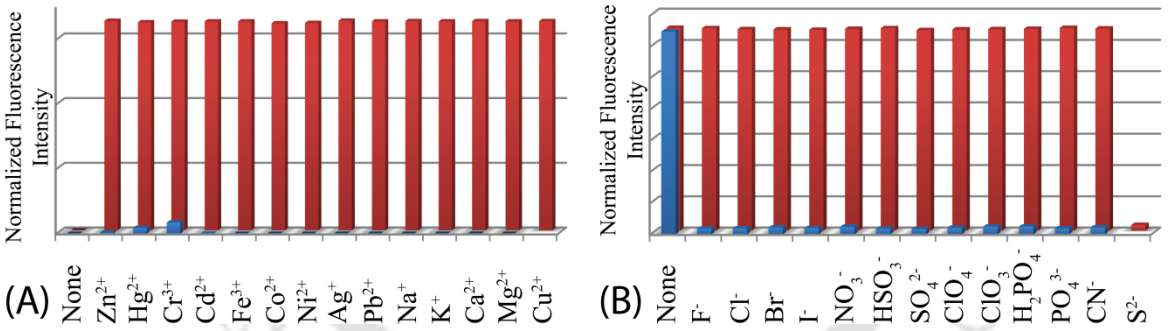

Figure 6.7 (A) Normalized fluorescence responses of **L_4** (10 μM) to various cations in CH_3CN/aqueous HEPES buffer (1 mM, pH 7.3; 1:4 v/v). The blue bars represent the emission intensities of **L_4** in the presence of cations of interest (50 μM). The red bars represent the change of the emission that occurs upon the subsequent addition of Cu^{2+} to the above solution; (B) Normalized fluorescence responses of **L_4-Cu** to various anions in CH_3CN/aqueous HEPES buffer (1 mM, pH 7.3; 1:4 v/v). The red bars represent the emission intensities of **L_4-Cu** in the presence of anions of interest (50 μM). The blue bars represent the change of the emission that occurs upon the subsequent addition of S^{2-} to the above solution. The intensities were recorded at 585 nm.

The sensing efficiency of **L_4** and **L_4-Cu** complex was further tested in presence of other cations and anions, which may interfere in estimation of copper and sulfide (Figure 6.7). The receptor **L_4** and the **L_4-Cu** complex both performed well in presence of other ions and sensed the respective analytes from a competitive environment.

6.6. Biological studies of L_4 in presence of Cu^{2+} and S^{2-}

Owing to its favorable binding properties with copper (II) and intense emission in visible region, it was conceived that compound **L_4** could be exploited for fluorescence imaging of live cells, particularly for sensitive detection of intracellular Cu^{2+}. However, to pursue this goal, it was pertinent to assess the cytotoxic effect of compound **L_4** on live cells. Varying concentrations of compound **L_4** and **L_4-Cu** complex were thus chosen and their cytotoxic effect on HeLa cells was ascertained following an exposure period of 24 h. The well-established MTT assay, which is based on mitochondrial dehydrogenase activity of viable cells, was adopted. It is quite evident from Figure 6.8 that compound **L_4** failed to exert any effect on the viability HeLa cells, irrespective of the chosen concentrations of the compound. However, exposure of HeLa cells to the lowest concentration of **L_4-Cu** complex (15 μM) resulted in a decline in cell viability. In presence of higher concentrations of **L_4-Cu** complex, the effect was more prominent and indicated a dose-dependent cytotoxic effect on HeLa cells. Previous literature reports also suggest cytotoxic and anti-proliferative effects of copper complex on cancer cells.[6.84,6.85] The viability of HeLa cells was not influenced by the solvent (DMSO) or the copper salt (Figure 6.8), substantiating that the observed cytotoxic effect could be attributed to **L_4-Cu** complex. The results obtained in the *in vitro* cytotoxic assay suggested that in order to pursue fluorescence imaging studies of **L_4-Cu** complex in live cells; it would be prudent to choose a working concentration below 15 μM for compound **L_4**. Hence, to assess the effectiveness of compound **L_4** as a probe for intracellular detection of Cu^{2+} by fluorescence microscopy, HeLa cells were treated with 10 μM **L_4** solution for 1 h followed by incubation with 20 μM $Cu(ClO_4)_2$ to promote formation of **L_4-Cu** complex. Based on the established 1:1 stoichiometry of binding between **L_4** and Cu^{2+} it can be reasonably

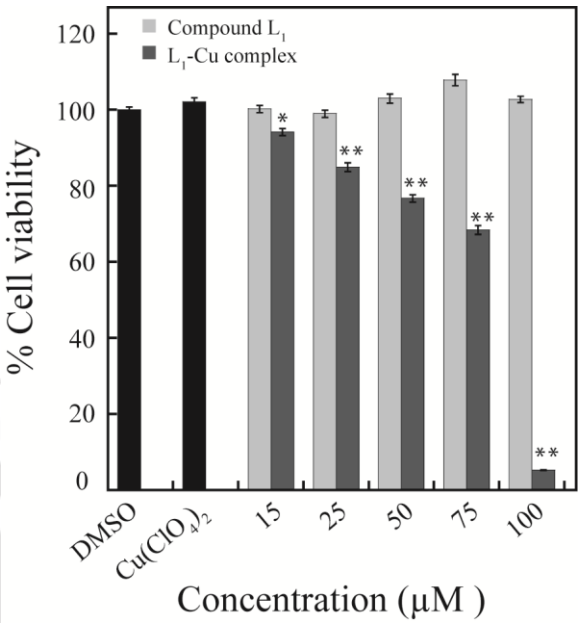

Figure 6.8 MTT assay to determine the cytotoxic effect of compound **L_4** and **L_4-Cu** complex on HeLa cells. Statistically significant values derived by ANOVA are indicated by asterisk marks. * indicates P value <0.05 and ** indicates P value <0.001.

assumed that the concentration of **L_4-Cu** complex formed in HeLa cells would be much lower than the concentration (15 μM) at which a marginal cytotoxic effect of the complex was observed (Figure 6.8).

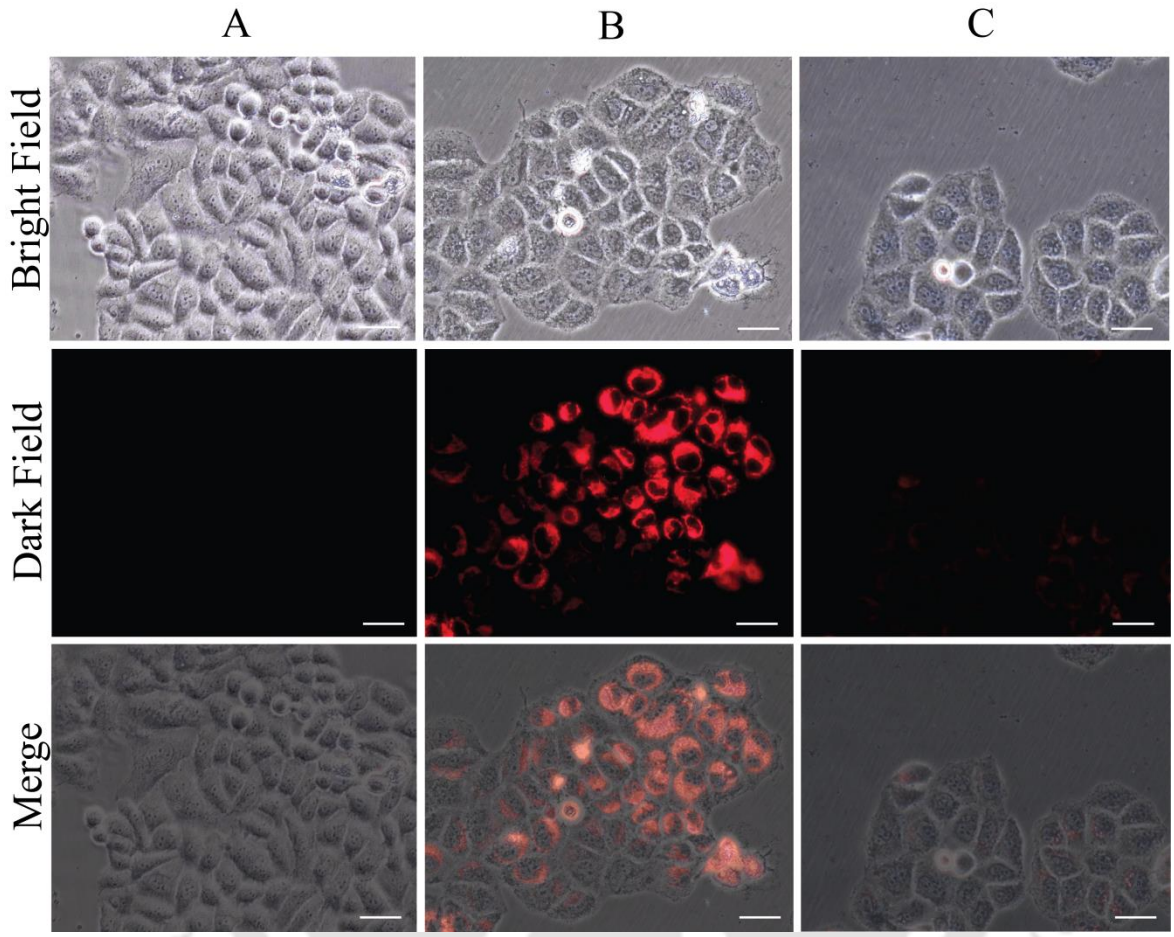

Figure 6.9 Fluorescence microscopic images of HeLa cells (A) after treating with 10 μM **L_4**, (under green light) (B) after adding 20 μM of Cu^{2+}, (under green light) to the **L_4** treated cells (C) after adding 30 μM S^{2-}, (under green light) to the (**L_4** + Cu^{2+}) treated cells. Scale bar for the images is 50 μm.

Fluorescence microscopic studies revealed a lack of fluorescence for HeLa cells treated with compound **L_4** alone (Figure 6.9, Panel A). Upon incubation with $Cu(ClO_4)_2$, a striking switch-ON fluorescence was observed inside HeLa cells, which indicated the formation of **L_4-Cu** complex, as observed earlier in solution studies. Further, an intense red fluorescence was conspicuous in the perinuclear region of HeLa cells (Figure 6.9, Panel B). Interestingly, sulfide sensing inside HeLa cells by **L_4-Cu** complex could also be pursued as evident from the remarkable switch-OFF of the red fluorescence emission inside cells following incubation with Na_2S solution (Figure 6.9, Panel C). Essentially, the fluorescence microscopic analysis strongly suggested that compound **L_4** could readily

cross the membrane barrier, permeate into HeLa cells and rapidly sense intracellular Cu^{2+} and S^{2-}. It is significant to mention here that brightfield images of treated cells did not reveal any gross morphological perturbations, which suggested that HeLa cells were viable. This finding is encouraging for future *in vivo* biomedical applications of the sensor.

6.7. Conclusion

In summary, we have developed an NIR sensitive receptor **L_4** which selectively binds with Cu^{2+} ions and propels a switch ON response in optical and fluorescence spectra in the visible region. Apart from the NIR and visible changes the FRET based fluorescence response makes it a dual probe for naked eye detection through change in color and fluorescence. The detection limit for Cu^{2+} was found to be much lower than the permissible Cu^{2+} concentration in drinking water as per standard norms. The complex formed between **L_4** and Cu^{2+} is dissociable only in presence of sulfide anion, which makes the **L_4-Cu** complex an efficient sensor for sulfide anions. From the extensive spectroscopic studies it is clear that the receptor **L_4** and **L_4-Cu** complex could be used as a ratiometric sensor for the detection of Cu^{2+} and S^{2-} based on RET process involving the donor indole and the acceptor Cu^{2+} bound xanthene moiety of **L_4**. The receptor **L_4** shows intense change in its fluorescence emission when bound to Cu^{2+} in physiological conditions. Hence, the effectiveness of compound **L_4** as a probe for intracellular detection of Cu^{2+} by fluorescence microscopy was also studied. Moreover, the fluorescence microscopic analysis strongly suggested that compound **L_4** could readily cross the membrane barrier, permeate into HeLa cells and rapidly sense intracellular Cu^{2+} and S^{2-}.

References

[6.1] M. C. Linder and M. Hazegh-Azam, *Am. J. Clin. Nutr.* 1996, **63**, 797S.

[6.2] R. Uauy, M. Olivares and M. Gonzalez, *Am. J. Clin. Nutr.* 1998, **67**, 952S.

[6.3] G. E. Cartwright and M. M. Wintrobe, *Am. J. Clin. Nutr.* 1964, **14**, 224.

[6.4] D. G. Barceloux, *J. Toxicol. Clin. Toxicol.*, 1999, **37**, 217.

[6.5] D. Strausak, J. F. Mercer, H. H. Dieter, W. Stremmel and G. Multhaup, *Brain Res. Bull.*, 2001, **55**, 175.

[6.6] P. D. Beer and P. A. Gale, *Angew. Chem., Int. Ed.*, 2001, **40**, 486.

[6.7] R. Martinez-Manez and F. Sancenon, *Chem. Rev.*, 2003, **103**, 4419.

[6.8] Hydrogen Sulfide; World Health Organization: Geneva, 1981 (Environmental Health Criteria, No. 19).

[6.9] R. E. Gosselin, R. P. Smith and H. C. Hodge, Hydrogen Sulfide. In Clinical Toxicology of Commercial Products, 5th ed.; Williams and Wilkins: Baltimore, MD, 1984; pp III-198−III-202.

[6.10] S. A. Patwardhan and S. M. Abhyankar, *Colourage*, 1988, **35**, 15.

[6.11] P. A. Patnaik, Comprehensive Guide to the Hazardous Properties of Chemical Substances, 3rd ed.; Wiley: New York, 2007.

[6.12] N. Shao, Y. Zhang, S. M. Cheung, R. H. Yang, W. H. Chan, T. Mo, K. A. Li and F. Liu, *Anal. Chem.*, 2005, **77**, 7294.

[6.13] D. W. Domaille, E. L. Que and C. J. Chang, *Nat. Chem. Biol.*, 2008, **4**, 168.

[6.14] K. M. K. Swamy, S. K. Ko, S. K. Kwon, H. N. Lee, C. Mao, J. M. Kim, K. H. Lee, J. Kim, I. Shin and J. Yoon, *Chem. Commun*., 2008, 5915.

[6.15] E. Kimura, *Pure Appl. Chem.*, 1986, **58**, 1461.

[6.16] Z. Zhou and C. J. Fahrni, *J. Am. Chem. Soc*., 2004, **126**, 8862.

[6.17] Y. Zhou, F. Wang, Y. Kim, S. J. Kim and J. Yoon, *Org. Lett*., 2009, **11**, 4442.

[6.18] L. Fabbrizzi, M. Licchelli, P. Pallavicini, A. Perotti and D. Sacchi, *Angew. Chem.*, 1994, **106**, 2051.

[6.19] E. L. Que, D. W. Domaille and C. J. Chang, *Chem. Rev.*, 2008, **108**, 1517.

[6.20] J. Cody and C. J. Fahrni, *Tetrahedron*, 2004, **60**, 11099.

[6.21] Y. Xiang, A. J. Tong and Y. Ju, *Org.Lett.*, 2006, **8**, 2863.

[6.22] G. K. Li, Z. X. Xu, C. F. Chen and Z. T. Huang, *Chem. Commun.*, 2008, 1774.

[6.23] S. Goswami, D. Sen and N. K. Das, *Org. Lett.*, 2010, **12**, 856.

[6.24] Z. Xu, J. Yoon nad D. R. Spring, *Chem. Commun.*, 2010, **46**, 2563.

[6.25] K. Kaur and S. Kumar, *Dalton Trans*., 2011, **40**, 2451.

[6.26] R. Martinez, F. Zapata, A. Caballero, A. Espinosa, A. Tarraga and P. Molina, *Org. Lett.*, 2006, **8**, 3235.

[6.27] E. Sanna, L. Martinez, C. Rotger, S. Blasco, J. Gonzalez, E. Garcia-Espana and A. Costa, *Org. Lett.*, 2010, **12**, 3840.

[6.28] M. Verma, A. F. Chaudhry and C. Fahrni, *J. Org. Biomol. Chem.*, 2010, **8**, 363.

[6.29] Y. Zheng, Q. Huo, P. Kele, F. M. Andreopoulos, S. M. Pham and R. M. Leblanc, *Org. Lett.*, 2001, **3**, 3277.

[6.30] L. Gao, J. Q. Wang, L. Huang, X. X. Fan, J. H. Zhu, Y. Wang and Z. G. Zou, *Inorg. Chem.*, 2007, **46**, 10287.

[6.31] V. S. Jisha, A. J. Thomas and D. Ramaiah, *J. Org. Chem.*, 2009, **74**, 6667.

[6.32] H. H. Wang, L. Xue, Z. J. Fang, G. P. Li and H. Jiang, *New J. Chem.*, 2010, **34**, 1239.

[6.33] T. Gunnlaugsson, J. P. Leonard and N. S. Murray, *Org. Lett.*, 2004, **6**, 1557.

[6.34] R. Martinez, A. Espinosa, A. Tarraga and P. Molina, *Org. Lett.*, 2005, **7**, 5869.

[6.35] Z. Xu, K. Baek, H. N. Kim, J. Cui, X. Qian, D. R. Spring, I. Shin and J. Yoon, *J. Am. Chem. Soc.*, 2010, **132**, 601.

[6.36] L. Yang, R. McRae, M. M. Henary, R. Patel, B. Lai, S. Vogt and C. J. Fahrni, *Proc. Natl. Acad. Sci. USA* 2005, **102**, 11179.

[6.37] E. W. Miller, L. Zeng, D. W. Domaille and C. J. Chang, *Nat. Protoc.*, 2006, **1**, 824.

[6.38] Z. Xu, S. J. Han, C. Lee, J. Yoon and D. R. Spring, *Chem. Commun.*, 2010, **46**, 1679.

[6.39] D. W. Domaille, L. Zeng and C. J. Chang, *J. Am. Chem. Soc.*, 2010, **132**, 1194.

[6.40] H. D. Axelrod, J. H. Cary, J. E. Bonelli and J. P. Lodge Jr., *Anal. Chem.*, 1969, **41**, 1856.

[6.41], M. F. Choi and P. Hawkins, *Anal. Chim. Acta*, 1997, **344**, 105.

[6.42] M. A. Spaziani, J. L. Davis, M. Tinani and M. K. Carroll, *Analyst*,1997, **122**, 1555.

[6.43] M. G. Choi, S. Cha, H. Lee, H. L. Jeon and S.-K. Chang, *Chem. Commun.*, 2009, 7390.

[6.44] X. F. Yang, L. Wang, H. Xu and M. Zhao, *Anal. Chim. Acta*, 2009, **631**, 91.

[6.45] L. Zhang, X. Lou, Y. Yu, J. Qin and Z. Li, *Macromolecules*, 2011, **44**, 5186.

[6.46] G. Patonay and M. D. Antoine, *Anal. Chem.*, 1991, **63**, 321A.

[6.47] R. B. Thompson, *Top. Fluoresc. Spectrosc.*, 1994, **4**, 151.

[6.48] S. Stoyanov, *Pract. Spectrosc.*, 2001, **25**, 35.

[6.49] J. Fabian, H. Nakazumi and M. Matsuoka, *Chem. Rev.*, 1992, **92**, 1197.

[6.50] J. V. Frangioni, *Curr. Opin. Chem. Biol.*, 2003, **7**, 626.

[6.51] B. A. Smith, W. J. Akers, W. M. Leevy, A. J. Lampkins, S. Z. Xiao, W. Wolter, M. A. Suckow, S. Achilefu and B. D. Smith, *J. Am. Chem. Soc.*, 2010, **132**, 67.

[6.52] M. Kodama and E. Kimura, *J. Chem. Soc. Dalton Trans.*, 1979, 325.

[6.53] D. Aldakov and J. P. Anzenbacher, *J. Am. Chem. Soc.*, 2004, **126**, 4752.

[6.54] A. Coskun, M. D. Yilmaz and E. U. Akkaya, *Org Lett.*, 2007, **9**, 607.

[6.55] B. Ozmen and E. U. Akkaya, *Tetrahedron Lett.*, 2000, **41**, 9185.

[6.56] E. Sasaki, H. Kojima, H. Nishimatsu, Y. Urano, K. Kikuchi, Y. Hirata and T. Nagano, *J. Am. Chem. Soc.*, 2005, **127**, 3684.

[6.57] X. Peng, F. Song, E. Lu, Y. Wang, W. Zhou, J. Fan and Y. Gao, *J. Am. Chem. Soc.*, 2005, **127**, 4170.

[6.58] B. Tang, H. Huang, K. Xu, L. Tong, G. Yang, X. Liu and L. An, *Chem. Commun.*, 2006, 3609.

[6.59] P. Carol, S. Sreejith and A. Ajayaghosh, *Chem. Asian J.*, 2007, **2**, 338.

[6.60] S. Yin, V. Leen, S. V. Snick, N. Boens and W. Dehaen, *Chem. Commun.*, 2010, **46**, 6329.

[6.61] M. Zhu, M. Yuan, X. Liu, J. Xu, J. Lv, C. Huang, H. Liu, Y. Li, S. Wang and D. Zhu, *Org. Lett.*, 2008, **10**, 1481.

[6.62] X. Chen, S-W. Nam, G-H. Kim, N. Song, Y. Jeong, I. Shin, S. K. Kim, J. Kim, S. Park and J. Yoon, *Chem. Commun.*, 2010, **46**, 8953.

[6.63] Y. Yang, T. Cheng, W. Zhu, Y. Xu and X. Qian, *Org. Lett.*, 2011, **13**, 264.

[6.64] X. Cao, W. Lin and L. He, *Org. Lett.*, 2011, **13**, 4716.

[6.65] D. Maity, A. K. Manna, D. Karthigeyan, T. K. Kundu, S. K. Pati and T. Govindaraju, *Chem. Eur. J.*, 2011, **17**, 11152.

[6.66] J. S. Kim, K. H. Noh, S. H. Lee, S. K. Kim, S. K. Kim and J. Yoon, *J. Org. Chem.*, 2003, **68**, 597.

[6.67] J. S. Kim, O. J. Shon, J. A. Rim and S. K. Kim, J. Yoon, *J. Org. Chem.*, 2002, **67**, 2348.

[6.68] L. Aoki, T. Sakaki and S. Shinkai, *J. Chem. Soc., Chem. Commun.*, 1992, 730.

[6.69] I. Leray, J. P. Lefevre, J. F. Delouis, J. Delaire and B. Valeur, *Chem. Eur. J.*, 2001, **7**, 4590.

[6.70] M. H. Lee, D. T. Quang, H. S. Jung, J. Yoon, C.-H. Lee and J. S. Kim, *J. Org. Chem.*, 2007, **72**, 4242.

[6.71] H. Zhang and D. M. Rudkevich, *Chem. Commun.*, 2007, 1238.

[6.72] A. E. Albers, V. S. Okreglak and C. J. Chang, *J. Am. Chem. Soc.*, 2006, **128**, 9640.

[6.73] M. H. Lee, H. J. Kim, S. Yoon, N. Park and J. S. Kim, *Org. Lett.*, 2008, **10**, 213.

[6.74] Z. Zhu, M. Yu, H. Yang, K. Huang, F. Li, T. Yi and C. Huang, *Chem. Commun.*, 2008, 3387.

[6.75] M. Royzen, Z. Dai and J. W. Canary, *J. Am. Chem. Soc.*, 2005, **127**, 1612.

[6.76] A. Ajayaghosh, P. Carol and S. Sreejith, *J. Am. Chem. Soc.*, 2005, **127**, 14962.

[6.77] K. Kiyose, H. Kojima, Y. Urano and T. Nagano, *J. Am. Chem. Soc.*, 2006, **128**, 6548.

[6.78] H. Takakusa, K. Kikuchi, Y. Urano, H. Kojima and T. Nagano, *Chem. Eur. J.*, 2003, **9**, 1479.

[6.79] J. R. Lakowicz, *Principles of Fluorescence Spectroscopy*, 3rd ed.; Springer: New York, 2008.

[6.80] C. Kar, M. D. Adhikari, A. Ramesh and G. Das *Inorg. Chem.*, 2013, **52**,743.

[6.81] X. Li, X. Gao, W. Shi and H. Ma, *Chem. Rev.* 2014, **114**, 590.

[6.82] P. Bose and P. Ghosh, *Chem. Commun.*, 2010, **46**, 2962.

[6.83] M. H. Lee, J.-S. Wu, J. W. Lee, J. H. Jung and J. S. Kim, *Org. Lett.*, 2007, **9**, 2501.

[6.84] K. Ghosh, P. Kumar, V. Mohan, U. P. Singh, S. Kasiri and S. S. Mandal, *Inorg. Chem.*, 2012, **51**, 3343.

[6.85] H. Thomadaki, A. Karaliota, C. Litos and A. Scorilas, *J. Med. Chem.*, 2008, **51**, 3713.

Appendix

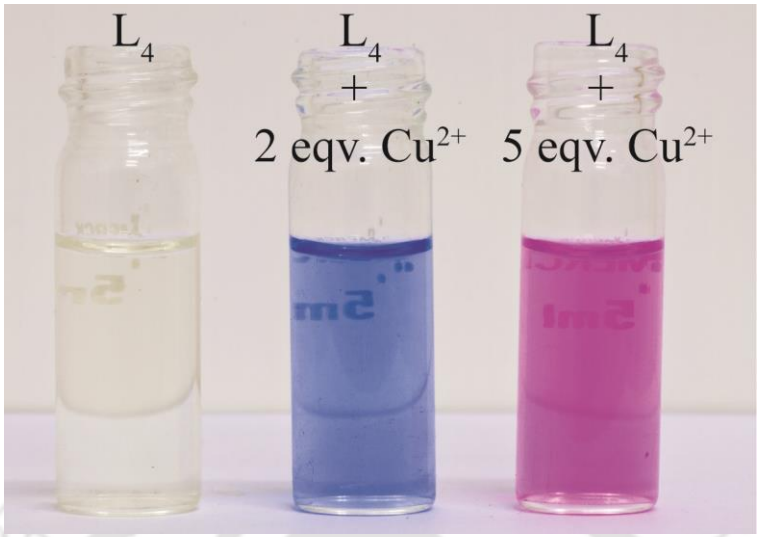

Figure A6.1 Visual change in the color of **L_4** upon addition of 2 eqv. and 5 eqv. of Cu^{2+} respectively.

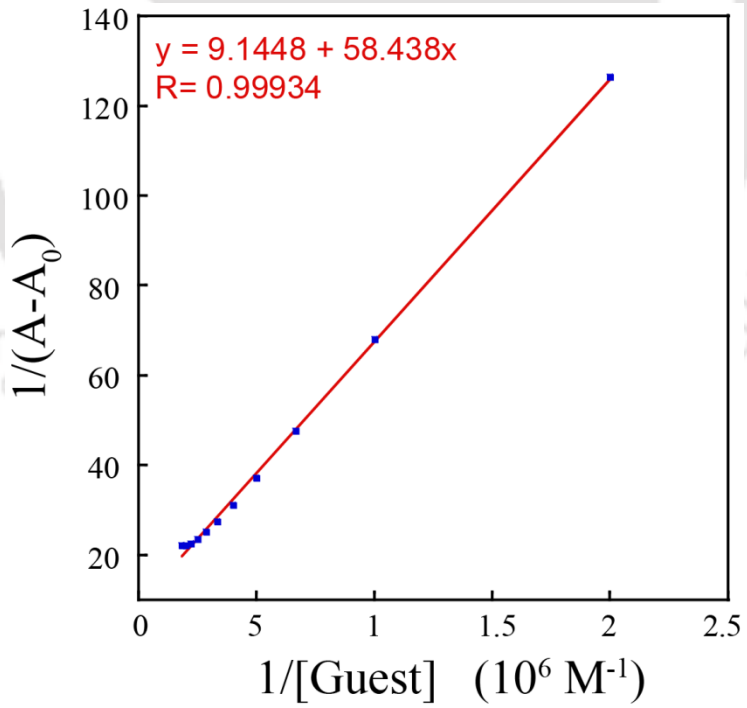

Figure A6.2 Bensei-Hildebrand plot obtained from the UV-Vis absorption (absorbance calculated from 702 nm) studies.

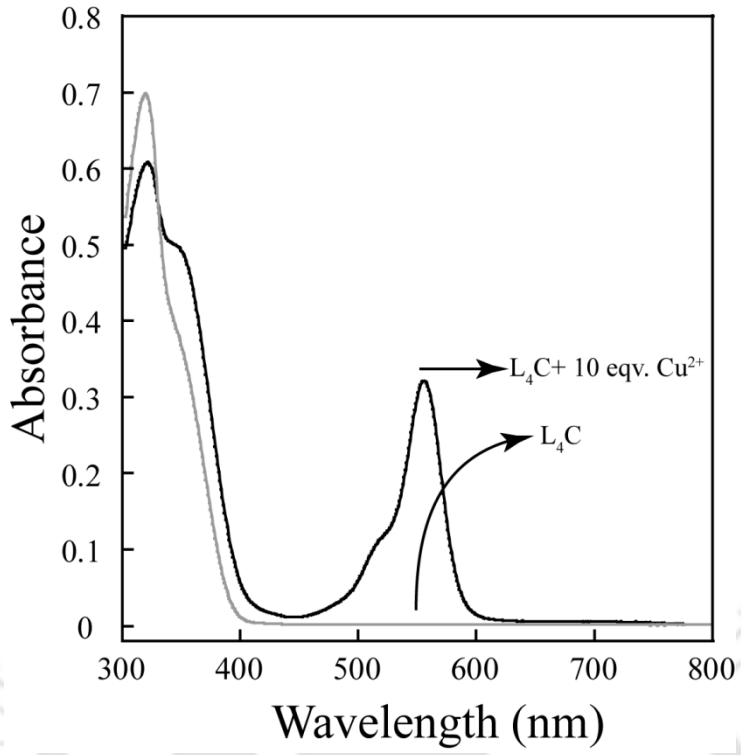

Figure A6.3 Changes of the of UV-Vis absorption of compound **L_4C** (10 μM) observed upon addition of 10 eqv. of $CuClO_4$ salt in a CH_3CN/aqueous HEPES buffer (1 mM, pH 7.3; 1:4 v/v).

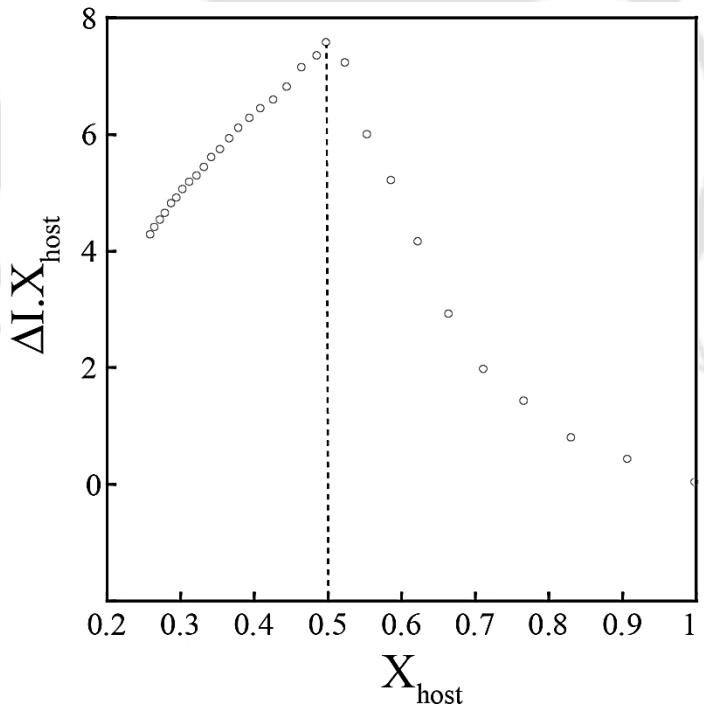

Figure A6.4 Job's plot between **L_4** and Cu^{2+} ions. Where X_{host} = the mole fraction of **L_4** and ΔI is the change ($I-I_0$) in the intensity (585 nm) of the emission spectra in presence of guest.

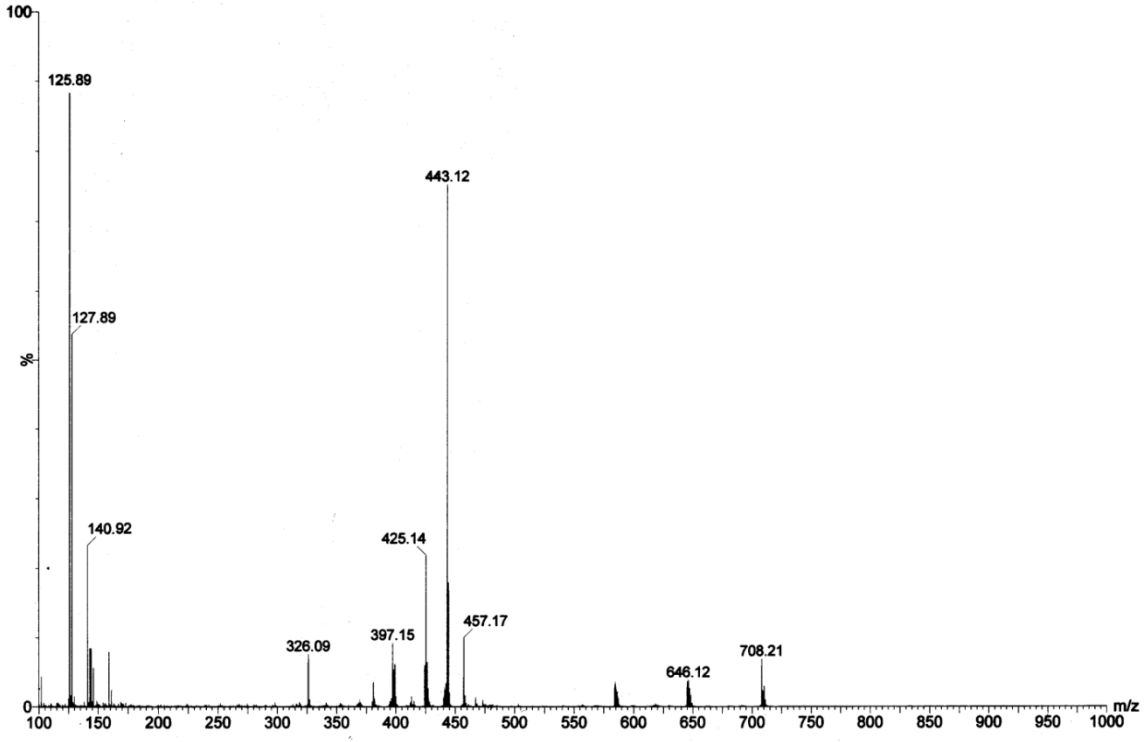

Figure A6.5 Mass spectrum of $\mathbf{L_4}$-Cu complex.

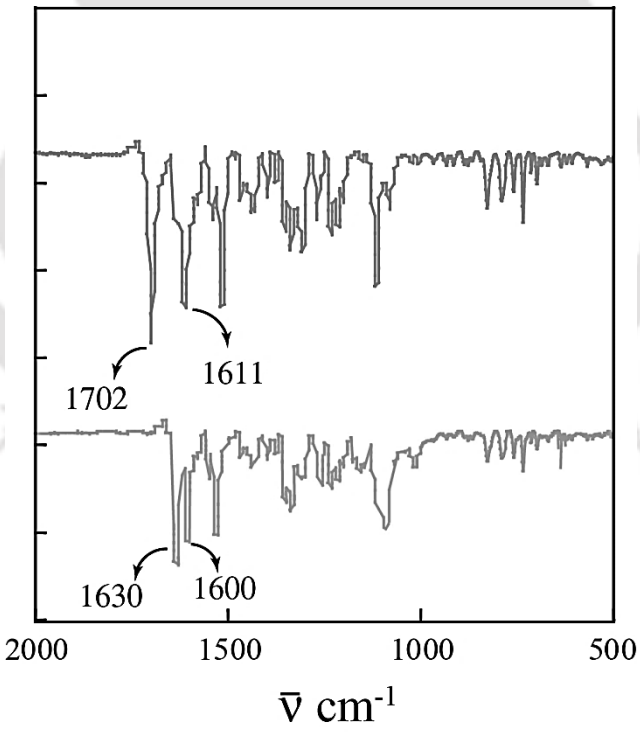

Figure A6.6 IR spectra $\mathbf{L_4}$ (above) and $\mathbf{L_4}$**-Cu** complex (below).

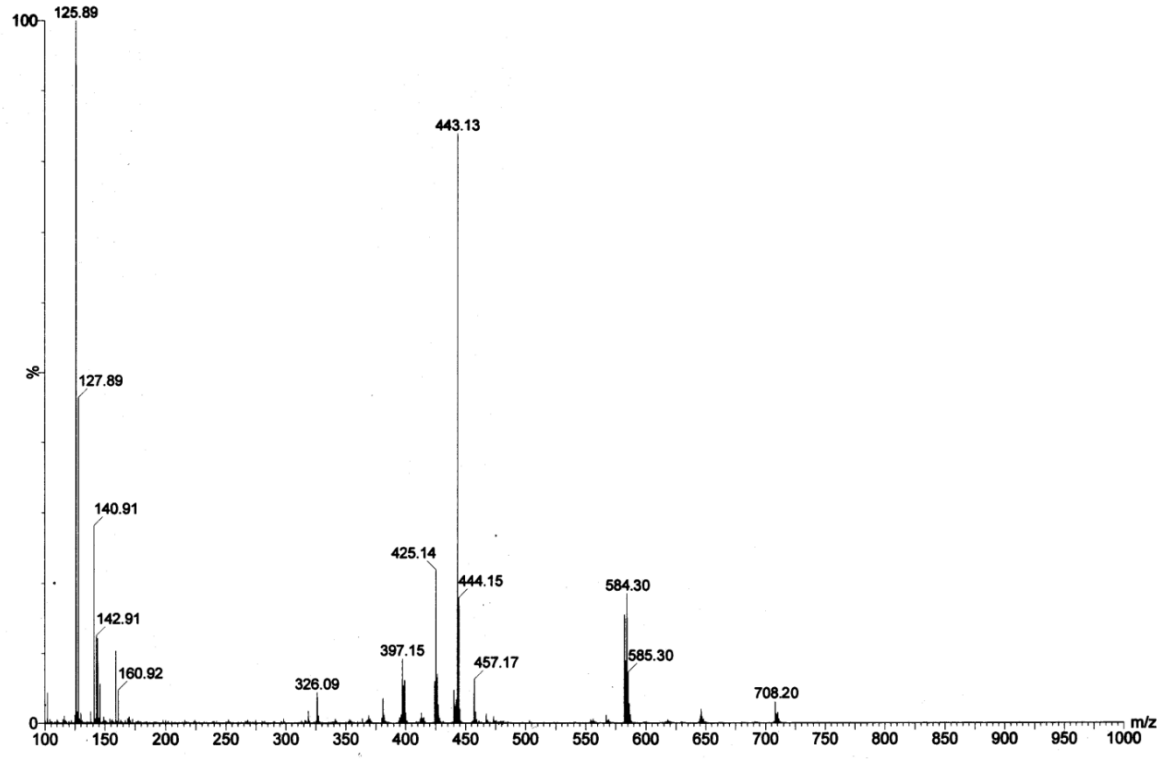

Figure A6.7 Mass spectrum of **L_4-Cu**+Sulfide

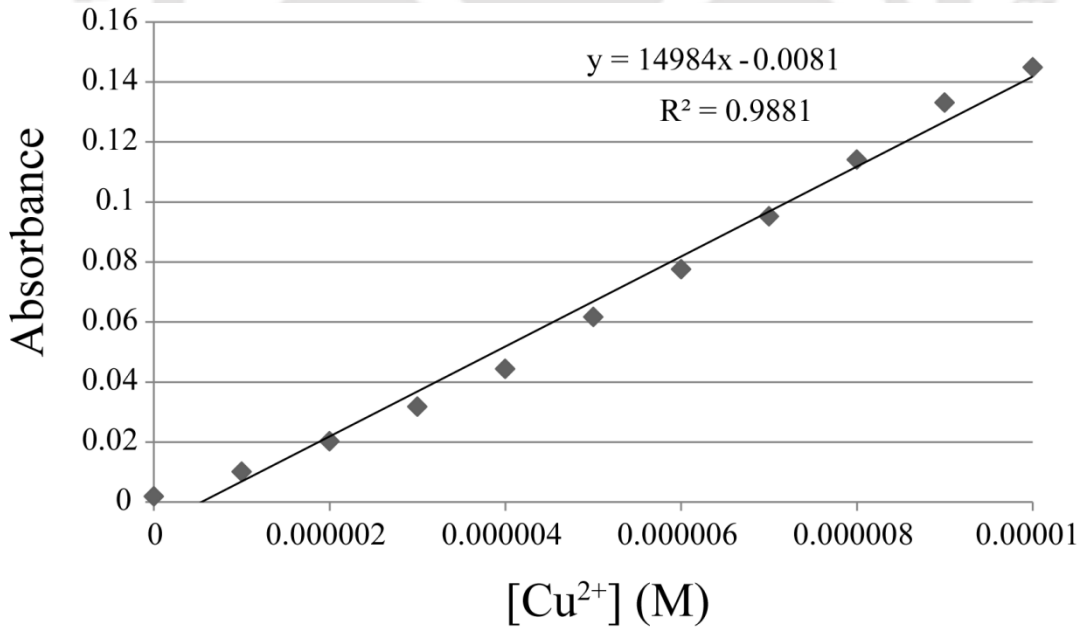

Figure A6.8 Absorbance versus Concentration plot for measuring the detection limit (3σ/k, here σ= 0.0000443847) of Cu^{2+} by **L_4**.

Table A3.1 selectivity coefficient of Cu^{2+} over other metal ions

Metal Ions	Selectivity Coefficient
Zn^{2+}	168.9547
Hg^{2+}	34.80567
Cr^{3+}	18.37764
Cd^{2+}	1187.959
Fe^{3+}	1834.24
Co^{2+}	1411.4
Ni^{2+}	1325.04
Ag^{+}	3811.765
Pb^{2+}	3800
Na^{+}	3805.882
K^{+}	3800
Ca^{2+}	3805.824
Mg^{2+}	3800

Conclusion and Future Perspective

To conclude, this thesis provides some significant results in the arena of 'supramolecular chemistry of cation and anion sensing', where the naked eye sensing capability of some newly synthesized imine based (Schiff base) fluorogenic receptors (**L_1-L_4**) were explored in solution state. In general, the present findings provide insight in designing simple and stable chemosensor molecules which can detect various ions in aqueous solution and inside living cells. The studies in the thesis also provide a route for gradual development in the design of the sensor molecules to obtain spectral response in the longer wavelength region of the spectra.

Receptor **L_1** containing a single imine linkage is the simplest structure among all the synthesized ligand, it has been shown to selectively detect Fe^{3+} ion *via* formation of chelation induced fluorescence emission mechanism and subsequently formed **L_1-Fe** complex undergoes dissociation selectively in presence of F^- ions. Thus **L_1** can be used for selective detection of Fe^{3+} and F^- in aqueous medium as well as biological milieu by switch ON/OFF green fluorescence. Whereas, receptor **L_2** which consist two imine linkage displays Cu^{2+} selective fluorescence switch ON at the yellow region of the emission spectra. The Cu^{2+} sensing ability of **L_2** is pertinent in complex environmental samples and inside mammalian cells. In case of **L_3** we have introduced an electron donor site and a binding site separated by a conjugated system, the binding of metal ions to **L_3** increase the possibility of charge transfer through the system and the fluorescence response is obtained at further longer region of the spectra. To further shift the optical as well as fluorescence response to far more longer region in chapter 6 we have chosen a well-known fluorophoric moiety, Rhodamine B and further modified it by introducing an indole moiety. The rhodamine based fluorophoric probe **L_4** has been shown to efficiently sense Cu^{2+} ions in the NIR region of the optical spectra and also exhibit switch ON red fluorescence. The **L_4-Cu** complex undergoes dissociation selectively in presence of S^{2-} ions with complete regeneration of the spectral properties. Overall, these results give a clear idea about some of the important factors for designing chemosensors, such as the type of donor-atoms, size and flexibility that determines the selectivity, efficiency and the wavelength region of the spectral response.

Fluorescence and colorimetric chemo-sensorial chemistry has grown considerably since the pioneering work of Sousa with the naphthalene compounds. After the Nobel Prize in supramolecular chemistry in 1987 to Charles J. Pedersen, Jean-Marie Lehn and Donald J. Cram, the design and application of fluorescent molecular devices increased exponentially. The possibility of a precise molecular recognition between a chemosensor and their guests has many applications in analytical chemistry, supramolecular science, biochemistry, physical chemistry, medicinal chemistry, toxicology, forensic sciences and applicable disciplines even to the modern nanosciences. However, for these applications to reach their prospective basic work is in tuning the receptor molecule in such a way that it is easily soluble in aqueous media and the spectral response is vivid and at longer end of the spectra. Although the results included in this thesis are extremely useful from a fundamental viewpoint, there is other challenging aspects in supramolecular chemistry that need to be developed, basically from an applicative approach. Research in these areas with a focus on technological and biomedical applications, based upon the remarkable cation, anion and neutral molecular sensing appear to be forthcoming.

Chirantan Kar

Academic Summary

2010 - Present	PhD student at Indian Institute of Technology Guwahati, India.
Thesis title:	"Design, synthesis and application of fluorogenic probes for selective detection of ionic analytes in physiological condition"
2007-2009:	Masters in Chemistry (Specialization: Organic Chemistry) University of North Bengal, West Bengal, India. 71.57%.
2004-2007:	Graduation (Chemistry), ABN Seal College, West Bengal, India. 62.50%.
2001-2003:	12th (Science), WBCHSE, 74.00%.
2001	10th , WBBSE, 81%.

Research Interest

Photochemistry, physical-organic chemistry, Physical-inorganic chemistry, synthesis and characterization of fluorescence probes, identification of unknown compounds and ions in environmental samples using spectroscopic techniques, application of new sensor technologies in biotechnology and environmental analyses.

Research Experience

PhD Research (January 2010 - Present)
Brief Research Topic:

- Synthesis and characterization of organic receptor molecules to obtain desired spectral properties.
- Studied the interaction between these newly synthesized receptors and various environmentally important ionic species.
- Explored the factors that control the selectivity of these fluorophoric receptors towards specific analytes.

- Also applied these chemosensor probes for detecting specific analytes in complex environmental (natural water samples) and biological (mammalian cells) milieu.
- Apart from the work involved in my thesis I have also gathered knowledge on protein fluorescence, protein small molecule interactions and protein aggregation studies

Expertise:

- Spectroscopic techniques (UV, Fluorescence, FT-IR, Atomic absorption), Optical and fluorescence microscopy, NMR spectroscopy, mass spectrometry, single crystal x-ray diffraction.

Publications

1. A simple and efficient fluorophoric probe for dual sensing of Fe^{3+} and F^{-}: application to bioimaging in native cellular iron pools and live cells, **Chirantan Kar**, Soham Samanta, Sandipan Mukherjee, Barun K. Datta, Aiyagari Ramesh and Gopal Das, ***New J. Chem.***, 2014, **DOI:** 10.1039/C4NJ00239C.
2. NIR- and FRET-Based Sensing of Cu^{2+} and S^{2-} in Physiological Conditions and in Live Cells, **Chirantan Kar**, Manab Adhikari, Aiyagari Ramesh and Gopal Das, ***Inorg. Chem.***, 2013, 52, 743.
3. A CHEF-based biocompatible turn ON ratiometric sensor for sensitive and selective probing of Cu^{2+}, **Chirantan Kar**, Manab Adhikari, Aiyagari Ramesh and Gopal Das, ***Sensor. Actuat. B-Chem.***, 2013, 188, 1132.
4. Zn^{2+} and Pyrophosphate Sensing: Selective Detection in Physiological Conditions and Application in DNA-Based Estimation of Bacterial Cell Numbers, Barun K. Datta, Sandipan Mukherjee, **Chirantan Kar**, Aiyagari Ramesh and Gopal Das, ***Anal. Chem.***, 2013, 85, 8369.
5. Selective sensing and efficient separation of Hg^{2+} from aqueous medium with a pyrene based amphiphilic ligand, **Chirantan Kar**, Manab Adhikari, Aiyagari Ramesh and Gopal Das, ***RSC Advances***., 2012, 2, 9201.
6. Prospective Antibacterial for Drug-resistant Pathogens: A Dual Warhead Amphiphile Designed to Track Interactions and Kill Pathogenic Bacteria by Membrane Damage and Cellular DNA Cleavage, Durairaj Thiyagarajan, Sudeep Goswami, **Chirantan Kar**, Gopal Das and Ramesh Aiyagari, ***Chem Commun.***, 2014, **DOI**: 10.1039/C4CC02354D.

7. Synthetic amphiphiles as therapeutic antibacterials: lessons on bactericidal efficacy and cytotoxicity and potential application as an adjuvant in antimicrobial chemotherapy, Sudeep Goswami, Manab Deb Adhikari, **Chirantan Kar**, Durairaj Thiyagarajan, Gopal Das and Aiyagari Ramesh, ***J. Mater. Chem. B***, 2013, 1, 2612.
8. A retrievable fluorescence "TURN ON" sensor for sulfide anions, **Chirantan Kar** and Gopal Das. ***J. Photoch Photobio. A: Chemistry***, 2013, 251, 128.
9. Benzimidazole functionalized tripodal receptor for selective recognition of iodide, **Chirantan Kar**, Arghya Basu and Gopal Das, ***Tetrahedron Lett.***, 2012, 53, 4754.
10. Role of N-Methyl-8-(Alkoxy)quinolinium Iodide in Suppression of Protein-Protein Interactions, Bimlesh Ojha, **Chirantan Kar** and Gopal Das, ***J. Chem. Sci.***, 2013**,** 125, 229.
11. Selective fluorescence sensor for Al^{3+} and Pb^{2+} in physiological condition by a benzene based tripodal receptor, Barun Kr. Dutta, **Chirantan Kar**, Arghya Basu and Gopal Das, ***Tetrahedron Lett.*** 2013, 54, 771.
12. Synthesis, crystal structure and bio-macromolecular interaction studies of pyridine-based thiosemicarbazone and its Ni(II) and Cu(II) complexesArghya Basu, Durairaj Thiyagarajan, **Chirantan Kar**, Aiyagari Ramesh and Gopal Das, ***RSC Adv.***, 2013, 3, 14088.
13. A novel amphiphilic thiosemicarbazone derivative for binding and selective sensing of human serum albumin, **Chirantan Kar**, Bimlesh Ojha and Gopal Das, ***Luminescence,*** 2013, 28, 339.
14. Excited-State Intermolecular Proton Transfer Induced TURN ON Fluorescent Chemosensor for Selective Detection of PO_4^{3-} Anion, **Chirantan Kar**, Sandeep Dey and Gopal Das, ***Sensor Lett.,*** 2011, 9, 1430.
15. A single Probe to sense Al^{3+} Colorimetrically and Cd^{2+} by Turn-On Fluorescence in Physiological Conditions and Live Cells, **Chirantan Kar**, Soham Samanta, Sandipan Mukherjee, Aiyagari Ramesh and Gopal Das. ***(Communicated)***.

Conference Attended

- "**MTIC**" 2013, IIT Roorkee, Uttarakhand, India (Poster presented)